

MODELING THE INTERACTION BETWEEN MICRO-CLIMATE FACTORS AND MOISTURE-RELATED SKIN-SUPPORT FRICTION DURING PATIENT REPOSITIONING IN BED

by

T. Z. Jagt

in partial fulfillment of the requirements for the degree of

Master of Science
in Applied Mathematics

at the faculty EEMCS of Delft University of Technology,
to be defended publicly on Thursday April 9, 2015 at 11:30 AM.

Student number:	1509489	
Supervisor:	Dr. ir. F. J. Vermolen	TU Delft
Thesis committee:	Prof. dr. ir. C. Vuik,	TU Delft
	Dr. ir. W. T. van Horssen,	TU Delft

This thesis is confidential and cannot be made public until April 9, 2015.

An electronic version of this thesis is available at <http://repository.tudelft.nl/>.

PREFACE

For the past year I have been working at the Delft University of Technology on mathematical models regarding pressure ulcers. This report describes the final product of this research. I would like to express my gratitude to those who made these results possible or contributed in any other way.

First of all I would like to thank the members of the examination committee. I would like to thank my daily supervisor Fred Vermolen for giving me the opportunity to work on this project, and helping me to take the time I needed. During the entire project he was always motivated and inspired me by listing the endless possibilities within this research. Through Fred I got the opportunity to go to the International Symposium of Computer Methods in Biomechanics and Biomedical Engineering (CMBBE), where I attended presentations of Amit Gefen himself, who has created the underlying models of this project ([1], [2]). I would like to thank Kees Vuik and Wim van Horsen for being part of the committee.

I would also like to thank my family, and especially my parents for supporting me not only during this thesis, but my entire education. With your trust and support the last years went by smoothly and enjoyable. I would like to thank you for helping me to stay focused during this final project and achieve the results discussed in this report. When things got hard or I got really nervous I could always count on you for help. Specifically, I would like to thank my sister Yara for reading this report and providing me with feedback. I would also like to thank my friends for sharing their own, similar, stories. Thank you for letting me realize once again that research almost never goes smooth.

At last I would like to thank Kevin Moerman who created the Gibbon Toolbox, for answering all my questions and taking the time to meet with me in person.

*T. Z. Jagt
Delft, April 2015*

CONTENTS

List of Figures	vii
List of Tables	ix
List of Abbreviations	xi
List of Symbols	xiii
1 Introduction	1
1.1 Pressure Ulcers	2
1.1.1 Skin Breakdown	3
1.2 Previous research	4
1.2.1 The effects of the micro climate	4
1.2.2 Choosing a software package	8
1.3 Outline of this thesis	11
2 Mathematical model	13
2.1 Deformation and stress	13
2.1.1 The deformation gradient	13
2.1.2 Push forward and pull back	15
2.1.3 The stress tensor	16
2.1.4 The strain tensor	20
2.1.5 The Principal stresses	22
2.1.6 The Maximum shear stress	23
2.2 Problem definition	24
2.2.1 The Problem	24
2.2.2 The Weak Formulation	27
2.3 Including the contact definitions	32
2.3.1 The two body contact problem	32
2.3.2 Including friction in the problem	33
2.3.3 Including the contact in the equations of motion	37
2.3.4 The Weak form including the contact tractions	37
2.4 Constructing the model using the Gibbon Toolbox and FEBio	39
2.4.1 The basic model	39
2.4.2 Adding the microclimate factors to the basic model	44
2.4.3 Further improving the model	45
3 The Numerical Method: Newton Raphson	49
3.1 The general Newton-Raphson method	49
3.1.1 One degree of freedom	49
3.1.2 The general solution	50
3.2 Applying the Newton-Raphson method to the problem without Contact	52
3.2.1 Linearization of the virtual work	52
3.2.2 Discretization of the virtual work	58
3.2.3 Discretization of the linearized virtual work	63
3.2.4 Formulating the Newton-Raphson scheme	66
3.3 Applying the Newton-Raphson method to the problem with Contact	68
3.3.1 Linearizing the Contact integral	68
3.3.2 Discretizing the contact integral	69
3.3.3 Discretizing the linearized contact integral	70

3.4	Quasi-Newton methods with Line Search	71
3.4.1	The Quasi-Newton method in FEBio; BFGS	71
3.4.2	The Line Search	72
4	Results	73
4.1	The objective	73
4.1.1	Skin failure	73
4.1.2	Other objectives	74
4.2	Results with the basic model	75
4.2.1	The small model (Model A) with Prescribed boundary conditions	75
4.2.2	The small model (Model A) with a body load	78
4.2.3	The big model (Model B) with Prescribed boundary conditions	81
4.2.4	Results of the Basic Model	82
4.3	Results of the model including microclimate factors	83
4.3.1	The small model with microclimate factors	84
4.4	Results of final model	86
4.4.1	Changing the Young's modulus	86
4.4.2	Adding Weight	88
4.4.3	Changing the temperature	89
4.5	Overall Results	92
5	Discussions and Conclusions	93
5.1	Conclusions	93
5.2	Discussion	94
5.3	Recommendations for future work	95
A	Elasticity, Stress and Strain	97
A.1	Elasticity	97
A.2	Stress and Strain	97
A.3	Hooke's Law	98
A.3.1	Isotropic materials	100
A.4	Plane stress and Plane strain	101
B	Contact Mechanics	105
B.1	Normal contact mechanics	106
B.1.1	The Hertzian Theory of Elastic Deformations	106
B.1.2	Contact models with adhesion	108
B.2	Tangential Contact Problems	109
B.2.1	Cattaneo problem	109
B.2.2	Half-space approaches	110
B.2.3	Forming a new stress distribution	112
B.2.4	Coulomb's Law of Friction	113
B.2.5	The contact mechanics model for contact between human and bed	114
B.3	The Signorini Problem	114
C	Matlab Codes	117
C.1	Effect of microclimate factors on the patients risk of pressure ulcers - Matlab code	117
C.2	Matlab code of the Final Model	119
D	FEBio files	127
D.1	FEBio file of the Final Model	127
	Bibliography	131

LIST OF FIGURES

1.1	Schematic representation of the yield point	3
1.2	Skin strength vs. shear stress	4
1.3	Model of the human body	4
1.4	Skin strength vs. shear stress	7
1.5	The effects of temperature and other factors on the critical time.	8
1.6	The software package Adina.	9
1.7	The predecessor PreView.	9
1.8	FEBio	9
1.9	The post processor PostView.	10
1.10	A schematic overview of the chosen software.	11
2.1	The deformation of a solid.	14
2.2	Volume change in the deformation of a body.	15
2.3	The traction vector in a deformable body.	16
2.4	The stress components.	17
2.5	An elemental tetrahedron.	17
2.6	The principal directions of the stress tensor.	22
2.7	Illustration of the notation used for the two body contact problem	32
2.8	Schematic of the parametrization of a contact surface. Source: [20].	34
2.9	The basic models.	40
2.10	Prescribed boundary conditions	42
2.11	Two methods of adding weight to the model.	46
2.12	The heat equation is solved along a simple rod.	47
3.1	Solving the one-degree-of-freedom nonlinear problem $f(x) = 0$.	50
3.2	Uniform surface pressure	57
3.3	Discretization of a general geometry.	59
4.1	Skin strength vs. shear stress	73
4.2	Deformation results of the small basic model with prescribed boundary conditions.	75
4.3	The maximum shear stress of the skin elements in the small basic model with prescribed boundary conditions.	76
4.4	The maximum shear stress of the skin compared with the shear strength for the small basic model with prescribed boundary conditions.	76
4.5	Deformation results of the small basic model with prescribed boundary conditions.	77
4.6	The maximum shear stress of the skin elements in the small basic model with prescribed boundary conditions.	77
4.7	The maximum shear stress of the skin compared with the shear strength for the small basic model with prescribed boundary conditions.	77
4.8	Deformation results of the small basic model with prescribed boundary conditions for different values of the Young's modulus.	78
4.9	The maximum shear stress of the skin for different values of the Young's modulus.	78
4.10	Twitches in the first few steps of the solution	79
4.11	Deformation results of the small basic model with a body load.	79
4.12	Downward displacement due to gravity for the small basic model.	80
4.13	The maximum shear stress of the skin elements in the small basic model with a body load.	80
4.14	The maximum shear stress of the skin compared with the shear strength for the small basic model with a body load.	80
4.15	The maximum shear stress in the small basic body.	81

4.16	Deformation results of the big basic model with prescribed boundary conditions.	81
4.17	The maximum shear stress of the skin elements in the big basic model with prescribed boundary conditions.	82
4.18	The maximum shear stress of the skin compared with the shear strength for the big basic model with prescribed boundary conditions.	82
4.19	The coefficient of friction for a skin temperature of $T_s = 30^\circ\text{C}$	83
4.20	Deformation results of the small model including microclimate factors with a body load.	84
4.21	The maximum shear stress of the skin elements in the small model including microclimate factors with a body load.	84
4.22	The maximum shear stress of the skin compared with the shear strength for the small model including microclimate factors with a body load.	85
4.23	Deformation results of the small model with a changing Young's modulus with a body load.	86
4.24	The downward of the small model with a changing Young's modulus.	86
4.25	The maximum shear stress of the skin elements in the small model with a changing Young's modulus with a body load.	87
4.26	The maximum shear stress of the skin compared with the shear strength for the small model with a changing Young's modulus with a body load.	87
4.27	Deformation results of the small model with additional weight modeled with a body load.	88
4.28	The downward of the small model with additional weight.	88
4.29	The maximum shear stress of the skin elements in the small model with additional weight modeled with a body load.	89
4.30	The maximum shear stress of the skin compared with the shear strength for the small model with additional weight modeled with a body load.	89
4.31	The accumulation of perspiration for different skin temperatures.	89
4.32	The coefficient of friction for different skin temperatures.	90
4.33	The shear strength of the skin for different skin temperatures.	90
4.34	Deformation results of the small model with $T_s = 35^\circ\text{C}$ modeled with a body load.	90
4.35	The maximum shear stress of the skin elements in the small model with $T_s = 35^\circ\text{C}$ modeled with a body load.	91
4.36	The maximum shear stress of the skin compared with the shear strength for the small model with $T_s = 35^\circ\text{C}$ modeled with a body load.	91
4.37	The maximum shear stress of the skin for all different models.	92
A.1	Plane Stress	101
A.2	Plane Strain	102
A.3	Comparison between plane stress and plane strain.	104
B.1	Contact with no force acting upon the contact.	106
B.2	Contact with a normal force acting upon the contact. Source: [4]	106
B.3	The center of the sphere moves down by a distance of $d = \delta_n$	109
B.4	Sticking and sliding domains in a round tangential contact.	113

LIST OF TABLES

1.1	Values used in the plots	7
2.1	The used units.	39
2.2	Dimensions of the two basic models.	40
2.3	Specifications of the materials	43
2.4	Values used in the calculation of the perspiration factor	45
2.5	The variables in the heat equation	47
2.6	The values in the heat equation	48
2.7	The loadcurve describing the Young's modulus	48
4.1	Three cases for the small basic model with prescribed boundary conditions.	75
4.2	A single case for the small basic model with a body load.	78
4.3	A single case for the big basic model with prescribed boundary conditions.	81
4.4	A single case for the small model including microclimate factors with a body load.	84
A.1	Relationships between the Coefficients of Elasticity	99

LIST OF ABBREVIATIONS

EPUAP	European Pressure Ulcer Advisory Panel
SPU	Superficial Pressure Ulcer
PK1 stress	First Piola-Kirchhoff stress tensor
PK1 traction	First Piola-Kirchhoff traction vector
PK2 stress	Second Piola-Kirchhoff stress tensor
BFGS	Broyden-Fletcher-Goldfarb-Shanno method
COF	Coefficient of Friction
ROI	Region of Interest

LIST OF MOST USED SYMBOLS

$\sigma_1, \sigma_2, \sigma_3$	The principal stresses
τ_{\max}	Maximum shear stress
F	Deformation gradient
X	Position in the reference/undeformed configuration
x	Position in the current/deformed configuration
ϕ	Mapping between reference and current configuration
J	Jacobian ($J = \det(\mathbf{F})$)
t(n)	Traction vector corresponding to the normal n
σ	Cauchy stress tensor
P	First Piola-Kirchhoff stress tensor
T	First Piola-Kirchhoff traction vector
S	Second Piola-Kirchhoff stress tensor
C	Right Cauchy-Green deformation tensor
c	Eulerian or spatial elasticity tensor
E	Green or Lagrangian strain tensor
δW	Virtual work
$D(\dots)[\mathbf{u}]$	Directional derivative in the direction of u
g	Gap function
\mathbf{t}_T	Frictional traction force
μ	Coefficient of friction
\mathbf{t}_N	Contact pressure
$\frac{\Delta V(t)}{V}$	The accumulated perspiration over time t within V
T_a	Ambient temperature (close to the region of interest)
T_s	Skin temperature
τ_w^s	Shear strength of the skin
$T(x, t)$	The temperature at time t and position x
$c(x)$	The specific heat
$\rho(x)$	The mass density
K_0	The thermal conductivity
H	The heat transfer coefficient

1

INTRODUCTION

Patients that are limited to spending most of their time lying in bed are prone to skin breakdown as a consequence of moisture development between the skin and mattress. This wetness results from transpiration or urine. Due to wetting of the skin, the mechanical properties of the skin change and the friction between the skin and the mattress increases. This increase implies that the shear forces at the interface between the skin and mattress increase when a patient is moved or relocated on bed for daily care. This mechanism increases the likelihood of the development of a superficial pressure ulcer.

In this research, we will analyze, use and improve the phenomenological model developed by Gefen ([1], [2]) for the simulation of micro-climate factors. This model contains an interaction between the amount of transpiration, the ambient temperature, the increase of humidity and the increase in the skin-support contact pressure. Furthermore, we will analyze and use a finite-element model for the mechanical support and equilibrium of tissue interacting with the mattress where the skin and subcutaneous tissue are incorporated. This interaction poses a contact problem where the surface of contact between the skin and mattress has to be determined. In this work, we will focus on the combination of the two models, where we aim at predicting the likelihood of the development of a superficial pressure ulcer in the course of time upon moving the patient over the surface of the mattress. This is done by using the finite-element method over the domain containing the tissue as well as the mattress. As an output parameter the shear stress will be important to estimate the time at which skin break-down (failure) occurs. Since the mechanical properties of skin change with local humidity, the skin will deteriorate in the course of time due to the build-up of moisture levels. In this MSc-thesis, we aim at a coupling of the micro-climate factors to the mechanical equilibrium which consists of a contact problem.

The basics of this thesis lie in the two articles

- "How do microclimate factors affect the risk for superficial pressure ulcers: A mathematical modeling study" by Amit Gefen [1], and
- "Modeling the effects of moisture-related skin-support friction on the risk for superficial pressure ulcers during patient repositioning in bed" by Eliav Shaked and Amit Gefen [2].

These articles both describe a mathematical model regarding pressure ulcers in bed-bound patients. The first one assesses a patients risk of getting a pressure ulcer. Here a pressure ulcer is said to develop when the strength of the skin is smaller than the stress obtained by the movement. The second article describes a way of calculating the shear stress of the skin during movement using the finite element method.

The goal of the thesis can be summarized as follows:

To create a combined model from the two models created by Amit Gefen, in which a patients risk of pressure ulcers can be assessed when considering not only the contact between the body and the bed, but also including the effects of microclimate factors.

1.1. PRESSURE ULCERS

A pressure ulcer is a special type of wound, caused by the appliance of stress on the skin. The official definition of a pressure ulcer is given by the European Pressure Ulcer Advisory Panel and says the following.

"A pressure ulcer is localized injury to the skin and/or underlying tissue usually over a bony prominence, as a result of pressure, or pressure in combination with shear. A number of contributing or confounding factors are also associated with pressure ulcers; the significance of these factors is yet to be elucidated." – <http://www.epuap.org>

Such a pressure ulcer can occur after a large pressure has been applied to the skin for a short period of time, or when a small pressure is applied for a long period of time. Pressure ulcers, also referred to as "bedsores" or "pressure sores", usually occur at bony prominences, which are the parts of the body that are usually in direct contact with the underlying surface such as a mattress. Examples of the most common locations are the shoulders and the shoulder blades, back of the head, heel, spine and tail bone.

The "European Pressure Ulcer Advisory Panel" (EPUAP) is a panel created to "support all European countries in their efforts to prevent and treat pressure ulcers". The overall mission of this panel is to

" provide the relief of persons suffering from or at risk of pressure ulcers, in particular through research and the education of the public and by influencing pressure ulcer policy in all European countries towards an adequate patient centered and cost effective pressure ulcer care." – <http://www.epuap.org> [3]

In order to improve the communication between the different countries regarding pressure ulcers, the EPUAP has created a "Quick Reference Guide" which has been translated into many different languages. In this reference guide guidelines are given that describe how a patients risk of pressure ulcers can be determined, and which factors should be taken into account. In this guide, the different types of pressure ulcers are also divided into four different categories. The categories and their (shortened) explanations are given below. The full explanation can be found on the EPUAP website [3].

Category/Stage I: Non-blanchable erythema Intact skin with non-blanchable redness of a localized area usually over a bony prominence. Darkly pigmented skin may not have visible blanching; its color may differ from the surrounding area. The area may be painful, firm, soft, warmer or cooler as compared to adjacent tissue. Category I may be difficult to detect in individuals with dark skin tones. May indicate "at risk" persons.

Category/Stage II: Partial thickness Partial thickness loss of dermis presenting as a shallow open ulcer with a red pink wound bed, without slough. May also present as an intact or open/ruptured serum-filled blister. Presents as a shiny or dry shallow ulcer without slough or bruising where bruising indicates deep tissue injury.

Category/Stage III: Full thickness skin loss Full thickness tissue loss. Subcutaneous fat may be visible but bone, tendon or muscle are not exposed. Slough may be present but does not obscure the depth of tissue loss. May include undermining and tunneling. The depth of a Category/Stage III pressure ulcer varies by anatomical location.

Category/Stage IV: Full thickness tissue loss Full thickness tissue loss with exposed bone, tendon or muscle. Slough or eschar may be present. Often includes undermining and tunneling. The depth of a Category/Stage IV pressure ulcer varies by anatomical location.

As can be seen in the definitions above, these different grades indicate the severity of the injury. In this thesis the main focus will lie on superficial pressure ulcers. According to Gefen ([1, 2]) these superficial ulcers correspond to the pressure ulcers from Grade I and Grade II.

As mentioned in the definition of pressure ulcers, many different factors influence a patients risk at the injuries. These factors include among others the age of the patient, whether or not the patient is healthy, the wetness of the skin and the stiffness of the skin. Many of these factors are related, for example a patient who has diabetes often has a stiffer skin.

A lot of research has been done and is being done to investigate these factors and decrease patients risk at

pressure ulcers. The models that are described in the articles that will be used in this thesis investigate the relation between the wetness of the skin (microclimate factors) and the risk of pressure ulcers. In the articles it is described that the temperature in the room has effect on the moisture level of the skin which has effect on the stiffness of the skin, hence again the factors are related.

1.1.1. SKIN BREAKDOWN

To minimize a patients risk at pressure ulcers it is important to know when pressure ulcers develop. A very simple way of looking at the development of these wounds is to look at it as the skin "failing" or breaking down. There are multiple theories on the failing of materials, depending on the types of these materials.

A solid material is called ductile when it has the ability to deform under tensile stress, for example when sliding along a different plane. Criteria used to predict the failure of these materials are also known as yield criteria. These criteria can be seen as defining the limit of elasticity in a material after which plastic deformation will occur. This means that some of the deformations will remain when the material is unloaded. The yield criteria try to ascertain the yield point at which the elastic region, in which unloading the material means the deformations are completely reversed, changes into the plastic region. Note that despite the quick transition from elastic to plastic behavior, in reality there is no distinct yield point due to continuity ([4]).

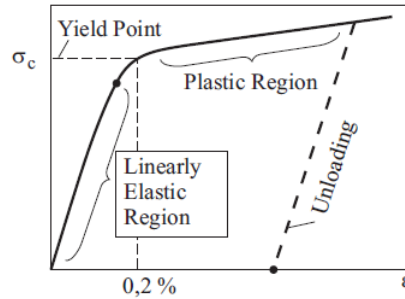


Figure 1.1: Schematic representation of a stress-strain diagram for many metals and non-metals. The transition from elastic to plastic behavior is fast but continuous and can therefore not truly be given by a single yield point. Source: [4]

Note that even though the definition of the yield point does not include actual failing of the material, it is the point at which permanent deformation occurs. In the context of the human body this will therefore be used as the failing point.

Below two of the most common yield criteria will be discussed ([5], [6]).

Maximum shear stress theory Also known as **the Tresca yield criterion**. This theory states that the material yields when the maximum shear stress τ exceeds the shear yield strength τ_y . For the principal stresses ordered as $\sigma_1 \geq \sigma_2 \geq \sigma_3$ the maximum shear stress is given equal to $\frac{1}{2}(\sigma_1 - \sigma_3)$ (see Sections 2.1.5 and 2.1.6). The yield point can hence be determined by solving equation (1.1):

$$\tau = \frac{1}{2}(\sigma_1 - \sigma_3) = \tau_y. \quad (1.1)$$

Maximum distortion energy criterion Also known as **the von Mises Criterion**. This criterion states that failure occurs when the von Mises stress squared σ_v exceeds the yield strength σ_y squared. Determining the yield point can be done by solving equation (1.2) where σ_1 , σ_2 and σ_3 are the principal stresses, i.e.

$$\sigma_v^2 = \frac{1}{2}[(\sigma_1 - \sigma_2)^2 + (\sigma_1 - \sigma_3)^2 + (\sigma_2 - \sigma_3)^2] = \sigma_y^2. \quad (1.2)$$

In this thesis the Maximum shear stress theory shall be used as this theory is also described by Gefen in [1]. In the article Gefen uses this theory to determine the critical time point for skin breakdown t^* which is in fact the time when the yield point is reached (see Figure 1.2). In Section 4.1.1 a more detailed explanation of the use of the Maximum shear stress theory in this thesis is given.

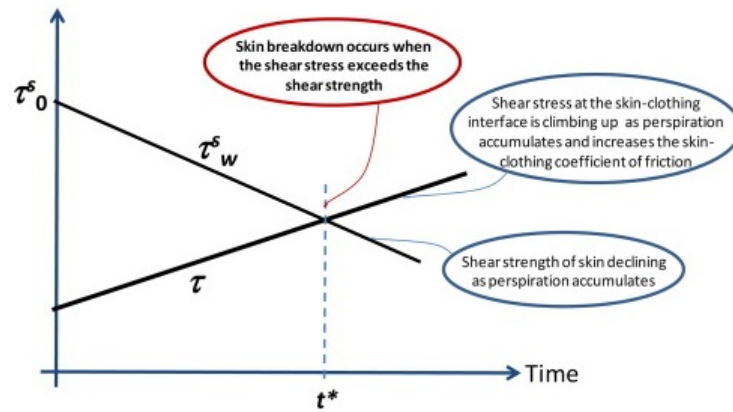


Figure 1.2: Skin break down will occur when the shear stress applied on the skin exceeds the shear strength of the skin. Source: [1]

1.2. PREVIOUS RESEARCH

This section will discuss the article on the effects of microclimate factors on the development of pressure ulcers written by Gefen [1] and the research that was done in the beginning of this thesis regarding the most suitable software.

1.2.1. THE EFFECTS OF THE MICRO CLIMATE

The paper by Amit Gefen [1] reviews a mathematical model which describes the effect of microclimate factors on the development of pressure ulcers.

In this section the assumptions, calculations and results of this article will be discussed.

In the article the risk of superficial pressure ulcers (SPUs) is being examined. Here superficial pressure ulcers will mean "skin damage associated with sustained mechanical loading".

The research described in the article continues on the idea that thermodynamic conditions within and around the skin tissue (i.e. the skin being wet) influences the risk of a patient getting a SPU. The term *microclimate* is used here to describe factors like the local temperature and moisture conditions of the skin. The area of interest will be the parts of the human body that are considered the weight-bearing regions ([7]¹). Previous papers described the effect of surface temperature, humidity, moisture and air movement as risk factors on the patients susceptibility. All these papers however, were based on purely experimental research. The article written by Gefen creates a mathematical model to prove that the microclimate factors are indeed risk factors.

In Figure 1.3 the part of the human body that is considered is shown. This *region of interest* (ROI) is "a small region of contact between the skin and a support (e.g. mattress or cushion), possibly with a covering sheet, some clothing or stocking in-between the skin and support".

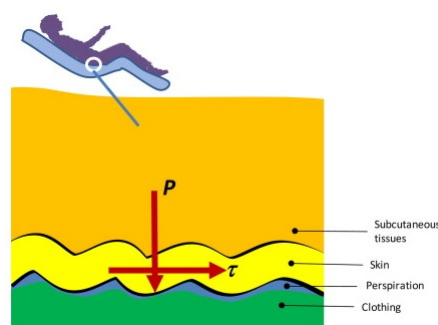


Figure 1.3: The model will consider a small weight-bearing part of the human body. Source: [1]

¹ Referred to by Gefen in [1].

Perspiration The first step that is taken in the article is to assume the expression of the perspiration accumulated over a certain time period within the available space. The following denotations are used.

Notation	Factor
ΔV	volume of perspiration
t	time
V	available space between the skin and the contact materials at the ROI
\dot{S}	rate of production of perspiration by the sweat glands contained on the ROI
\dot{D}	rate of drainage of perspiration out of the ROI via the contact materials
\dot{E}	rate of evaporation of perspiration.

With the factors above, the accumulated perspiration over time t within V is assumed to be

$$\frac{\Delta V(t)}{V} = \int_0^t (\dot{S} - \dot{E} - \dot{D}) dt \quad (1.3)$$

Now the rate of production of perspiration can be assumed to start with an ambient temperature T_a (temperature within the ROI) of 30°C . It can also be assumed that the production is proportional to the temperature gradient $T_a - 30^\circ\text{C}$. Using this \dot{S} can be formulated as

$$\dot{S} = \alpha \frac{T_a - 30^\circ\text{C}}{T_a^{\max} - T_s^{\min}}. \quad (1.4)$$

Here α is a dimensionless proportionality constant, T_a^{\max} is the maximal ambient temperature and is equal to 40°C and T_s^{\min} is the minimal skin temperature, equal to 30°C .

In a similar way the evaporation rate is formulated.

$$\dot{E} = \beta \frac{T_a - T_s}{T_a^{\max} - T_s^{\min}} (1 - RH) \quad (1.5)$$

Here β is another dimensionless proportionality constant, T_s is the skin temperature and RH is the relative humidity at the liquid free-space of the ROI. In the article a more detailed definition is given.

"The RH is defined as the ratio between the amount of water vapor at the ROI and the maximum amount of water vapor that the ROI can hold, and hence, the RH ranges between 0 and 1." - Amit Gefen, [1]

With this definition it can be noted that $RH = 1 - \frac{\Delta V(t)}{V}$. In the paper, however, Gefen mentions but does not use this definition; RH is simply assumed constant².

Lastly an expression for the drainage of perspiration \dot{D} is given. This is simply given as a single dimensionless effective permeability coefficient

$$\dot{D} = \gamma. \quad (1.6)$$

This constant weighs together the contributions of permeabilities of all contact materials. If for instance $\gamma = 0$, there is no drainage of perspiration at all.

To establish a model that is, mathematically speaking, simple enough to solve, the assumption is made that the ambient temperature, skin temperature and relative humidity do not change in time, and thus are independent of t . With these assumptions and using equations (1.4), (1.5) and (1.6) equation (1.3) becomes

²Note that when $RH = 1 - \frac{\Delta V(t)}{V}$ would be used equation (1.5) would simplify to

$$\dot{E} = \beta \frac{T_a - T_s}{T_a^{\max} - T_s^{\min}} \frac{\Delta V(t)}{V}$$

and equation (1.3) could be solved exact.

$$\frac{\Delta V(t)}{V} = \left[\alpha \frac{T_a - 30^\circ\text{C}}{T_a^{\max} - T_s^{\min}} + \beta \frac{T_a - T_s}{T_a^{\max} - T_s^{\min}} (1 - RH) + \gamma \right] \cdot t, \quad (1.7)$$

with t such that $0 \leq \Delta V(t)/V \leq 1$.

The coefficient of friction Another factor in the model described in the article is the *coefficient of friction* (COF) between the skin and a contacting covering sheet or clothing. This coefficient strongly depends on the volume of perspiration accumulated over the skin.

For instance, for the contact between dry skin and common hospital textiles the COF is equal to approximately 0.4. For contact between wet skin and the same textiles the COF will increase to approximately 0.9. Using this, an expression for the COF (denoted as μ) between the skin and the covering sheet or clothing in the ROI is described for the model;

$$\mu = 0.5 \frac{\Delta V(t)}{V} + 0.4. \quad (1.8)$$

This equation shows that the accumulation of perspiration on the skin will consequently increase the shear forces f between the skin and the contact materials over time.

For the shear forces f it holds that $f = \mu N$ where N is the body weight force applied perpendicularly to the skin-support or skin-clothing contact area at the weight-bearing region. This body weight force N is assumed to be constant over time since the patient is not moving. Despite this fact, μ does increase with time as can be obtained from equation (1.8). As a consequence the shear stress between the skin and the contact materials will increase over time, as the amount of perspiration increases. This shear stress τ is equal to the shear force normalized by the contact area A which gives $\tau = \mu N/A$. Because the pressure P delivered to the skin from the support surface at the skin-support or clothing-support region of contact is given as $P = N/A$ the shear stress can be written in terms of this pressure, that is $\tau = \mu P$. Substituting the expression of the COF (equation (1.8)) into this relationship the following equation holds for the ROI.

$$\tau = \left(0.5 \frac{\Delta V(t)}{V} + 0.4 \right) \cdot P \quad (1.9)$$

Here the pressure P depends on the stiffness of the support, and will increase as the stiffness of the support increases ([8]³). Since τ is linearly proportional to P , the same dependency on the stiffness of the support will hold.

Skin Breakdown When the shear stress applies on the skin (given by equation (1.9)) exceeds the shear strength of the skin, skin break down will occur (Figure 1.4). It was shown before that the shear stress will increase over time as perspiration accumulates. The shear strength of the skin will however decline. A reference is given to ([9]) regarding the fact that the shear strength reduces "by a factor 5 for a completely hydrated skin with respect to dry skin." Using this an expression of the shear strength of the skin τ_w^s is given.

$$\tau_w^s = \left(1 - 0.8 \frac{\Delta V(t)}{V} \right) \tau_0^s \quad (1.10)$$

Here τ_0^s is the shear strength of dry skin.

Since the skin breaks down when the shear stress applied on the skin exceeds the shear strength of the skin, the next step is to find the time t^* for which the shear stress is equal to the shear strength of the skin, hence where $\tau = \tau_w^s$. This equality yields

$$t^* = \frac{\tau_0^s - 0.4P}{(0.5P + 0.8\tau_0^s) \left\{ \frac{[\alpha - \beta(1-RH)]T_a + \beta(1-RH)T_s - \alpha \cdot 30^\circ\text{C}}{T_a^{\max} - T_s^{\min}} - \gamma \right\}} \quad (1.11)$$

With this equation it is possible to examine the effect of the different factors on this critical time t^* .

³Referred to by Gefen in [1].

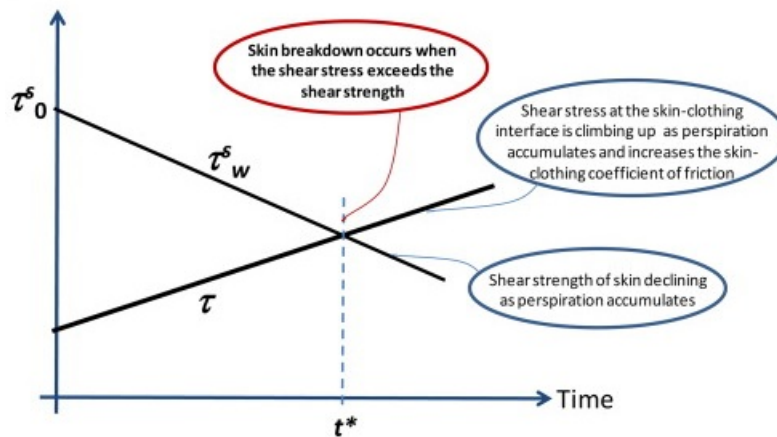


Figure 1.4: Skin break down will occur when the shear stress applied on the skin exceeds the shear strength of the skin. Source: [1]

CALCULATIONS

In the article, the effect of the microclimate factors T_a , RH and T_s as well as interacting factors P and permeability γ on the critical time for skin breakdown is examined. In order to study the effects of these factors on the critical time, several plots were made in which the factors were given various values. In every plot, the critical time (t^*) is plotted against the skin temperature (T_s) and one of the other factors is being varied. In Table 1.1 the values for all parameters are given. Note that whenever one of the factors is being varied, the others are equal to the values given in this table [1].

The Matlab code used to repeat the calculations can be found in Appendix (C.1).

Table 1.1: These parameter values are used in the plots shown in Figure 1.5 .

Parameters	τ_0^s	P	α	β	γ	T_a	RH
Value	70 kPa	7 kPa	2	1	0.1	35°C	0.5

RESULTS

In the article the results are given using the plots shown in Figure 1.5. It can be seen in the figures that all the factors which have been examined do have effect on the critical time.

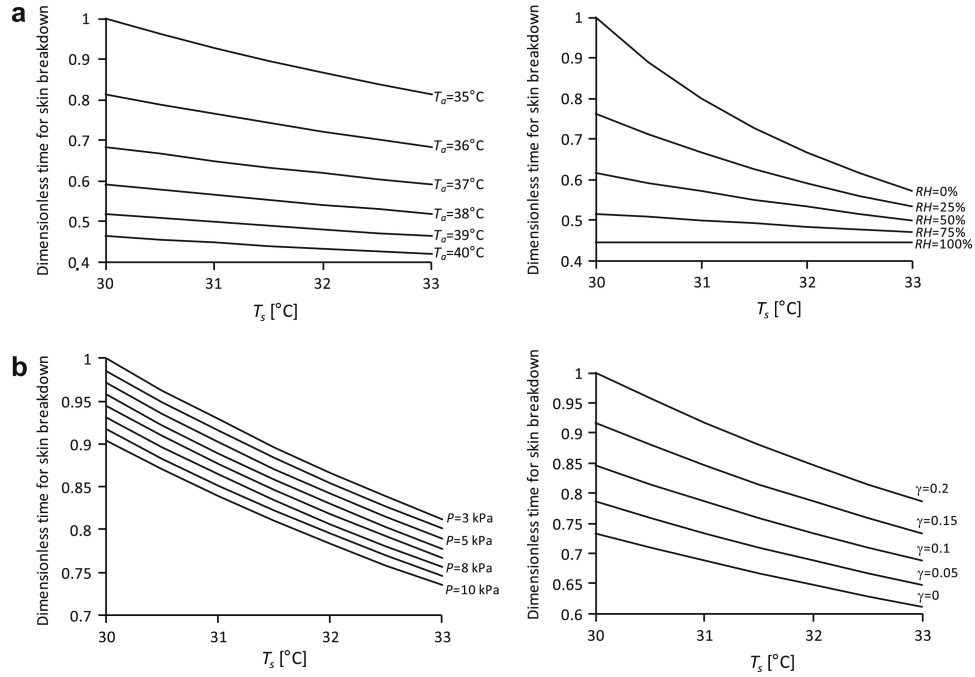


Figure 1.5: The calculated dimensionless critical times for skin breakdown versus the skin temperature (T_s) for different values of (a) the microclimate parameters of ambient temperature (T_a) (left panel) and relative humidity (RH) (right panel), and (b) the interacting parameters of pressure delivered from the support (P) (left panel) and permeability to perspiration (γ) of the materials contacting the skin or being in close proximity to the skin (right panel). The following values were assigned to the model variables in these simulations: $\tau_0^S = 70$ kPa, $P = 7$ kPa*, $\alpha = 2$, $\beta = 1$, and $\gamma = 0.13$, $T_a = 35^\circ\text{C}^*$ and $RH = 0.53$. * denotes; where not altered as detailed in the specific panel. Source: [1]

1.2.2. CHOOSING A SOFTWARE PACKAGE

In this thesis the goal is to combine the two models regarding pressure ulcers created by Gefen ([1], [2]). As one of the models uses the finite element method to solve the problem, a suitable software package had to be found. This software needs to be widely accessible and easy to change, that is, it should be possible to add features such as the effect of microclimate factors. The second model of Gefen originally was implemented using software called Adina ([10]), hence the first software we checked was Adina.

ADINA - FINITE ELEMENT ANALYSIS SOFTWARE

The software package called Adina ([10]) allows the user to model 2D problems which are solved using Finite Element Methods. It has a graphic interface hence the user does not need any programming skills.

To be able to fully use the software it needs to be purchased. A free trial version can be obtained⁴ but when using this version the number of nodes is limited to 900.

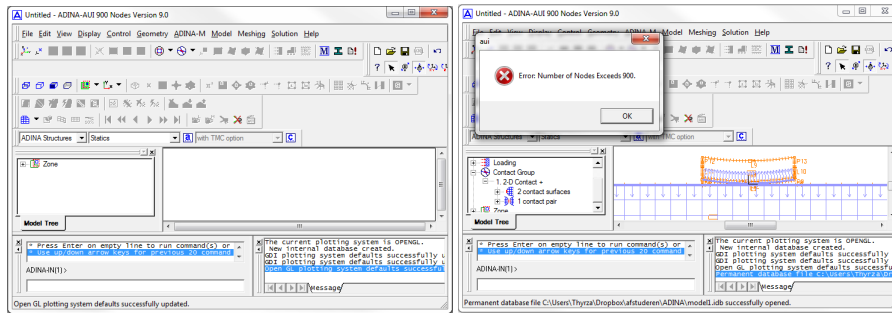
As the software is not open source the user does not have the opportunity to obtain details regarding the calculations from the code. Using Adina the user is obligated to buy the full version, but even when purchased is limited to working with 2D problems in a graphic interface, unable to combine the model with other mathematical models. Due to these limitations we decided to look at other software packages and discard the use of Adina.

FEBIO

FEBio ([11]) is software constructed to solve medical problems using a Finite Element Analysis. The software is open source and is created by the University of Utah using C++. The software is originally constructed together with two other programs; PreView ([12]) and PostView ([13]).

PreView Also constructed by the University of Utah, PreView is the original predecessor of FEBio. Quite similar to Adina, the problem can be modeled using a graphical interface. Opposite to Adina, FEBio is only capable to solve problems in 3D.

⁴The trial version can be downloaded at <http://www.adina.com/n900.shtml>.

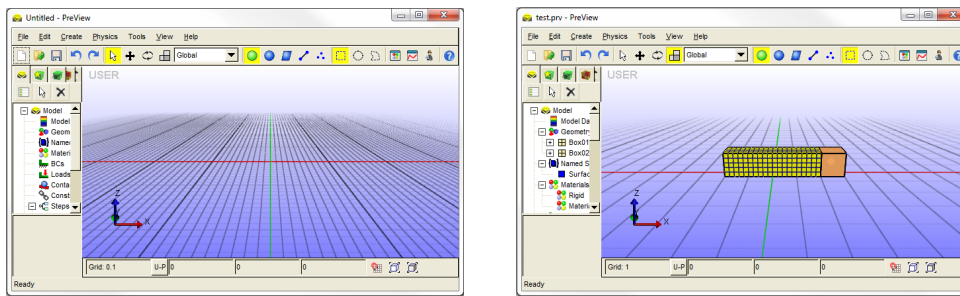


(a) Opening Adina the user is presented with many options. (b) When building a model in the trial version the user is limited to 900 nodes.

Figure 1.6: The software package Adina.

In PreView the user has to implement the geometries, boundary conditions, types of contact and so on. Since PreView can only build basic geometries it is possible to import more advanced geometries built using other software. Besides information regarding the problem, various details about solving the problem can be defined in PreView. Examples of these details are the maximum number of retries for each time step and the solution method.

Once the model is complete a FEBIO (.feb) file is made, which can be run using FEBio.



(a) The basic screen of PreView. (b) Simple geometries can be created in PreView.

Figure 1.7: The predecessor PreView.

FEBio Once the .feb file has been generated the user can run this file in FEBio which solves the modeled problem. On Windows the program can be run directly from PreView, from a command prompt or from the Programs Menu. In running FEBio the user will see a command prompt on the screen which shows the details of every time step (see Figure 1.8). When finished solving the problem FEBio will simply stop and the output will be saved in several files.

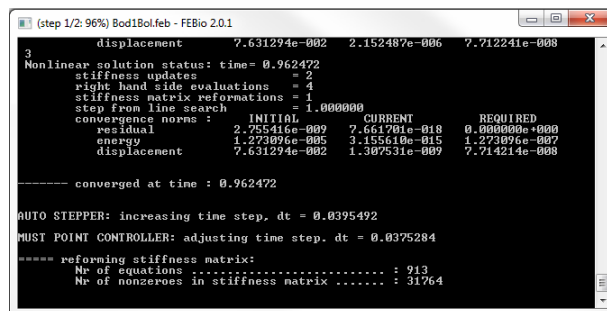


Figure 1.8: FEBio while solving a problem.

PostView Once the problem is solved using FEBio, the output can be viewed in the post processor PostView. In this program the user can view different outputs such as the stresses, strains and deformations of the bodies at every time step. Similar to Adina, the package consisting of FEBio, PreView and PostView is very graphic.

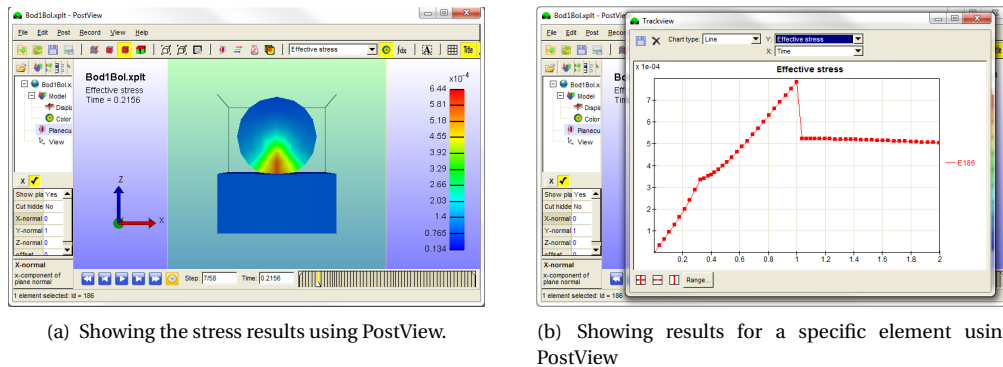


Figure 1.9: PostView can be used to view many different outputs.

The user can implement the model by choosing the correct settings. As the package exists of three different programs, the user also has the opportunity to choose a different method for creating the .feb file. The user for example can write the file manually using the XML language. This opportunity is very convenient because it means we could use a mathematical program such as Matlab to write the .feb file and to add the effects of micro-climate factors such as sweat.

Another advantage of FEBio is that the software is open source, it is therefore possible to view and even change the source code.

MATLAB

The goal in this thesis is to combine two mathematical models. Working with mathematical models the most common first computational environment to use is Matlab. Since Matlab allows the user to implement mathematical models in which functions can be called, Matlab is very suitable to model the micro-climate factors for a bedbound patient. However, since Matlab itself does not have a Finite Element Solver for large problems, this solver would have to be implemented separately which would be very time consuming.

As FEBio is a Finite Element solver in which Bio-mechanical problems can be solved and Matlab is a program in which the micro-climate factors can be modeled, it would be very convenient if we could combine these two programs.

THE GIBBON TOOLBOX

When further investigating the possibilities of FEBio combined with Matlab, we came across the Gibbon Toolbox ([14]). This is a set of Matlab codes in which a problem is modeled, a FEBio file is created, FEBio is called to solve the problem, and which then shows the user specified output. Basically this toolbox allows the user to replace PreView (and PostView) with Matlab, but still use FEBio to actually solve the problem.

THE FINAL SOFTWARE CHOICE

Using the information described above a final choice for the software was made. Instead of choosing a single program the choice was made to use the combination of Matlab, the Gibbon Toolbox and FEBio. Using Matlab and the Gibbon Toolbox a .feb file will be generated in which the problem including the micro-climate factors will be described. When completely defined, the model will then be solved using FEBio. Once solved, the results will be viewed using either Matlab, PostView or a combination. A schematic overview of this can be seen in Figure 1.10.

Note that this section does not cover all possible software packages. Other programs, such as Abaqus ([15]) have not been considered in the choice because they are quite similar to FEBio and Adina.



Figure 1.10: A schematic overview of the chosen software. The logos were retrieved from [14], [11] and [13]

1.3. OUTLINE OF THIS THESIS

This document is organized in the following chapters:

- Chapter 2 describes the mathematical model that is solved in this thesis. In the final sections the implementation of the model in the software is discussed.
- Chapter 3 gives the details on the numerical method that is used to solve the problem.
- Chapter 4 is subdivided into three sections, each discussing the results obtained with a part of the model. The first section discusses the basic model, the second section discusses the results of the model in which microclimate factors are included. The last section discusses the final model which is enhanced with the improvements discussed in Chapter 2.4.3.
- Chapter 5 includes the conclusions, remarks and ideas concerning future research.
- Appendix A gives additional information regarding stress and strain, as well as some information regarding constitutive laws such as Hooke's Law.
- Appendix B provides additional information on contact mechanics. Different solving methods are described.
- Appendix C contains the Matlab code of the final model.
- Appendix D contains the FEBio file of the final model.

2

MATHEMATICAL MODEL

In this chapter the mathematical model will be discussed. The first section will contain the necessary definitions regarding stress and deformation. In the second section (Section 2.2) the problem will be given in mathematical equations. The section will start with discussing the basic principles of mechanics, after which the actual problem will be derived. Section 2.3 will then elaborate on the mathematical model by including the contact information. Lastly, Section 2.4 explains the model as it is constructed using the software. It should be noted that Sections 2.2 and 2.3 give the mathematical problem as implemented in FEBio, whereas Section 2.4 only provides the details that are needed to solve the model.

2.1. DEFORMATION AND STRESS

In contact between solids and the deformation of solids the concepts of elasticity, stress and strain are very important. In the subject of pressure ulcers, stress especially is important. In this section mostly deformation and stress will be discussed. More information on elasticity, stress and strain is provided in Appendix A. The knowledge used in this section and its subsections is acquired a.o. from the books Theory of Elasticity, by S. Timoshenko and J.N. Goodier [16], Nonlinear Continuum Mechanics for Finite Element Analysis by Javier Bonet and Richard D. Wood [17], and Introduction to Finite Element Analysis Using MATLAB® and Abaqus by Amar Khennane, chapter 5 [18]. More information on stress and strain can be found in Appendix A.

2.1.1. THE DEFORMATION GRADIENT

When considering a deforming body one has a reference configuration (the undeformed body) and a current configuration (the deformed body). During the deformation many quantities can change such as the area of a part of the body, the volume, and even the density. This is illustrated in Figure 2.1.

To be able to link the quantities of the reference configuration to the quantities of the current deformation (or even during the deformation) the deformation gradient \mathbf{F} is introduced. This tensor makes it possible to describe the relative spatial position of two neighboring particles after deformation in terms of their relative material position before deformation.

When the motion of the deformable body at time t is described by a mapping $\mathbf{x} = \boldsymbol{\phi}(\mathbf{X}, t)$ between the initial positions denoted by \mathbf{X} and the current positions denoted by \mathbf{x} , the *deformation gradient* is defined as

$$\mathbf{F} = \frac{\partial \boldsymbol{\phi}}{\partial \mathbf{X}} = \nabla \boldsymbol{\phi}. \quad (2.1)$$

Note that here $\boldsymbol{\phi}$ is a vector and hence \mathbf{F} is a matrix.

This definition is derived from the following idea. Consider a material particle P in the reference configuration and a material particle Q_1 in the neighborhood of P . The position of Q_1 relative to P is given by the elemental vector $d\mathbf{X}_1$.

$$d\mathbf{X}_1 = \mathbf{X}_{Q_1} - \mathbf{X}_P \quad (2.2)$$

After the body is deformed, both Q_1 and P will have deformed to spatial positions given by

$$\mathbf{x}_P = \boldsymbol{\phi}(\mathbf{X}_P, t) \quad (2.3a)$$

$$\mathbf{x}_{Q_1} = \boldsymbol{\phi}(\mathbf{X}_{Q_1}, t). \quad (2.3b)$$

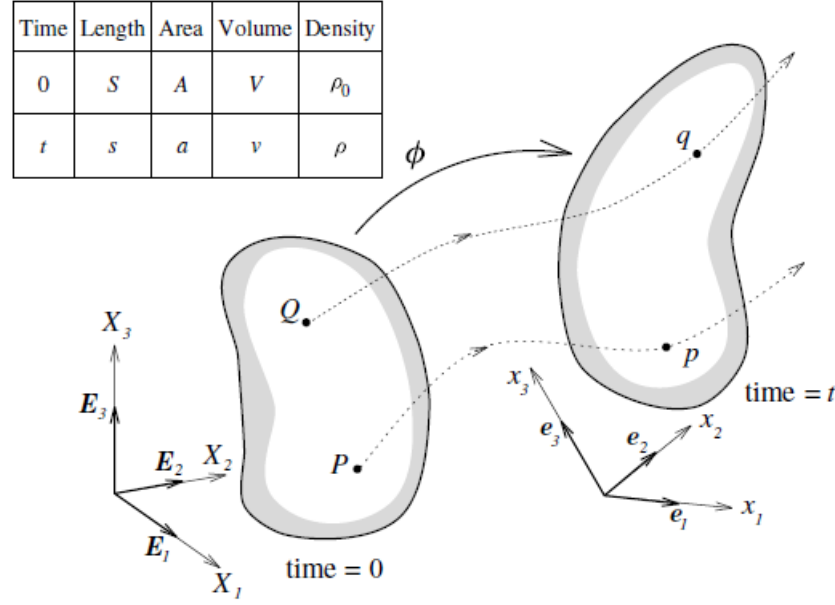


Figure 2.1: Many quantities change in the deformation of a body. Source: [17]

Applying the deformation and using equation (2.2) the elemental vector becomes

$$d\mathbf{x}_1 = \mathbf{x}_{q_1} - \mathbf{x}_p = \boldsymbol{\phi}(\mathbf{X}_p + d\mathbf{X}_1, t) - \boldsymbol{\phi}(\mathbf{X}_p, t). \quad (2.4)$$

Using the definition of \mathbf{F} and assuming $\|d\mathbf{X}_1\|$ to be sufficiently small, this can be rewritten as

$$d\mathbf{x}_1 = \mathbf{F}d\mathbf{X}_1. \quad (2.5)$$

Note that the motion of the deformable body can also be expressed as

$$\mathbf{x} = \mathbf{x}(\mathbf{X}, t). \quad (2.6)$$

In this case the deformation gradient is given by

$$\mathbf{F} = \frac{\partial \mathbf{x}}{\partial \mathbf{X}}. \quad (2.7)$$

When considering only a single elemental material vector $d\mathbf{X}$, the corresponding vector $d\mathbf{x}$ in the deformed (spatial) configuration is given by

$$d\mathbf{x} = \mathbf{F}d\mathbf{X}. \quad (2.8)$$

The inverse of the deformation gradient can be used to express the reference position of a particle in terms of the position in the current configuration. The inverse is given by

$$\mathbf{F}^{-1} = \frac{\partial \mathbf{X}}{\partial \mathbf{x}} = \nabla \boldsymbol{\phi}^{-1}. \quad (2.9)$$

CHANGE IN VOLUME

The deformation gradient can be used to express many quantities, among which is the change in volume when a body deforms [17]. Consider an infinitesimal vector element in the material (reference) configuration defined by the following three edges (see Figure 2.2).

$$d\mathbf{X}_1 = dX_1 \mathbf{E}_1 \quad (2.10a)$$

$$d\mathbf{X}_2 = dX_2 \mathbf{E}_2 \quad (2.10b)$$

$$d\mathbf{X}_3 = dX_3 \mathbf{E}_3 \quad (2.10c)$$

Here \mathbf{E}_1 , \mathbf{E}_2 and \mathbf{E}_3 are the orthogonal unit vectors which means that the edges of the volume element are parallel to the Cartesian axes.

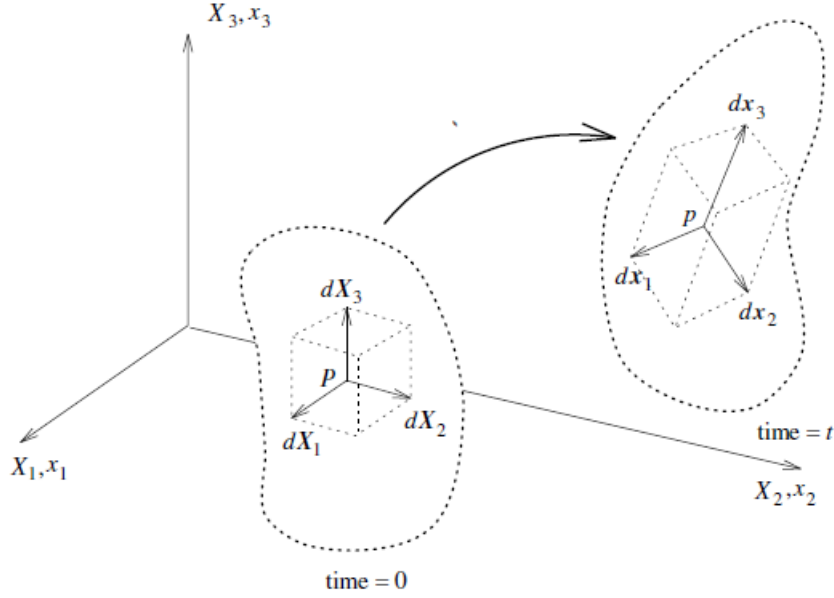


Figure 2.2: The volume change of an element caused by the deformation of a body. Source: [17]

The elemental material volume is obviously given by

$$dV = dX_1 dX_2 dX_3. \quad (2.11)$$

The deformed volume can be derived by first considering the spatial vectors that define the element in the spatial configuration.

$$d\mathbf{x}_1 = \mathbf{F}d\mathbf{X}_1 = \frac{\partial \boldsymbol{\phi}}{\partial X_1} dX_1 \quad (2.12a)$$

$$d\mathbf{x}_2 = \mathbf{F}d\mathbf{X}_2 = \frac{\partial \boldsymbol{\phi}}{\partial X_2} dX_2 \quad (2.12b)$$

$$d\mathbf{x}_3 = \mathbf{F}d\mathbf{X}_3 = \frac{\partial \boldsymbol{\phi}}{\partial X_3} dX_3 \quad (2.12c)$$

Using these elemental vectors the deformed volume is given by

$$\begin{aligned} dv &= |d\mathbf{x}_1 \cdot (d\mathbf{x}_2 \times d\mathbf{x}_3)| \\ &= \left| \frac{\partial \boldsymbol{\phi}}{\partial X_1} \cdot \left(\frac{\partial \boldsymbol{\phi}}{\partial X_2} \times \frac{\partial \boldsymbol{\phi}}{\partial X_3} \right) dX_1 dX_2 dX_3 \right| \end{aligned} \quad (2.13)$$

It can be noted that the triple product in equation (2.13) is the determinant of the deformation gradient \mathbf{F} . Using this the volume change caused by deformation can be expressed using the Jacobian J .

$$dv = JdV, \quad J = \det \mathbf{F} \quad (2.14)$$

This expression will be used later on in this section.

2.1.2. PUSH FORWARD AND PULL BACK

In the previous section the deformation gradient is introduced as the relationship between the undeformed (material) and deformed (spatial) quantities. Many studies in literature however, use the concepts of *push forward* and *pull back* to express these relationships.

Push forward is used to express the spatial form in terms of the material form. For example, the elemental vector $d\mathbf{x}$ is the push forward equivalent of the material vector $d\mathbf{X}$, which is expressed as

$$d\mathbf{x} = \boldsymbol{\phi}_* [d\mathbf{X}] = \mathbf{F}d\mathbf{X}. \quad (2.15)$$

Pull back is used to express the material form in terms of the spatial form. Taking the same example, the material vector $d\mathbf{X}$ is the pull back equivalent of the spatial vector $d\mathbf{x}$, expressed as

$$d\mathbf{X} = \phi_*^{-1} [d\mathbf{x}] = \mathbf{F}^{-1} d\mathbf{x}. \quad (2.16)$$

Note that ϕ_* denotes an operation, which is evaluated differently for different operands [] [17].

2.1.3. THE STRESS TENSOR

If one applies pressure or other external forces on the outside of an object and this object is being restrained against rigid body movement, this pressure will be noted inside the object as internal forces are induced. These internal forces have a certain intensity, i.e. a certain amount of force per unit area of the surface on which they act. This intensity of the internal forces is called stress. The dimension of stress is pressure, hence it is mostly measured in terms of pascal (Pa).

THE CAUCHY STRESS TENSOR

The traction vector When considering a deformable body in its current position one can study the forces applied by one part of the body (R_1) on the remaining part of the body (R_2). This is illustrated in Figure 2.3.

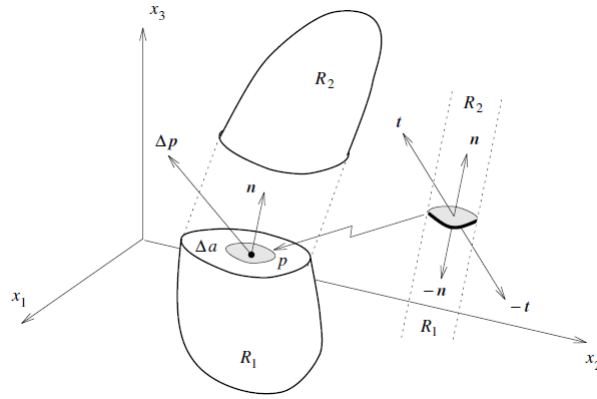


Figure 2.3: The traction vector on an element of area Δa in a deformable body. Source: [17]

Now consider the element of area Δa to normal \mathbf{n} in the neighborhood of spatial point p as shown in Figure 2.3. Suppose the resultant force on this area is equal to $\Delta \mathbf{p}$, then the traction \mathbf{t} vector corresponding to the normal \mathbf{n} at p is defined as [17]

$$\mathbf{t}(\mathbf{n}) = \lim_{\Delta a \rightarrow 0} \frac{\Delta \mathbf{p}}{\Delta a}. \quad (2.17)$$

The above relation between \mathbf{t} and \mathbf{n} should satisfy Newton's third law which states that "when one body exerts a force on a second body, the second body simultaneously exerts a force equal in magnitude and opposite in direction on the first body."

In terms of the traction vector \mathbf{t} this means that

$$\mathbf{t}(-\mathbf{n}) = -\mathbf{t}(\mathbf{n}). \quad (2.18)$$

One can express the three traction vectors associated with the three Cartesian directions \mathbf{e}_1 , \mathbf{e}_2 and \mathbf{e}_3 in a component form, in which the first notion of a stress tensor appears (see Figure 2.4).

$$\mathbf{t}(\mathbf{e}_1) = \sigma_{11}\mathbf{e}_1 + \sigma_{21}\mathbf{e}_2 + \sigma_{31}\mathbf{e}_3 \quad (2.19a)$$

$$\mathbf{t}(\mathbf{e}_2) = \sigma_{12}\mathbf{e}_1 + \sigma_{22}\mathbf{e}_2 + \sigma_{32}\mathbf{e}_3 \quad (2.19b)$$

$$\mathbf{t}(\mathbf{e}_3) = \sigma_{13}\mathbf{e}_1 + \sigma_{23}\mathbf{e}_2 + \sigma_{33}\mathbf{e}_3 \quad (2.19c)$$

A relationship has now been given between the traction vector \mathbf{t} corresponding to the Cartesian directions \mathbf{e}_i and the components σ_{ij} . However, a more general relationship between the the traction vector \mathbf{t} corresponding to a general direction \mathbf{n} and the components σ_{ij} is desired. In order to obtain such a relationship it is sufficient to study the translational equilibrium of elemental tetrahedron as shown in Figure 2.5.

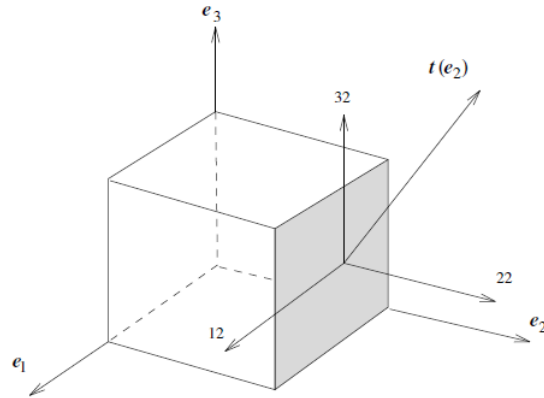


Figure 2.4: It is possible to express the traction vectors in a component form, introducing the notion of a stress tensor. Source: [17]

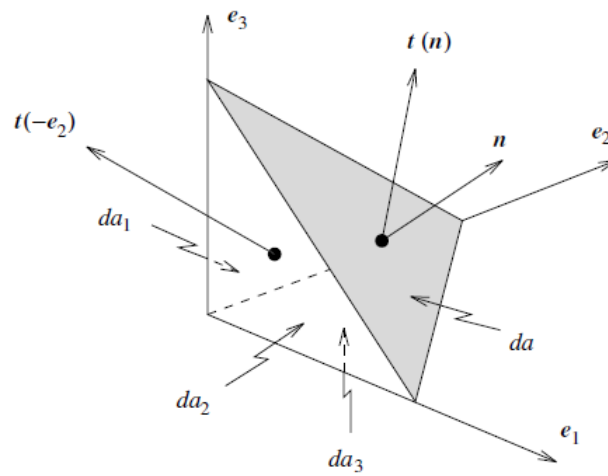


Figure 2.5: Considering the translational equilibrium of an elemental tetrahedron one can obtain a relationship between the traction vector \mathbf{t} corresponding to a general direction \mathbf{n} and the components σ_{ij} . Source: [17]

Taking \mathbf{f} to be the force per unit volume acting on the body at point p , the equilibrium of the tetrahedron is given as

$$\mathbf{t}(\mathbf{n})da + \sum_{i=1}^3 \mathbf{t}(-\mathbf{e}_i)da_i + \mathbf{f}dv = \mathbf{0}. \tag{2.20}$$

In this equation $da_i = (\mathbf{n} \cdot \mathbf{e}_i)da$ is the projection of the area da onto the plane orthogonal to the Cartesian direction i and dv is the volume of the tetrahedron. This expression can be rewritten by dividing the equation by da , using Newton's third law and equations (2.19a)–(2.19c) and noting that $dv/da \rightarrow 0$.

$$\begin{aligned} \mathbf{t}(\mathbf{n}) &= -\sum_{j=1}^3 \mathbf{t}(-\mathbf{e}_j) \frac{da_j}{da} - \mathbf{f} \frac{dv}{da} \\ &= \sum_{j=1}^3 \mathbf{t}(\mathbf{e}_j)(\mathbf{n} \cdot \mathbf{e}_j) \\ &= \sum_{i,j=1}^3 \sigma_{ij}(\mathbf{e}) \end{aligned} \tag{2.21}$$

Using the tensor product $(\mathbf{e}_j \cdot \mathbf{n})\mathbf{e}_i$ can be rewritten as $(\mathbf{e}_i \otimes \mathbf{e}_j)\mathbf{n}$. Substituting this into equation 2.21 gives

$$\begin{aligned}\mathbf{t}(\mathbf{n}) &= \sum_{i,j=1}^3 \sigma_{ij}(\mathbf{e}_i \otimes \mathbf{e}_j)\mathbf{n} \\ &= \left[\sum_{i,j=1}^3 \sigma_{ij}(\mathbf{e}_i \otimes \mathbf{e}_j) \right] \mathbf{n}.\end{aligned}\quad (2.22)$$

With this the *Cauchy stress tensor* $\boldsymbol{\sigma}$ is identified which relates the normal vector \mathbf{n} to the traction vector \mathbf{t} as

$$\mathbf{t}(\mathbf{n}) = \boldsymbol{\sigma}\mathbf{n}; \quad \boldsymbol{\sigma} = \sum_{i,j=1}^3 \sigma_{ij}(\mathbf{e}_i \otimes \mathbf{e}_j). \quad (2.23)$$

The Cauchy stress tensor In the previous paragraph the Cauchy stress tensor has been defined. When considering such a stress tensor, it is usually resolved into two components: a normal stress which is perpendicular to the area one looks at, and a shearing stress which acts in the plane of this area. To denote these components of the Cauchy stress, the symbols $\boldsymbol{\sigma}$ and $\boldsymbol{\tau}$ are often used. Here $\boldsymbol{\sigma}$ denotes the normal stresses and $\boldsymbol{\tau}$ denotes the shearing stresses.

To indicate the direction of the plane on which the stress is acting, subscripts to the components x , y and z are used. This means that when working in the Euclidean space the normal stresses are denoted by σ_x , σ_y and σ_z . The subscript x for example indicates that the stress is acting on a plane normal to the x -axis. It is agreed to take the normal stress positive when it produces tension and negative in the case it produces compression.

The shearing stresses are denoted by τ_{xy} , τ_{xz} , τ_{yx} , τ_{yz} , τ_{zx} and τ_{zy} or simply by σ_{xy} , σ_{xz} , σ_{yx} , σ_{yz} , σ_{zx} and σ_{zy} . Here $\tau_{ij} = \sigma_{ij}$. Note that the shearing stresses have two subscripts each. The first letter in the subscript indicates the direction of the normal to the plane under consideration. The second letter is then indicating the direction of the component of the stress. For example, considering the sides of a cube perpendicular to the z -axis, the component in the x -direction will be denoted by τ_{zx} .

In the paragraph above it becomes clear that stress has three symbols to describe the normal stresses (σ_x , σ_y and σ_z) and six symbols to describe the shearing stresses (τ_{xy} , τ_{xz} , τ_{yx} , τ_{yz} , τ_{zx} and τ_{zy}).

Dividing the area one is looking at into very small elements, one can deduce that the shearing stress can be described using three symbols instead of one. This deduction can be done considering the equilibrium of the small elements. The following symmetry relations will be found:

$$\begin{aligned}\tau_{xy} &= \tau_{yx} & \tau_{xz} &= \tau_{zx} & \tau_{yz} &= \tau_{zy} \\ \sigma_{xy} &= \sigma_{yx} & \sigma_{xz} &= \sigma_{zx} & \sigma_{yz} &= \sigma_{zy}\end{aligned} \quad (2.24)$$

Using these equations one finds that there are six components of stress, σ_x , σ_y , σ_z , $\tau_{xy} = \tau_{yx}$, $\tau_{xz} = \tau_{zx}$ and $\tau_{yz} = \tau_{zy}$, at every point in the object.

These stress components are sometimes denoted in matrix style, which gives us the stress matrix

$$\boldsymbol{\sigma} = \begin{bmatrix} \sigma_x & \tau_{xy} & \tau_{xz} \\ \tau_{yx} & \sigma_y & \tau_{yz} \\ \tau_{zx} & \tau_{zy} & \sigma_z \end{bmatrix}.$$

Using (2.24) it can be seen that the matrix above is symmetric. Sometimes in engineering a vector notation is used. In that case the stress is denoted as

$$\vec{\boldsymbol{\sigma}} = \left\{ \begin{array}{l} \sigma_x \\ \sigma_y \\ \sigma_z \\ \tau_{xy} \\ \tau_{yz} \\ \tau_{xz} \end{array} \right\} = \left\{ \begin{array}{l} \sigma_{xx} \\ \sigma_{yy} \\ \sigma_{zz} \\ \sigma_{xy} \\ \sigma_{yz} \\ \sigma_{xz} \end{array} \right\} = \left\{ \begin{array}{l} \sigma_{11} \\ \sigma_{22} \\ \sigma_{33} \\ \sigma_{12} \\ \sigma_{23} \\ \sigma_{13} \end{array} \right\}.$$

THE PIOLA-KIRCHHOFF STRESS TENSOR

While the Cauchy stress tensor is the most used form of the stress tensor, it is sometimes necessary to use another form. The Cauchy stress tensor is sometimes called *the true stress* because it is a true measure of the force per unit area in the current, deformed, configuration [19]. When working with large deformations however, there is a clear distinction between the current configuration which is the deformed configuration and a reference or undeformed configuration. In this case different ways of defining the action of surfaces need to be defined. One of these methods is using the Piola-Kirchhoff stress tensor instead of the Cauchy stress.

The first Piola-Kirchhoff stress tensor Consider both an undeformed (reference) and a deformed configuration of a material as well as a vector element of surface in the reference configuration $\mathbf{N}dS$. Here \mathbf{N} is the unit normal on the area and dS is the area of the element. Now during the deformation the particles that make up the area will move, eventually occupying an element defined as $\mathbf{n}ds$ in the deformed configuration, where \mathbf{n} is the normal and ds the area of this new element. By the definition of the Cauchy stress the force $\Delta\mathbf{p}$ acting on the surface element in the deformed configuration is equal to

$$\Delta\mathbf{p} = \boldsymbol{\sigma}\mathbf{n}ds. \quad (2.25)$$

Using this idea *the first Piola-Kirchhoff stress tensor* \mathbf{P} is defined by

$$\Delta\mathbf{p} = \mathbf{P}\mathbf{N}dS. \quad (2.26)$$

This first Piola-Kirchhoff stress tensor (or PK1 stress) relates the force acting in the deformed and current configuration to the surface element in the undeformed reference configuration.

Similar to the (Cauchy) traction vector used in Section 2.1.3 a PK1 traction vector \mathbf{T} exists for which holds that

$$\mathbf{T} = \mathbf{P}\mathbf{N} \quad \mathbf{T} = \frac{\Delta\mathbf{p}}{ds}. \quad (2.27)$$

Note that unlike the Cauchy traction the PK1 traction is a fictitious quantity. Where the Cauchy traction is the actual physical force per area on the element in the current configuration, the PK1 traction is the force acting on an element in the current configuration divided by the area of the corresponding element in the reference configuration.

The relation between the Cauchy and the first Piola-Kirchhoff stresses In some situations one would like to switch from the Piola-Kirchhoff stress to the Cauchy stress or vice versa. In order to do this the relation between the Cauchy stresses and PK1 stresses shall be discussed.

From the definitions given above it follows that

$$\boldsymbol{\sigma}\mathbf{n}ds = \mathbf{P}\mathbf{N}dS. \quad (2.28)$$

We can now apply *Nanson's formula*, which gives the relation between areas in the current configuration and areas in the reference configuration as

$$\mathbf{n}ds = \mathbf{J}\mathbf{F}^{-T}\mathbf{N}dS, \quad (2.29)$$

where ds is the area in the current configuration and dS the area in the reference configuration.

Using this formula the relation between the Cauchy and PK1 stresses can be easily obtained from 2.28.

The relation between the Cauchy and PK1 stresses

$$\mathbf{P} = \mathbf{J}\boldsymbol{\sigma}\mathbf{F}^{-T} \quad (2.30a)$$

$$\boldsymbol{\sigma} = \mathbf{J}^{-1}\mathbf{P}\mathbf{F}^T \quad (2.30b)$$

The second Piola-Kirchhoff stress tensor A second Piola-Kirchhoff stress tensor \mathbf{S} is defined as [19]

$$\mathbf{S} = J\mathbf{F}^{-1}\boldsymbol{\sigma}\mathbf{F}^{-T}, \quad (2.31)$$

where J is still the determinant of \mathbf{F} . For brevity this tensor shall be called the PK2 stress. It can be interpreted as follows. Consider the force vector $\Delta\mathbf{p}$ in the current configuration and find the corresponding vector in the undeformed body using $\bar{\Delta}\mathbf{p} = \mathbf{F}^{-1}\Delta\mathbf{p}$. The PK2 stress can be seen as this fictitious force $\bar{\Delta}\mathbf{p}$ divided by the area element in the reference configuration [19].

Even though the stress is a fictitious quantity, it is used as a measure of the forces in the material. This is done for three reasons.

1. The PK2 stress is symmetric:

$$\mathbf{S} = \mathbf{S}^T. \quad (2.32)$$

This can be checked by looking at the definition:

$$(\mathbf{F}^{-1}\boldsymbol{\sigma}\mathbf{F}^{-T})^T = (\boldsymbol{\sigma}\mathbf{F}^{-T})^T (\mathbf{F}^{-1})^T \quad (2.33a)$$

$$= \mathbf{F}^{-1}\boldsymbol{\sigma}^T\mathbf{F}^{-T} \quad (2.33b)$$

$$= \mathbf{F}^{-1}\boldsymbol{\sigma}\mathbf{F}^{-T}, \quad (2.33c)$$

where the last step holds due to the symmetry of $\boldsymbol{\sigma}$.

2. The second reason the PK2 stress is used is that in combination with the Euler-Lagrange strain \mathbf{E} (see Section 2.1.4) the Virtual Work equation in material form can be defined (see Section 2.2.2).
3. The PK2 stress is parameterized by material coordinates only, which means that it is a material tensor field. This is similar to the Cauchy stress being a spatial tensor field.

Note that the PK1 stress and PK2 stress are related as follows.

The relation between the PK1 and PK2 stresses

$$\mathbf{P} = \mathbf{F}\mathbf{S} \quad (2.34a)$$

$$\mathbf{S} = \mathbf{F}^{-1}\mathbf{P} \quad (2.34b)$$

2.1.4. THE STRAIN TENSOR

Besides inducing internal forces when one applies pressure or other external forces on the outside of an object while this object is being restrained against rigid body movement, material points inside the body can be displaced. When this displacement causes the distance between two points in the body to change one speaks of straining. In other words, strain is the change in a dimension divided by the original dimension; when working in \mathbb{R}^1 , strain is the displacement of a point per unit length. In this section the strain tensors in both material form and spatial form shall be given. Additional information on the strain can be found in Appendix A.

THE CAUCHY-GREEN TENSORS

Consider once again two elemental vectors $d\mathbf{X}_1$ and $d\mathbf{X}_2$ in the reference configuration, which change to $d\mathbf{x}_1$ and $d\mathbf{x}_2$ in deformation. By the definition of the deformation gradient \mathbf{F} the following expression can be formed

$$d\mathbf{x}_1 \cdot d\mathbf{x}_2 = \mathbf{F}d\mathbf{X}_1 \cdot \mathbf{F}d\mathbf{X}_2 \quad (2.35a)$$

$$= d\mathbf{X}_1 \cdot \mathbf{F}^T\mathbf{F}d\mathbf{X}_2 \quad (2.35b)$$

$$= d\mathbf{X}_1 \cdot \mathbf{C}d\mathbf{X}_2. \quad (2.35c)$$

The tensor \mathbf{C} introduced in 2.35c is known as the *right Cauchy-Green deformation tensor* [17] and defined as

$$\mathbf{C} = \mathbf{F}^T\mathbf{F}. \quad (2.36)$$

As \mathbf{C} operates on the material vectors $d\mathbf{X}_1$ and $d\mathbf{X}_2$, \mathbf{C} is called a material tensor quantity.

Similarly it is possible to express the spatial vectors $d\mathbf{x}_1$ and $d\mathbf{x}_2$ in terms of the material vectors $d\mathbf{X}_1$ and $d\mathbf{X}_2$ using the deformation gradient.

$$d\mathbf{X}_1 \cdot d\mathbf{X}_2 = \mathbf{F}^{-1} d\mathbf{x}_1 \cdot \mathbf{F}^{-1} d\mathbf{x}_2 \quad (2.37a)$$

$$= d\mathbf{x}_1 \cdot \mathbf{F}^{-T} \mathbf{F}^{-1} d\mathbf{x}_2 \quad (2.37b)$$

$$= d\mathbf{x}_1 \cdot (\mathbf{F}\mathbf{F}^T)^{-1} d\mathbf{x}_2 \quad (2.37c)$$

$$= d\mathbf{x}_1 \cdot \mathbf{b}^{-1} d\mathbf{x}_2. \quad (2.37d)$$

This way the *left Cauchy-Green deformation tensor* also known as the *Finger tensor* \mathbf{b} is defined as [17]

$$\mathbf{b} = \mathbf{F}\mathbf{F}^T. \quad (2.38)$$

As \mathbf{b}^{-1} operates on the spatial vectors $d\mathbf{x}_1$ and $d\mathbf{x}_2$, the tensor \mathbf{b} is called a spatial tensor quantity.

Note that the Cauchy-Green tensors provide information on the change in angle between the two vectors and the stretch of the line elements.

From the right Cauchy-Green tensor the *Eulerian or spatial elasticity tensor* \mathbf{c} can be obtained using the concept of push forward [17].

$$\mathbf{c} = J^{-1} \phi_* [\mathbf{C}]; \quad \mathbf{c} = \sum_{\substack{i,j,k,l=1 \\ I,J,K,L=1}}^3 J^{-1} F_{iI} F_{jJ} F_{kK} F_{lL} C_{IJKL} \mathbf{e}_i \otimes \mathbf{e}_j \otimes \mathbf{e}_k \otimes \mathbf{e}_l \quad (2.39)$$

THE GREEN STRAIN TENSOR

A general measure of deformation is the change in the scalar product of two elemental vectors. Using the definitions given above, this change can now be found in terms of the Cauchy-Green tensor.

$$\frac{1}{2} (d\mathbf{x}_1 \cdot d\mathbf{x}_2 - d\mathbf{X}_1 \cdot d\mathbf{X}_2) = \frac{1}{2} (d\mathbf{X}_1 \cdot \mathbf{C} d\mathbf{X}_2 - d\mathbf{X}_1 \cdot d\mathbf{X}_2) \quad (2.40a)$$

$$= d\mathbf{X}_1 \cdot \left(\frac{1}{2} (\mathbf{C} - \mathbf{I}) \right) d\mathbf{X}_2 \quad (2.40b)$$

$$= d\mathbf{X}_1 \cdot \mathbf{E} d\mathbf{X}_2 \quad (2.40c)$$

Here the *Green strain tensor* \mathbf{E} , also known as the *Lagrangian strain tensor* is defined by

$$\mathbf{E} = \frac{1}{2} (\mathbf{C} - \mathbf{I}), \quad (2.41)$$

where \mathbf{C} is the right Cauchy-Green deformation tensor and \mathbf{I} is the identity matrix.

Note that the Green strain tensor directly gives information on the change in the scalar product of two elemental vectors.

THE ALMANSI STRAIN TENSOR

Similar to the Green strain tensor a strain tensor exists which provides information in terms of the spatial element vectors. The change in scalar product is now expressed as

$$\frac{1}{2} (d\mathbf{x}_1 \cdot d\mathbf{x}_2 - d\mathbf{x}_1 \cdot d\mathbf{x}_2) = \frac{1}{2} (d\mathbf{x}_1 \cdot d\mathbf{x}_2 - d\mathbf{x}_1 \cdot \mathbf{b}^{-1} d\mathbf{x}_2) \quad (2.42a)$$

$$= d\mathbf{x}_1 \cdot \left(\frac{1}{2} (\mathbf{I} - \mathbf{b}^{-1}) \right) d\mathbf{x}_2 \quad (2.42b)$$

$$= d\mathbf{x}_1 \cdot \mathbf{e} d\mathbf{x}_2. \quad (2.42c)$$

Here \mathbf{e} is called the *Almansi strain tensor* or the *Eulerian strain tensor* defined by

$$\mathbf{e} = \frac{1}{2} (\mathbf{I} - \mathbf{b}^{-1}). \quad (2.43)$$

This strain tensor also provides direct information on the change in the scalar product of two elemental vectors.

Note that the Green strain tensor and the Almansi strain tensor can be expressed in one another using the push forward and pull back concept as follows:

$$\mathbf{E} = \phi_*^{-1} [\mathbf{e}] = \mathbf{F}^T \mathbf{e} \mathbf{F} \quad \text{Pull back,} \quad (2.44a)$$

$$\mathbf{e} = \phi_* [\mathbf{E}] = \mathbf{F}^{-T} \mathbf{E} \mathbf{F}^{-1} \quad \text{Push forward.} \quad (2.44b)$$

2.1.5. THE PRINCIPAL STRESSES

A very common way of working with the stress of a body is to consider the *principal stresses*. These stresses are equal to the Cauchy stresses when the basis is changed in such a way that the shear stresses become equal to zero. This is done as follows [18].

Suppose the basis that is used is given by $(\vec{e}_1, \vec{e}_2, \vec{e}_3)$ and the stress vector is given by $\vec{T} = \sigma \vec{n}$. Now suppose that for this basis the stress vector on the cutting plane $P(\vec{n})$ is not parallel to the normal \vec{n} (see Figure 2.6). The goal is to find a cutting plane $P(\vec{n}')$ for which $\vec{T} = \sigma \vec{n}' = \lambda \vec{n}'$ with λ a scalar and \vec{n}' is parallel to \vec{T} . Taking this plane together with two other planes which are mutually perpendicular will form a basis of the tensor, better known as *the principal basis*. Note that this basis is made of the principal directions of the stress tensor which, due to the symmetry of σ , are the orthonormal eigenvectors of σ .

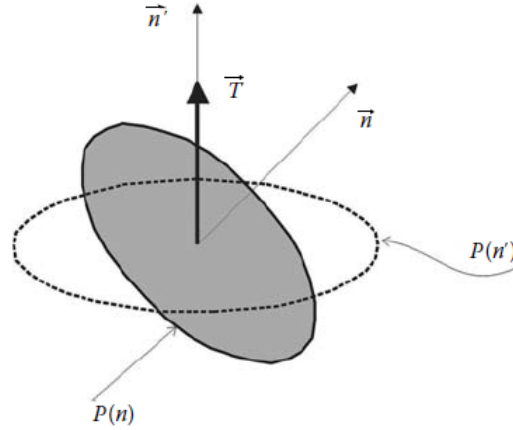


Figure 2.6: When the stress tensor is considered in a basis in which the stress in parallel to the normal one obtains the principal stresses. Source: [18]

In the principal basis the stress tensor reduces to its diagonal form and is given as

$$\sigma = \begin{pmatrix} \sigma_1 & 0 & 0 \\ 0 & \sigma_2 & 0 \\ 0 & 0 & \sigma_3 \end{pmatrix} \quad (2.45)$$

Here σ_1 , σ_2 and σ_3 are *the principal stresses*. Note that these stresses are the roots of the characteristic equation of the stress tensor σ given by

$$\sigma = \begin{pmatrix} \sigma_{11} & \sigma_{12} & \sigma_{13} \\ \sigma_{21} & \sigma_{22} & \sigma_{23} \\ \sigma_{31} & \sigma_{32} & \sigma_{33} \end{pmatrix}. \quad (2.46)$$

The roots can be calculated by solving

$$\begin{vmatrix} \sigma_{11} - \lambda & \sigma_{12} & \sigma_{13} \\ \sigma_{21} & \sigma_{22} - \lambda & \sigma_{23} \\ \sigma_{31} & \sigma_{32} & \sigma_{33} - \lambda \end{vmatrix} = 0. \quad (2.47)$$

which obtains the characteristic equation

$$\lambda^3 - I_1 \lambda^2 + I_2 \lambda - I_3 = 0, \quad (2.48)$$

where I_i are the stress invariants.

$$I_1 = \sigma_{11} + \sigma_{22} + \sigma_{33} \quad (2.49a)$$

$$= \text{tr } \sigma$$

$$I_2 = \sigma_{11}\sigma_{22} + \sigma_{22}\sigma_{33} + \sigma_{11}\sigma_{33} - \sigma_{12}^2 - \sigma_{23}^2 - \sigma_{31}^2 \quad (2.49b)$$

$$= \frac{1}{2} [\text{tr}(\sigma)^2 - \text{tr}(\sigma^2)] = \frac{1}{2} (\sigma_{ii}\sigma_{jj} - \sigma_{ij}\sigma_{ji})$$

$$I_3 = \sigma_{11}\sigma_{22}\sigma_{33} + 2\sigma_{12}\sigma_{23}\sigma_{31} - \sigma_{12}^2\sigma_{33} - \sigma_{23}^2\sigma_{11} - \sigma_{31}^2\sigma_{22} \quad (2.49c)$$

$$= \det(\sigma)$$

Note that due to the symmetry of the Cauchy stress tensor there are three real roots λ_i for the characteristic equations. These roots are the principal stresses, which are often ordered as $\sigma_1 \geq \sigma_2 \geq \sigma_3$, using equations (2.49a)–(2.49c).

$$\sigma_1 = \max(\lambda_1, \lambda_2, \lambda_3) \quad (2.50a)$$

$$\sigma_2 = I_1 - \sigma_1 - \sigma_3 \quad (2.50b)$$

$$\sigma_3 = \min(\lambda_1, \lambda_2, \lambda_3) \quad (2.50c)$$

The stress invariants I_i can also be given in terms of the principal stresses:

$$I_1 = \sigma_1 + \sigma_2 + \sigma_3, \quad (2.51a)$$

$$I_2 = \sigma_1\sigma_2 + \sigma_2\sigma_3 + \sigma_3\sigma_1, \quad (2.51b)$$

$$I_3 = \sigma_1\sigma_2\sigma_3. \quad (2.51c)$$

The principal stresses and directions do not depend on the chosen axes to describe the stress as they are properties of the stress tensor. The stress invariants I_1 , I_2 and I_3 are invariant under coordinate transformation [19].

2.1.6. THE MAXIMUM SHEAR STRESS

In Section 2.1.3 the shear stress τ has been defined. A common measure when working with shear stresses is the *maximum shear stress* τ_{\max} . As the stresses depend on the basis in which they are considered it is clear that on a certain plane the stresses will be maximal.

The maximum shear stress is given in terms of the principal stresses ($\sigma_1 \geq \sigma_2 \geq \sigma_3$) as

$$\tau_{\max} = \frac{1}{2}(\sigma_1 - \sigma_3). \quad (2.52)$$

2.2. PROBLEM DEFINITION

The issue that is being considered is the problem of a bedbound patient who has a risk of the development of pressure ulcers. From the moment the patient lies in the bed the skin will experience a certain stress level. If the skin of the patient is exposed during a longer period of time, the stress level can increase which will weaken the skin. When a patient is then being moved across the bed by a caretaker, the skin can break down. Following the method described by Gefen and Shaked in [2], the following problem will be implemented.

- A human body is at rest on a mattress. Shaked and Gefen worked with a 2D model in which the body was modeled by a circle and the mattress by a rectangle. As FEBio uses 3D models the body shall now be modeled as a sphere and the mattress will be represented by a box.
- Due to gravity the body immerses into the mattress which will cause both the human skin and the mattress to deform.
- After a while a caregiver will move the body 10cm across the mattress (horizontal sliding) and 1cm towards the mattress. This latter movement is due to the additional loading the caregiver applies to reposition the patient.

This section contains information on the exact problem which FEBio solves, i.e. the problem described above written in mathematical equations. The general problem given by the equations of motion shall be given in Section 2.2.1. This will be followed by a derivation of the weak form (Section 2.2.2) after which the finite element method which is implemented in FEBio (Sections 3.2 and 3.4) shall be discussed. Both sections closely follow the derivations given in [17], as this is the literature work on which the implementation in FEBio is based.

In Section 2.3 it will be described how FEBio deals with contact problems. The information in this section is gained from [20]. Additional information on contact mechanics is given in Appendix B.

2.2.1. THE PROBLEM

As FEBio is a program in which many various problems can be implemented, different starting points are used for several types of problems. In this thesis only the case of solid materials shall be considered.

In general when looking at solid materials a good place to start mathematically is with the basic principles from mechanics. These principles can be Newton's Laws, or the equivalent set of dynamics laws Euler's Laws. In this thesis we will start from Euler's Laws to derive the Equations of motion, specifically Euler's first Law: the Principle of Linear Momentum.

A distinction will be made between two types of descriptions [17].

The material description is also known as the Lagrangian description. In this description the variation of a quantity such as the material density ρ over the body is described with respect to the original (or initial) coordinate \mathbf{X} used to label a material particle in the continuum at time $t = 0$ as

$$\rho = \rho(\mathbf{X}, t).$$

Here a change in time t means that the same material particle \mathbf{X} has a different density ρ , hence interest is focused on the material particle X .

The spatial description is also known as the Eulerian description. In this description the quantities will be described with respect to the position in the current configuration \mathbf{x} , currently occupied by a material particle in the continuum at time t . For instance, the material density ρ will be described as

$$\rho = \rho(\mathbf{x}, t).$$

A change in time t implies that a different density is observed at the same spatial position \mathbf{x} , now probably occupied by a different particle. Interest is focused on a spatial position \mathbf{x} .

The implementation in FEBio uses the spatial description, however, the material description is used to simplify certain derivations.

THE PRINCIPLE OF LINEAR MOMENTUM

In the Principle of Linear Momentum the momentum of an object is defined as a measure of an objects tendency to keep moving once it is set in motion.

Spatial form In the spatial form the linear momentum \mathbf{p} is equal to the product of the body's mass and its velocity.

$$\mathbf{p} = m\mathbf{v} \quad (2.53)$$

When considering the change in an objects momentum over time one obtains

$$\dot{\mathbf{p}} = \frac{d\mathbf{p}}{dt} = \frac{d(m\mathbf{v})}{dt} = m \frac{d\mathbf{v}}{dt} = m\mathbf{a}. \quad (2.54)$$

Here we used that the mass of the body is constant in time, hence $\frac{dm}{dt} = 0$. Equation (2.54) can be rewritten using Newton's second law which states that $\mathbf{F} = m\mathbf{a}$. This gives

$$\mathbf{F} = \frac{d}{dt}(m\mathbf{v}) \quad (2.55)$$

which is known as the *principle of linear momentum*, or *the balance of linear momentum*. Looking at the equation it states that the rate of change of the momentum is equal to the applied force. When the applied forces are equal to zero (there are no forces applied to the system) this law is called the *law of conservation of (linear) momentum*. In this case the total momentum of the system remains constant.

The principles as they are given above are applied to a particle and therefore should be expanded to hold for a continuum. We shall do this by considering a material volume v in the current configuration. Given this finite portion has a spatial mass density $\rho(\mathbf{x}, t)$ and a spatial velocity field $\mathbf{v}(\mathbf{x}, t)$ the total linear momentum of this mass is given as

$$\mathbf{L}(t) = \int_v \rho(\mathbf{x}, t)\mathbf{v}(\mathbf{x}, t) dV. \quad (2.56)$$

Considering the rate of change of the momentum the principle of linear momentum states that

$$\dot{\mathbf{L}}(t) = \frac{d}{dt} \int_v \rho(\mathbf{x}, t)\mathbf{v}(\mathbf{x}, t) dV = \mathbf{F}(t), \quad (2.57)$$

where $\mathbf{F}(t)$ is the resultant of the forces acting on the finite portion. Note that we are working with material volume, which contains the same particles of matter at all times. The amount of space occupied by these particles may change over time.

The above equation includes a derivative of an integral, which we would like to rewrite. This can be done by using the law of mass conservation, which states that for a density ρ and \mathbf{v} the velocity of the element

$$\frac{\partial \rho}{\partial t} + \nabla \cdot (\rho\mathbf{v}) = 0. \quad (2.58)$$

Using this we can obtain the following for F a property per unit mass and V a material volume, where the first equality is known as Reynolds' transport theorem for a material element.

$$\begin{aligned} \frac{d}{dt} \left(\int_V \rho F dV \right) &= \int_V \frac{\partial \rho F}{\partial t} dV + \int_S \rho F (\mathbf{v} \cdot \mathbf{n}) dS \\ &= \int_V \left(\frac{\partial \rho}{\partial t} F + \rho \frac{\partial F}{\partial t} + \nabla \cdot (\rho \mathbf{v} F) \right) dV \\ &= \int_V \left(F \left[\frac{\partial \rho}{\partial t} + \nabla \cdot (\rho \mathbf{v}) \right] + \rho \left[\frac{\partial F}{\partial t} + \mathbf{v} \cdot \nabla F \right] \right) dV \\ &= \int_V \rho \left[\frac{\partial F}{\partial t} + \mathbf{v} \cdot \nabla F \right] dV \\ &= \int_V \rho \frac{DF}{Dt} dV \end{aligned}$$

Here $\frac{DF}{Dt}$ is the material derivative of the property F , given by

$$\frac{DF}{Dt} = \frac{\partial F}{\partial t} + \mathbf{v} \cdot \nabla F. \quad (2.59)$$

It can be found that the material derivative of the velocity \mathbf{v} itself is equal to the acceleration.

$$\begin{aligned}\frac{D\mathbf{v}}{Dt} &= \frac{\partial\mathbf{v}}{\partial t} + \mathbf{v} \cdot \nabla\mathbf{v} \\ &= \frac{\partial\mathbf{v}}{\partial t} + v_x \frac{\partial\mathbf{v}}{\partial x} + v_y \frac{\partial\mathbf{v}}{\partial y} + v_z \frac{\partial\mathbf{v}}{\partial z} \\ &= \frac{d}{dt}\mathbf{v}(t, x, y, z) \\ &= \dot{\mathbf{v}}.\end{aligned}$$

We obtain

$$\dot{\mathbf{L}}(t) = \int_v \rho(\mathbf{x}, t) \dot{\mathbf{v}}(\mathbf{x}, t) dv = \mathbf{F}(t). \quad (2.60)$$

We can further rewrite this linear momentum principle by evaluating the resultant force $\mathbf{F}(t)$ acting on the body. This force exists of the surface tractions \mathbf{t} acting over the surface elements and the body forces \mathbf{b} which act on the volume elements. Using this the resultant force can be written as

$$\mathbf{F}(t) = \int_s \mathbf{t} ds + \int_v \mathbf{b} dv. \quad (2.61)$$

Substituting this into equation (2.60) we can express

The Principle of the Linear Momentum in the spatial form as

$$\int_v \rho(\mathbf{x}, t) \dot{\mathbf{v}}(\mathbf{x}, t) dv = \int_s \mathbf{t} ds + \int_v \mathbf{b} dv. \quad (2.62)$$

Material form The linear momentum of a mass element in material form is given by $\rho_0 \mathbf{V} dV$, where \mathbf{V} is the same velocity as \mathbf{v} which is used in the spatial form. The only difference is that now the velocity is expressed in the material coordinates \mathbf{X} and $\rho dv = \rho_0 dV$. Similar to the spatial form, the *total linear momentum* can be given as an integral over the volume V in the reference configuration:

$$\mathbf{L}(t) = \int_V \rho_0(\mathbf{X}) \mathbf{V}(\mathbf{X}, t) dV. \quad (2.63)$$

Using this and the law of mass conservation the principle of linear momentum is now given by

$$\dot{\mathbf{L}}(t) = \frac{d}{dt} \int_V \rho_0(\mathbf{X}) \mathbf{V}(\mathbf{X}, t) dV = \int_V \rho_0 \frac{d\mathbf{V}}{dt} dV = \mathbf{F}(t). \quad (2.64)$$

The forces \mathbf{F} are the external forces acting on the current configuration, which means that we have to work with the first Piola-Kirchhoff stress, since this stress measures the actual force in the current configuration, however per unit surface area in the reference configuration. With this stress the surface force acting on the surface element ds in the current configuration can be given using the first Piola-Kirchhoff traction vector \mathbf{T} as $d\mathbf{f}_{surf} = \mathbf{t} ds = \mathbf{T} dS$, where \mathbf{t} is the Cauchy traction vector. Similarly the body force can be given by the reference body force \mathbf{B} , which is the actual body force acting on the current configuration per unit volume in the reference configuration. One obtains $d\mathbf{f}_{body} = \mathbf{b} dv = \mathbf{B} dV$.

Using these two definitions the resultant force is

$$\mathbf{F}(t) = \int_S \mathbf{T} dS + \int_V \mathbf{B} dV. \quad (2.65)$$

After substituting this into equation (2.64) we obtain

The Principle of the Linear Momentum in the material form

$$\int_V \rho_0 \frac{d\mathbf{V}}{dt} dV = \int_S \mathbf{T} dS + \int_V \mathbf{B} dV. \quad (2.66)$$

THE EQUATIONS OF MOTION

Spatial form From the Principle of Linear Momentum we can derive the equations of motion, which describe the problem that needs to be solved in FEBio. To do this we shall start by rewriting the integral over the surface

$$\int_s \mathbf{t} ds.$$

Cauchy's Law states that there exists a Cauchy stress tensor $\boldsymbol{\sigma}$ that relates the normal vector \mathbf{n} to the traction vector \mathbf{t} as [17]

$$\mathbf{t} = \boldsymbol{\sigma} \mathbf{n}. \quad (2.67)$$

Applying this law to the integral over the surface gives us

$$\int_s \mathbf{t} ds = \int_s \boldsymbol{\sigma} \mathbf{n} ds. \quad (2.68)$$

The divergence theorem, also known as Gauss' Theorem, states that the volume integral of the divergence of any continuously differentiable vector \mathbf{A} is the closed surface integral of the outward normal component of \mathbf{A} [21]

$$\iiint_R \nabla \cdot \mathbf{A} dV = \iint_S \mathbf{A} \cdot \hat{\mathbf{n}} dS. \quad (2.69)$$

Since the Cauchy stress tensor $\boldsymbol{\sigma}$ is continuously differentiable this theorem can be applied to the integral in 2.68.

$$\int_s \boldsymbol{\sigma} \mathbf{n} ds = \int_v \nabla \cdot \boldsymbol{\sigma} dv \quad (2.70)$$

Note that in literature both $\mathbf{t} = \boldsymbol{\sigma} \mathbf{n}$ and $\mathbf{t} = \mathbf{n} \boldsymbol{\sigma}$ are used. These are both correct, since the stress tensor $\boldsymbol{\sigma}$ is symmetric ($\boldsymbol{\sigma} = \boldsymbol{\sigma}^T$).

The Principle of Linear Momentum (equation (2.62)) can therefore be written as

$$\int_v \nabla \cdot \boldsymbol{\sigma} + \mathbf{b} dv = \int_v \rho \dot{\mathbf{v}} dv. \quad (2.71)$$

Now the equations of motion are equal to

Equations of Motion in the spatial form:

$$\nabla \cdot \boldsymbol{\sigma} + \mathbf{b} = \rho \frac{d\mathbf{v}}{dt} \quad (2.72)$$

Material Form Similar to the Cauchy stresses in the spatial form, there exists a Piola-Kirchhoff stress tensor \mathbf{P} for which $\mathbf{T} = \mathbf{P}\mathbf{N}$. Together with the divergence theorem this can be used to rewrite the principle of linear momentum given in equation (2.66). We obtain

$$\int_V [div \mathbf{P} + \mathbf{B}] dV = \int_V \rho_0 \frac{d\mathbf{V}}{dt} dV. \quad (2.73)$$

Now the equations of motion are equal to

Equations of Motion in the material form:

$$div \mathbf{P} + \mathbf{B} = \rho_0 \frac{d\mathbf{V}}{dt} \quad (2.74)$$

2.2.2. THE WEAK FORMULATION

In the previous section the problem for solid materials is described using the equations of motions. When solving this problem using the Finite Element Method we start by converting the strong form (equations of motion and boundary conditions) into the weak form which is known as the principle of virtual work.

SPATIAL FORM

Starting with the equations of motion in the spatial form (equation (2.72)) the weak form is derived by multiplying the equation by a test function $\delta \mathbf{v}$ which represents a virtual velocity and integrate over the volume v . By doing so we obtain

$$\int_v \delta \mathbf{v} (\nabla \cdot \boldsymbol{\sigma} + \mathbf{b}) dV = \int_v \delta \mathbf{v} (\rho \frac{d\mathbf{v}}{dt}) dV. \quad (2.75)$$

The above equation can be rewritten using the fact that $(\boldsymbol{\sigma} = \boldsymbol{\sigma}^T)$ and the identity

$$\nabla (A^T \cdot b) = b \cdot (\nabla \cdot A) + A : (\nabla b),$$

or, in a different order,

$$b \cdot (\nabla \cdot A) = \nabla (A^T \cdot b) - A : (\nabla b).$$

We obtain

$$\int_v \delta \mathbf{v} (\nabla \cdot \boldsymbol{\sigma}) dV = \int_v \nabla \cdot (\boldsymbol{\sigma} \cdot \delta \mathbf{v}) dV - \int_v \boldsymbol{\sigma} : (\nabla \delta \mathbf{v}) dV, \quad (2.76)$$

from which follows that

$$\int_v \delta \mathbf{v} (\rho \frac{d\mathbf{v}}{dt}) dV = \int_v [\nabla \cdot (\boldsymbol{\sigma} \cdot \delta \mathbf{v}) - \boldsymbol{\sigma} : (\nabla \delta \mathbf{v}) + \delta \mathbf{v} \cdot \mathbf{b}] dV. \quad (2.77)$$

Here the divergence theorem (equation (2.69)) can be applied followed by Cauchy's law (equation (2.67)).

$$\begin{aligned} \int_v \delta \mathbf{v} (\rho \frac{d\mathbf{v}}{dt}) dV &= \int_{\partial v} [(\boldsymbol{\sigma} \cdot \delta \mathbf{v}) \cdot \mathbf{n}] da - \int_v \boldsymbol{\sigma} : (\nabla \delta \mathbf{v}) dV + \int_v [\delta \mathbf{v} \cdot \mathbf{b}] dV \\ &= \int_{\partial v} (\mathbf{t} \cdot \delta \mathbf{v}) da - \int_v \boldsymbol{\sigma} : (\nabla \delta \mathbf{v}) dV + \int_v [\delta \mathbf{v} \cdot \mathbf{b}] dV, \end{aligned} \quad (2.78)$$

where we used that

$$(\boldsymbol{\sigma} \cdot \delta \mathbf{v}) \cdot \mathbf{n} \equiv \sigma_{ij} \delta v_j n_i = \delta v_j \sigma_{ji} n_i \equiv \delta \mathbf{v} \cdot (\boldsymbol{\sigma} \cdot \mathbf{n}) = \delta \mathbf{v} \cdot \mathbf{t} = \mathbf{t} \cdot \delta \mathbf{v}.$$

Changing the order of these integrals we obtain:

$$- \int_v \delta \mathbf{v} (\rho \frac{d\mathbf{v}}{dt}) dV = \int_v \boldsymbol{\sigma} : (\nabla \delta \mathbf{v}) dV - \int_v [\mathbf{b} \cdot \delta \mathbf{v}] dV - \int_{\partial v} (\mathbf{t} \cdot \delta \mathbf{v}) da. \quad (2.79)$$

FEBio allows the user to choose between quasi-static and a dynamic analysis, where the quasi-static analysis is the default setting. In the quasi-static analysis the inertial effects, given by the ρ -term, are ignored and an equilibrium solution is sought. This means that they work with the equations of equilibrium in which the acceleration $\frac{d\mathbf{v}}{dt}$ is taken equal to zero and hence

$$\int_v \boldsymbol{\sigma} : (\nabla \delta \mathbf{v}) dV - \int_v [\mathbf{b} \cdot \delta \mathbf{v}] dV - \int_{\partial v} (\mathbf{t} \cdot \delta \mathbf{v}) da = 0. \quad (2.80)$$

Note that this equation includes the expression $\nabla \delta \mathbf{v}$. As $\delta \mathbf{v}$ is an arbitrary virtual velocity, the gradient of this velocity is by definition the virtual velocity gradient $\delta \mathbf{l}$, defined as

$$\delta \mathbf{l} = \nabla \delta \mathbf{v} = \frac{\partial \delta \mathbf{v}}{\partial \mathbf{x}} = \begin{pmatrix} \frac{\partial \delta v_x}{\partial x} & \frac{\partial \delta v_x}{\partial y} & \frac{\partial \delta v_x}{\partial z} \\ \frac{\partial \delta v_y}{\partial x} & \frac{\partial \delta v_y}{\partial y} & \frac{\partial \delta v_y}{\partial z} \\ \frac{\partial \delta v_z}{\partial x} & \frac{\partial \delta v_z}{\partial y} & \frac{\partial \delta v_z}{\partial z} \end{pmatrix}. \quad (2.81)$$

Using this, equation (2.80) becomes

$$\int_v \boldsymbol{\sigma} : \delta \mathbf{l} dV - \int_v [\mathbf{b} \cdot \delta \mathbf{v}] dV - \int_{\partial v} (\mathbf{t} \cdot \delta \mathbf{v}) da = 0. \quad (2.82)$$

As a final step the virtual velocity gradient is expressed in terms of the symmetric virtual rate of deformation $\delta \mathbf{d}$ and the antisymmetric virtual spin tensor $\delta \mathbf{w}$ as

$$\delta \mathbf{l} = \delta \mathbf{d} + \delta \mathbf{w}, \quad (2.83)$$

where

$$\delta \mathbf{d} = \frac{1}{2}(\delta \mathbf{I} + \delta \mathbf{I}^T), \text{ and} \quad (2.84a)$$

$$\delta \mathbf{w} = \frac{1}{2}(\delta \mathbf{I} - \delta \mathbf{I}^T). \quad (2.84b)$$

Assuming the rotational motion of the particles is equal to zero, the spatial virtual work equation can be formulated using spatial quantities only.

The spatial virtual work equation:

$$\delta W = \int_V \boldsymbol{\sigma} : \delta \mathbf{d} \, dv - \int_V \mathbf{b} \cdot \delta \mathbf{v} \, dv - \int_{\partial V} \mathbf{t} \cdot \delta \mathbf{v} \, da = 0. \quad (2.85)$$

MATERIAL FORM

The virtual work equation in material form can be derived in two different ways. First of all, it can be derived directly from the equations of motion. Secondly it is possible to derive the material form from the spatial form. In this section the entire virtual work equation shall be derived from the equations of motion, after which only a part of the virtual work equation shall be derived from the spatial form. Even though the results are the same the latter way is used later on in the Newton Raphson Method and is therefore shown here.

Derivation from the equations of motion Starting with the equations of motion in material form (equation (2.74)) the derivation of the Principle of Virtual Work in material form is quite similar to the derivation of the spatial form.

$$div \mathbf{P} + \mathbf{B} = \rho_0 \frac{d\mathbf{V}}{dt} \quad (2.86)$$

The first step is to multiply both sides by a test function $\delta \mathbf{V}$ and to take the integral over the volume V .

$$\int_V \delta \mathbf{V} (div \mathbf{P} + \mathbf{B}) \, dV = \int_V \delta \mathbf{V} \left(\rho_0 \frac{d\mathbf{V}}{dt} \right) \, dV. \quad (2.87)$$

Note that unlike the Cauchy stress tensor $\boldsymbol{\sigma}$, the PK1 stress tensor \mathbf{P} is not symmetric. Using

$$b \cdot (\nabla \cdot A) = \nabla \cdot (A^T \cdot b) - A : (\nabla b),$$

one therefore obtains

$$\int_V \delta \mathbf{V} (\nabla \cdot \mathbf{P}) \, dV = \int_V \nabla \cdot (\mathbf{P}^T \cdot \delta \mathbf{V}) \, dV - \int_V \mathbf{P} : (\nabla \delta \mathbf{V}) \, dv. \quad (2.88)$$

Substituting this into equation (2.87) gives

$$\int_V \delta \mathbf{V} \left(\rho_0 \frac{d\mathbf{V}}{dt} \right) \, dV = \int_V [\nabla \cdot (\mathbf{P}^T \cdot \delta \mathbf{V}) - \mathbf{P} : (\nabla \delta \mathbf{V}) + \delta \mathbf{V} \cdot \mathbf{B}] \, dV. \quad (2.89)$$

Here the divergence theorem (equation (2.69)) can be applied after which one can use that $\mathbf{P}\mathbf{N} = \mathbf{T}$.

$$\begin{aligned} \int_V \delta \mathbf{V} \left(\rho_0 \frac{d\mathbf{V}}{dt} \right) \, dV &= \int_{\partial V} [\mathbf{P}^T \cdot \delta \mathbf{V}] \cdot \mathbf{N} \, dA - \int_V \mathbf{P} : (\nabla \delta \mathbf{V}) \, dV + \int_V [\delta \mathbf{V} \cdot \mathbf{B}] \, dV \\ &= \int_{\partial V} [\delta \mathbf{V} \cdot \mathbf{P}] \cdot \mathbf{N} \, dA - \int_V \mathbf{P} : (\nabla \delta \mathbf{V}) \, dV + \int_V [\delta \mathbf{V} \cdot \mathbf{B}] \, dV \\ &= \int_{\partial V} [\mathbf{T} \cdot \delta \mathbf{V}] \, dA - \int_V \mathbf{P} : (\nabla \delta \mathbf{V}) \, dV + \int_V [\delta \mathbf{V} \cdot \mathbf{B}] \, dV \end{aligned} \quad (2.90)$$

Changing the order of these integrals, gives

$$- \int_V \delta \mathbf{V} \left(\rho_0 \frac{d\mathbf{V}}{dt} \right) \, dV = \int_V \mathbf{P} : (\nabla \delta \mathbf{V}) \, dV - \int_V [\mathbf{B} \cdot \delta \mathbf{V}] \, dV - \int_{\partial V} (\mathbf{T} \cdot \delta \mathbf{V}) \, dA. \quad (2.91)$$

Similar to the spatial case the acceleration $\frac{d\mathbf{V}}{dt}$ is taken equal to zero because the inertial effects are ignored and an equilibrium solution is sought, which gives

The material virtual work equation:

$$\delta W = \int_V \mathbf{P} : (\nabla \delta \mathbf{V}) dV - \int_V [\mathbf{B} \cdot \delta \mathbf{V}] dV - \int_{\partial V} (\mathbf{T} \cdot \delta \mathbf{V}) dA = 0. \quad (2.92)$$

Derivation from the spatial form The second way of determining the material form of the virtual work equation is through the spatial form. Here only a part of the equation shall be derived, as this is the only part that is needed. We start with the following expression in the spatial form [17]:

$$\int_v \boldsymbol{\sigma} : \delta \mathbf{d} dv. \quad (2.93)$$

In this derivation the virtual work shall be expressed using the second Piola-Kirchhoff stress tensor \mathbf{S} and the time derivative of the Green strain tensor \mathbf{E} .

First of all the time derivative of the Lagrangian strain tensor will be considered. This tensor $\dot{\mathbf{E}}$ is known as the *material strain rate tensor* [17]. Here $\mathbf{E} = \frac{1}{2}(\mathbf{C} - \mathbf{I})$ is the Lagrangian strain tensor. The derivative is now obtained by

$$\dot{\mathbf{E}} = \frac{1}{2}\dot{\mathbf{C}} = \frac{1}{2}(\dot{\mathbf{F}}^T \mathbf{F} + \mathbf{F}^T \dot{\mathbf{F}}). \quad (2.94)$$

Here $\mathbf{C} = \mathbf{F}^T \mathbf{F}$ is the right Cauchy-Green deformation tensor as defined in equation (2.36).

The material strain rate tensor gives the current rate of change of the scalar product of two elemental vectors in terms of the initial elemental vectors as

$$\frac{d}{dt}(d\mathbf{x}_1 \cdot d\mathbf{x}_2) = 2d\mathbf{X}_1 \cdot \dot{\mathbf{E}}d\mathbf{X}_2. \quad (2.95)$$

The rate of change of the scalar product can also be expressed in terms of $d\mathbf{x}_1$ and $d\mathbf{x}_2$ as

$$\begin{aligned} \frac{1}{2} \frac{d}{dt}(d\mathbf{x}_1 \cdot d\mathbf{x}_2) &= d\mathbf{X}_1 \cdot \dot{\mathbf{E}}d\mathbf{X}_2 \\ &= \mathbf{F}^{-1} d\mathbf{x}_1 \cdot \dot{\mathbf{E}}\mathbf{F}^{-1} d\mathbf{x}_2 \\ &= d\mathbf{x}_1 \cdot (\mathbf{F}^{-T} \dot{\mathbf{E}}\mathbf{F}^{-1}) d\mathbf{x}_2. \end{aligned} \quad (2.96)$$

In this equation the *rate of deformation tensor* \mathbf{d} is introduced which is defined as

$$\mathbf{d} = \mathbf{F}^{-T} \dot{\mathbf{E}}\mathbf{F}^{-1}. \quad (2.97)$$

Another way of defining the rate of deformation tensor is by using the *velocity gradient* \mathbf{l} . This gradient is defined as

$$\mathbf{l} = \frac{\partial \mathbf{v}(\mathbf{x}, t)}{\partial \mathbf{x}} = \nabla \mathbf{v}, \quad (2.98)$$

where $\mathbf{v}(\mathbf{x}, t)$ is the velocity as a function of the spatial coordinates. Another way of defining \mathbf{l} is by

$$\mathbf{l} = \dot{\mathbf{F}}\mathbf{F}^{-1}. \quad (2.99)$$

With these definitions of the velocity gradient the rate of deformation tensor can be given by

$$\mathbf{d} = \frac{1}{2}(\mathbf{l} + \mathbf{l}^T). \quad (2.100)$$

Note that the material strain rate tensor and the rate of deformation tensor can be expressed in one another using the push forward and pull back concept as follows:

$$\dot{\mathbf{E}} = \boldsymbol{\Psi}_*^{-1} [\mathbf{d}] = \mathbf{F}^T \mathbf{d} \mathbf{F} \quad \text{Pull back,} \quad (2.101a)$$

$$\mathbf{d} = \boldsymbol{\Psi}_* [\dot{\mathbf{E}}] = \mathbf{F}^{-T} \dot{\mathbf{E}}\mathbf{F}^{-1} \quad \text{Push forward.} \quad (2.101b)$$

Using these new definitions, the virtual work equation can be rewritten into the material form [17].

$$\int_v \boldsymbol{\sigma} : \delta \mathbf{d} \, dv = \int_V J \boldsymbol{\sigma} : (\mathbf{F}^{-T} \delta \dot{\mathbf{E}} \mathbf{F}^{-1}) \, dV \quad (2.102a)$$

$$= \int_V \text{tr}(\mathbf{F}^{-1} J \boldsymbol{\sigma} \mathbf{F}^{-T} \delta \dot{\mathbf{E}}) \, dV \quad (2.102b)$$

$$= \int_V \mathbf{S} : \delta \dot{\mathbf{E}} \, dV \quad (2.102c)$$

Note that this part is equal to the part $\int_V \mathbf{P} : (\nabla \delta \mathbf{V}) \, dV$ in equation (2.92).

2.3. INCLUDING THE CONTACT DEFINITIONS

One of the most difficult parts of solving the model is the contact between the skin and the mattress. As further explained in Appendix B, the biggest problem is the number of unknowns. As one cannot predict the movement and deformation of both bodies, the contact area between the bodies is also unknown.

FEBio includes many options regarding contact and coupling. These different options are further explained in Section 2.4.1. In this model the contact is between two deformable bodies which will also be the contact type that will be described in this section. This section will start with a definition of the two body contact problem (Section 2.3.1), after which it will be included in the equations of motion (Section 2.3.3). As the contact will also be solved using the Newton-Raphson method the equations of motion including the contribution of the contact tractions will be converted to the virtual work equation (Section 2.3.4).

The definitions and derivations in this section closely follow the information given in [20], as this is the book that was used for the implementation in FEBio.

2.3.1. THE TWO BODY CONTACT PROBLEM

Before discussing the problem some notation shall be introduced [20]. The two bodies that are considered in the reference configuration are denoted by $\Omega^{(i)} \subset \mathbb{R}^3$ for $i = 1, 2$. The bodies are put in motion, described by $\boldsymbol{\varphi}^{(i)}$ which will cause them to come into contact. Points within the first body $\bar{\Omega}^{(1)}$ are denoted by \mathbf{X} in the reference configuration and \mathbf{x} in the current configuration. Points in the second body $\bar{\Omega}^{(2)}$ are denoted by \mathbf{Y} and \mathbf{y} respectively. The boundary of each body in the reference configuration is denoted as $\partial\Omega^{(i)}$ and is subdivided into three regions $\Gamma_c^{(i)}$, $\Gamma_\sigma^{(i)}$ and $\Gamma_u^{(i)}$, such that

$$\Gamma_c^{(i)} \cup \Gamma_\sigma^{(i)} \cup \Gamma_u^{(i)} = \partial\Omega^{(i)}, \quad \text{and} \quad \Gamma_c^{(i)} \cap \Gamma_\sigma^{(i)} = \Gamma_c^{(i)} \cup \Gamma_u^{(i)} = \Gamma_u^{(i)} \cup \Gamma_\sigma^{(i)} = \emptyset. \quad (2.103)$$

The three regions are defined as follows:

- $\Gamma_c^{(i)}$ is the part of the boundary that is in contact with the other body,
- $\Gamma_\sigma^{(i)}$ is the part of the boundary where tractions are applied, and
- $\Gamma_u^{(i)}$ is the part of the boundary where the solution (the displacement $\bar{\mathbf{u}}^{(i)}$) is prescribed.

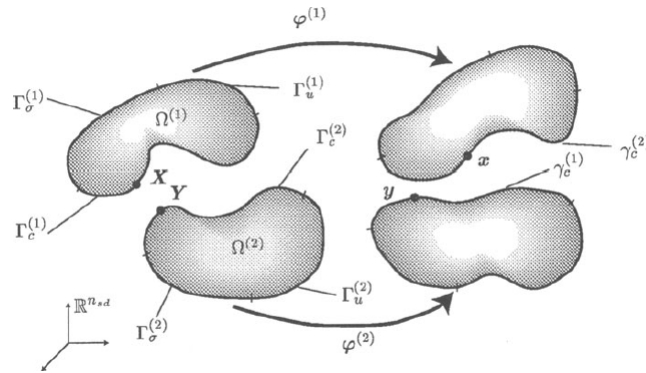


Figure 2.7: The basic notation used in the two body contact problem. Source: [20].

In the current configuration the counterpart of the contact boundary is designated as $\gamma_c^{(i)} = \boldsymbol{\varphi}_t^{(i)}(\Gamma_c^{(i)})$, $i = 1, 2$. An overview of the notation is given in Figure 2.7.

Recall from Section 2.2.1 that the equations of motion in the material form are given by equation (2.74) where \mathbf{P} is the first Piola-Kirchhoff stress, \mathbf{B} the prescribed body force, ρ_0 the reference density and $\frac{d\mathbf{V}}{dt}$ the material acceleration field:

$$\text{div}\mathbf{P} + \mathbf{B} = \rho_0 \frac{d\mathbf{V}}{dt}. \quad (2.104)$$

As this equation must hold for each body separately, the equation can be written for body i as

$$\text{div}\mathbf{P}^{(i)} + \mathbf{B}^{(i)} = \rho_0^{(i)} \mathbf{A}^{(i)}, \quad \text{where} \quad \mathbf{A}^{(i)} = \frac{d\mathbf{V}^{(i)}}{dt}. \quad (2.105)$$

Similarly in the spatial form:

$$\nabla \cdot \boldsymbol{\sigma}^{(i)} + \mathbf{b}^{(i)} = \rho^{(i)} \mathbf{a}^{(i)}, \quad \text{where } \mathbf{a}^{(i)} = \frac{d\mathbf{v}^{(i)}}{dt}. \quad (2.106)$$

The corresponding initial and boundary conditions are given by

$$\mathbf{P}^{(i)} \mathbf{N}^{(i)} = \bar{\mathbf{T}}^{(i)} \quad \text{in } \Gamma_\sigma^{(i)}, \text{ for all } t, \quad (2.107a)$$

$$\boldsymbol{\varphi}^{(i)} = \bar{\boldsymbol{\varphi}}^{(i)} \quad \text{in } \Gamma_u^{(i)}, \text{ for all } t, \quad (2.107b)$$

$$\dot{\boldsymbol{\varphi}}^{(i)} \Big|_{t=0} = \mathbf{V}_0^{(i)} \quad \text{in } \bar{\Omega}^{(i)}, \quad (2.107c)$$

$$\boldsymbol{\varphi}^{(i)} \Big|_{t=0} = \mathbf{I} \quad (\text{the identity mapping}) \quad \text{in } \bar{\Omega}^{(i)}. \quad (2.107d)$$

Here $\mathbf{N}^{(i)}$ is the outward normal to $\partial\Omega^{(i)}$ in the reference configuration, $\bar{\mathbf{T}}^{(i)}$ is the specified traction field on $\Gamma_\sigma^{(i)}$, $\bar{\boldsymbol{\varphi}}^{(i)}$ is the specified displacement field on $\Gamma_u^{(i)}$ and $\mathbf{V}_0^{(i)}$ is the specified initial velocity field for body i .

The final element that needs to be introduced before introducing the contact element in the equation of motion are the contact conditions describing the response on $\Gamma_c^{(1)}$ (or $\Gamma_c^{(2)}$). The first step in introducing these conditions is terming the two bodies.

1. The first body has the surface that will be used to parametrize the contact. The positions of points belonging to this surface will be monitored with respect to the location of the second surface. This surface is termed the *slave* or *contactor* surface.
2. The surface of the second body is termed the *master* or *target* surface.

In this section the first body shall be parametrized, that is $\Gamma_c^{(1)}$ is the slave surface, and $\Gamma_c^{(2)}$ is the master surface.

Now for a given point \mathbf{X} on the slave reference contact surface $\Gamma_c^{(1)}$, there is a point $\bar{\mathbf{Y}}(\mathbf{X})$ on the master contact surface ($\Gamma_c^{(2)}$) that is 'closest' to point \mathbf{X} . This point $\bar{\mathbf{Y}}(\mathbf{X})$ is defined according to the following *closest point projection*:

$$\bar{\mathbf{Y}}(\mathbf{X}) = \arg \min_{\mathbf{Y} \in \Gamma_c^{(2)}} \left\| \boldsymbol{\varphi}_t^{(1)}(\mathbf{X}) - \boldsymbol{\varphi}_t^{(2)}(\mathbf{Y}) \right\|. \quad (2.108)$$

With this definition of the closest point, the *gap function* $g(\mathbf{X}, t)$ can be written as

$$g(\mathbf{X}, t) = -\mathbf{v} \left(\boldsymbol{\varphi}_t^{(1)}(\mathbf{X}) - \boldsymbol{\varphi}_t^{(2)}(\bar{\mathbf{Y}}(\mathbf{X})) \right), \quad (2.109)$$

where \mathbf{v} is the outward unit normal to $\gamma_{c_t}^{(2)}$ at $\bar{\mathbf{y}} = \boldsymbol{\varphi}_t^{(2)}(\bar{\mathbf{Y}})$. Note that when $g > 0$ it means that \mathbf{X} has penetrated body 2, which is not allowed when dealing with contact. From this the contact constraint condition can be derived as being

$$g(\mathbf{X}, t) \leq 0. \quad (2.110)$$

2.3.2. INCLUDING FRICTION IN THE PROBLEM

Now that the contact problem has been described, the effects of friction can be included. Since the contact is described from the position of points $\mathbf{X} \in \Gamma_c^{(1)}$ opposing the surface $\Gamma_c^{(2)}$, the goal is to write the frictional governing equations in a similar way. For this some new notation needs to be introduced. The notation starts with assuming that $\Gamma_c^{(2)}$ can be described as

$$\Gamma_c^{(2)} = \boldsymbol{\Psi}_0^{(2)}(\mathcal{A}^{(2)}), \quad \text{and} \quad \gamma_{c_t}^{(2)} = \boldsymbol{\Psi}_t^{(2)}(\mathcal{A}^{(2)}), \quad (2.111)$$

where $\mathcal{A}^{(2)} \subset \mathbb{R}^2$ is a parametrization of the contact surface, see Figure 2.8.

This parametrization $\mathcal{A}^{(2)}$ and the mappings $\boldsymbol{\Psi}_0^{(2)}$ and $\boldsymbol{\Psi}_t^{(2)}$ are assumed to be smooth for simplicity [20]. Typical points of $\mathcal{A}^{(2)}$ will be denoted by $\boldsymbol{\xi}$. The point of $\mathcal{A}^{(2)}$ corresponding to $\bar{\mathbf{Y}}(\mathbf{X}, t)$ will be denoted by $\bar{\boldsymbol{\xi}}(\mathbf{X}, t)$.

It is convenient to define bases associated with each point \mathbf{X} , which are advected with \mathbf{X} as it moves. These bases shall be called the *slip advected bases*. The first one that will be defined is one in the reference configuration of the sliding surface ($\Gamma_c^{(2)}$). The second is defined in the current configuration ($\gamma_{c_t}^{(2)}$).

$$\mathbf{T}_\alpha := \boldsymbol{\Psi}_{0,\alpha}^{(2)}(\bar{\boldsymbol{\xi}}(\mathbf{X}, t)), \quad \text{and} \quad \boldsymbol{\tau}_\alpha := \boldsymbol{\Psi}_{t,\alpha}^{(2)}(\bar{\boldsymbol{\xi}}(\mathbf{X}, t)), \quad \alpha = 1, \dots, n_{sd} - 1. \quad (2.112)$$

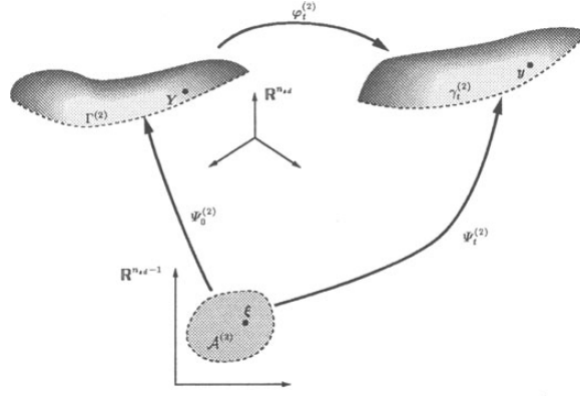


Figure 2.8: Schematic of the parametrization of a contact surface. Source: [20].

Here n_{sd} is the number of spatial dimensions. Note that \mathbf{T}_α and $\boldsymbol{\tau}_\alpha$ are always associated with a material point \mathbf{X} and are evaluated according to its current (closest point) projection to $\Gamma_c^{(2)}$, parametrized by $\bar{\xi}(\mathbf{X}, t)$. When characterizing potential frictional response the most important variable is the relative velocity between \mathbf{X} and its opposing point $\bar{\mathbf{Y}}(\mathbf{X}, t)$. This relative velocity can be expressed both in the spatial configuration and the reference configuration, by an appeal to the slip advected bases introduced in equation (2.112). We consider the time derivative of the relative position vector between $\mathbf{x} = \boldsymbol{\varphi}^{(1)}(\mathbf{X})$ and its contact point $\bar{\mathbf{y}} = \boldsymbol{\varphi}^{(2)}(\bar{\mathbf{Y}}(\mathbf{X}))$ during perfect sliding (when $g = \dot{g} = 0$) and the two points remain coincident in space [20].

$$\begin{aligned} 0 &= \frac{d}{dt} [\boldsymbol{\varphi}^{(1)}(\mathbf{X}, t) - \boldsymbol{\varphi}^{(2)}(\bar{\mathbf{Y}}(\mathbf{X}, t), t)] \\ &= \mathbf{V}^{(1)}(\mathbf{X}, t) - \mathbf{V}^{(2)}(\bar{\mathbf{Y}}(\mathbf{X}, t), t) - \mathbf{F}_t^{(2)}(\boldsymbol{\Psi}_0^{(2)}(\bar{\xi}(\mathbf{X}, t))) \frac{d}{dt} [\bar{\mathbf{Y}}(\mathbf{X}, t)] \end{aligned} \quad (2.113)$$

Here $\mathbf{F}_t^{(2)}$ is the deformation gradient of body (2) at time t . From this equation it follows that the relative velocity may be represented in terms of vectors in the tangent spaces $\Gamma_c^{(2)}$ and $\gamma_c^{(2)}$ while sliding is occurring. The *spatial relative velocity* \mathbf{v}_T and the *convective relative velocity* $\boldsymbol{\nu}_T$ are defined as

$$\mathbf{v}_T := \mathbf{F}_t^{(2)} \left(\boldsymbol{\Psi}_0^{(2)}(\bar{\xi}(\mathbf{X}, t)) \right) \frac{d}{dt} [\bar{\mathbf{Y}}(\mathbf{X}, t)], \quad (2.114a)$$

$$= \mathbf{V}^{(1)}(\mathbf{X}, t) - \mathbf{V}^{(2)}(\bar{\mathbf{Y}}(\mathbf{X}, t), t) \quad \text{by equation (2.113), and}$$

$$\boldsymbol{\nu}_T := \frac{d}{dt} [\bar{\mathbf{Y}}(\mathbf{X}, t)], \quad (2.114b)$$

$$= \dot{\bar{\xi}}^\alpha(\mathbf{X}, t) \mathbf{T}_\alpha \quad \text{as the point in } \mathcal{A}^{(2)} \text{ corresponding to } \bar{\mathbf{Y}}(\mathbf{X}, t) \text{ is denoted by } \bar{\xi}(\mathbf{X}, t).$$

It can be shown that $\boldsymbol{\nu}_T$ is the pull back of \mathbf{v}_T by $\boldsymbol{\varphi}_t^{(2)}$ and since

$$\boldsymbol{\tau}_\alpha = \mathbf{F}_t^{(2)} \mathbf{T}_\alpha, \quad (2.115)$$

it follows that

$$\boldsymbol{\nu}_T = \dot{\bar{\xi}}^\alpha(\mathbf{X}, t) \boldsymbol{\tau}_\alpha. \quad (2.116)$$

It can be derived ([20]) that the $\dot{\bar{\xi}}^\alpha$ are the components of the convected relative velocity \mathcal{V}_T with respect to the \mathbf{T}_α basis, and are likewise the components of the spatial relative velocity \mathbf{v}_T with respect to the $\boldsymbol{\tau}_\alpha$ basis.

More generally, the components $\dot{\bar{\xi}}^\alpha(\mathbf{X}, t)$ of $\boldsymbol{\nu}_T$ and \mathbf{v}_T in their respective basis can be interpreted using the closest point projection given in equation (2.108). This can even be done for the case where $g \neq 0$. It can be noted that since the projection of $\mathbf{x} = \boldsymbol{\varphi}_t^{(1)}(\mathbf{X})$ onto $\gamma_{c_t}^{(2)}$ is normal to $\gamma_{c_t}^{(2)}$ at $\bar{\mathbf{y}} = \boldsymbol{\varphi}_t^{(2)}(\bar{\mathbf{Y}}(\mathbf{X}))$, we can write [20]

$$\boldsymbol{\tau}_\alpha \cdot [\boldsymbol{\varphi}_t^{(1)}(\mathbf{X}, t) - \boldsymbol{\varphi}_t^{(2)}(\bar{\mathbf{Y}}(\mathbf{X}, t), t)] = 0, \quad \alpha = 1, 2. \quad (2.117)$$

Taking the material time derivative of this expression yields

$$0 = [\mathbf{V}^{(1)}(\mathbf{X}) - \mathbf{V}^{(2)}(\bar{\mathbf{Y}}(\mathbf{X})) - \boldsymbol{\tau}_\gamma \dot{\bar{\xi}}^\gamma] \cdot \boldsymbol{\tau}_\alpha - g \mathbf{v} \cdot [\mathbf{V}_{,\alpha}^{(2)}(\bar{\mathbf{Y}}(\mathbf{X})) + \boldsymbol{\varphi}_{t,\alpha\beta}^{(2)}(\bar{\xi}) \dot{\bar{\xi}}^\beta]. \quad (2.118)$$

This can be rewritten as

$$A_{\alpha\beta} \dot{\bar{\xi}}^\beta = [\mathbf{V}^{(1)}(\mathbf{X}) - \mathbf{V}^{(2)}(\bar{\mathbf{Y}}(\mathbf{X}))] \boldsymbol{\tau}_\alpha - g \mathbf{v} \cdot [\mathbf{V}_{,\alpha}^{(2)}(\bar{\mathbf{Y}}(\mathbf{X}))], \quad (2.119)$$

where the quantity $A_{\alpha\beta}$ is defined as

$$A_{\alpha\beta} := m_{\alpha\beta} + g \kappa_{\alpha\beta}. \quad (2.120)$$

In this equation $\kappa_{\alpha\beta} := \mathbf{v} \cdot \boldsymbol{\varphi}_{t,\alpha\beta}^{(2)}(\bar{\mathbf{Y}})$ denotes the components of the surface curvature at $\bar{\xi}$ [20], and $m_{\alpha\beta} := \boldsymbol{\tau}_\alpha \cdot \boldsymbol{\tau}_\beta$ refers to the components of the metric tensor.

In the case of perfect sliding, i.e. when $g = 0$, equation (2.119) simplifies to

$$\dot{\bar{\xi}}^\alpha = [\mathbf{V}^{(1)}(\mathbf{X}) - \mathbf{V}^{(2)}(\bar{\mathbf{Y}}(\mathbf{X}))] \boldsymbol{\tau}_\alpha. \quad (2.121)$$

Here $\boldsymbol{\tau}_\alpha = m^{\alpha\beta} \boldsymbol{\tau}_\beta$ represents the dual basis to $\boldsymbol{\tau}_\beta$.

It can be obtained that in the case of perfect sliding the $\dot{\bar{\xi}}^\alpha$ represent the projection of the relative material velocity $\mathbf{V}^{(1)}(\mathbf{X}) - \mathbf{V}^{(2)}(\bar{\mathbf{Y}}(\mathbf{X}))$ into the (spatial) tangent plane at $\boldsymbol{\varphi}_t^{(2)}(\bar{\mathbf{Y}}(\mathbf{X}))$.

To formulate the frictional model a distinction shall be made between two frameworks: the *spatial kinematic frame* and the *convected kinematic frame*.

Starting with the spatial kinematic frame, the spatial relative velocity \mathbf{v}_T will be used in the equations. Note that even though the quantity is associated with the material point \mathbf{X} , it is a vector resolved in terms of spatial bases $\boldsymbol{\tau}_\alpha$. Considering the Piola-Kirchhoff contact traction $\mathbf{T}(\mathbf{X}, t)$, one finds that this vector can also be written in terms of spatial bases. Recall that the Piola traction is defined as

$$\mathbf{T}(\mathbf{X}, t) := \mathbf{P}(\mathbf{X}, t) \mathbf{N}(\mathbf{X}), \quad (2.122)$$

where \mathbf{P} is the first Piola-Kirchhoff stress and \mathbf{N} the outward surface normal in the initial configuration.

A frictional traction vector can be defined by resolving the Piola traction $\mathbf{T}(\mathbf{X}, t)$ in terms of the spatial basis to obtain the (spatial) frictional traction \mathbf{t}_T :

$$\mathbf{t}_T(\mathbf{X}, t) := -\mathbf{T}(\mathbf{X}, t) + \mathbf{t}_N(\mathbf{X}, t) \mathbf{v}, \quad (2.123)$$

where \mathbf{t}_N is the contact pressure, which is positive if it is compressive, and \mathbf{v} is the outward normal to $\gamma_c^{(2)}$ at $\boldsymbol{\varphi}_t^{(2)}(\bar{\mathbf{Y}}(\mathbf{X}, t))$. The minus sign ensures that \mathbf{t}_T physically represents the frictional traction exerted by \mathbf{X} on the surface $\Gamma_c^{(2)}$.

Considering the convected kinematic frame allows for the frictional traction to be defined in the convected basis. The convected frictional traction $\mathcal{F}_T(\mathbf{X}, t)$ is defined as the pull back of \mathbf{t}_T induced by $\boldsymbol{\varphi}_t^{(2)}$:

$$\begin{aligned} \mathcal{F}_T(\mathbf{X}, t) &:= \mathbf{F}_t^{(2)T}(\bar{\mathbf{Y}}(\mathbf{X}, t)) \mathbf{t}_T(\mathbf{X}, t) \\ &= \mathbf{t}_{T_\alpha}(\mathbf{X}, t) \mathbf{T}^\alpha. \end{aligned} \quad (2.124)$$

In this equation the last line holds due to the fact that $\mathbf{T}^\alpha = \mathbf{F}_t^{(2)T} \boldsymbol{\tau}^\alpha$.

COULOMB FRICTION

With the two frameworks defined above we can now turn to friction. FEBio supports contact with Coulomb friction, which is the most common form of friction (see Appendix B.2.4). The friction will be formulated within both frameworks. The Coulomb law for large sliding problems shall be given in the unregularized form, which is not differentiable at the origin and allows for description of perfect sticking behavior [20].

The Coulomb law states that the frictional traction force \mathbf{t}_T should always be smaller than or equal to the contact pressure \mathbf{t}_N multiplied by a coefficient of friction μ :

$$\|\mathbf{t}_T\| \leq \mu \mathbf{t}_N. \quad (2.125)$$

In the spatial slip advected frame the Coulomb law can be expressed as

$$\begin{aligned}
g &\leq 0 \\
\mathbf{t}_N &\geq 0 \\
\mathbf{t}_N g &= 0 \\
\Psi(\mathbf{t}_T, \mathbf{t}_N) &:= \|\mathbf{t}_T\| - \mu \mathbf{t}_N \leq 0, \\
\mathbf{v}_T^b &= \dot{\gamma} \frac{\mathbf{t}_T}{\|\mathbf{t}_T\|}, \\
\dot{\gamma} &\geq 0, \\
\dot{\gamma} \Psi &= 0.
\end{aligned} \tag{2.126}$$

Here $\mathbf{v}_T^b = m_{\alpha\beta} \dot{\xi}^\beta \tau^\alpha$, with $m_{\alpha\beta} = \boldsymbol{\tau}_\alpha \cdot \boldsymbol{\tau}_\beta$ as before, and $\|(\bullet)\|$ indicating the Euclidean norm of the vector (\bullet) . The indices $\alpha, \beta, \gamma, \dots$ run between 1 and $n_{sd} - 1$. Equation (2.126) can be written in components (with respect to the τ^α basis) as

$$\begin{aligned}
g &\leq 0 \\
\mathbf{t}_N &\geq 0 \\
\mathbf{t}_N g &= 0 \\
\Psi(\mathbf{t}_T, \mathbf{t}_N) &:= [\mathbf{t}_{T_\alpha} m^{\alpha\beta} \mathbf{t}_{T_\beta}]^{1/2} - \mu \mathbf{t}_N \leq 0, \\
m_{\alpha\beta} \dot{\xi}^\beta \tau^\alpha &= \dot{\gamma} \frac{\mathbf{t}_{T_\alpha}}{[\mathbf{t}_{T_\beta} m^{\beta\gamma} \mathbf{t}_{T_\gamma}]^{1/2}}, \\
\dot{\gamma} &\geq 0, \\
\dot{\gamma} \Psi &= 0.
\end{aligned} \tag{2.127}$$

In the convective slip advected frame the Coulomb law can be written as

$$\begin{aligned}
g &\leq 0 \\
\mathbf{t}_N &\geq 0 \\
\mathbf{t}_N g &= 0 \\
\Psi(\mathcal{F}_T, \mathbf{t}_N) &:= \|\mathcal{F}_T\| - \mu \mathbf{t}_N \leq 0, \\
\mathcal{V}_T^b &= \dot{\gamma} \frac{\mathcal{F}_T}{\|\mathcal{F}_T\|}, \\
\dot{\gamma} &\geq 0, \\
\dot{\gamma} \Psi &= 0.
\end{aligned} \tag{2.128}$$

With respect to the \mathbf{T}^α basis this can be written in components as

$$\begin{aligned}
g &\leq 0 \\
\mathbf{t}_N &\geq 0 \\
\mathbf{t}_N g &= 0 \\
\Psi(\mathbf{t}_T, \mathbf{t}_N) &:= [\mathbf{t}_{T_\alpha} M^{\alpha\beta} \mathbf{t}_{T_\beta}]^{1/2} - \mu \mathbf{t}_N \leq 0, \\
M_{\alpha\beta} \dot{\xi}^\beta \tau^\alpha &= \dot{\gamma} \frac{\mathbf{t}_{T_\alpha}}{[\mathbf{t}_{T_\beta} M^{\beta\gamma} \mathbf{t}_{T_\gamma}]^{1/2}}, \\
\dot{\gamma} &\geq 0, \\
\dot{\gamma} \Psi &= 0.
\end{aligned} \tag{2.129}$$

Here $M_{\alpha\beta} = \mathbf{T}_\alpha \cdot \mathbf{T}_\beta$ is the material metric. Note that though the expressions given in (2.127) and (2.129) are very similar, they are not entirely identical. Where the spatial description uses spatial metrics $m^{\alpha\beta}$ to compute lengths, the convective frame uses reference metrics $M^{\alpha\beta}$ for this. This results in a spatial traction \mathbf{t}_T in the spatial frame which satisfies Coulombs law, while in the convective frame \mathcal{F}_T is forced to satisfy this law. When the deformation of $\Gamma_c^{(2)}$ is small however, these differences vanish.

2.3.3. INCLUDING THE CONTACT IN THE EQUATIONS OF MOTION

With the definitions given in the previous section, the total problem including the contact constraints is given by [20]:

$$div \mathbf{P}^{(i)} + \mathbf{B}^{(i)} = \rho_0^{(i)} \mathbf{A}^{(i)}, \quad \text{where } \mathbf{A}^{(i)} = \frac{d\mathbf{V}^{(i)}}{dt}. \quad (2.130)$$

The corresponding initial boundary conditions are given by

$$\mathbf{P}^{(i)} \mathbf{N}^{(i)} = \bar{\mathbf{T}}^{(i)} \quad \text{in } \Gamma_\sigma^{(i)}, \text{ for all } t \quad (2.131a)$$

$$\boldsymbol{\varphi}^{(i)} = \bar{\boldsymbol{\varphi}}^{(i)} \quad \text{in } \Gamma_u^{(i)}, \text{ for all } t \quad (2.131b)$$

$$\dot{\boldsymbol{\varphi}}^{(i)} \Big|_{t=0} = \mathbf{V}_0^{(i)} \quad \text{in } \bar{\Omega}^{(i)} \quad (2.131c)$$

$$\boldsymbol{\varphi}^{(i)} \Big|_{t=0} = \mathbf{I} \quad (\text{the identity mapping}) \quad \text{in } \bar{\Omega}^{(i)} \quad (2.131d)$$

Note that thus far the problem is stated the same as the problem without contact. Now the additional information that needs to be incorporated into the problem are the contact conditions. For all $\mathbf{X} \in \Gamma_c^{(1)}$, decomposing the Piola-Kirchhoff traction at \mathbf{X} as $\mathbf{T} = -\mathbf{t}_{T_\alpha} \boldsymbol{\tau}^\alpha + \mathbf{t}_N \mathbf{v}$, the contact conditions are

$$\mathbf{t}_N \geq 0 \quad (2.132a)$$

$$g \leq 0 \quad (2.132b)$$

$$\mathbf{t}_N g = 0, \quad (2.132c)$$

where the frictional tractions are given in either the spatial slip advected frame or the convective slip advected frame:

- The spatial, slip advected frame:

$$\begin{aligned} \Psi(\mathbf{t}_T, \mathbf{t}_N) &:= [\mathbf{t}_{T_\alpha} m^{\alpha\beta} \mathbf{t}_{T_\beta}]^{1/2} - \mu \mathbf{t}_N \leq 0, \\ m_{\alpha\beta} \dot{\xi}^\beta \boldsymbol{\tau}^\alpha &= \dot{\gamma} \frac{\mathbf{t}_{T_\alpha}}{[\mathbf{t}_{T_\beta} m^{\beta\gamma} \mathbf{t}_{T_\gamma}]^{1/2}}, \\ \dot{\gamma} &\geq 0, \\ \dot{\gamma} \Psi &= 0. \end{aligned}$$

- The convective, slip advected frame:

$$\begin{aligned} \Psi(\mathbf{t}_T, \mathbf{t}_N) &:= [\mathbf{t}_{T_\alpha} M^{\alpha\beta} \mathbf{t}_{T_\beta}]^{1/2} - \mu \mathbf{t}_N \leq 0, \\ M_{\alpha\beta} \dot{\xi}^\beta \boldsymbol{\tau}^\alpha &= \dot{\gamma} \frac{\mathbf{t}_{T_\alpha}}{[\mathbf{t}_{T_\beta} M^{\beta\gamma} \mathbf{t}_{T_\gamma}]^{1/2}}, \\ \dot{\gamma} &\geq 0, \\ \dot{\gamma} \Psi &= 0. \end{aligned}$$

2.3.4. THE WEAK FORM INCLUDING THE CONTACT TRACTIONS

In Section 2.2.2 the virtual work equation in material form is given as

$$\delta W(\boldsymbol{\Psi}, \delta \mathbf{v}) = \int_V \mathbf{P} : (\nabla \delta \mathbf{v}) dV - \int_V [\mathbf{B} \cdot \delta \mathbf{v}] dV - \int_{\partial V} (\mathbf{T} \cdot \delta \mathbf{v}) dA = 0. \quad (2.133)$$

Here \mathbf{P} is the PK1 stress, \mathbf{B} the body force and \mathbf{T} the surface traction.

In the two body contact problem including friction this weak form shall only change slightly.

First of all, the above equation must hold for each body (i) , $i = 1, 2$. Secondly, the equation will be in terms of the motion of body (i) $\boldsymbol{\varphi}^{(i)}$ and a weighting (test) function $\boldsymbol{\omega}^{(i)}$, where

$$\begin{aligned} \boldsymbol{\varphi} &: \bar{\Omega}^{(1)} \cup \bar{\Omega}^{(2)} \rightarrow \mathbb{R}^3, \\ \boldsymbol{\omega} &: \bar{\Omega}^{(1)} \cup \bar{\Omega}^{(2)} \rightarrow \mathbb{R}^3. \end{aligned} \quad (2.134)$$

Thirdly, the integral over the surface (∂V) describing the surface tractions can be written as the integral over the part of the surface where tractions are present $(\Gamma_\sigma^{(i)})$. Last of all, an additional term appears in the virtual

work equation, describing the contact problem. This term will be an integral over the part of the surface where the body is in contact with the other body ($\Gamma_c^{(i)}$). With these changes, the virtual work equation for each body can be written as

$$\delta W^{(i)}(\boldsymbol{\varphi}^{(i)}, \boldsymbol{\omega}^{(i)}) = \int_{\Omega^{(i)}} \nabla \boldsymbol{\omega}^{(i)} : \mathbf{P}^{(i)} d\Omega - \int_{\Omega^{(i)}} \boldsymbol{\omega}^{(i)} \cdot \mathbf{B}^{(i)} d\Omega - \int_{\Gamma_\sigma^{(i)}} \boldsymbol{\omega}^{(i)} \cdot \mathbf{T}^{(i)} d\Gamma - \int_{\Gamma_c^{(i)}} \boldsymbol{\omega}^{(i)} \cdot \mathbf{T}^{(i)} d\Gamma = 0. \quad (2.135)$$

As this equation must hold for each body the total virtual work equation for the two body contact problem can be expressed as the summation over the bodies.

$$\begin{aligned} \delta W(\boldsymbol{\varphi}, \boldsymbol{\omega}) &:= \sum_{i=1}^2 \delta W^{(i)}(\boldsymbol{\varphi}^{(i)}, \boldsymbol{\omega}^{(i)}) \\ &= \sum_{i=1}^2 \left\{ \underbrace{\int_{\Omega^{(i)}} \nabla \boldsymbol{\omega}^{(i)} : \mathbf{P}^{(i)} d\Omega - \int_{\Omega^{(i)}} \boldsymbol{\omega}^{(i)} \cdot \mathbf{B}^{(i)} d\Omega - \int_{\Gamma_\sigma^{(i)}} \boldsymbol{\omega}^{(i)} \cdot \mathbf{T}^{(i)} d\Gamma}_{\delta W^{int,ext}(\boldsymbol{\varphi}, \boldsymbol{\omega})} \right\} \\ &\quad - \underbrace{\sum_{i=1}^2 \int_{\Gamma_c^{(i)}} \boldsymbol{\omega}^{(i)} \cdot \mathbf{T}^{(i)} d\Gamma}_{\delta W^c(\boldsymbol{\varphi}, \boldsymbol{\omega})} = 0. \end{aligned} \quad (2.136)$$

Note that $\delta W^{int,ext}(\boldsymbol{\varphi}, \boldsymbol{\omega})$ denotes the internal and external virtual work that has been discussed before. $\delta W^c(\boldsymbol{\varphi}, \boldsymbol{\omega})$ denotes the contact virtual work, and is also known as the *contact integral*. In short equation (2.136) can be written as

$$\delta W(\boldsymbol{\varphi}, \boldsymbol{\omega}) = \delta W^{int,ext}(\boldsymbol{\varphi}, \boldsymbol{\omega}) + \delta W^c(\boldsymbol{\varphi}, \boldsymbol{\omega}) = 0. \quad (2.137)$$

Note that the contact integral includes two integrals, one over each contact surface. This expression can be converted to an expression including only one integral using the assumption made earlier that all contact quantities are parametrized by $\mathbf{X} \in \Gamma_c^{(1)}$. The conversion can be achieved by enforcing linear momentum across the contact interface [20]. This is done by requiring that the differential contact force induced on body (2) at $\tilde{\mathbf{Y}}$ be equal and opposite to that produced on body (1) at \mathbf{X} , that is

$$\mathbf{t}_t^{(2)}(\tilde{\mathbf{Y}}(\mathbf{X})) d\Gamma_c^{(2)} = \mathbf{t}_t^{(1)}(\mathbf{X}) d\Gamma_c^{(1)}. \quad (2.138)$$

Using this the contact integral can be given as

$$\delta W^c(\boldsymbol{\varphi}, \boldsymbol{\omega}) = - \int_{\Gamma_c^{(1)}} \mathbf{t}_t^{(1)}(\mathbf{X}) [\boldsymbol{\omega}^{(1)}(\mathbf{X}) - \boldsymbol{\omega}^{(2)}(\tilde{\mathbf{Y}}(\mathbf{X}))] d\Gamma. \quad (2.139)$$

This can be simplified using the linearized variation of the gap function δg and the linearized variation of $\tilde{\boldsymbol{\xi}}$.

$$\begin{aligned} \delta W^c(\boldsymbol{\varphi}, \boldsymbol{\omega}) &= - \int_{\Gamma_c^{(1)}} [\mathbf{t}_N \mathbf{v} - t_{Ta} \boldsymbol{\tau}^\alpha] \cdot [\boldsymbol{\omega}^{(1)}(\mathbf{X}) - \boldsymbol{\omega}^{(2)}(\tilde{\mathbf{Y}}(\mathbf{X}))] d\Gamma \\ \delta W^c(\boldsymbol{\varphi}, \boldsymbol{\omega}) &= \int_{\Gamma_c^{(1)}} [t_{Ni} \delta g + t_{Ta} \delta \tilde{\boldsymbol{\xi}}^\alpha] d\Gamma, \end{aligned} \quad (2.140)$$

where

$$\delta g = -\mathbf{v} \cdot [\boldsymbol{\omega}^{(1)}(\mathbf{X}) - \boldsymbol{\omega}^{(2)}(\tilde{\mathbf{Y}}(\mathbf{X}))], \quad \text{and} \quad (2.141)$$

$$\delta \tilde{\boldsymbol{\xi}}^\alpha = \boldsymbol{\tau}^\alpha \cdot [\boldsymbol{\omega}^{(1)}(\mathbf{X}) - \boldsymbol{\omega}^{(2)}(\tilde{\mathbf{Y}}(\mathbf{X}))] \quad (\text{when } g = 0). \quad (2.142)$$

2.4. CONSTRUCTING THE MODEL USING THE GIBBON TOOLBOX AND FEBIO

2.4.1. THE BASIC MODEL

In this section an overview of the different components of the model is given. This will be done in a setup similar to the general FEBio file.

THE UNITS

FEBio allows the user to choose its own set of units. It is up to the user to verify if the set is indeed **consistent**. Before discussing the entire model an overview will therefore be given of used units.

Table 2.1: The used units.

Units		
Time	seconds	s
Length	millimeter	mm
Mass	kilogram	kg
Density	mass per unit volume	kg/mm ³
Force	millinewton	kg·mm/s ² , mN
Stress	Kilo Pascal	mN/mm ² , kPa

GENERAL INFORMATION

Before defining the actual problem, some general information has to be provided in the .feb file. Details like the type of problem and the name of the problem have to be given here.

FEBio allows the user to choose from five different problem modules, which define the type of analysis that FEBio performs. The module types will be briefly discussed below [22].

Solid The solid type deals with structural mechanics problems. The user has the choice between a quasi-static analysis and a dynamic analysis.

Biphasic The biphasic module type allows the user to solve problems in which fluids flow. One can choose to use a steady-state analysis or a transient analysis.

Solute This type is very similar to the biphasic analysis but also includes problems that include solute transport. Similar to the biphasic problem the user can choose between a steady-state analysis or a transient analysis.

Multiphasic Even more elaborate is the multiphasic type in which the user can analyse problems including chemical reactions.

Heat The heat type can be used to solve heat transfer problems. Again one has the option to choose for a steady-state analysis or a transient analysis.

In the descriptions above one can see that besides the modules the user can also choose between some analysis types. In the solid type, which is the module that is used in this project, one can choose between a quasi-static analysis and a dynamic analysis. The difference between these two analysis types is that in the quasi-static analysis the inertial effects are ignored and an equilibrium solution is sought. In a dynamic analysis the inertial effects are included. Note that even though the quasi-static analysis looks for an equilibrium solution, it is still possible to simulate time dependent effects.

In this project the Solid module with a quasi-static analysis has been used.

Besides the analysis type the user also needs to specify some control information such as the initial step size dt for the Newton method and total number of time steps. As the method does not always converge for large step sizes the user needs to specify the minimum step size that the program can use and the number of retries that it is allowed to use. As the problem is solved using BFGS (see Section 3.4.1) the user can specify the maximum number of stiffness updates. Many of these control parameters have a default value which means that the user is not obliged to define them. When not defined the program will automatically use the default values. Which values do need to be given can be found in the user manual of FEBio [22].

GEOMETRY AND MESH

When starting to build the model using the Gibbon Toolbox and FEBio the first thing that was noted was that this model would have to be in 3D instead of 2D. In this model the body is therefore modeled by a sphere instead of a circle and the bed is modeled as a box. To represent the different skin layers (i.e. skin and subcutaneous tissue) multiple spheres were modeled within each other. The mattress and the human body are implemented separately, positioned to make sure they only touch each other in a single point.

The dimensions of the model During the project two different sized models have been used. Details regarding these two models are given in Table 2.2. In working with the models the sizes of the spheres were sometimes altered to see the effect on the stress levels. Table 2.2 however gives the general dimensions.

Table 2.2: Dimensions of the two basic models.

	Model A (small)	Model B (big)
Width mattress	12 mm	400 mm
Thickness mattress	12 mm	400 mm
Height mattress	6 mm	50 mm
Inner radius subcutaneous tissue	2 mm	163 mm
Outer radius subcutaneous tissue	4 mm	178 mm
Inner radius skin	4 mm	178 mm
Outer radius skin	6 mm	180 mm

To give a better idea regarding the geometry of the model, both models A and B are shown in Figure 2.9. One can see that both models are currently hollow and the body only exists of skin and subcutaneous tissue.

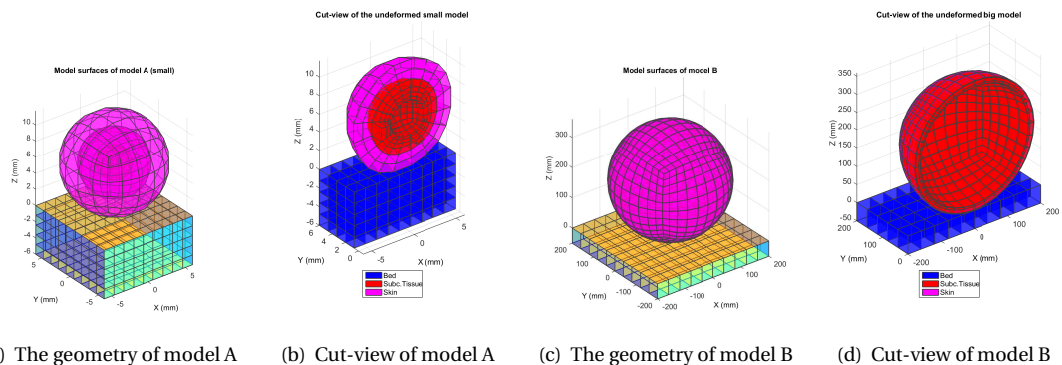


Figure 2.9: The geometry and cut-view overviews of the basic models.

Meshing the geometry Working in Matlab there are multiple ways of implementing the geometry and mesh. The first option is to model a sphere and a box and then use some software to mesh the volumes. This software could for instance be TetGen ([23]). Another option is to immediately mesh the bodies while creating them. In implementing the model the latter option was used. This was done using a function from the Gibbon Toolbox in Matlab [14]. Multiple functions are available, depending on the type of elements the user wants. In this model we use 8-node hexahedral elements (hex8).

While creating the mattress, the box is immediately subdivided into elements. When defining the size of the box the user also has to define the number of elements that should fill each dimension. This can be done in different ways. The first possibility is simply stating the number of elements that have to be in the width, thickness and height. Another possibility is stating the size of the elements and defining the number of elements by checking how many elements of that size can fit in the box. Of course when doing so the number of elements need to be rounded. In the code below the latter option is shown.

```

1 %% Creating the box (mattress)
  sampleWidth=400; %width of the mattress
  sampleThickness=400; %thickness of the mattress
  sampleHeight=50; %height of the mattress
  pointSpacing=40.3;% size of the elements
6
  %the number of elements in the width of the box
  numElementsWidth=round(sampleWidth/pointSpacing);
  %the number of elements in the thickness of the box
  numElementsThickness=round(sampleThickness/pointSpacing);
11 %the number of elements in the height of the box
  numElementsHeight=round(sampleHeight/pointSpacing);

```

Meshing the spheres is done rather similarly. The user starts with defining the inner and outer radius of the first sphere. This is the inner sphere, which represents the subcutaneous tissue. Immediately the user can define whether or not the sphere should be hollow or not. If it is hollow the sphere with the inner radius will be left empty. If not, the inner sphere and the mantel around the sphere will be united into one sphere. When defining the dimensions of the inner sphere the user also has to specify the number of elements that should be in the core, and the number of elements that should be in the mantel. These numbers are then used to construct the actual sphere. Given the number of elements that the user has specified to be in the core, a cube is constructed in which each dimension exists of the specified number of elements. This cube is then changed into a sphere. Note that the number of elements specified to be in the core is not the actual number of elements in the core.

Once the core is constructed the mantel is constructed upon this sphere. The user has specified the number of elements that the mantel should contain and the thickness of the mantel. On every element of the outer face of the core a new element is build, of which the thickness is equal to the thickness of the mantel divided by the number of elements in the mantel. Again the number that is specified is not equal to the actual number of elements in the mantel.

```

%% Creating the first sphere (Subcutaneous tissue)
sphereRadius=178; %What is the outer radius of the first sphere
3 sphereRadiusInner=163; %What is the inner radius of the first sphere

% How many elements should each dimension of the cube contain?
cPar.numElementsCore=10;
% In how many elements should the thickness of the mantel be divided?
8 cPar.numElementsMantel=3;
% 1 means the sphere is hollow; 0 means the core will be filled.
cPar.Totaq=1;
%Creating sphere
[meshStruct]=hexMeshSphere(cPar);

```

When this is done only the first sphere has been constructed (the subcutaneous tissue). For the second sphere (the skin), another mantel will be constructed around the subcutaneous tissue. Here again the user needs to specify the thickness of the mantel and the number of elements in the mantel, after which the mantel is constructed in the same way as described above.

BOUNDARY CONDITIONS AND LOADS

In the model there are two different types of boundary conditions that can be used. The first one is the fixed boundary condition, in which the movement of the boundary is set to zero in a certain direction. The second type is the prescribed boundary condition. Another possibility to make the body move is by using a body force such as gravity.

Fixed boundary conditions In the fixed boundary conditions the movement of a surface in a certain direction is set equal to zero. In the model we set the movement of the bottom of the mattress in all directions equal to zero. Besides that, the body existing of the spheres is not allowed to move in the y -direction. When only considering the downward motion we also fix the bodies in the x -direction.

Prescribed boundary conditions and body forces Using a prescribed boundary condition one can order a certain surface to move in a prescribed direction. In doing this both the direction and the magnitude of the movement has to be given. When using a body force such as gravity the user only has to specify the acceleration (so force per unit mass). In the case of gravity the acceleration is equal to 9.81 N/kg . As the unit for the force used in this project is mN , the acceleration will need to be equal to $9.81 \cdot 10^3 \text{ mN/kg}$. In this project both prescribed boundary conditions and body forces have been used to model the downward movement of the patient. Despite using gravity is more realistic, it makes the problem harder to solve. While using prescribed movement is easier to solve the effect of the boundary condition strongly depends on the surface it is linked to. For instance, forcing the outer surface of the skin to move down for a millimeter is very different from forcing the inner surface of the subcutaneous tissue to move down one millimeter. This difference can be clearly seen in Figure 2.10.

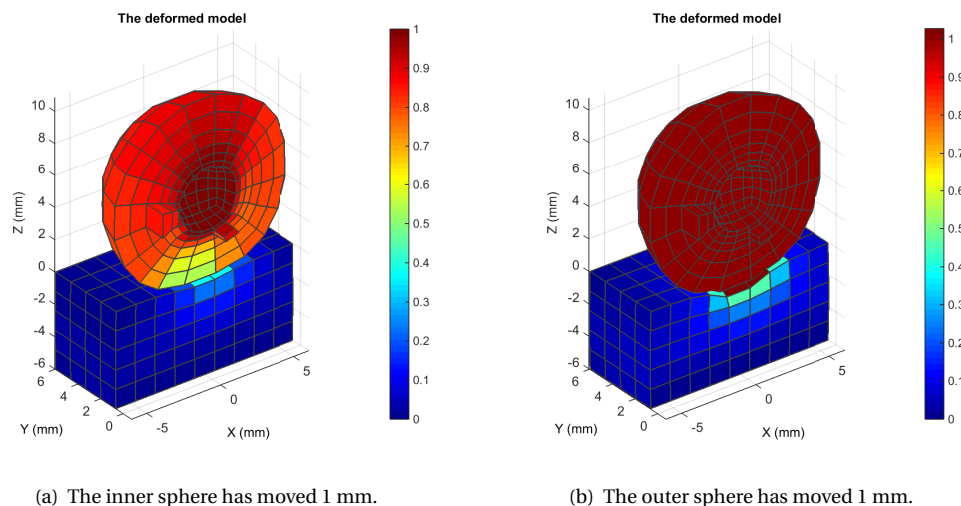


Figure 2.10: Using a prescribed boundary condition to simulate the downward motion gives different results when applied to different surfaces. The colours indicate the amount the body has moved.

It is clear that applying the boundary condition to the inner sphere results in a more deformed body, while applying it to the outer sphere results in a more deformed mattress.

Besides the downward motion of the body a sideways movement of sliding across the mattress has also been included in this project. For this the prescribed boundary condition is used, applied to the inner sphere.

Loadcurves in FEBio As mentioned before the user can specify the direction and magnitude of the movement when using a prescribed boundary condition and the magnitude when using a body force. These actions can be even further controlled by adding a loadcurve to the movements. This allows the user to determine how fast the body should move. The loadcurve simply states how much the body should have moved at a certain time point. For example one could give a boundary condition the loadcurve $[0 \ 0; \ 1 \ 0.5; \ 2 \ 1]$ and the value (magnitude) 10mm . This means that when the time starts ($t = 0$) the body should not have moved ($u = 0$). Then at the first time step the body should have moved halfway ($u = 5$) and at the second time

step ($t = 2$) the body should have moved 10mm. It is also possible to have loadcurves such as $\sin(t)$. Besides loads and boundary conditions the loadcurves can also be used for many other properties.

THE MATERIALS

FEBio offers many different materials that can be used to model the problem. These materials are subdivided into eight different groups.

1. Elastic solids
2. Viscoelastic solids
3. Multigeneration solids
4. Biphasic materials
5. Triphasic and Multiphasic materials
6. Chemical reactions
7. Rigid bodies

In this thesis only materials from the elastic solids group have been used. As was done in the article of Gefen [2] the mattress, subcutaneous tissue and the skin have been modeled using isotropic elastic materials. To use this material in FEBio the user only has to specify the Young's modulus and the Poisson's ratio. An optional parameter is the density of the material. If not specified FEBio will take this value equal to 1. In the project the following values were used.

Table 2.3: The isotropic elastic materials are completely specified by the Young's modulus, the Poisson's ratio and the density.

		The mattress	The subcutaneous tissue	The skin
Young's modulus	E (kPa)	10	2	15.2
Poisson's ratio	ν (-)	0.3	0.48	0.49
Density	ρ (kg/mm ³)	30e-9	971e-9	1100e-9

For each material FEBio has implemented its own constitutive equations describing the relation between the Cauchy stress and strain tensors. When working with isotropic elastic materials the constitutive equations are given by Hooke's Law, which is explained in Appendix A.3.

CONTACT

The most important components of this model is the contact between the human body and the mattress. This contact can be easily modeled in FEBio as they have many different options for contact problems. Similar to the materials, the different contact interfaces are divided into multiple groups.

1. Sliding interfaces
2. Biphasic contact
3. Biphasic-Solute and Multiphasic contact
4. Rigid Wall interfaces
5. Tied interfaces
6. Tied Biphasic interfaces
7. Rigid interfaces
8. Rigid joints

In the contact between a human body and a mattress we are dealing with two deformable bodies. In this thesis we are only interested in the sliding interfaces.

Within the group of sliding interfaces FEBio has defined six options depending on what the user wants.

sliding with gaps is the original implementation of sliding contact in FEBio. The contact problem is posed as a nonlinear constrained optimization problem. It uses nodal integration to integrate the contact equations.

facet-to-facet sliding is identical to *sliding with gaps* but uses a more accurate integration rule; the Gaussian quadrature. This sliding interface often converges when the above method does not.

sliding-tension-compression can be used to model problems in which separation of the contact surfaces along the direction normal to the interface needs to be prevented while still allowing tangential sliding.

sliding2 is similar to *facet-to-facet sliding* but is different in the linearization of the contact forces. This results in different stiffness matrices. As the formulation in this method is non-symmetric it will require more memory and running time. It also supports biphasic contact.

sliding3 is similar to *sliding2* but also supports biphasic-solute contact.

sliding-multiphasic is again similar to *sliding3* but supports multiphasic contact.

In this thesis only the *sliding with gaps* interface and the *facet-to-facet sliding* interface have been used. For both interfaces the user needs to specify certain information, starting with the contact surfaces of the problems. Each contact problem has a master surface and a slave surface. As stated in the user manual of FEBio:

"The slave surface is the surface over which the contact equations are integrated and on which the tractions are calculated. The master surface is used to measure the gap function and to define the necessary kinematic quantities such as surface normals and tangents." – *user manual FEBio* [22]

As one can imagine, using this definition means that the result can depend on the users choice of master and slave surface. When such problems occur FEBio offers an option that swaps the master and slave surfaces during the analysis.

Once the surfaces are defined, some properties regarding the contact need to be defined such as the penalty factor which is used to help the program enforce the contact constraints. When not defined by the user FEBio will take the default settings that are given in the user manual [22].

Currently *sliding with gaps* is the only contact in FEBio which supports friction between the two bodies. As friction is a very big part of the stress of the human body this is the main sliding interface that shall be used.

DIVIDING THE MODEL INTO STEPS

To further enhance the model FEBio has the option to let the user add time steps. The user can define boundary conditions and contact interfaces which will only hold during a specific step or during the whole analysis. In this project at least two steps are needed.

1. In the first step the patient lies down on the bed, hence the sphere will move towards the bed. This can be implemented using a prescribed boundary condition or a body force.
2. In the second step the patient is being moved across the bed due to a prescribed boundary condition. During this step, right before the patient is being moved across the bed the patient will move even further down towards the bed. This is caused by the extra weight of the caretaker.

2.4.2. ADDING THE MICROCLIMATE FACTORS TO THE BASIC MODEL

In Section 1.2.1 a mathematical model describing the effects of microclimate factors on the risk of pressure ulcers is described. To implement this model, multiple aspects need to be noted.

- The model looks at the effect of microclimate factors when the patient does not move.
- In this model only a downward force is present, not a sideways.
- Both the coefficient of friction between the body and bed and the strength of the skin change due to the microclimate factors.

- The model starts from a point where the temperature in the region of interest has stabilized.

To use the same assumptions as the mathematical model of Gefen, the new model will consist of three steps. First of all there will be a time step describing the downward motion, in which the body comes in contact with the mattress. At the end of this first step we assume that the temperature in the region of interest has stabilized and the body is at rest. In the second step the effects of the microclimate factors will be included into the model. This will be done by changing the coefficient of friction between the skin and the mattress and the strength of the skin. At the end of the second step the skin will be assumed weakest. The third step which can then be taken is the movement across the bed. Since the skin is weak at this point one will assume the stress in this step to be very high.

Step 1 Step 1 is mostly what has been shown before. A body force is applied which causes the human body represented by the sphere to move downwards towards the bed. Once in contact with the bed both the body and the mattress will deform.

Step 2 This step represents the effects of the microclimate factors. In this time the friction between the skin and the bed will change. Changing this in time is done by adding a load curve as explained in Section 2.4.1, which basically means that instead of a constant the coefficient of friction will now be time dependent. The loadcurve is equal to the function given in equation (1.8). Note that to be able to use this function the production of perspiration also needs to be calculated. The perspiration factor $\frac{\Delta V(t)}{V}$ is calculated using equation (1.7):

$$\frac{\Delta V(t)}{V} = \left[\alpha \frac{T_a - 30^\circ\text{C}}{T_a^{\max} - T_s^{\min}} + \beta \frac{T_a - T_s}{T_a^{\max} - T_s^{\min}} (1 - RH) + \gamma \right] \cdot t, \quad (2.143)$$

with t such that $0 \leq \Delta V(t)/V \leq 1$. Table 2.4 shows the values that are used in this calculation.

Table 2.4: The parameter values that are used in the calculation of the perspiration factor.

Parameters	T_a	T_s	T_a^{\max}	T_s^{\min}	α	β	γ	RH
Value	35°C	30°C	40°C	30°C	2	1	0.1	0.5

The strength of the skin as a function of the time is calculated as given in equation (1.10):

$$\tau_w^s = \left(1 - 0.8 \frac{\Delta V(t)}{V} \right) \tau_0^s, \quad (2.144)$$

with

$$\tau_0^s = 70\text{kPa}.$$

Instead of calculating the shear stress of the skin using equation (1.9) the stress will be calculated using the Finite Element Method in FEBio.

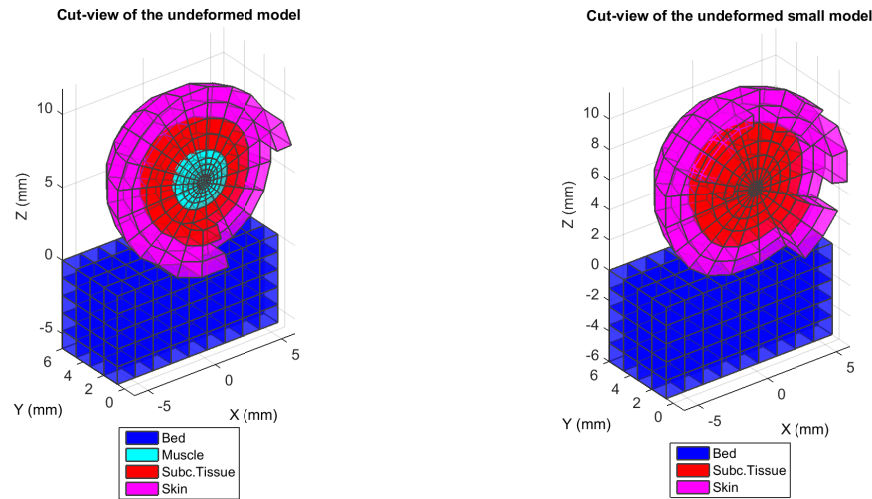
Step 3 This final step is the step in which the body will be moved across the bed.

2.4.3. FURTHER IMPROVING THE MODEL

ADDING WEIGHT TO THE MODEL

The model that has been constructed thus far only exists of a hollow sphere made up of skin and subcutaneous tissue. The stress levels that can be reached using this model are obviously not very close to the stress levels of the skin of an actual patient. To obtain results which are closer to reality more weight was therefore added to the model by simply filling (most of) the hole in the middle. Two methods can be used to achieve this.

1. The size of the hollow sphere inside the model is reduced, hence the inner radius of the sphere representing the subcutaneous tissue will be made smaller.
2. An additional sphere is added within the other spheres, representing either muscle or bone.



(a) Adding a new sphere in the center of the model.

(b) Reducing the size of the hollow sphere in the center.

Figure 2.11: Two methods are used to add weight to the model

The two methods are illustrated on the small model (model A) in Figure 2.11.

When adding a new sphere to the core of the model it can represent either muscle or bone. When modeling bone a rigid sphere can be used. When modeling muscle a special muscle material implemented in FEBio can be used.

HEAT EQUATION TO OBTAIN A VALUE FOR THE SKIN TEMPERATURE

In the article on how microclimate factors affect the risk of pressure ulcers written by Gefen [1], one of the factors that is taken into account is the temperature of the skin T_{skin} or T_s . In the article the temperature gets varied between 30 and 33 degrees Celsius as the time it takes for the stress level of the skin to reach a certain value is plotted against the skin temperature (see Figure 1.5). As the temperature of the skin is one of the variables in the formula of the strength of the skin and the formula giving the coefficient of friction a value has to be chosen to use in the model. In the previous section the chosen temperature was 30°C. Note that this value was chosen without any particular reason other than that the article mentioned the temperature would be in the range from 30°C to 33°C. To find a more accurate value of the temperature, or at least a more reasoned value, a simplified heat equation was solved for this problem.

The general heat equation that was considered for this problem is given by equation (2.145) ([21]).

$$c\rho \frac{\partial T}{\partial t} = \frac{\partial}{\partial x} \left(K_0 \frac{\partial T}{\partial x} \right) + Q \quad (2.145)$$

The different variables which occur in this equation are explained in Table 2.5.

For simplicity it is assumed that there is no heat source present, which results in $Q = 0$.

As the goal is to ascertain a value for the skin temperature a model needs to be created including boundary conditions and initial values. A small rod is being considered, taken from the sphere representing the body. This is illustrated in Figure 2.12.

The following two assumptions are made which will lead to the boundary conditions.

1. The temperature at the core of the body is a constant T_A .
2. At the other end of the rod the skin is in contact with the air. At the skin there will therefore be a process of heat transfer called convection. The temperature of the skin will therefore depend on the surrounding temperature and the heat transfer coefficient H which is the proportionality constant describing the amount of heat transfer.

Table 2.5: The variables in the heat equation

Symbol	Explanation
$T(x, t)$	The temperature at time t and position x .
$c(x)$	The specific heat. This quantity specifies the amount of heat energy that needs to be supplied to a unit mass of a substance to raise its temperature one unit.
$\rho(x)$	The mass density; the mass per unit volume
K_0	The thermal conductivity. It measures the ability of a material to conduct heat. A lower value of K_0 corresponds to a poorer conductor of heat energy.
$Q(x, t)$	Denotes the heat source. It gives the heat energy per unit volume generated per unit time.

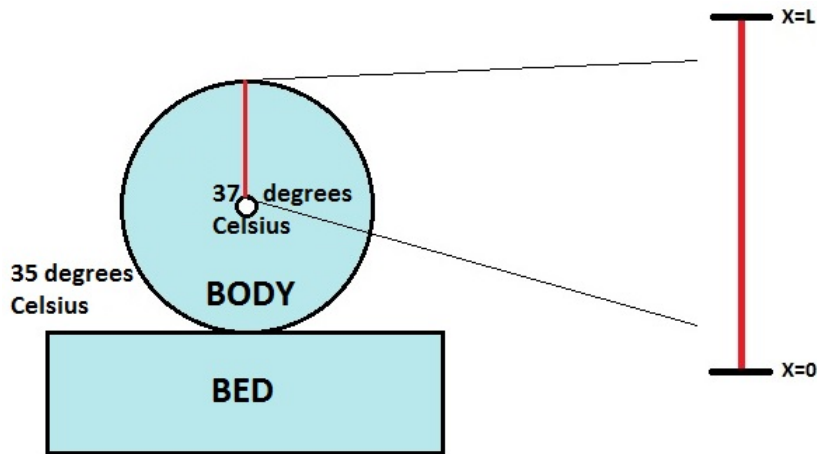


Figure 2.12: The heat equation is solved along a simple rod taken from the simplified geometry of the actual problem.

With the above two assumptions the following boundary conditions are determined.

$$T(0, t) = T_A \quad \text{A prescribed temperature} \quad (2.146a)$$

$$-K_0(L) \frac{\partial T}{\partial x}(L, t) = H [T(L, t) - T_B(t)] \quad \text{Newton's law of cooling} \quad (2.146b)$$

One final assumption that is made is that the boundary conditions are time independent (steady). The *equilibrium* or *steady-state solution* of the problem is the solution in which the temperature distribution does not depend on the time. This means that $T(x, t) = T(x)$ and hence $\frac{\partial T}{\partial t} = 0$. Searching for this solution the heat equation becomes

$$\frac{\partial}{\partial x} \left(K_0 \frac{\partial T}{\partial x} \right) = 0 \quad (2.147)$$

All the information given above leaves the following problem to be solved. As the solution is assumed to be time independent there is no need to use partial derivatives.

$$\frac{d}{dx} \left(K_0 \frac{dT}{dx} \right) = 0 \quad (2.148a)$$

$$T(0, t) = T_A \quad (2.148b)$$

$$-K_0(L) \frac{dT}{dx}(L, t) = H [T(L, t) - T_B(t)] \quad (2.148c)$$

Note that the skin temperature T_s is given by $T(L, t)$ and hence the above problem needs to be solved for $T(L, t)$.

Integrating equation (2.148a) twice and substituting the boundary conditions gives

$$T(L, t) = \frac{H L T_B(t) + K_0 T_A}{K_0 + H L}. \quad (2.149)$$

To actually determine the skin temperature the values of the variables in equation (2.149) needs to be acquired.

It is assumed that the temperature of the core of the body is equal to 37°C . As is done in the article on microclimate factors [1] the temperature of the air close to the body will be taken equal to $T_B = 35^\circ\text{C}$. The value of the thermal conductivity is retrieved from the website It's for health [24]. On this website many tissue properties are given for many different tissues among which the skin. The thermal conductivity of the skin is given to be $K_0 = 0.37 \text{ W/m}/^\circ\text{C}$.

The heat transfer coefficient H that will be used here is the heat transfer coefficient of the skin. In the article Convective and radiative heat transfer coefficients for individual human body segments [25] the convective heat transfer coefficient is given for different body parts. As the model that is created in this thesis would most likely resemble the heel of a foot the value that is chosen here is the value given for the foot. The article then offers a value for a standing person and for a seated person. In this case the value for the standing person was chosen, however this is not done for any particular reason. The value is given to be $H = 5.1 \text{ W}/\text{m}^2\text{K}$.

The used values are summarized in Table 2.6.

Table 2.6: The values in the heat equation

Variable	T_A	T_B	K_0	H	L
Value	310.15°K	308.15°K	$0.37 \text{ W}/\text{m}/^\circ\text{C}$	$5.1 \text{ W}/\text{m}^2/^\circ\text{K}$	0.180 m

Note that the unit of K_0 is $\text{W}/\text{m}/^\circ\text{C}$, which depends on $^\circ\text{C}$ while the rest of the variables use the temperature in $^\circ\text{K}$. However, as the thermal conductivity is given in W/m per $^\circ\text{C}$, it depends on the change in temperature instead of the temperature itself. As the change in temperature is the same in $^\circ\text{C}$ as it is in $^\circ\text{K}$, the difference in units does not matter in this case.

Taking the values given in the table the skin temperature is obtained as

$$T_s = T(L, t) = 308.7245^\circ\text{K} \approx 35.57^\circ\text{C}. \quad (2.150)$$

It is clear that this value is not the same as the 30°C that was used before, and it is not even in the range of $30 - 33^\circ\text{C}$.

Note that the heat equation that was solved here is a very simple equation, applied to a very simple model. Besides this, we also solved the steady state problem, which in real life will not actually occur. Another point that should be noted is that the values of the heat transfer rate and the heat conductivity might not be accurate. There are many articles describing these values, and many different values are mentioned.

CHANGING THE YOUNG'S MODULUS OF THE SKIN

In adding microclimate factors to the model, two factors have actually been added. First of all the strength of the skin is included in the model, which is time dependent. Secondly the coefficient of friction between the skin and the mattress is made time dependent, such that the longer the patient is at rest in the bed the more coefficient will increase. An element which is not included is the effect of the sweat on the skin itself. As it is well known, the skin does actually change when exposed to fluids for a longer period of time (think for instance of taking a bath during which the skin of your fingers get wrinkled).

In the model the change in the skin resulting from the sweating will be modeled by making the Young's modulus of the skin E , which defines the elasticity of the skin, a time dependent factor. The method of changing the Young's modulus comes from the article describing the finite element method for the contact between the human body and a mattress written by Gefen [2]. In this article it is stated that the Young's modulus of the skin depends on the age of the patient and whether or not the patient is healthy. In the article three different values of the Young's modulus are mentioned; 15.2, 50 and 100 kPa, in which the higher value corresponds to a stiffer skin. As it is known that the skin becomes stiffer when exposed to water for a period of time, it is a reasonable start to use these values. To ensure the elastic modulus changes through time, a loading curve is linked to the value. A loading curve shall be attached corresponding to the values in Table 2.7.

Table 2.7: The loadcurve describing the Young's modulus

Time t (s)	0	1	1.5	2
Young's modulus E (kPa)	15.2	15.2	50	100

3

THE NUMERICAL METHOD: NEWTON RAPHSON

The problem stated in Chapter 2 is solved in FEBio using a numerical method called the Newton-Raphson Method, combined with the Finite Element Method. This chapter will discuss how exactly FEBio solves the given problem and how the Newton-Raphson method works.

3.1. THE GENERAL NEWTON-RAPHSON METHOD

One of the most common methods to solve nonlinear equations of the form $\mathcal{F}(\mathbf{x}) = 0$ is called the Newton-Raphson method. This method, simply known as the Newton method, is an iterative method in which the function is linearized using the (directional) derivative, after which the solution is approached by starting with an initial guess \mathbf{x}_0 and then updating this guess. In other words, consider an initial guess \mathbf{x}_0 and a general change or increment \mathbf{u} for which hopefully $\mathbf{x} = \mathbf{x}_0 + \mathbf{u}$ is a little closer to the real solution. To fully explain the method we shall start off by explaining the problem when working with one degree of freedom. The information in this section closely follows the derivation given in [17].

3.1.1. ONE DEGREE OF FREEDOM

Consider a one-degree-of-freedom nonlinear equation

$$f(x) = 0. \quad (3.1)$$

The Newton method starts by making an initial guess of the solution x_0 . In the neighborhood of this guess the function $f(x)$ can be expressed using a Taylor's series, giving the following.

$$f(x) = f(x_0) + \left. \frac{df}{dx} \right|_{x_0} (x - x_0) + \frac{1}{2} \left. \frac{d^2f}{dx^2} \right|_{x_0} (x - x_0)^2 + \dots \quad (3.2)$$

Defining u as the increment in x ($u = (x - x_0)$) we can linearize the above equation by truncating the Taylor's expression and obtain

$$f(x) \approx f(x_0) + \left. \frac{df}{dx} \right|_{x_0} u. \quad (3.3)$$

Note that this is a linear function in u . The derivative in the above equation is more commonly expressed as

$$Df(x_0)[u] = \left. \frac{df}{dx} \right|_{x_0} u \approx f(x_0 + u) - f(x_0), \quad (3.4)$$

where $Df(x_0)[u]$ denotes a derivative of f at x_0 operating on u .

As the goal is to solve $f(x) = 0$, the Newton-Raphson method requires $f(x_k + u)$ to converge to zero and hence vanish. Using this the linear equation (3.3) becomes

$$f(x_k) + Df(x_k)[u] = 0. \quad (3.5)$$

Now realizing that u is defined as the increment in x , the new value x_{k+1} can be obtained by calculating u . The Newton-Raphson method for problems with one degree of freedom can therefore be given as in equation (3.6). This method is also illustrated in Figure 3.1.

$$u = [-Df(x_k)]^{-1} f(x_k) = \left[-\frac{df}{dx} \Big|_{x_k} \right]^{-1} f(x_k): \quad x_{k+1} = x_k + u. \quad (3.6)$$

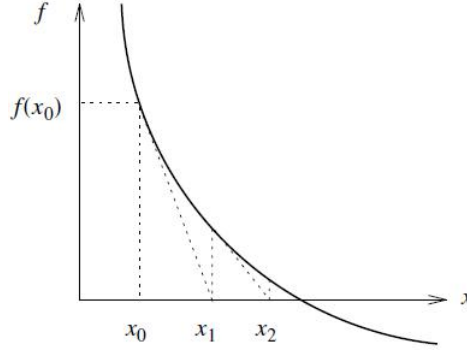


Figure 3.1: Solving the one-degree-of-freedom nonlinear problem $f(x) = 0$ using Newton-Raphson. Source: [17].

3.1.2. THE GENERAL SOLUTION

Having looked at the simple one-degree-of-freedom case we shall now look at the more general problem with more degrees of freedom.

Instead of solving $f(x) = 0$ we now want to solve

$$\mathcal{F}(\mathbf{x}) = 0 \quad (3.7)$$

where the function $\mathcal{F}(\mathbf{x})$ can represent anything with multiple degrees of freedom. Think for instance of a system of nonlinear (differential) equations. Note that the unknowns \mathbf{x} could also be sets of functions, which makes the problem even more complicated.

When starting to solve the problem given in equation (3.7) we again start with an initial guess \mathbf{x}_0 . Taking an increment \mathbf{u} , a new $\mathbf{x} = \mathbf{x}_0 + \mathbf{u}$ is generated which hopefully is closer to the actual solution.

In the problem with one-degree-of-freedom the function was expressed in the neighborhood of the guess using a Taylor's series. The difficult part in the current problem is expressing the derivative of \mathcal{F} with respect to \mathbf{x} which could itself be a function. This difficulty is managed by introducing a single artificial parameter ϵ with which a nonlinear function \mathbf{F} in ϵ can be established as

$$\mathbf{F}(\epsilon) = \mathcal{F}(\mathbf{x}_0 + \epsilon \mathbf{u}). \quad (3.8)$$

Note that $\mathbf{F}(\epsilon) \neq \mathcal{F}(\mathbf{x})$.

Having defined $\mathbf{F}(\epsilon)$ we can express this function with a Taylor's series about $\epsilon = 0$, where $\mathbf{x} = \mathbf{x}_0$. We obtain

$$\mathbf{F}(\epsilon) = \mathbf{F}(0) + \frac{d\mathbf{F}}{d\epsilon} \Big|_{\epsilon=0} \epsilon + \frac{1}{2} \frac{d^2\mathbf{F}}{d\epsilon^2} \Big|_{\epsilon=0} \epsilon^2 + \dots \quad (3.9)$$

Using the definition of $\mathbf{F}(\epsilon)$ this expression can be rewritten as an expression in \mathcal{F} .

$$\mathcal{F}(\mathbf{x}_0 + \epsilon \mathbf{u}) = \mathcal{F}(\mathbf{x}_0) + \epsilon \frac{d}{d\epsilon} \Big|_{\epsilon=0} \mathcal{F}(\mathbf{x}_0 + \epsilon \mathbf{u}) + \frac{\epsilon^2}{2} \frac{d^2}{d\epsilon^2} \Big|_{\epsilon=0} \mathcal{F}(\mathbf{x}_0 + \epsilon \mathbf{u}) + \dots \quad (3.10)$$

Now it is possible for us to obtain the change in the nonlinear function $\mathcal{F}(\mathbf{x})$ by simply truncating this Taylor's series. We get

$$\mathcal{F}(\mathbf{x}_0 + \epsilon \mathbf{u}) - \mathcal{F}(\mathbf{x}_0) = \epsilon \left. \frac{d}{d\epsilon} \right|_{\epsilon=0} \mathcal{F}(\mathbf{x}_0 + \epsilon \mathbf{u}). \quad (3.11)$$

As we introduced ϵ as an artificial parameter we can now eliminate it from the equation. We can do this by taking $\epsilon = 1$ and thereby obtaining

$$\mathcal{F}(\mathbf{x}_0 + \epsilon \mathbf{u}) - \mathcal{F}(\mathbf{x}_0) \approx 1 \left. \frac{d}{d\epsilon} \right|_{\epsilon=0} \mathcal{F}(\mathbf{x}_0 + \epsilon \mathbf{u}). \quad (3.12)$$

It can now be observed that the right side of this equation is in fact the directional derivative of $\mathcal{F}(\mathbf{x})$ at \mathbf{x}_0 in the direction of \mathbf{u} . Using this and adding $\mathcal{F}(\mathbf{x}_0)$ to both sides of the equation we can rewrite equation (3.12) as

$$\mathcal{F}(\mathbf{x}_0 + \epsilon \mathbf{u}) \approx \mathcal{F}(\mathbf{x}_0) + D\mathcal{F}(\mathbf{x}_0)[\mathbf{u}]. \quad (3.13)$$

As we want to solve $\mathcal{F}(\mathbf{x}) = 0$ we would like $\mathcal{F}(\mathbf{x}_0 + \epsilon \mathbf{u})$ to vanish, hence giving us

$$\mathcal{F}(\mathbf{x}_0) + D\mathcal{F}(\mathbf{x}_0)[\mathbf{u}] = 0. \quad (3.14)$$

The equation above is linear with respect to \mathbf{u} , which means that we can now establish the general Newton-Raphson method.

The Newton-Raphson method:

$$D\mathcal{F}(\mathbf{x}_k)[\mathbf{u}] = -\mathcal{F}(\mathbf{x}_k) : \quad \mathbf{x}_{k+1} = \mathbf{x}_k + \mathbf{u} \quad (3.15)$$

3.2. APPLYING THE NEWTON-RAPHSON METHOD TO THE PROBLEM WITHOUT CONTACT

The problem we want to solve using the Newton-Raphson method is the virtual work equation (2.85):

$$\delta W(\boldsymbol{\phi}, \delta \mathbf{v}) = \int_v \boldsymbol{\sigma} : \delta \mathbf{d} dv - \int_v \mathbf{b} \cdot \delta \mathbf{v} dv - \int_{\partial v} \mathbf{t} \cdot \delta \mathbf{v} da = 0. \quad (3.16)$$

Here $\boldsymbol{\phi}$ is the configuration and $\delta \mathbf{v}$ the virtual velocity.

Using the Newton-Raphson method the solution to equation (3.16) shall be found by iteratively solving

$$\delta W(\boldsymbol{\phi}_k, \delta \mathbf{v}) + D\delta W(\boldsymbol{\phi}_k, \delta \mathbf{v})[\mathbf{u}] = 0. \quad (3.17)$$

Note that the trial solution will now be a trial configuration $\boldsymbol{\phi}_k$.

In order to solve the problem using this method, several steps have to be taken.

1. The virtual work equation needs to be linearized, i.e. the directional derivative of $\delta W(\boldsymbol{\phi}, \delta \mathbf{v})$ needs to be derived. This is done in Section 3.2.1.
2. The virtual work equation needs to be discretized. This is done in Section 3.2.2.
3. The linearized virtual work equation needs to be discretized, which is done in Section 3.2.3.
4. The Newton-Raphson scheme has to be formulated. This final step is shown in Section 3.2.4.

3.2.1. LINEARIZATION OF THE VIRTUAL WORK

The directional derivative that needs to be calculated in order to linearize is in fact the directional derivative of the virtual work equation at a configuration $\boldsymbol{\phi}_k$ in the direction of \mathbf{u} . Simply put this means that the directional derivative $D\delta W(\boldsymbol{\phi}_k, \delta \mathbf{v})[\mathbf{u}]$ is the change in δW caused by the changing of $\boldsymbol{\phi}_k$ into $\boldsymbol{\phi}_k + \mathbf{u}$. During this change the virtual velocity $\delta \mathbf{v}$ has to remain constant.

Finding the directional derivative of the virtual work equation will be done in two parts, as the virtual work equation can be divided into two components: the internal and external virtual work. Here

$$\delta W_{int}(\boldsymbol{\phi}, \delta \mathbf{v}) = \int_v \boldsymbol{\sigma} : \delta \mathbf{d} dv, \quad (3.18a)$$

$$\delta W_{ext}(\boldsymbol{\phi}, \delta \mathbf{v}) = \int_v \mathbf{b} \cdot \delta \mathbf{v} dv + \int_{\partial v} \mathbf{t} \cdot \delta \mathbf{v} da, \quad (3.18b)$$

$$D\delta W(\boldsymbol{\phi}_k, \delta \mathbf{v})[\mathbf{u}] = D\delta W_{int}(\boldsymbol{\phi}_k, \delta \mathbf{v})[\mathbf{u}] - D\delta W_{ext}(\boldsymbol{\phi}_k, \delta \mathbf{v})[\mathbf{u}]. \quad (3.18c)$$

THE DIRECTIONAL DERIVATIVE OF THE INTERNAL VIRTUAL WORK

To determine the directional derivative of the internal virtual work equation we will use the material form of the virtual work. We do this as it is more convenient due to the fact that the initial elemental volume dV is constant during the linearization [17]. Once formulated, the directional derivative shall be transformed into the spatial form.

In the material form the internal virtual work component is given by equation (2.92):

$$\delta W_{int}(\boldsymbol{\phi}, \delta \mathbf{v}) = \int_V \mathbf{P} : (\nabla \delta \mathbf{V}) dV, \quad (3.19)$$

or, equally, by equation (2.102c):

$$\delta W_{int}(\boldsymbol{\phi}, \delta \mathbf{v}) = \int_V \mathbf{S} : \delta \dot{\mathbf{E}} dV. \quad (3.20)$$

In deriving the directional derivative the latter formulation shall be used.

Calculating the directional derivative we will use the product rule for the directional derivative which states that if $\mathcal{F}(\mathbf{x}) = \mathcal{F}_1(\mathbf{x}) \cdot \mathcal{F}_2(\mathbf{x})$, then

$$D\mathcal{F}(\mathbf{x}_0)[\mathbf{u}] = D\mathcal{F}_1(\mathbf{x}_0)[\mathbf{u}] \cdot \mathcal{F}_2(\mathbf{x}_0) + \mathcal{F}_1(\mathbf{x}_0) \cdot D\mathcal{F}_2(\mathbf{x}_0)[\mathbf{u}]. \quad (3.21)$$

Using this we obtain

$$D\delta W_{int}(\boldsymbol{\phi}, \delta \mathbf{v})[\mathbf{u}] = \int_V D(\delta \dot{\mathbf{E}} : \mathbf{S})[\mathbf{u}] dV \quad (3.22)$$

$$= \int_V \delta \dot{\mathbf{E}} : D\mathbf{S}[\mathbf{u}] dV + \int_V \mathbf{S} : D\delta \dot{\mathbf{E}}[\mathbf{u}] dV. \quad (3.23)$$

The first part that will be discussed is the directional derivative of \mathbf{S} .

In order to obtain this directional derivative, a different definition of the stress must first be given. Working with elastic materials, the constitutive behavior is only dependent on the current state of deformation. In this conditions any stress measure at a particle \mathbf{X} is the function of the current deformation gradient \mathbf{F} corresponding to this particle.

In this situation, elasticity can be expressed as

$$\mathbf{P} = \mathbf{P}(\mathbf{F}(\mathbf{X}), \mathbf{X}). \quad (3.24)$$

The direct dependency upon \mathbf{X} allows for the possible inhomogeneity of the material.

A material is termed *hyperelastic* when the work done by the stresses during a deformation process is dependent only on the initial state at time t_0 and the final configuration at time t . The behavior of the material is said to be path-independent in this case [17]. Working with path-independent behavior and noting that the PK1 stress \mathbf{P} is work conjugate with the rate of deformation gradient $\dot{\mathbf{F}}$, an *elastic potential* W per unit undeformed volume can be established as the work done by the stresses from the initial to the current position as [17]

$$W(\mathbf{F}(\mathbf{X}), \mathbf{X}) = \int_{t_0}^t \mathbf{P}(\mathbf{F}(\mathbf{X}), \mathbf{X}) : \dot{\mathbf{F}} dt, \quad (3.25a)$$

$$\dot{W} = \mathbf{P} : \dot{\mathbf{F}}. \quad (3.25b)$$

Assuming it is possible to construct $W(\mathbf{F}, \mathbf{X})$ defining a material [17], the rate of change of the potential can alternatively be given as

$$\dot{W} = \sum_{i,j=1}^3 \frac{\partial W}{\partial F_{ij}} \dot{F}_{ij}, \quad (3.26)$$

from which it follows that the PK1 stress tensor can be written as

$$\mathbf{P}(\mathbf{F}(\mathbf{X}), \mathbf{X}) = \frac{\partial W(\mathbf{F}(\mathbf{X}), \mathbf{X})}{\partial \mathbf{F}}. \quad (3.27)$$

Since second-order tensors such as stress and strain that are used to describe the material behavior must be objective, it follows that W must remain invariant when the current configuration undergoes a rigid body rotation. This implies that W depends on \mathbf{F} only via the stretch component \mathbf{U} and is independent of the rotation component \mathbf{R} . Instead of expressing W as a function of \mathbf{U} , the potential shall be given as a function of the right Cauchy-Green deformation tensor \mathbf{C} , which is defined as $\mathbf{C} = \mathbf{U}^2 = \mathbf{F}^T \mathbf{F}$. The potential is written as

$$W(\mathbf{F}(\mathbf{X}), \mathbf{X}) = W(\mathbf{C}(\mathbf{X}), \mathbf{X}). \quad (3.28)$$

It follows that

$$\dot{W} = \frac{\partial W}{\partial \mathbf{C}} : \dot{\mathbf{C}} = \frac{1}{2} \mathbf{S} : \dot{\mathbf{C}} \quad (3.29a)$$

$$\mathbf{S}(\mathbf{C}(\mathbf{X}), \mathbf{X}) = 2 \frac{\partial W}{\partial \mathbf{C}} = \frac{\partial W}{\partial \mathbf{E}}. \quad (3.29b)$$

With the definition of the second Piola-Kirchhoff stress given in equation (3.29b) the directional derivative can be obtained as

$$\begin{aligned} DS_{IJ}[\mathbf{u}] &= \left. \frac{d}{d\epsilon} \right|_{\epsilon=0} S_{IJ}(E_{KL}[\boldsymbol{\phi} + \epsilon \mathbf{u}]) \\ &= \sum_{K,L=1}^3 \frac{\partial S_{IJ}}{\partial E_{KL}} \left. \frac{d}{d\epsilon} \right|_{\epsilon=0} E_{KL}[\boldsymbol{\phi} + \epsilon \mathbf{u}] \\ &= \sum_{K,L=1}^3 \frac{\partial S_{IJ}}{\partial E_{KL}} DE_{KL}[\mathbf{u}]. \end{aligned} \quad (3.30)$$

More concisely:

$$D\mathbf{S}[\mathbf{u}] = \mathcal{C} : D\mathbf{E}[\mathbf{u}], \quad (3.31)$$

where \mathcal{C} is the symmetric fourth-order tensor known as the *Lagrangian* or *material elasticity tensor*, defined as [17]

$$\mathcal{C} = \frac{\partial \mathbf{S}}{\partial \mathbf{E}} = 2 \frac{\partial \mathbf{S}}{\partial \mathbf{C}}. \quad (3.32)$$

Having obtained the directional derivative of the second Piola-Kirchhof stress tensor we can continue deriving the directional derivative of the virtual work equation. Substituting the directional derivative of \mathbf{S} , given in equation (3.31), into equation (3.23) obtains

$$D\delta W_{int}(\boldsymbol{\phi}, \delta \mathbf{v})[\mathbf{u}] = \int_V \delta \dot{\mathbf{E}} : \mathcal{C} : D\mathbf{E}[\mathbf{u}] dV + \int_V \mathbf{S} : D\delta \dot{\mathbf{E}}[\mathbf{u}] dV. \quad (3.33)$$

It should be noted that the first integrand holds since the material elasticity tensor \mathcal{C} is a fourth-order tensor. By definition the double contraction of a fourth-order tensor with a second order tensor gives a second-order tensor¹ [17].

Starting with the expression $D\mathbf{E}[\mathbf{u}]$ the definition $\bar{\mathbf{E}} = \frac{1}{2}(\mathbf{F}^T \mathbf{F} - \mathbf{I})$ will be used. Applying the product rule of the directional derivative it can be given as

$$D\mathbf{E}[\mathbf{u}] = \frac{1}{2}(\mathbf{F}^T D\mathbf{F}[\mathbf{u}] + D\mathbf{F}^T[\mathbf{u}]\mathbf{F}). \quad (3.34)$$

It is clear that in order to obtain this directional derivative, the directional derivative of the deformation gradient \mathbf{F} has to be known. To get this derivative consider a small displacement $\mathbf{u}(\mathbf{x})$ from the deformed configuration given by $\mathbf{x} = \boldsymbol{\phi}_t(\mathbf{X}) = \boldsymbol{\phi}(\mathbf{X}, t)$. The directional derivative of \mathbf{F} in the direction of \mathbf{u} can be derived as [17]

$$\begin{aligned} D\mathbf{F}(\boldsymbol{\phi}_t)[\mathbf{u}] &= \left. \frac{d}{d\epsilon} \right|_{\epsilon=0} \mathbf{F}(\boldsymbol{\phi}_t + \epsilon \mathbf{u}) \\ &= \left. \frac{d}{d\epsilon} \right|_{\epsilon=0} \frac{\partial(\boldsymbol{\phi}_t + \epsilon \mathbf{u})}{\partial \mathbf{X}} \\ &= \left. \frac{d}{d\epsilon} \right|_{\epsilon=0} \left(\frac{\partial \boldsymbol{\phi}_t}{\partial \mathbf{X}} + \frac{\epsilon \mathbf{u}}{\partial \mathbf{X}} \right) \\ &= \frac{\partial \mathbf{u}}{\partial \mathbf{X}} \\ &= (\nabla \mathbf{u})\mathbf{F}. \end{aligned} \quad (3.35)$$

Using this, the Green strain can be linearized at the deformed configuration in the direction of \mathbf{u} as

$$\begin{aligned} D\mathbf{E}[\mathbf{u}] &= \frac{1}{2}(\mathbf{F}^T D\mathbf{F}[\mathbf{u}] + D\mathbf{F}^T[\mathbf{u}]\mathbf{F}) \\ &= \frac{1}{2}(\mathbf{F}^T \nabla \mathbf{u} \mathbf{F} + \mathbf{F}^T (\nabla \mathbf{u})^T \mathbf{F}) \\ &= \frac{1}{2} \mathbf{F}^T (\nabla \mathbf{u} + (\nabla \mathbf{u})^T) \mathbf{F} \\ &= \frac{1}{2} \mathbf{F}^T \boldsymbol{\epsilon} \mathbf{F}. \end{aligned} \quad (3.36)$$

Here $\boldsymbol{\epsilon}$ is the small strain tensor defined by

$$\boldsymbol{\epsilon} = \frac{1}{2}(\nabla \mathbf{u} + (\nabla \mathbf{u})^T). \quad (3.37)$$

¹The double contraction of a fourth-order tensor \mathcal{C} with a second-order tensor is defined as

$$\mathcal{C} : (\mathbf{u} \otimes \mathbf{v}) = (\mathcal{C} \mathbf{v})\mathbf{u},$$

and hence yields a second-order tensor.

The other directional derivative that needs to be formed is $D\delta\dot{\mathbf{E}}[\mathbf{u}]$. For this the definition of $\dot{\mathbf{E}}$ is used together with the fact that $\delta\dot{\mathbf{E}}$ is a function of $\delta\mathbf{v}$ and the configuration ϕ , which gives

$$\delta\dot{\mathbf{E}} = \frac{1}{2} \left(\delta\dot{\mathbf{F}}^T \mathbf{F} + \mathbf{F}^T \delta\dot{\mathbf{F}} \right), \quad (3.38)$$

where [17]

$$\delta\dot{\mathbf{F}} = \frac{\partial \delta\mathbf{v}}{\partial \mathbf{X}} = \nabla_0 \delta\mathbf{v}. \quad (3.39)$$

Note that the directional derivative of \mathbf{F} in the direction of \mathbf{u} , when \mathbf{u} is given as a function of the initial position of the body particles \mathbf{X} , is given by

$$D\mathbf{F}[\mathbf{u}] = \frac{\partial \mathbf{u}(\mathbf{X})}{\partial \mathbf{X}} = \nabla_0 \mathbf{u}, \quad (3.40)$$

where ∇_0 indicates the gradient with respect to the coordinates at the initial configuration.

Using this equation (3.38) becomes

$$D\delta\dot{\mathbf{E}} = \frac{1}{2} \left((\nabla_0 \delta\mathbf{v})^T \nabla_0 \mathbf{u} + (\nabla_0 \mathbf{u})^T \nabla_0 \delta\mathbf{v} \right). \quad (3.41)$$

Since the virtual velocities $\delta\mathbf{v}$ are not a function of the configuration, the term $\nabla_0 \delta\mathbf{v}$ remains constant. With this observation and noting the symmetry of \mathbf{S} , the linearized principle of virtual work in the material or Lagrangian form can be given as

$$D\delta W_{int}(\phi, \delta\mathbf{v})[\mathbf{u}] = \int_V \delta\dot{\mathbf{E}} : \mathcal{C} : D\mathbf{E}[\mathbf{u}] dV + \int_V \mathbf{S} : ((\nabla_0 \mathbf{u})^T \nabla_0 \delta\mathbf{v}) dV. \quad (3.42)$$

Using the fact that $\delta\dot{\mathbf{E}}$ can be expressed as $D\mathbf{E}[\delta\mathbf{v}]^2$, equation (3.42) can be rewritten to the final symmetric form [17]

$$D\delta W_{int}(\phi, \delta\mathbf{v})[\mathbf{u}] = \int_V D\mathbf{E}[\delta\mathbf{v}] : \mathcal{C} : D\mathbf{E}[\mathbf{u}] dV + \int_V \mathbf{S} : ((\nabla_0 \mathbf{u})^T \nabla_0 \delta\mathbf{v}) dV. \quad (3.43)$$

Equation (3.43) now gives the linearized internal virtual work in the material form. The next step is to transform this back to the spatial form, which will lead to much simplification. The following relationships shall be used to express the materially based quantities in terms of spatially based quantities.

$$D\mathbf{E}[\mathbf{u}] = \phi_*^{-1} [\boldsymbol{\varepsilon}] = \mathbf{F}^T \boldsymbol{\varepsilon} \mathbf{F} \quad \boldsymbol{\varepsilon} = \frac{1}{2} (\nabla \mathbf{u} + (\nabla \mathbf{u})^T) \quad (3.44a)$$

$$D\mathbf{E}[\delta\mathbf{v}] = \phi_*^{-1} [\delta\mathbf{d}] = \mathbf{F}^T \delta\mathbf{d} \mathbf{F} \quad \delta\mathbf{d} = \frac{1}{2} (\nabla \delta\mathbf{v} + (\nabla \delta\mathbf{v})^T) \quad (3.44b)$$

$$J\boldsymbol{\sigma} = \phi_* [\mathbf{S}] = \mathbf{F} \mathbf{S} \mathbf{F}^T \quad (3.44c)$$

$$JdV = dv \quad (3.44d)$$

$$J\mathbf{c} = \phi_* [\mathcal{C}] \quad Jc_{ijkl} = \sum_{I,J,K,L=1}^3 F_{iI} F_{jJ} F_{kK} F_{lL} \mathcal{C}_{IJKL} \quad (3.44e)$$

With these transformations the first integrand of equation (3.43) can be expressed in the spatial form as

$$D\mathbf{E}[\delta\mathbf{v}] : \mathcal{C} : D\mathbf{E}[\mathbf{u}] = \delta\mathbf{d} : \mathbf{c} : \boldsymbol{\varepsilon} dv, \quad (3.45)$$

where \mathbf{c} is the fourth-order *spatial elasticity tensor*.

In the second integrand the gradient ∇_0 appears, which is the gradient with respect to the initial particle coordinates. Using equation (3.35) these terms can be related to the spatial gradient.

$$\nabla_0 \mathbf{u} = (\nabla \mathbf{u}) \mathbf{F} \quad (3.46a)$$

$$\nabla_0 \delta\mathbf{v} = (\nabla \delta\mathbf{v}) \mathbf{F} \quad (3.46b)$$

²It is known that $D\mathbf{E}[\mathbf{u}] = \frac{1}{2} \mathbf{F}^T [\nabla \mathbf{u} + (\nabla \mathbf{u})^T] \mathbf{F}$, and hence $D\mathbf{E}[\delta\mathbf{v}] = \frac{1}{2} \mathbf{F}^T [\nabla \delta\mathbf{v} + (\nabla \delta\mathbf{v})^T] \mathbf{F}$. From the definition $\nabla \delta\mathbf{v} = \delta\mathbf{l}$ it follows that $D\mathbf{E}[\delta\mathbf{v}] = \frac{1}{2} \mathbf{F}^T [\delta\mathbf{l} + (\delta\mathbf{l})^T] \mathbf{F}$. Considering the definition $\dot{\mathbf{E}} = \mathbf{F}^T \mathbf{d} \mathbf{F}$, it is clear to see that $\delta\dot{\mathbf{E}} = \mathbf{F}^T \delta\mathbf{d} \mathbf{F}$. Using the definition of $\mathbf{d} = \frac{1}{2} (\mathbf{l} + \mathbf{l}^T)$, it is clear that $\delta\mathbf{d} = \frac{1}{2} (\delta\mathbf{l} + \delta\mathbf{l}^T)$. Substituting this into $\delta\dot{\mathbf{E}}$ gives $\delta\dot{\mathbf{E}} = \mathbf{F}^T (\frac{1}{2} (\delta\mathbf{l} + \delta\mathbf{l}^T)) \mathbf{F} = \frac{1}{2} \mathbf{F}^T [\delta\mathbf{l} + (\delta\mathbf{l})^T] \mathbf{F}$, hence $\delta\dot{\mathbf{E}} = D\mathbf{E}[\mathbf{u}]$.

Using these expressions and the transformations given before the second integrand can be re-expressed in a spatial framework as

$$\mathbf{S} : ((\nabla_0 \mathbf{u})^T \nabla_0 \delta \mathbf{v}) = \boldsymbol{\sigma} : [((\nabla \mathbf{u})^T \nabla \delta \mathbf{v})] dv. \quad (3.47)$$

Combining equations (3.45) and (3.47) now gives the linearized internal virtual work equation (3.43) as

The spatial or Eulerian linearized equilibrium equations

$$D\delta W_{int}(\boldsymbol{\phi}, \delta \mathbf{v})[\mathbf{u}] = \int_V \delta \mathbf{d} : \mathbf{c} : \boldsymbol{\varepsilon} dv + \int_V \boldsymbol{\sigma} : [((\nabla \mathbf{u})^T \nabla \delta \mathbf{v})] dv. \quad (3.48)$$

A final observation that can be made regarding this equation is the fact that this linearized virtual work equation is symmetric in $\delta \mathbf{v}$ and \mathbf{u} , that is,

$$D\delta W_{int}(\boldsymbol{\phi}, \delta \mathbf{v})[\mathbf{u}] = D\delta W_{int}(\boldsymbol{\phi}, \mathbf{u})[\delta \mathbf{v}]. \quad (3.49)$$

This symmetry is due to the identical functional relationship between $\delta \mathbf{d}$ and $\delta \mathbf{v}$ and $\boldsymbol{\varepsilon}$ and \mathbf{u} and the symmetry of \mathbf{c} and $\boldsymbol{\sigma}$. The symmetry of the directional derivative will result in a symmetric tangent stiffness matrix in the discretization step.

THE DIRECTIONAL DERIVATIVE OF THE EXTERNAL VIRTUAL WORK

Now that the internal virtual work has been linearized the next step is to linearize the external virtual work. Recall that the external virtual work is given by equation (3.18b):

$$\delta W_{ext}(\boldsymbol{\phi}, \delta \mathbf{v}) = \int_V \mathbf{b} \cdot \delta \mathbf{v} dv + \int_a \mathbf{t} \cdot \delta \mathbf{v} da. \quad (3.50)$$

Note that there are contributions from body forces \mathbf{b} and surface tractions \mathbf{t} . In the linearization of the external virtual work these two cases shall be considered separately, starting with the body forces.

The most common example of a body force, and also the type that is used in this project, is the gravity loading $\mathbf{b} = \rho \mathbf{g}$. Here ρ is the density and \mathbf{g} is the acceleration due to gravity. By performing a pull back on the body force component in equation (3.50), it is easy to show that the loading is not deformation-dependent, which causes the directional derivative to vanish. To see this note that the current density ρ can be written in terms of the initial density as $\rho = \rho_0 / J$ [17]. Substituting this into equation (3.50) the first integrand becomes

$$\delta W_{ext}^{\mathbf{b}}(\boldsymbol{\phi}, \delta \mathbf{v}) = \int_V \frac{\rho_0}{J} \mathbf{g} \cdot \delta \mathbf{v} dv = \int_V \rho_0 \mathbf{g} \cdot \delta \mathbf{v} dV. \quad (3.51)$$

As none of the terms in this expression depend on the current configuration the linearization is superfluous;

$$D\delta W_{ext}^{\mathbf{b}}(\boldsymbol{\phi}, \delta \mathbf{v})[\mathbf{u}] = 0. \quad (3.52)$$

Considering the surface forces this section will only discuss the case of uniform normal pressure. Assuming an applied uniform pressure p acting on a surface a having a pointwise normal \mathbf{n} , the traction force can be written as $\mathbf{t} = p\mathbf{n}$. The virtual work component becomes

$$\delta W_{ext}^p(\boldsymbol{\phi}, \delta \mathbf{v}) = \int_a p \mathbf{n} \cdot \delta \mathbf{v} da. \quad (3.53)$$

In this expression the magnitude of the area element and the orientation of the normal both depend on the displacement. Any deformation therefore results in a change in the equilibrium condition and the emergence of a stiffness term [17]. The expression needs to be linearized which will be done using an arbitrary parametrization of the surface as shown in Figure 3.2.

In terms of the parametrization one can write the normal and area elements in terms of the tangent vectors $\frac{\partial \mathbf{x}}{\partial \xi}$ and $\frac{\partial \mathbf{x}}{\partial \eta}$.

$$\mathbf{n} = \frac{\frac{\partial \mathbf{x}}{\partial \xi} \times \frac{\partial \mathbf{x}}{\partial \eta}}{\left\| \frac{\partial \mathbf{x}}{\partial \xi} \times \frac{\partial \mathbf{x}}{\partial \eta} \right\|} \quad (3.54a)$$

$$da = \left\| \frac{\partial \mathbf{x}}{\partial \xi} \times \frac{\partial \mathbf{x}}{\partial \eta} \right\| d\xi d\eta \quad (3.54b)$$

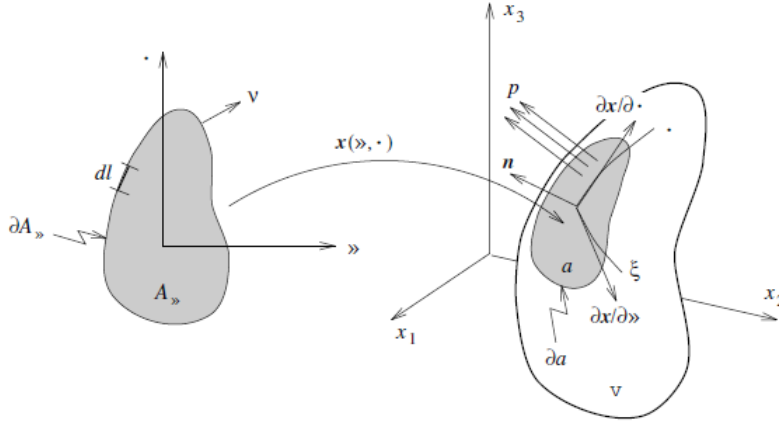


Figure 3.2: The linearization of the external virtual work is done using an arbitrary parametrization of the surface. Source: [17].

With these expressions equation (3.53) can be expressed in the parameter plane as

$$\delta W_{ext}^p(\boldsymbol{\phi}, \delta \mathbf{v}) = \int_{A_\xi} p \delta \mathbf{v} \cdot \left(\frac{\partial \mathbf{x}}{\partial \xi} \times \frac{\partial \mathbf{x}}{\partial \eta} \right) d\xi d\eta. \quad (3.55)$$

Here only the vectors $\frac{\partial \mathbf{x}}{\partial \xi}$ and $\frac{\partial \mathbf{x}}{\partial \eta}$ are displacement-dependent. These terms linearize to $\frac{\partial \mathbf{u}}{\partial \xi}$ and $\frac{\partial \mathbf{u}}{\partial \eta}$ respectively. Using this and using the product rule and the triple product, the linearized expression becomes

$$D\delta W_{ext}^p(\boldsymbol{\phi}, \delta \mathbf{v})[\mathbf{u}] = \int_{A_\xi} p \left[\frac{\partial \mathbf{x}}{\partial \xi} \cdot \left(\frac{\partial \mathbf{u}}{\partial \eta} \times \delta \mathbf{v} \right) - \frac{\partial \mathbf{x}}{\partial \eta} \cdot \left(\frac{\partial \mathbf{u}}{\partial \xi} \times \delta \mathbf{v} \right) \right] d\xi d\eta. \quad (3.56)$$

Note that in this expression \mathbf{u} and $\delta \mathbf{v}$ cannot be interchanged without altering the result, which means that the expression is unsymmetric. This will in general yield an unsymmetric tangent matrix component. It is however possible for the special but common case where the position of points along the boundary ∂a is fixed or prescribed to obtain a symmetric matrix. This is possible since in this case equation (3.56) can be rewritten using the triple product multiple times along with the following integration theorems.

$$\int_V \nabla f dV = \int_{\partial V} f \mathbf{n} dA \quad (3.57a)$$

$$\int_V \nabla \mathbf{v} dV = \int_{\partial V} \mathbf{v} \otimes \mathbf{n} dA \quad (3.57b)$$

$$\int_V \nabla \cdot \mathbf{v} dV = \int_{\partial V} \mathbf{v} \cdot \mathbf{n} dA \quad (3.57c)$$

$$\int_V \nabla \cdot \mathbf{S} dV = \int_{\partial V} \mathbf{S} \mathbf{n} dA \quad (3.57d)$$

Here V is a volume with boundary surface ∂V , \mathbf{n} is the unit normal to this surface, f is a scalar field, \mathbf{v} a tensor field or a vector field and \mathbf{S} a second-order tensor for which $(\mathbf{S} \otimes \mathbf{n}) : \mathbf{I} = \mathbf{S} \mathbf{n}$. Furthermore $\nabla \mathbf{v}$ denotes the gradient and $\nabla \cdot \mathbf{v}$ denotes the divergence.

With these theorems and the triple product equation (3.56) can be rewritten as [17]

$$\begin{aligned}
D\delta W_{ext}^p(\boldsymbol{\phi}, \delta\mathbf{v})[\mathbf{u}] &= \int_{A_\xi} p \left[\frac{\partial \mathbf{x}}{\partial \xi} \cdot \left(\frac{\partial \mathbf{u}}{\partial \eta} \times \delta\mathbf{v} \right) - \frac{\partial \mathbf{x}}{\partial \eta} \cdot \left(\frac{\partial \mathbf{u}}{\partial \xi} \times \delta\mathbf{v} \right) \right] d\xi d\eta \\
&= \int_{A_\xi} p \left[\frac{\partial \mathbf{u}}{\partial \eta} \cdot \left(\delta\mathbf{v} \times \frac{\partial \mathbf{x}}{\partial \xi} \right) - \frac{\partial \mathbf{u}}{\partial \xi} \cdot \left(\delta\mathbf{v} \times \frac{\partial \mathbf{x}}{\partial \eta} \right) \right] d\xi d\eta \\
&= \int_{A_\xi} p \left[\frac{\partial}{\partial \eta} \left(\frac{\partial \mathbf{x}}{\partial \xi} \cdot (\mathbf{u} \times \delta\mathbf{v}) \right) - \frac{\partial}{\partial \xi} \left(\frac{\partial \mathbf{x}}{\partial \eta} \cdot (\mathbf{u} \times \delta\mathbf{v}) \right) \right] d\xi d\eta \\
&\quad - \int_{A_\xi} p \left[\frac{\partial \mathbf{x}}{\partial \xi} \cdot \left(\mathbf{u} \times \frac{\partial \delta\mathbf{v}}{\partial \eta} \right) - \frac{\partial \mathbf{x}}{\partial \eta} \cdot \left(\mathbf{u} \times \frac{\partial \delta\mathbf{v}}{\partial \xi} \right) \right] d\xi d\eta \\
&= \int_{A_\xi} p \left[\frac{\partial \mathbf{x}}{\partial \xi} \cdot \left(\frac{\partial \delta\mathbf{v}}{\partial \eta} \times \mathbf{u} \right) - \frac{\partial \mathbf{x}}{\partial \eta} \cdot \left(\frac{\partial \delta\mathbf{v}}{\partial \xi} \times \mathbf{u} \right) \right] d\xi d\eta \\
&\quad + \oint_{\partial A_\xi} p (\mathbf{u} \times \delta\mathbf{v}) \cdot \left(v_\eta \frac{\partial \mathbf{x}}{\partial \xi} - v_\xi \frac{\partial \mathbf{x}}{\partial \eta} \right) dl.
\end{aligned} \tag{3.58}$$

Here $\mathbf{v} = [v_\xi, v_\eta]^T$ is the vector in the parameter plane normal to ∂A_ξ .

In the special case in which the positions along ∂a are fixed or prescribed, both the iterative displacement \mathbf{u} and the virtual velocity $\delta\mathbf{v}$ are zero along ∂A_ξ . In this case the second integral in equation (3.58) vanishes.

The final expression for the linearized external work used in FEBio anticipates closed boundary conditions and is constructed by adding half equation (3.56) and (3.58) [17].

$$\begin{aligned}
D\delta W_{ext}^p(\boldsymbol{\phi}, \delta\mathbf{v})[\mathbf{u}] &= \frac{1}{2} \int_{A_\xi} p \frac{\partial \mathbf{x}}{\partial \xi} \cdot \left[\left(\frac{\partial \mathbf{u}}{\partial \eta} \times \delta\mathbf{v} \right) + \left(\frac{\partial \delta\mathbf{v}}{\partial \eta} \times \mathbf{u} \right) \right] d\xi d\eta \\
&\quad - \frac{1}{2} \int_{A_\xi} p \frac{\partial \mathbf{x}}{\partial \eta} \cdot \left[\left(\frac{\partial \mathbf{u}}{\partial \xi} \times \delta\mathbf{v} \right) + \left(\frac{\partial \delta\mathbf{v}}{\partial \xi} \times \mathbf{u} \right) \right] d\xi d\eta
\end{aligned} \tag{3.59}$$

It is easily seen that the discretization of this equation will lead to a symmetric component of the tangent matrix.

3.2.2. DISCRETIZATION OF THE VIRTUAL WORK

The first step in solving the problem with the Newton-Raphson method was to linearize the virtual work equation. Now that this is done the next step is to consider the entire problem in elements, that is, discretize the virtual work.

Before actually discretizing the virtual work equation several definitions will be given.

GENERAL DISCRETIZATION

Figure 3.3 illustrates the discretization of a general geometry. As can be seen the discretization is done in the initial configuration using isoparametric elements. With these elements the initial geometry can be interpolated in terms of the particles \mathbf{X}_a defining the initial position of the element nodes as

$$\mathbf{X} = \sum_{a=1}^n N_a(\xi_1, \xi_2, \xi_3) \mathbf{X}_a. \tag{3.60}$$

Here $N_a(\xi_1, \xi_2, \xi_3)$ are the standard shape functions and n denotes the number of nodes. Note that during the deformation the nodes and elements are permanently attached to the material particles with which they were initially associated [17]. With this definition, the motion is described in terms of the current position $\mathbf{x}_a(t)$ of the nodal particles as

$$\mathbf{x} = \sum_{a=1}^n N_a \mathbf{x}_a(t). \tag{3.61}$$

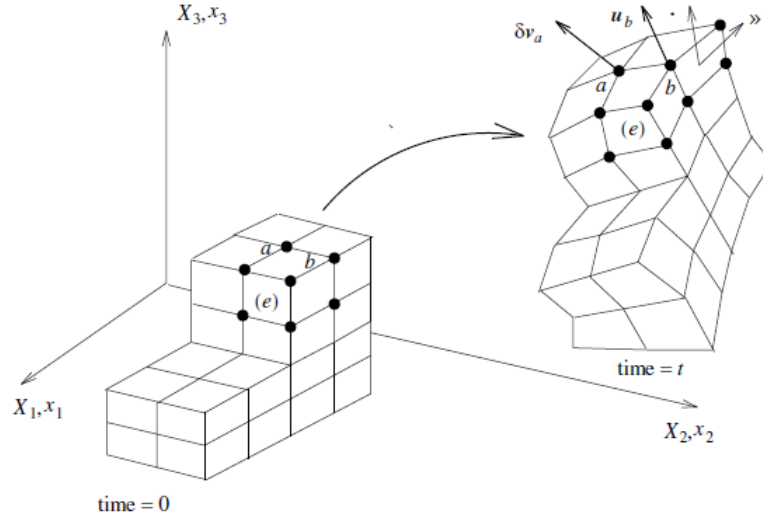


Figure 3.3: Discretization of a general geometry. Source: [17].

From this expression the real and virtual velocity interpolation can be obtained by differentiating with respect to time:

$$\mathbf{v} = \sum_{a=1}^n N_a \mathbf{v}_a, \quad (3.62a)$$

$$\delta \mathbf{v} = \sum_{a=1}^n N_a \delta \mathbf{v}_a. \quad (3.62b)$$

Similarly the displacement \mathbf{u} can be interpolated as

$$\mathbf{u} = \sum_{a=1}^n N_a \mathbf{u}_a. \quad (3.63)$$

In order to interpolate the deformation gradient \mathbf{F} over an element, equation (3.61) is differentiated with respect to the initial coordinates, obtaining after some rewriting,

$$\mathbf{F} = \sum_{a=1}^n \mathbf{x}_a \otimes \nabla_0 N_a, \quad (3.64)$$

where $\nabla_0 N_a = \frac{\partial N_a}{\partial \mathbf{X}}$ can be related to $\nabla_\xi N_a = \frac{\partial N_a}{\partial \xi}$ using the chain rule and equation (3.60). This obtains

$$\frac{\partial N_a}{\partial \mathbf{X}} = \left(\frac{\partial \mathbf{X}}{\partial \xi} \right)^{-T} \frac{\partial N_a}{\partial \xi}, \quad (3.65a)$$

$$\frac{\partial \mathbf{X}}{\partial \xi} = \sum_{a=1}^n \mathbf{X}_a \otimes \nabla_\xi N_a. \quad (3.65b)$$

These equations can also be written in matrix form, yielding

$$\mathbf{F} = \begin{bmatrix} F_{11} & F_{12} & F_{13} \\ F_{21} & F_{22} & F_{23} \\ F_{31} & F_{32} & F_{33} \end{bmatrix}; \quad F_{ij} = \sum_{a=1}^n x_{a,i} \frac{\partial N_a}{\partial X_j}, \quad (3.66)$$

and,

$$\frac{\partial \mathbf{X}}{\partial \xi} = \begin{bmatrix} \frac{\partial X_1}{\partial \xi_1} & \frac{\partial X_1}{\partial \xi_2} & \frac{\partial X_1}{\partial \xi_3} \\ \frac{\partial X_2}{\partial \xi_1} & \frac{\partial X_2}{\partial \xi_2} & \frac{\partial X_2}{\partial \xi_3} \\ \frac{\partial X_3}{\partial \xi_1} & \frac{\partial X_3}{\partial \xi_2} & \frac{\partial X_3}{\partial \xi_3} \end{bmatrix}; \quad \frac{\partial X_I}{\partial \xi_\alpha} = \sum_{a=1}^n X_{a,I} \frac{\partial N_a}{\partial \xi_\alpha}. \quad (3.67)$$

Using equation (3.64) other quantities such as the Cauchy-Green tensors can be obtained as,

$$\mathcal{C} = \mathbf{F}^T \mathbf{F} = \sum_{a,b} (\mathbf{x}_a \cdot \mathbf{x}_b) \nabla_0 N_a \otimes \nabla_0 N_b; \quad (3.68a)$$

$$C_{IJ} = \sum_{k=1}^3 F_{kI} F_{kJ}, \quad (3.68b)$$

$$\mathbf{b} = \mathbf{F} \mathbf{F}^T = \sum_{a,b} (\nabla_0 N_a \cdot \nabla_0 N_b) \mathbf{x}_a \otimes \mathbf{x}_b; \quad (3.68c)$$

$$b_{ij} = \sum_{K=1}^3 F_{iK} F_{jK}. \quad (3.68d)$$

The final quantities that shall be discretized here are the real and virtual rate of deformation and the linear strain tensor. Recall that these quantities are defined as follows:

$$\mathbf{d} = \frac{1}{2} (\mathbf{l} + \mathbf{l}^T), \quad (3.69a)$$

$$\mathbf{l} = \nabla \mathbf{v}, \quad (3.69b)$$

$$\boldsymbol{\varepsilon} = \frac{1}{2} (\nabla \mathbf{u} + (\nabla \mathbf{u})^T). \quad (3.69c)$$

Introducing equation (3.62a) and equation (3.62b) into the definitions given in equation (3.69a) and equation (3.69b) respectively, and introducing equation (3.63) into equation (3.69c) gives the discretized definitions.

$$\mathbf{d} = \frac{1}{2} \sum_{a=1}^n (\mathbf{v}_a \otimes \nabla N_a + \nabla N_a \otimes \mathbf{v}_a) \quad (3.70a)$$

$$\delta \mathbf{d} = \frac{1}{2} \sum_{a=1}^n (\delta \mathbf{v}_a \otimes \nabla N_a + \nabla N_a \otimes \delta \mathbf{v}_a) \quad (3.70b)$$

$$\boldsymbol{\varepsilon} = \frac{1}{2} \sum_{a=1}^n (\mathbf{u}_a \otimes \nabla N_a + \nabla N_a \otimes \mathbf{u}_a) \quad (3.70c)$$

Here $\nabla N_a = \partial N_a / \partial \mathbf{x}$ can be obtained from the derivations of the shape functions [17].

$$\frac{\partial N_a}{\partial \mathbf{x}} = \left(\frac{\partial \mathbf{x}}{\partial \boldsymbol{\xi}} \right)^{-T} \frac{\partial N_a}{\partial \boldsymbol{\xi}} \quad (3.71a)$$

$$\frac{\partial \mathbf{x}}{\partial \boldsymbol{\xi}} = \sum_{a=1}^n \mathbf{x}_a \otimes \nabla_{\boldsymbol{\xi}} N_a \quad (3.71b)$$

$$\frac{\partial x_i}{\partial \xi_{\alpha}} = \sum_{a=1}^n x_{a,i} \otimes \frac{\partial N_a}{\partial \xi_{\alpha}} \quad (3.71c)$$

DISCRETIZATION OF THE VIRTUAL WORK

Now that many quantities have been discretized the goal is to discretize the virtual work equation. Recall that the virtual work equation is given by

$$\delta W(\boldsymbol{\phi}, \delta \mathbf{v}) = \int_v \boldsymbol{\sigma} : \delta \mathbf{d} \, dv - \int_v \mathbf{b} \cdot \delta \mathbf{v} \, dv - \int_{\partial v} \mathbf{t} \cdot \delta \mathbf{v} \, da. \quad (3.72)$$

We will consider the virtual work by looking at an element (e) and one of its nodes a . Instead of considering the whole virtual work only the contribution of the single virtual nodal velocity $\delta \mathbf{v}_a$ occurring at the node a will be considered. Using the interpolations of $\delta \mathbf{v}$ and $\delta \mathbf{d}$ given in equations (equation (3.62b)) and (equation (3.70b)) respectively, the contribution is given in equation (3.73). In the internal energy term the symmetry of $\boldsymbol{\sigma}$ has been used to obtain this simplified form

$$\delta W^{(e)}(\boldsymbol{\phi}, N_a \delta \mathbf{v}_a) = \int_{v^{(e)}} \boldsymbol{\sigma} : (\delta \mathbf{v}_a \otimes \nabla N_a) \, dv - \int_{v^{(e)}} \mathbf{b} \cdot (N_a \delta \mathbf{v}_a) \, dv - \int_{\partial v^{(e)}} \mathbf{t} \cdot (N_a \delta \mathbf{v}_a) \, da. \quad (3.73)$$

This can be rewritten using the following properties of the tensor product (\otimes), the trace (tr) and the double product ($:$).

By definition for two second-order tensors \mathbf{A} and \mathbf{B} , $\mathbf{A} : \mathbf{B} = \text{tr}(\mathbf{A}^T \mathbf{B}) = \text{tr}(\mathbf{B} \mathbf{A}^T) = \text{tr}(\mathbf{A} \mathbf{B}^T)$. The tensor product of three vectors \mathbf{u} , \mathbf{v} and \mathbf{w} is by definition $(\mathbf{u} \otimes \mathbf{v})\mathbf{w} = (\mathbf{w} \cdot \mathbf{v})\mathbf{u}$. From this it follows that for a tensor \mathbf{S}

$$\mathbf{S}(\mathbf{u} \otimes \mathbf{v})\mathbf{w} = \mathbf{S}[(\mathbf{u} \otimes \mathbf{v})\mathbf{w}] = \mathbf{S}\mathbf{u}(\mathbf{v} \cdot \mathbf{w}) = (\mathbf{S}\mathbf{u} \otimes \mathbf{v})\mathbf{w}.$$

The last property that is needed is the property of the trace, which states that

$$\text{tr}(\mathbf{u} \otimes \mathbf{v}) = \sum_{i=1}^n (\mathbf{u} \otimes \mathbf{v})_{ii} = \sum_{i=1}^n u_i v_i = \mathbf{u} \cdot \mathbf{v}.$$

Using these three properties it can be shown that

$$\mathbf{S} : (\mathbf{u} \otimes \mathbf{v}) = \text{tr}(\mathbf{S}^T (\mathbf{u} \otimes \mathbf{v})) = \text{tr}((\mathbf{u} \otimes \mathbf{v})\mathbf{S}^T) = \text{tr}(\mathbf{u} \otimes \mathbf{S}\mathbf{v}) = \mathbf{u} \cdot \mathbf{S}\mathbf{v}.$$

With this final property and the fact that the virtual nodal velocities do not depend on the intergration equation (3.73) can be re-expressed as [17]

$$\delta W^{(e)}(\boldsymbol{\phi}, N_a \delta \mathbf{v}_a) = \delta \mathbf{v}_a \left(\int_{v^{(e)}} \boldsymbol{\sigma} \nabla N_a dv - \int_{v^{(e)}} N_a \mathbf{b} dv - \int_{\partial v^{(e)}} N_a \mathbf{t} da \right). \quad (3.74)$$

Having this equation, it can be divided into two components; a term describing the internal equivalent nodal forces $\mathbf{T}_a^{(e)}$ and a term describing the external nodal forces $\mathbf{F}_a^{(e)}$. This obtains

$$\delta W^{(e)}(\boldsymbol{\phi}, N_a \delta \mathbf{v}_a) = \delta \mathbf{v}_a (\mathbf{T}_a^{(e)} - \mathbf{F}_a^{(e)}) \quad (3.75a)$$

where,

$$\mathbf{T}_a^{(e)} = \int_{v^{(e)}} \boldsymbol{\sigma} \nabla N_a dv; \quad T_{a,i}^{(e)} = \sum_{j=1}^3 \sigma_{ij} \frac{\partial N_a}{\partial x_j}, \quad (3.75b)$$

$$\mathbf{F}_a^{(e)} = \int_{v^{(e)}} N_a \mathbf{b} dv + \int_{\partial v^{(e)}} N_a \mathbf{t} da. \quad (3.75c)$$

Note that the Cauchy stress tensor $\boldsymbol{\sigma}$ depends on the materials and the corresponding constitutive equations.

Equation (3.75a) gives the contribution to the virtual work equation from a single element (e) attached to node a . The contribution from all element $e_1 \dots e_{m_a}$ containing node a , that is $a \in e$, is given as

$$\delta W(\boldsymbol{\phi}, N_a \delta \mathbf{v}_a) = \sum_{\substack{e=1 \\ a \in e}}^{m_a} \delta W^{(e)}(\boldsymbol{\phi}, N_a \delta \mathbf{v}_a) = \delta \mathbf{v}_a \cdot (\mathbf{T}_a - \mathbf{F}_a), \quad (3.76a)$$

with

$$\mathbf{T}_a = \sum_{\substack{e=1 \\ a \in e}}^{m_a} \mathbf{T}_a^{(e)}, \quad (3.76b)$$

$$\mathbf{F}_a = \sum_{\substack{e=1 \\ a \in e}}^{m_a} \mathbf{F}_a^{(e)}. \quad (3.76c)$$

Taking the summation over all the nodes N in the mesh the total contribution $\delta W(\boldsymbol{\phi}, \delta \mathbf{v})$ is obtained.

$$\delta W(\boldsymbol{\phi}, \delta \mathbf{v}) = \sum_{a=1}^N \delta W^{(e)}(\boldsymbol{\phi}, N_a \delta \mathbf{v}_a) = \sum_{a=1}^N \delta \mathbf{v}_a \cdot (\mathbf{T}_a - \mathbf{F}_a) = 0. \quad (3.77)$$

As this equation must hold for any arbitrary virtual nodal velocities, the discretized equilibrium equations emerge as

$$\mathbf{R}_a = \mathbf{T}_a - \mathbf{F}_a = \mathbf{0}, \quad (3.78)$$

for the nodal residual force \mathbf{R}_a . It can be seen that for this equation to be satisfied, the internal and equivalent external forces need to be in equilibrium at each node $a = 1, \dots, N$. For convenience the above residual force and the internal and external forces can be written as arrays, as,

$$\mathbf{T} = \begin{bmatrix} \mathbf{T}_1 \\ \mathbf{T}_2 \\ \vdots \\ \mathbf{T}_n \end{bmatrix}; \quad \mathbf{F} = \begin{bmatrix} \mathbf{F}_1 \\ \mathbf{F}_2 \\ \vdots \\ \mathbf{F}_n \end{bmatrix}; \quad \mathbf{R} = \begin{bmatrix} \mathbf{R}_1 \\ \mathbf{R}_2 \\ \vdots \\ \mathbf{R}_n \end{bmatrix}. \quad (3.79)$$

With these formulations and writing the virtual velocities in a vector as

$$\delta \mathbf{v} = \begin{bmatrix} \delta v_1 \\ \delta v_2 \\ \vdots \\ \delta v_n \end{bmatrix}, \quad (3.80)$$

The discretized virtual work equation (3.77) can be re-expressed as

$$\delta W(\phi, \delta \mathbf{v}) = \delta \mathbf{v}^T \mathbf{R} = \delta \mathbf{v}^T (\mathbf{T} - \mathbf{F}) = 0. \quad (3.81)$$

When noting that the internal equivalent forces are nonlinear functions of the current nodal positions \mathbf{x}_a the complete nonlinear equilibrium equations can be assembled as

$$\mathbf{R}(\mathbf{x}) = \mathbf{T}(\mathbf{x}) - \mathbf{F}(\mathbf{x}) = \mathbf{0}, \quad \text{where } \mathbf{x} = \begin{bmatrix} \mathbf{x}_1 \\ \mathbf{x}_2 \\ \vdots \\ \mathbf{x}_n \end{bmatrix}, \quad (3.82)$$

where \mathbf{x} is the array containing all nodal positions.

MATRIX NOTATION

A more common method of denoting the discretized equilibrium equations is using matrix formulations. To do this the symmetric Cauchy stress and rate of deformation tensor are re-established as vectors including six independent elements

$$\underline{\sigma} = \begin{bmatrix} \sigma_{11} \\ \sigma_{22} \\ \sigma_{33} \\ \sigma_{12} \\ \sigma_{13} \\ \sigma_{23} \end{bmatrix}; \quad \mathbf{d} = \begin{bmatrix} d_{11} \\ d_{22} \\ d_{33} \\ 2d_{12} \\ 2d_{13} \\ 2d_{23} \end{bmatrix}. \quad (3.83)$$

Note that the off-diagonal terms of the deformation tensor are doubled to ensure that $\mathbf{d}^T \underline{\sigma}$ gives the correct internal energy

$$\int_v \underline{\sigma} : \mathbf{d} dv = \int_v \mathbf{d}^T \underline{\sigma} dv. \quad (3.84)$$

The rate of deformation \mathbf{d} can be given as

$$\mathbf{d} = \sum_{a=1}^n \mathbf{B}_a \mathbf{v}_a, \quad \text{where } \mathbf{B}_a = \begin{bmatrix} \frac{\partial N_a}{\partial x_1} & 0 & 0 \\ 0 & \frac{\partial N_a}{\partial x_2} & 0 \\ 0 & 0 & \frac{\partial N_a}{\partial x_3} \\ \frac{\partial N_a}{\partial x_2} & \frac{\partial N_a}{\partial x_1} & 0 \\ \frac{\partial N_a}{\partial x_3} & 0 & \frac{\partial N_a}{\partial x_1} \\ 0 & \frac{\partial N_a}{\partial x_3} & \frac{\partial N_a}{\partial x_2} \end{bmatrix}. \quad (3.85)$$

With these definitions the discretized virtual work equation (3.72) can be written as

$$\delta W(\boldsymbol{\phi}, N_a \delta \mathbf{v}_a) = \int_{v^{(e)}} (\mathbf{B}_a \delta \mathbf{v}_a)^T \underline{\boldsymbol{\sigma}} dv - \int_{v^{(e)}} \mathbf{b} \cdot (N_a \delta \mathbf{v}_a) dv - \int_{\partial v^{(e)}} \mathbf{t} \cdot (N_a \delta \mathbf{v}_a) da. \quad (3.86)$$

With these notations the element equivalent nodal forces $\mathbf{T}_a^{(e)}$ are expressed as

$$\mathbf{T}_a^{(e)} = \int_{v^{(e)}} \mathbf{B}_a^T \underline{\boldsymbol{\sigma}} dv. \quad (3.87)$$

3.2.3. DISCRETIZATION OF THE LINEARIZED VIRTUAL WORK

Now that the virtual work equation is discretized the final step is to discretize the linearized virtual work. For convenience the linearized virtual work shall again be split into the internal and external components.

$$D\delta W(\boldsymbol{\phi}_k, \delta \mathbf{v})[\mathbf{u}] = D\delta W_{int}(\boldsymbol{\phi}_k, \delta \mathbf{v})[\mathbf{u}] - D\delta W_{ext}(\boldsymbol{\phi}_k, \delta \mathbf{v})[\mathbf{u}] \quad (3.88)$$

The component describing the internal virtual work shall be subdivided even further into a constitutive and initial stress component, as

$$\begin{aligned} D\delta W_{int}(\boldsymbol{\phi}, \delta \mathbf{v})[\mathbf{u}] &= D\delta W_c(\boldsymbol{\phi}, \delta \mathbf{v})[\mathbf{u}] + D\delta W_\sigma(\boldsymbol{\phi}, \delta \mathbf{v})[\mathbf{u}] \\ &= \int_v \delta \mathbf{d} : \mathbf{c} : \boldsymbol{\varepsilon} dv + \int_v \boldsymbol{\sigma} : [((\nabla \mathbf{u}))^T \nabla \delta \mathbf{v}] dv. \end{aligned} \quad (3.89)$$

DISCRETIZATION OF THE CONSTITUTIVE COMPONENT OF THE INTERNAL WORK

The first component that will be discretized is the constitutive component of the internal work

$$D\delta W_c(\boldsymbol{\phi}, \delta \mathbf{v})[\mathbf{u}] = \int_v \delta \mathbf{d} : \mathbf{c} : \boldsymbol{\varepsilon} dv. \quad (3.90)$$

To discretize this in matrix form the small strain vector $\boldsymbol{\varepsilon}$ is written in a similar way as the rate of deformation \mathbf{d} in equation (3.85):

$$\underline{\boldsymbol{\varepsilon}} = \begin{bmatrix} \varepsilon_{11} \\ \varepsilon_{22} \\ \varepsilon_{33} \\ 2\varepsilon_{12} \\ 2\varepsilon_{13} \\ 2\varepsilon_{23} \end{bmatrix}; \quad \underline{\boldsymbol{\varepsilon}} = \sum_{a=1}^n \mathbf{B}_a \mathbf{v}_a, \quad \text{where } \mathbf{B}_a = \begin{bmatrix} \frac{\partial N_a}{\partial x_1} & 0 & 0 \\ 0 & \frac{\partial N_a}{\partial x_2} & 0 \\ 0 & 0 & \frac{\partial N_a}{\partial x_3} \\ \frac{\partial N_a}{\partial x_2} & \frac{\partial N_a}{\partial x_1} & 0 \\ \frac{\partial N_a}{\partial x_3} & 0 & \frac{\partial N_a}{\partial x_1} \\ 0 & \frac{\partial N_a}{\partial x_3} & \frac{\partial N_a}{\partial x_2} \end{bmatrix}. \quad (3.91)$$

The spatial constitutive matrix \mathbf{D} is constructed from the components of \mathbf{c} such that $\delta \mathbf{d} : \mathbf{c} : \boldsymbol{\varepsilon} = \delta \mathbf{d}^T \mathbf{D} \underline{\boldsymbol{\varepsilon}}$. The resulting symmetric matrix is [17]

$$\mathbf{D} = \frac{1}{2} \begin{bmatrix} 2c_{1111} & 2c_{1122} & 2c_{1133} & c_{1112} + c_{1121} & c_{1113} + c_{1131} & c_{1123} + c_{1132} \\ & 2c_{2222} & 2c_{2233} & c_{2212} + c_{2221} & c_{2213} + c_{2231} & c_{2223} + c_{2232} \\ & & 2c_{3333} & c_{3312} + c_{3321} & c_{3313} + c_{3331} & c_{3323} + c_{3332} \\ & & & c_{1212} + c_{1221} & c_{1213} + c_{1231} & c_{1223} + c_{1232} \\ & & & & c_{1313} + c_{1331} & c_{1323} + c_{1332} \\ & & & & & c_{2323} + c_{2332} \end{bmatrix}. \quad (3.92)$$

With these the constitutive component of the linearized internal virtual work can be written as

$$D\delta W_c(\boldsymbol{\phi}, \delta \mathbf{v})[\mathbf{u}] = \int_v \delta \mathbf{d} : \mathbf{c} : \boldsymbol{\varepsilon} dv = \int_v \delta \mathbf{d}^T \mathbf{D} \underline{\boldsymbol{\varepsilon}} dv. \quad (3.93)$$

Substituting equations (3.85) and (3.91) the contribution of a single element (e) associated with the two nodes a and b is obtained as

$$\begin{aligned} D\delta W_c^{(e)}(\boldsymbol{\phi}, N_a \delta \mathbf{v}_a)[N_b \mathbf{u}] &= \int_{v^{(e)}} \mathbf{B}_a \delta \mathbf{v}_a^T \mathbf{D} (\mathbf{B}_b \mathbf{u}_b) dv \\ &= \delta \mathbf{v}_a \left(\int_{v^{(e)}} \mathbf{B}_a^T \mathbf{D} \mathbf{B}_b dv \right) \end{aligned} \quad (3.94)$$

$$= \delta \mathbf{v}_a \mathbf{K}_{c,ab}^{(e)}. \quad (3.95)$$

Here $\mathbf{K}_{c,ab}^{(e)}$ is

The constitutive component of the tangent matrix relating node a to node b in element (e):

$$\mathbf{K}_{c,ab}^{(e)} = \int_{v^{(e)}} \mathbf{B}_a^T \mathbf{D} \mathbf{B}_b dv. \quad (3.96)$$

DISCRETIZATION OF THE INITIAL COMPONENT OF THE INTERNAL WORK

The second term that shall be discretized is the initial component of the internal work, that is,

$$D\delta W_\sigma(\boldsymbol{\phi}, \delta \mathbf{v})[\mathbf{u}] = \int_v \boldsymbol{\sigma} : [((\nabla \mathbf{u}))^T \nabla \delta \mathbf{v}] dv. \quad (3.97)$$

To discretize this expression the gradients $\nabla \mathbf{u}$ and $\nabla \delta \mathbf{v}$ can be easily interpolated from equations (3.62b) and (3.63).

$$\nabla \delta \mathbf{v} = \sum_{a=1}^n \delta \mathbf{v}_a \otimes \nabla N_a \quad (3.98a)$$

$$\nabla \mathbf{u} = \sum_{b=1}^n \mathbf{u}_b \otimes \nabla N_b \quad (3.98b)$$

Substituting these expressions into equation (3.97) and using the property $\mathbf{S} : (\mathbf{u} \otimes \mathbf{v}) = \mathbf{u} \cdot \mathbf{S} \mathbf{v}$ for vectors \mathbf{u} and \mathbf{v} , the contribution to the linearized virtual work of the initial stress component for element (e) linking nodes a and b can be derived [17]:

$$\begin{aligned} D\delta W_\sigma(\boldsymbol{\phi}, N_a \delta \mathbf{v})[N_b \mathbf{u}_b] &= \int_v \boldsymbol{\sigma} : [((\nabla \mathbf{u}_b))^T \nabla \delta \mathbf{v}_a] dv \\ &= \int_{v^{(e)}} \boldsymbol{\sigma} : [(\delta \mathbf{v}_a \cdot \mathbf{u}_b) \nabla N_b \otimes \nabla N_a] dv \\ &= (\delta \mathbf{v}_a \cdot \mathbf{u}_b) \int_{v^{(e)}} \nabla N_a \cdot \boldsymbol{\sigma} \nabla N_b dv. \end{aligned} \quad (3.99)$$

It can be noted that the final integral is a scalar, and that $\delta \mathbf{v}_a \cdot \mathbf{u}_b = \delta \mathbf{v}_a \cdot \mathbf{I} \mathbf{u}_b$. Using this the contribution can be rewritten as

$$\begin{aligned} D\delta W_\sigma(\boldsymbol{\phi}, N_a \delta \mathbf{v})[N_b \mathbf{u}_b] &= (\delta \mathbf{v}_a \cdot \mathbf{u}_b) \int_{v^{(e)}} \nabla N_a \cdot \boldsymbol{\sigma} \nabla N_b dv \\ &= \delta \mathbf{v}_a \cdot \left(\int_{v^{(e)}} \nabla N_a \cdot \boldsymbol{\sigma} \nabla N_b \mathbf{I} dv \right) \mathbf{u}_b \\ &= \delta \mathbf{v}_a \cdot \mathbf{K}_{\sigma,ab}^{(e)} \mathbf{u}_b. \end{aligned}$$

Here $\mathbf{K}_{\sigma,ab}^{(e)}$ is

The initial component of the tangent matrix relating node a to node b in element (e) (also known as the initial stress matrix):

$$\mathbf{K}_{\sigma,ab}^{(e)} = \int_{v^{(e)}} (\nabla N_a \cdot \boldsymbol{\sigma} \nabla N_b) \mathbf{I} dv. \quad (3.100)$$

DISCRETIZATION OF THE EXTERNAL WORK

The final component that needs to be discretized is the linearized external work component

$$\begin{aligned} D\delta W_{ext}^p(\boldsymbol{\phi}, \delta \mathbf{v})[\mathbf{u}] &= \frac{1}{2} \int_{A_\xi} p \frac{\partial \mathbf{x}}{\partial \xi} \left[\left(\frac{\partial \mathbf{u}}{\partial \eta} \times \delta \mathbf{v} \right) + \left(\frac{\partial \delta \mathbf{v}}{\partial \eta} \times \mathbf{u} \right) \right] d\xi d\eta \\ &\quad - \frac{1}{2} \int_{A_\xi} p \frac{\partial \mathbf{x}}{\partial \eta} \left[\left(\frac{\partial \mathbf{u}}{\partial \xi} \times \delta \mathbf{v} \right) + \left(\frac{\partial \delta \mathbf{v}}{\partial \xi} \times \mathbf{u} \right) \right] d\xi d\eta. \end{aligned} \quad (3.101)$$

As mentioned in linearizing the external force component, the body forces are independent of the motion and therefore do not contribute to the linearized external work. In the discretization of the linearized external work (3.101) surface elements are therefore needed. In the isoparametric volume interpolation there is a corresponding surface representation in terms of ξ and η [17].

$$\mathbf{x}(\xi, \eta) = \sum_{a=1}^n N_a \mathbf{x}_a \quad (3.102)$$

Here n denotes the number of nodes on each surface element. Similarly

$$\delta \mathbf{v}(\xi, \eta) = \sum_{a=1}^n N_a \delta \mathbf{v}_a, \text{ and} \quad (3.103a)$$

$$\mathbf{u}(\xi, \eta) = \sum_{a=1}^n N_a \mathbf{u}_a. \quad (3.103b)$$

Substituting this into equation (3.101) the contribution to the linearized external virtual work from surface element (e) associated with nodes a and b can be given as [17]

$$\begin{aligned} D\delta W_{ext}^{p(e)}(\boldsymbol{\phi}, N_a \delta \mathbf{v}_a)[N_b \mathbf{u}_b] &= (\delta \mathbf{v}_a \times \mathbf{u}_b) \cdot \frac{1}{2} \int_{A_\xi} p \frac{\partial \mathbf{x}}{\partial \xi} \left(\frac{\partial N_a}{\partial \eta} N_b - \frac{\partial N_b}{\partial \eta} N_a \right) d\xi d\eta \\ &\quad - (\delta \mathbf{v}_a \times \mathbf{u}_b) \cdot \frac{1}{2} \int_{A_\xi} p \frac{\partial \mathbf{x}}{\partial \eta} \left(\frac{\partial N_a}{\partial \xi} N_b - \frac{\partial N_b}{\partial \xi} N_a \right) d\xi d\eta \\ &= (\delta \mathbf{v}_a \times \mathbf{u}_b) \cdot \mathbf{k}_{p,ab}. \end{aligned} \quad (3.104)$$

Here $\mathbf{k}_{p,ab}$ is the vector of stiffness coefficients, given by

$$\mathbf{k}_{p,ab} = \frac{1}{2} \int_{A_\xi} p \frac{\partial \mathbf{x}}{\partial \xi} \left(\frac{\partial N_a}{\partial \eta} N_b - \frac{\partial N_b}{\partial \eta} N_a \right) d\xi d\eta - \frac{1}{2} \int_{A_\xi} p \frac{\partial \mathbf{x}}{\partial \eta} \left(\frac{\partial N_a}{\partial \xi} N_b - \frac{\partial N_b}{\partial \xi} N_a \right) d\xi d\eta. \quad (3.105)$$

The contribution to the linearized external work can be reinterpreted as

$$D\delta W_{ext}^{p(e)}(\boldsymbol{\phi}, N_a \delta \mathbf{v}_a)[N_b \mathbf{u}_b] = \delta \mathbf{v}_a \cdot \mathbf{K}_{p,ab}^{(e)} \mathbf{u}_b. \quad (3.106)$$

Here $\mathbf{K}_{p,ab}^{(e)}$ is

The external pressure component of the tangent matrix relating node a to node b in element (e):

$$\mathbf{K}_{p,ab}^{(e)} = \boldsymbol{\varepsilon} \mathbf{k}_{p,ab}^{(e)}; \quad [\mathbf{K}_{p,ab}^{(e)}]_{ij} = \sum_{k=1}^3 \varepsilon_{ijk} [\mathbf{k}_{p,ab}^{(e)}]_k; \quad i, j = 1, 2, 3. \quad (3.107)$$

Here $\varepsilon_{ijk} = \pm 1$ or zero, depending on the parity of the ijk permutation.

THE TOTAL DISCRETIZED LINEARIZED VIRTUAL WORK EQUATION

In the previous sections the different components of the linearized virtual work equation have been discretized. The final step that needs to be taken is now to combine all of these components. This can be done as follows

$$D\delta W^{(e)}(\boldsymbol{\phi}, N_a \delta \mathbf{v}_a)[N_b \mathbf{u}_b] = \delta \mathbf{v} \cdot \mathbf{K}_{ab}^{(e)} \mathbf{u}_b, \quad (3.108a)$$

where

$$\mathbf{K}_{ab}^{(e)} = \mathbf{K}_{c,ab}^{(e)} + \mathbf{K}_{\sigma,ab}^{(e)} - \mathbf{K}_{p,ab}^{(e)}. \quad (3.108b)$$

Here the entire linearized virtual work is discretized for element (e) linking nodes a and b in terms of the substiffness matrix $\mathbf{K}_{ab}^{(e)}$.

Note that this discretization only considers a single element. To assemble the total linearized virtual work three steps have to be taken.

1. The contribution to a node a from node b associated with all elements (e) (1 to $m_{a,b}$) containing nodes a and b can be obtained using a summation over all these elements:

$$D\delta W(\boldsymbol{\phi}, N_a \delta \mathbf{v}_a)[N_b \mathbf{u}_b] = \sum_{\substack{e=1 \\ a,b \in e}}^{m_{a,b}} D\delta W^{(e)}(\boldsymbol{\phi}, N_a \delta \mathbf{v}_a)[N_b \mathbf{u}_b]. \quad (3.109a)$$

2. The contribution to a node a from all nodes $b = 1, \dots, n_a$ which are connected to a can be obtained using a summation over all the nodes b :

$$D\delta W(\boldsymbol{\phi}, N_a \delta \mathbf{v}_a)[\mathbf{u}] = \sum_{b=1}^{n_a} D\delta W(\boldsymbol{\phi}, N_a \delta \mathbf{v}_a)[N_b \mathbf{u}_b]. \quad (3.109b)$$

3. The total contribution can be obtained by summing over all elements a :

$$D\delta W(\boldsymbol{\phi}, \delta \mathbf{v})[\mathbf{u}] = \sum_{a=1}^n D\delta W(\boldsymbol{\phi}, N_a \delta \mathbf{v}_a)[\mathbf{u}]. \quad (3.109c)$$

Expressing the virtual velocities $\delta \mathbf{v}$ and the nodal displacements \mathbf{u} as

$$\delta \mathbf{v} = \begin{bmatrix} \delta \mathbf{v}_1 \\ \delta \mathbf{v}_2 \\ \vdots \\ \delta \mathbf{v}_n \end{bmatrix}, \text{ and} \quad (3.110a)$$

$$\mathbf{u} = \begin{bmatrix} \mathbf{u}_1 \\ \mathbf{u}_2 \\ \vdots \\ \mathbf{u}_n \end{bmatrix}, \quad (3.110b)$$

and assembling the tangent stiffness matrix \mathbf{K} using the nodal components as

$$\mathbf{K} = \begin{bmatrix} \mathbf{K}_{11} & \mathbf{K}_{12} & \cdots & \mathbf{K}_{1n} \\ \mathbf{K}_{21} & \mathbf{K}_{22} & \cdots & \mathbf{K}_{2n} \\ \vdots & \vdots & \ddots & \vdots \\ \mathbf{K}_{n1} & \mathbf{K}_{n2} & \cdots & \mathbf{K}_{nn} \end{bmatrix}, \quad (3.110c)$$

one obtains, in a different notation,

The total discretized linearized virtual work equation

$$D\delta W(\boldsymbol{\phi}, \delta \mathbf{v})[\mathbf{u}] = \delta \mathbf{v}^T \mathbf{K} \mathbf{u}. \quad (3.111)$$

3.2.4. FORMULATING THE NEWTON-RAPHSON SCHEME

Recall that using the Newton-Raphson method the virtual work equation needs to be solved, which means that equation (3.112) needs to be solved iteratively.

$$D\delta W(\boldsymbol{\phi}_k, \delta \mathbf{v})[\mathbf{u}] = -\delta W(\boldsymbol{\phi}_k, \delta \mathbf{v}) \quad (3.112)$$

In the previous sections the components in this equations were discretized, resulting in

$$\delta W(\boldsymbol{\phi}, \delta \mathbf{v}) = \delta \mathbf{v}^T \mathbf{R}, \quad \text{and } D\delta W(\boldsymbol{\phi}, \delta \mathbf{v})[\mathbf{u}] = \delta \mathbf{v}^T \mathbf{K} \mathbf{u}. \quad (3.113a)$$

Substituting this into equation (3.112) the Newton-Raphson equation for this problem is obtained

$$\delta \mathbf{v}^T \mathbf{K} \mathbf{u} = -\delta \mathbf{v}^T \mathbf{R}. \quad (3.114)$$

As the virtual velocities $\delta \mathbf{v}$ are arbitrary, the discretized Newton-Raphson scheme becomes

$$\mathbf{K}(\mathbf{x}_k) \cdot \mathbf{u} = -\mathbf{R}(\mathbf{x}_k), \quad \mathbf{x}_{k+1} = \mathbf{x}_k + \mathbf{u}. \quad (3.115)$$

When solving this using the Newton-Raphson method the stiffness matrix \mathbf{K} and the residual vector \mathbf{R} are re-evaluated for each iteration k . The displacement increment \mathbf{u} is then calculated by multiplying both sides of the equation by the inverse of \mathbf{K} .

The re-evaluating of the stiffness matrix and its inverse requires a lot of computation time and this process is therefore, especially for large problems, expensive. A solution for this is the use of a Quasi-Newton method, which is a method that does not re-evaluate the stiffness matrix at every step, but updates it instead (see Section 3.4).

3.3. APPLYING THE NEWTON-RAPHSON METHOD TO THE PROBLEM WITH CONTACT

3.3.1. LINEARIZING THE CONTACT INTEGRAL

To solve the two body contact problem using the Newton-Raphson method, the virtual work equation given in equation (2.136) needs to be linearized, as the Newton-Raphson equation is

$$\delta W^{int,ext}(\boldsymbol{\varphi}_k, \boldsymbol{\omega}) + \delta W^c(\boldsymbol{\varphi}_k, \boldsymbol{\omega}) + \Delta \delta W^{int,ext}(\boldsymbol{\varphi}_k, \boldsymbol{\omega}) + \Delta \delta W^c(\boldsymbol{\varphi}_k, \boldsymbol{\omega}) = 0, \quad (3.116)$$

where the directional derivative is denoted by Δ for brevity.

In the previous section the internal and external work have already been linearized, so in order to solve the equation only the contact integral has yet to be linearized. This section will not discuss the entire linearization, as the process is similar to the process used in Section 3.2.1.

The directional derivative that needs to be computed is

$$\Delta \delta W^c(\boldsymbol{\varphi}, \boldsymbol{\omega}) = \Delta \left(\int_{\Gamma_c^{(1)}} [\mathbf{t}_{N_t} \delta g + \mathbf{t}_{T_{at}} \delta \bar{\boldsymbol{\xi}}^\alpha] d\Gamma \right). \quad (3.117)$$

As the integral is evaluated in the contact surface of the reference configuration ($\Gamma_c^{(1)}$), only the integrand varies with the motion which means that the derivative can be moved inside the integral [20]:

$$\Delta \delta W^c(\boldsymbol{\varphi}, \boldsymbol{\omega}) = - \int_{\Gamma_c^{(1)}} \Delta [\mathbf{t}_N \delta g + \mathbf{t}_{T_{at}} \delta \bar{\boldsymbol{\xi}}^\alpha] d\Gamma_c^{(1)}. \quad (3.118)$$

Starting with the normal contact terms, the directional derivative of \mathbf{t}_N can be computed as

$$\begin{aligned} \Delta \mathbf{t}_N &= \Delta \{ \epsilon_N \langle g \rangle \}, \\ &= \epsilon_N \frac{\partial \langle g \rangle}{\partial g} \Delta g, \\ &= H(g) \epsilon_N \Delta g. \end{aligned} \quad (3.119)$$

Here $\epsilon_N > 0$ is the normal penalty parameter, and the notation $\langle \bullet \rangle$ is defined as:

$$\langle x \rangle := \begin{cases} x & \text{if } x \geq 0, \\ 0 & \text{if } x < 0. \end{cases} \quad (3.120)$$

Furthermore, $H(g)$ is the *Heaviside function*, which is equal to 1 if $g > 0$ and equal to zero if $g < 0$. It can also be derived that

$$\Delta g = -\mathbf{v} \cdot [\Delta \boldsymbol{\varphi}^{(1)}(\mathbf{X}) - \Delta \boldsymbol{\varphi}^{(2)}(\bar{\mathbf{Y}}(\mathbf{X}))]. \quad (3.121)$$

To compute $\Delta(\delta g)$, equation (2.141) is linearized. This obtains

$$\begin{aligned} \Delta(\delta g) &= g[\mathbf{v} \cdot \boldsymbol{\omega}_{,\gamma}^{(2)}(\bar{\mathbf{Y}}(\mathbf{X})) + \boldsymbol{\kappa}_{\alpha\gamma}(\bar{\mathbf{Y}}(\mathbf{X})) \delta \bar{\boldsymbol{\xi}}^\alpha] m^{\gamma\beta} [\mathbf{v} \cdot \Delta \boldsymbol{\varphi}_{,\beta}^{(2)}(\bar{\mathbf{Y}}(\mathbf{X})) + \boldsymbol{\kappa}_{\alpha\beta}(\bar{\mathbf{Y}}(\mathbf{X})) \Delta \bar{\boldsymbol{\xi}}^\alpha] \\ &\quad + \delta \bar{\boldsymbol{\xi}}^\beta \mathbf{v} \cdot [\Delta \boldsymbol{\varphi}_{,\beta}^{(2)}(\bar{\mathbf{Y}}(\mathbf{X}))] + \Delta \bar{\boldsymbol{\xi}}^\beta \mathbf{v} \cdot [\boldsymbol{\omega}_{,\beta}^{(2)}(\bar{\mathbf{Y}}(\mathbf{X}))] + \boldsymbol{\kappa}_{\alpha\beta}(\bar{\mathbf{Y}}(\mathbf{X})) \delta \bar{\boldsymbol{\xi}}^\beta \Delta \bar{\boldsymbol{\xi}}^\alpha. \end{aligned} \quad (3.122)$$

Here

$$A_{\alpha\beta} \Delta \bar{\boldsymbol{\xi}}^\beta = [\Delta \boldsymbol{\varphi}^{(1)}(\mathbf{X}) - \Delta \boldsymbol{\varphi}^{(2)}(\bar{\mathbf{Y}}(\mathbf{X}))] \boldsymbol{\tau}_\alpha - g \mathbf{v} \cdot [\Delta \boldsymbol{\varphi}_{,\alpha}^{(2)}(\bar{\mathbf{Y}}(\mathbf{X}))], \quad (3.123)$$

where the quantity $A_{\alpha\beta}$ is defined as

$$A_{\alpha\beta} := m_{\alpha\beta} + g \boldsymbol{\kappa}_{\alpha\beta}.$$

Using the above expressions the linearized contact integral is given by [20]

$$\begin{aligned} \Delta \delta W^c(\boldsymbol{\varphi}, \boldsymbol{\omega}) &= \Delta \left(\int_{\Gamma_c^{(1)}} [\mathbf{t}_{N_t} \delta g + \mathbf{t}_{T_{at}} \delta \bar{\boldsymbol{\xi}}^\alpha] d\Gamma \right) \\ &= \int_{\Gamma_c^{(1)}} [\Delta(\mathbf{t}_N \delta g) + \Delta \mathbf{t}_{T_\alpha} \delta \bar{\boldsymbol{\xi}}^\alpha + \mathbf{t}_{T_\alpha} \Delta(\delta \bar{\boldsymbol{\xi}}^\alpha)] d\Gamma, \end{aligned} \quad (3.124)$$

where

$$\begin{aligned}
\Delta(\mathbf{t}_N \delta g) &= \Delta(\mathbf{t}_N) \delta g + \mathbf{t}_N \Delta(\delta g) \\
&= H(g) \epsilon_N \delta g \Delta g \\
&\quad + \mathbf{t}_N \left\{ g[\mathbf{v} \cdot \boldsymbol{\omega}_{,\gamma}^{(2)}(\bar{\mathbf{Y}}(\mathbf{X})) + \kappa_{\alpha\gamma}(\bar{\mathbf{Y}}(\mathbf{X})) \delta \bar{\xi}^\alpha] m^{\gamma\beta} [\mathbf{v} \cdot \Delta \boldsymbol{\varphi}_{,\beta}^{(2)}(\bar{\mathbf{Y}}(\mathbf{X})) + \kappa_{\alpha\beta}(\bar{\mathbf{Y}}(\mathbf{X})) \Delta \bar{\xi}^\alpha] \right. \\
&\quad + \delta \bar{\xi}^\beta \mathbf{v} \cdot [\Delta \boldsymbol{\varphi}_{,\beta}^{(2)}(\bar{\mathbf{Y}}(\mathbf{X}))] + \Delta \bar{\xi}^\beta \mathbf{v} \cdot [\boldsymbol{\omega}_{,\beta}^{(2)}(\bar{\mathbf{Y}}(\mathbf{X}))] \\
&\quad \left. + \kappa_{\alpha\beta}(\bar{\mathbf{Y}}(\mathbf{X})) \delta \bar{\xi}^\beta \Delta \bar{\xi}^\alpha \right\}, \tag{3.125}
\end{aligned}$$

and

$$\begin{aligned}
A_{\alpha\beta} \Delta(\delta \bar{\xi}^\beta) &= -\boldsymbol{\tau}_\alpha \cdot \boldsymbol{\omega}_{,\beta}^{(2)}(\bar{\mathbf{Y}}(\mathbf{X})) \Delta \bar{\xi}^\beta - \boldsymbol{\tau}_\alpha \cdot \Delta \boldsymbol{\varphi}_{t,\beta}^{(2)}(\bar{\mathbf{Y}}(\mathbf{X})) \delta \bar{\xi}^\beta \\
&\quad - \left[\boldsymbol{\tau}_\alpha \cdot \boldsymbol{\varphi}_{t,\beta\gamma}^{(2)}(\bar{\mathbf{Y}}(\mathbf{X})) + g \mathbf{v} \cdot \boldsymbol{\varphi}_{t,\alpha\beta\gamma}^{(2)}(\bar{\mathbf{Y}}(\mathbf{X})) \right] \delta \bar{\xi}^\beta \Delta \bar{\xi}^\gamma \\
&\quad - \delta \bar{\xi}^\beta \boldsymbol{\tau}_\beta \cdot \left[\Delta \boldsymbol{\varphi}_{t,\alpha}^{(2)}(\bar{\mathbf{Y}}(\mathbf{X})) + \boldsymbol{\varphi}_{t,\alpha\gamma}^{(2)}(\bar{\mathbf{Y}}(\mathbf{X})) \Delta \bar{\xi}^\gamma \right] \\
&\quad - \Delta \bar{\xi}^\beta \boldsymbol{\tau}_\beta \cdot \left[\boldsymbol{\omega}_{,\alpha}^{(2)}(\bar{\mathbf{Y}}(\mathbf{X})) + \boldsymbol{\varphi}_{t,\alpha\gamma}^{(2)}(\bar{\mathbf{Y}}(\mathbf{X})) \delta \bar{\xi}^\gamma \right] \\
&\quad - g \mathbf{v} \cdot \left[\boldsymbol{\omega}_{,\alpha\beta}^{(2)}(\bar{\mathbf{Y}}(\mathbf{X})) + \Delta \boldsymbol{\varphi}_{t,\alpha\beta}^{(2)}(\bar{\mathbf{Y}}(\mathbf{X})) \delta \bar{\xi}^\beta \right] \\
&\quad + [\boldsymbol{\omega}^{(1)}(\mathbf{X}) - \boldsymbol{\omega}^{(2)}(\bar{\mathbf{Y}}(\mathbf{X}))] \cdot \left[\Delta \boldsymbol{\varphi}_{t,\alpha}^{(2)}(\bar{\mathbf{Y}}(\mathbf{X})) + \boldsymbol{\varphi}_{t,\alpha\gamma}^{(2)}(\bar{\mathbf{Y}}(\mathbf{X})) \Delta \bar{\xi}^\gamma \right] \\
&\quad + [\Delta \boldsymbol{\varphi}^{(1)}(\mathbf{X}) - \Delta \boldsymbol{\varphi}^{(2)}(\bar{\mathbf{Y}}(\mathbf{X}))] \cdot \left[\boldsymbol{\omega}_{t,\alpha}^{(2)}(\bar{\mathbf{Y}}(\mathbf{X})) + \boldsymbol{\varphi}_{t,\alpha\gamma}^{(2)}(\bar{\mathbf{Y}}(\mathbf{X})) \Delta \bar{\xi}^\gamma \right]. \tag{3.126}
\end{aligned}$$

The quantity $A_{\alpha\beta}$ is defined as before, as $A_{\alpha\beta} := m_{\alpha\beta} + g \kappa_{\alpha\beta}$ and $\kappa_{\alpha\beta}$ is $\kappa_{\alpha\beta} := \mathbf{v} \cdot \boldsymbol{\varphi}_{t,\alpha\beta}^{(2)}(\bar{\mathbf{Y}}(\mathbf{X}))$ [20].

3.3.2. DISCRETIZING THE CONTACT INTEGRAL

Solving the problem with the Finite Element Method needs for both the contact integral and the linearized contact integral to be discretized. In this section the discretization of the contact integral will be given. Recall that the contact integral is given as

$$\delta W^c(\boldsymbol{\varphi}, \boldsymbol{\omega}) = \int_{\Gamma_c^{(1)}} \left[\mathbf{t}_{N_t} \delta g + \mathbf{t}_{T_{at}} \delta \bar{\xi}^\alpha \right] d\Gamma, \tag{3.127}$$

where

$$\delta g = -\mathbf{v} \cdot [\boldsymbol{\omega}^{(1)}(\mathbf{X}) - \boldsymbol{\omega}^{(2)}(\bar{\mathbf{Y}}(\mathbf{X}))], \quad \text{and} \tag{3.128a}$$

$$\delta \bar{\xi}^\alpha = \boldsymbol{\tau}^\alpha \cdot [\boldsymbol{\omega}^{(1)}(\mathbf{X}) - \boldsymbol{\omega}^{(2)}(\bar{\mathbf{Y}}(\mathbf{X}))] \quad (\text{when } g = 0). \tag{3.128b}$$

When discretizing the contact integral the first step is the contact surface discretization. This step is very important as all development of the contact depends only on the configurations and variations evaluated on the contact surfaces, not on values in the interiors. Recall that in Section 2.3.2 $\mathcal{A}^{(2)}$ was defined as a parametrization of the contact surface of the second body, with typical points $\boldsymbol{\xi} \in \mathcal{A}^{(2)}$:

$$\Gamma_c^{(2)} = \boldsymbol{\Psi}_0^{(2)}(\mathcal{A}^{(2)}), \quad \text{and} \quad \boldsymbol{\gamma}_c^{(2)} = \boldsymbol{\Psi}_t^{(2)}(\mathcal{A}^{(2)}). \tag{3.129}$$

A similar relation will now be assumed between $\mathcal{A}^{(1)}$ and $\Gamma_c^{(1)}$, $\boldsymbol{\Psi}_t^{(1)}$, and the typical points in $\mathcal{A}^{(1)}$ will be denoted as $\boldsymbol{\eta}$.

The discretization of the contact surface $\boldsymbol{\varphi}^{(1)}$ of the first body is given, with $\boldsymbol{\eta} \in \mathcal{A}^{(1)e}$, as

$$\boldsymbol{\varphi}^{(1)e}(\boldsymbol{\eta}) = \sum_{a=1}^{n_{nes}} N_a(\boldsymbol{\eta}) \mathbf{d}_a^{(1)}(t), \tag{3.130a}$$

where $\mathbf{d}_a^{(1)}(t)$ is a nodal value of $\boldsymbol{\varphi}^{(1)}$, n_{nes} is the number of nodes per element surface, and $N_a(\boldsymbol{\eta})$ denotes a standard Lagrangian shape function. The interpolation of $\boldsymbol{\omega}^{(1)}$ can similarly be conceived as

$$\boldsymbol{\omega}^{(1)e}(\boldsymbol{\eta}) = \sum_{a=1}^{n_{nes}} N_a(\boldsymbol{\eta}) \mathbf{c}_a^{(1)}, \tag{3.130b}$$

where $\mathbf{c}_a^{(1)}$ is a nodal value of $\boldsymbol{\omega}^{(1)}$ which is independent of time. With these definitions one can also write

$$\mathbf{X}^e(\boldsymbol{\eta}) = \sum_{a=1}^{n_{nes}} N_a(\boldsymbol{\eta}) \mathbf{X}_a. \tag{3.130c}$$

The above definitions can similarly be given for the contact surface of the second body, with $\xi \in \mathcal{A}^{(2)e}$:

$$\boldsymbol{\varphi}^{(2)e}(\xi) = \sum_{b=1}^{n_{nes}} N_b(\xi) \mathbf{d}_b^{(2)}(t), \quad (3.131a)$$

where $\mathbf{d}_b^{(2)}(t)$ is a nodal value of $\boldsymbol{\varphi}^{(2)}$,

$$\boldsymbol{\omega}^{(2)e}(\xi) = \sum_{b=1}^{n_{nes}} N_b(\xi) \mathbf{c}_b^{(2)}, \quad (3.131b)$$

where $\mathbf{c}_b^{(2)}$ is a nodal value of $\boldsymbol{\omega}^{(2)}$ which is again independent of time, and

$$\mathbf{Y}^e = \sum_{b=1}^{n_{nes}} N_b(\xi) \mathbf{X}_b. \quad (3.131c)$$

With these discrete fields the contact integral can now be discretized. It is first noted that the integration can be written as a sum over the n_{sel} surface element areas

$$\delta W^c(\boldsymbol{\varphi}, \boldsymbol{\omega}) = \sum_{e=1}^{n_{sel}} \int_{\Gamma_c^{(1)e}} [\mathbf{t}_N \delta g + \mathbf{t}_{T_\alpha} \delta \bar{\xi}^\alpha] d\Gamma. \quad (3.132)$$

Using a quadrature rule³, the integration can be approximated using a quadrature rule

$$\delta W^c(\boldsymbol{\varphi}, \boldsymbol{\omega}) \approx \sum_{e=1}^{n_{sel}} \left\{ \sum_{k=1}^{n_{int}} W^k j(\boldsymbol{\eta}^k) [\mathbf{t}_N(\boldsymbol{\eta}^k) \delta g(\boldsymbol{\eta}^k) + \mathbf{t}_{T_\alpha}(\boldsymbol{\eta}^k) \delta \bar{\xi}^\alpha(\boldsymbol{\eta}^k)] \right\}, \quad (3.133)$$

where n_{int} is the number of integration points per element surface of $\Gamma_c^{(1)}$. In this approximation W^k is the quadrature weight corresponding to local quadrature point k . The Jacobian of the transformation between the parent and reference domains is denoted by j . The (local) parent coordinate of quadrature point k is denoted by $\boldsymbol{\eta}^k \in \mathcal{A}^{(1)e}$. Defining the vector $\delta \boldsymbol{\Psi}^{c^k}$ of nodal variations corresponding to quadrature point k and the (local) contact force vector corresponding to quadrature point k \mathbf{f}^{c^k} , equation 3.133 can be rewritten as [20]

$$\delta W^c(\boldsymbol{\varphi}, \boldsymbol{\omega}) \approx \sum_{e=1}^{n_{sel}} \left\{ \sum_{k=1}^{n_{int}} W^k j(\boldsymbol{\eta}^k) \delta \boldsymbol{\Psi}^{c^k} \cdot \mathbf{f}^{c^k} \right\}. \quad (3.134)$$

3.3.3. DISCRETIZING THE LINEARIZED CONTACT INTEGRAL

The discretization of the linearized contact integral can be derived in two ways. First of all the linearized contact integral given in equation (3.124) can be derived directly. Secondly, the discretized contact integral given in equation (3.134) can be linearized. Both ways result in the following discretized contact integral:

$$\begin{aligned} \Delta \delta W^c(\boldsymbol{\varphi}, \boldsymbol{\omega}) &\approx \sum_{e=1}^{n_{sel}} \left\{ \sum_{k=1}^{n_{int}} W^k j(\boldsymbol{\eta}^k) \left[\Delta(\mathbf{t}_N(\boldsymbol{\eta}^k) \delta g(\boldsymbol{\eta}^k)) \right. \right. \\ &\quad \left. \left. + \Delta \mathbf{t}_{T_\alpha}(\boldsymbol{\eta}^k) \delta \bar{\xi}^\alpha(\boldsymbol{\eta}^k) + \mathbf{t}_{T_\alpha}(\boldsymbol{\eta}^k) \Delta(\delta \bar{\xi}^\alpha(\boldsymbol{\eta}^k)) \right] \right\} \\ &= \sum_{e=1}^{n_{sel}} \left\{ \sum_{k=1}^{n_{int}} W^k j(\boldsymbol{\eta}^k) \delta \boldsymbol{\Psi}^{c^k} \cdot \mathbf{k}^{c^k} \Delta \delta \boldsymbol{\Psi}^{c^k} \right\}, \end{aligned} \quad (3.135)$$

where \mathbf{k}^{c^k} is the local contact stiffness.

³In FEBio different quadrature rules are used dependent on the contact interface (see Section 2.4.1). In the sliding-with-gaps interface for example, nodal integration is used, whereas the facet-to-facet interface uses Gaussian quadrature.

3.4. QUASI-NEWTON METHODS WITH LINE SEARCH

As mentioned above, a quasi-Newton method is based on the Newton method, but only approximates or updates the stiffness matrix \mathbf{K} . Many possibilities for estimating this stiffness matrix exist, from calculating the matrix only at the first step and then simply keeping it, to calculating it once every several steps. The method that is used in FEBio is called the Broyden-Fletcher-Goldfarb-Shanno (BFGS) method. To improve the model a little, a line search is added to the solution method.

3.4.1. THE QUASI-NEWTON METHOD IN FEBIO; BFGS

The Broyden-Fletcher-Goldfarb-Shanno (BFGS) method does not re-evaluate the stiffness matrix \mathbf{K} at every iteration, it updates it. When updating it should satisfy the following equation

$$\mathbf{K}_k \mathbf{d}_k = \mathbf{G}_k, \quad (3.136)$$

where $\mathbf{d}_k = \mathbf{x}_k - \mathbf{x}_{k-1}$ is a displacement increment and $\mathbf{G}_k = \mathbf{R}_{k-1} - \mathbf{R}_k$ is an increment in the residual.

The first step in updating the stiffness matrix \mathbf{K} is calculating a displacement increment which defines a direction for the displacement increment that is actually used [26]

$$\mathbf{u} = \mathbf{K}_{k-1}^{-1} \mathbf{R}_{k-1}. \quad (3.137)$$

With this the actual displacement increment is given by

$$\mathbf{x}_k = \mathbf{x}_{k-1} + s\mathbf{u}. \quad (3.138)$$

The scalar s is determined from a line search (see Section 3.4.2) and it is used to optimize the increment. Once the displacement increment is known, the residual matrix \mathbf{R}_k can be evaluated. With the equations given above one can also evaluate \mathbf{d}_k and the residual increment \mathbf{G}_k .

The BFGS method now uses the following steps to update the stiffness matrix.

1. The vectors \mathbf{v} and \mathbf{w} are calculated, which are given by

$$\mathbf{v}_k = - \left(\frac{\mathbf{d}_k^T \mathbf{G}_k}{\mathbf{d}_k^T \mathbf{K}_{k-1} \mathbf{d}_k} \right)^{\frac{1}{2}} \mathbf{K}_{k-1} \mathbf{d}_k - \mathbf{G}_k, \text{ and} \quad (3.139a)$$

$$\mathbf{w}_k = \frac{\mathbf{d}_k}{\mathbf{d}_k^T \mathbf{G}_k}. \quad (3.139b)$$

Here $\mathbf{K}_{k-1} \mathbf{d}_k = s\mathbf{R}_{k-1}$.

2. The vectors defined in the first step are used to form the $n \times n$ matrix \mathbf{A}

$$\mathbf{A}_k = \mathbf{I} + \mathbf{v}_k \mathbf{w}_k^T. \quad (3.140)$$

3. In the final step the stiffness matrix is updated as

$$\mathbf{K}_k^{-1} = \mathbf{A}_k^T \mathbf{K}_{k-1}^{-1} \mathbf{A}_k. \quad (3.141)$$

A condition number c of the updating matrix \mathbf{A} is defined in FEBio as

$$c = \left(\frac{\mathbf{d}_k^T \mathbf{G}_k}{\mathbf{d}_k^T \mathbf{K}_{k-1} \mathbf{d}_k} \right)^{\frac{1}{2}}. \quad (3.142)$$

This number is used to decide whether or not the update should be performed. When the number exceeds a preset tolerance the update will not be performed, as this update might be numerically dangerous.

3.4.2. THE LINE SEARCH

In the BFGS-method a line search is used to optimize the displacement increment. The line search does not affect the direction of the displacement increment, but it does control the magnitude of the increment using the scalar s :

$$\mathbf{x}_k = \mathbf{x}_{k-1} + s\mathbf{u}.$$

The value of s is usually chosen so that the residual force $\mathbf{R}(\mathbf{x}_k + s\mathbf{u})$ at the end of the iteration is orthogonal to \mathbf{u} [26]:

$$R(s) = \mathbf{u}^T \mathbf{R}(\mathbf{x}_k + s\mathbf{u}) = 0. \quad (3.143)$$

It is often sufficient to obtain s such that

$$|R(s)| < \rho |R(0)|,$$

where $\rho = 0.9$ is used in FEBio. Usually $s = 1$ satisfies this equation. When this is not the case, s is approximated using an approximation of $R(s)$ in s . FEBio uses

$$R(s) \approx (1-s)R(0) + R(1)s^2 = 0, \quad (3.144)$$

which yields

$$s = \frac{r}{2} \pm \sqrt{\left(\frac{r}{2}\right)^2 - r}, \quad \text{where } r = \frac{R(0)}{R(1)}. \quad (3.145)$$

There are now multiple possibilities:

- $r < 0$: the square root is positive. This obtains

$$s_1 = \frac{r}{2} + \sqrt{\left(\frac{r}{2}\right)^2 - r}.$$

- $r > 0$: the parameter s can be obtained using the value that minimizes the quadratic function, hence

$$s_1 = \frac{r}{2}.$$

The new value is entered into equation (3.144). If the equation is satisfied the parameter s is found. If not, a new value is calculated using now $R(s_1)$ instead of $R(1)$ [26]. This is repeated until a value for s is found for which equation (3.144) is satisfied.

4

RESULTS

4.1. THE OBJECTIVE

In this chapter the results obtained with the different models will be presented. The main goal of this project is to see whether the stress exceeds the strength of the skin, which will cause skin breakdown. Before giving the results this failure theory will therefore be repeated here. More objectives are explained in Section 4.1.2

4.1.1. SKIN FAILURE

In Section 1.2.1 it is stated by Gefen that skin breakdown will occur when the shear stress exceeds the shear strength of the skin. This theory is commonly known as the maximum shear stress theory, which was briefly described in Section 1.1.1.

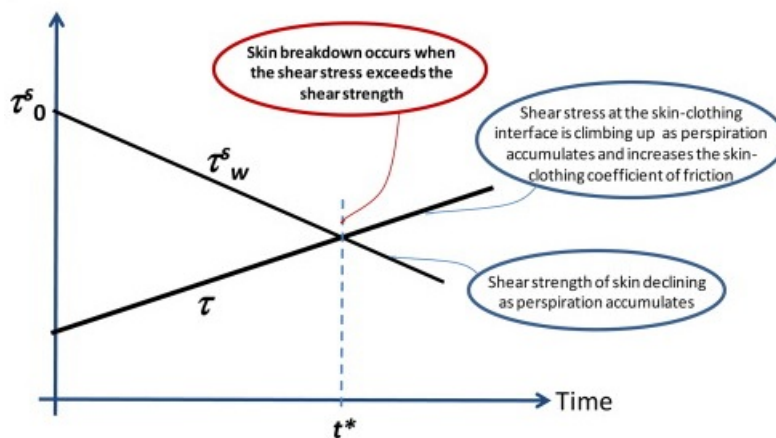


Figure 4.1: Skin break down will occur when the shear stress applied on the skin exceeds the shear strength of the skin. Source: [1]

In the article on microclimate factors [1], both the stress and the strength of the skin are described as functions of the perspiration. However, as mentioned in Section 2.4.2 in this project the stress is calculated using the finite element method in FEBio.

One of the possibilities of FEBio is to save different types of output, such as the stress (both normal and shear) of every element at every time step. Another possible output involves the eigenvalues of the stress tensor of every element at every time step. However, to get information regarding the skin breakdown, we need the maximum shear stress. This quantity cannot be chosen as an output in FEBio, which means it has to be calculated using the definitions given in Sections 2.1.5 and 2.1.6. Here the stresses and the eigenvalues are needed.

The quantities that will be compared here are

1. The shear strength, defined in [1] as

$$\tau_w^s = \left(1 - 0.8 \frac{\Delta V(t)}{V}\right) \tau_0^s, \quad (4.1)$$

where $\frac{\Delta V(t)}{V}$ is the volume of perspiration ΔV accumulated over a time period t within the available space V between the skin and contacting materials and τ_0^s is the shear strength of dry skin set equal to 70kPa.

2. The maximum shear stress, calculated from the Cauchy stresses obtained by FEBio. Using the definitions of the principal stresses ($\sigma_1 \geq \sigma_2 \geq \sigma_3$) the maximum shear stress is given as $\tau = \frac{1}{2}(\sigma_1 - \sigma_3)$.

4.1.2. OTHER OBJECTIVES

Apart from failure of the skin, there are many other quantities in the model that are of interest. Two of the other topics that will be discussed in this chapter are given below.

1. The location of the maximum stress is very important in the discussion of pressure ulcers, since for deep pressure ulcers the breakdown starts inside the body instead of on the skin. Note that this is only interesting when working with the body load.
2. The material values are dependent on the age and the health of the patient. The effect of this dependence can be considered by plotting the maximum shear stress of different patients (with different values of the Young's modulus) in one figure.

4.2. RESULTS WITH THE BASIC MODEL

In this section some results obtained with the basic models will be given. In the basic model the following two steps are taken.

1. In the first step the body undergoes a downward motion caused by either a body force or prescribed boundary condition of which the last is applied on the inner sphere.
2. In the second step the body moves across the bed, modeled using a prescribed boundary condition. The condition is applied to the same surface as the prescribed boundary condition in step 1.

In the model the Young's modulus of the skin and the coefficient of friction remain constant.

Different cases will be discussed, using the different contact interfaces (sliding with gaps and facet-to-facet sliding (see Section 2.4.1)) and using different downward motion techniques (body force and prescribed boundary conditions (see Section 2.4.1)). We only consider the prescribed boundary conditions applied to the inner sphere of the model. This is done since this is closest to reality.

4.2.1. THE SMALL MODEL (MODEL A) WITH PRESCRIBED BOUNDARY CONDITIONS

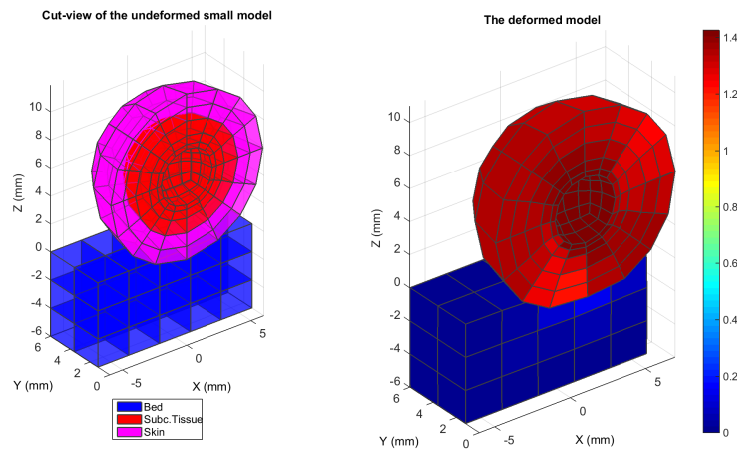
Working with the small basic model using prescribed boundary conditions, three cases are considered. The first case uses the sliding with gaps contact interface while the second case uses the facet-to-facet interface in which there is no friction. The two cases are summarized in Table 4.1. In both cases the standard values for the materials are used, which are given in Section 2.4.1. The third case is used to compare the results for different patients, i.e. different values of the Young's modulus.

Table 4.1: Three cases for the small basic model with prescribed boundary conditions.

	The downward movement	The sideways movement	The contact interface	Friction coefficient
Case 1	1 mm	1 mm	sliding with gaps	0.2
Case 2	1 mm	1 mm	facet-to-facet	no friction
Case 3	1 mm	0.9 mm	facet-to-facet	no friction

CASE 1

In the first case the sliding with gaps interface is used with a friction coefficient of 0.2. The deformation results of this case are given in Figure 4.2.



(a) The undeformed basic model.

(b) The deformed basic model.

Figure 4.2: Deformation results of the small basic model with prescribed boundary conditions.

It is clear that for the most part the body deforms, whereas the mattress only deforms a little. In Figure 4.3 the statistics of the maximum shear stress of the skin elements is plotted. The red line denotes the maximum

value of the maximum shear stress at each time step taken from the values of all the elements. The green line denotes the minimum value and the blue line denotes the average value. An observation that can be made

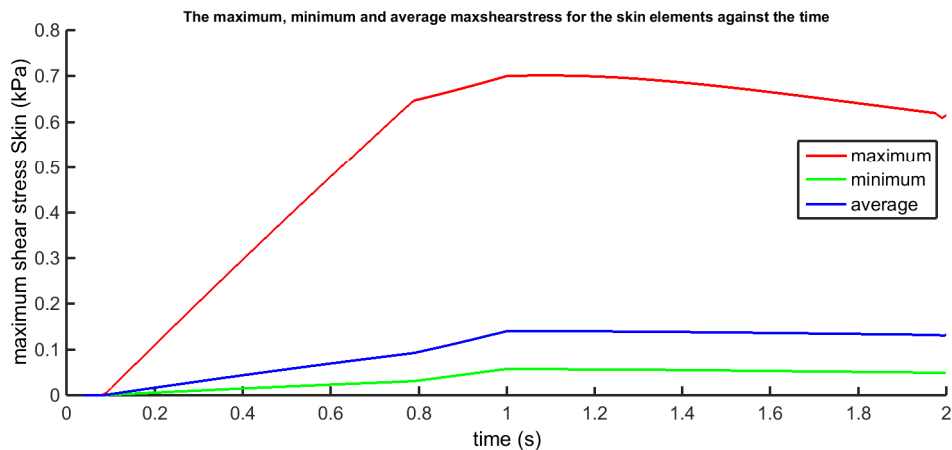


Figure 4.3: The maximum shear stress of the skin elements in the small basic model with prescribed boundary conditions.

from this figure is the fact that the maximum shear stress decreases in the second time step when the patient is moved across the bed. Figure 4.4 shows the maximum values of the maximum shear stress (denoted by the red line) and the shear strength of the skin (denoted by the blue line). The shear strength of the skin is calculated using equation (4.1), where the accumulation of perspiration is described in Section 1.2.1.

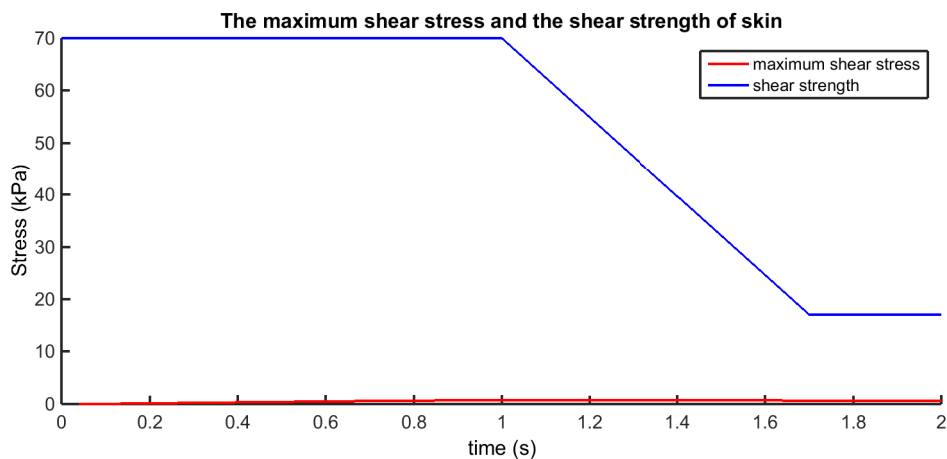


Figure 4.4: The maximum shear stress of the skin compared with the shear strength for the small basic model with prescribed boundary conditions.

From this figure it is clear that the maximum shear stress of the skin is much smaller than the strength of the skin, which means that in this model the skin will not 'break' and pressure ulcers will likely not develop.

CASE 2

In the second case the contact interface was changed to facet-to-facet. As this interface does not take friction into account it is more likely to converge. Taking the same displacement values, the deformation of the model (shown in Figure 4.5) is approximately the same as when modeled with the sliding with gaps contact interface.

Looking at the maximum shear stress though, some differences with respect to the other contact interface can be seen. Looking at Figure 4.6 it can be seen that instead of simply decreasing the maximum shear stress slightly varies when the patient is being moved. It can also be seen that the maximum shear stress is smaller in this case than in case 1. Figure 4.7 shows the plot with both the maximum values of the maximum shear stress and the shear strength of the skin. Similar to in case 1 the lines do not intersect, hence there will be no skin failure.

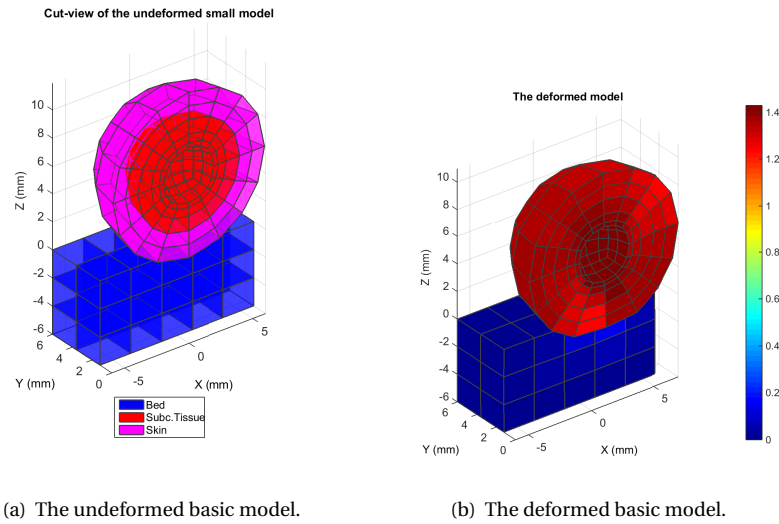


Figure 4.5: Deformation results of the small basic model with prescribed boundary conditions.

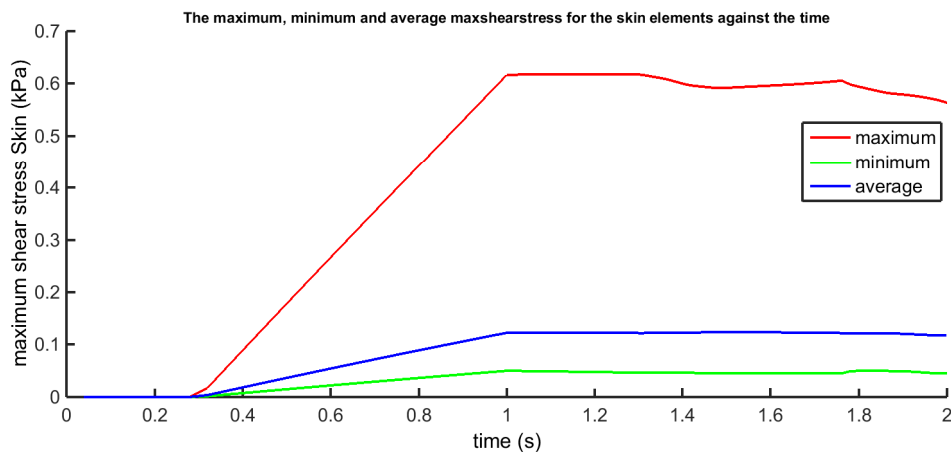


Figure 4.6: The maximum shear stress of the skin elements in the small basic model with prescribed boundary conditions.

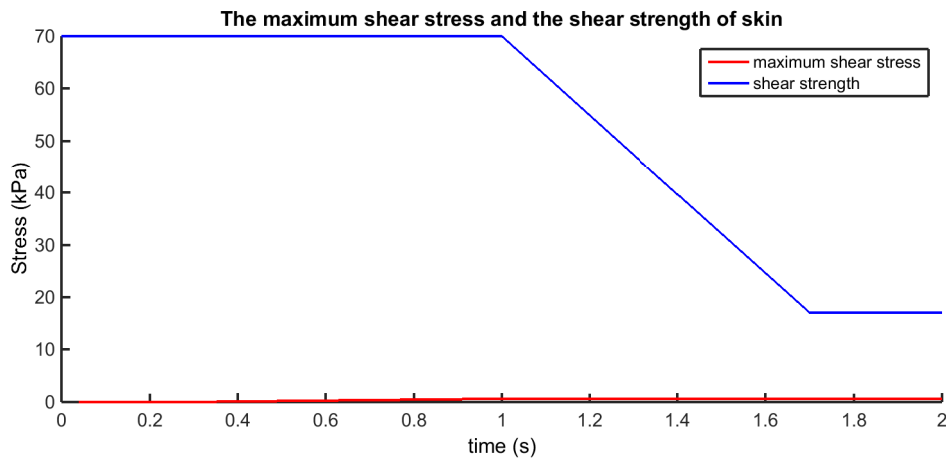
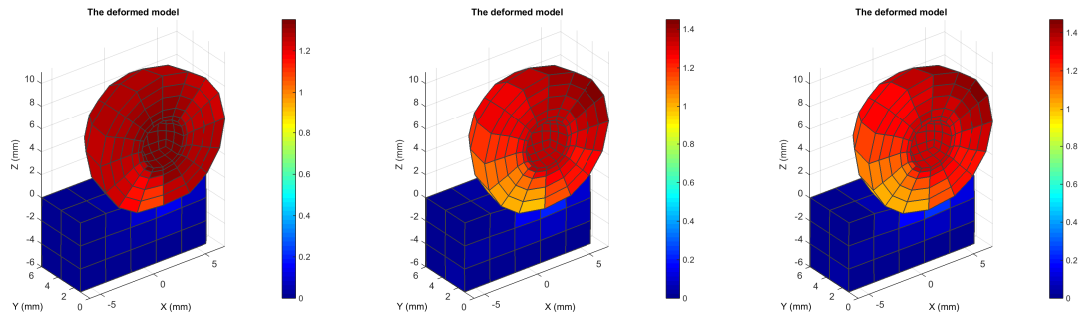


Figure 4.7: The maximum shear stress of the skin compared with the shear strength for the small basic model with prescribed boundary conditions.

CASE 3

In this last case the same model is solved three times, only changing the Young's modulus of the skin. The contact interface that is used here is the facet-to-facet interface, as this converges better. It can be seen that,



(a) The deformed basic model with Young's modulus 15.2 kPa. (b) The deformed basic model with Young's modulus 50 kPa. (c) The deformed basic model with Young's modulus 100 kPa.

Figure 4.8: Deformation results of the small basic model with prescribed boundary conditions for different values of the Young's modulus.

although small, there are differences in the amount of deformation. More interesting however, is the result shown in Figure 4.9. Here the maximum shear stress is plotted for the three different values of the Young's modulus. It is clear that when the Young's modulus is larger, that is, the skin is stiffer, the maximum shear stress is higher. It can be noted however, that there is still no skin failure as the values of the stress remain far below 70 kPa.

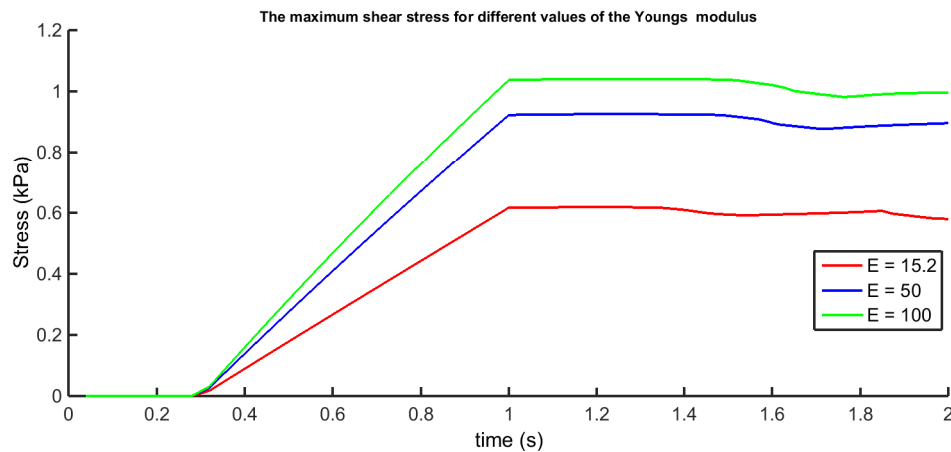


Figure 4.9: The maximum shear stress of the skin for different values of the Young's modulus.

4.2.2. THE SMALL MODEL (MODEL A) WITH A BODY LOAD

Having considered the small model with prescribed boundary conditions, we will now turn to the small model where the body load is applied. Before giving the results it must be noted that the model does not converge as well when working with a body load. The first thing that is done to improve the convergence is the use a coarser mesh. Secondly, instead of using multiple materials such as subcutaneous tissue and skin, only skin is used in this model.

As the convergence is an issue here only one case will be considered.

Table 4.2: A single case for the small basic model with a body load.

	The applied acceleration	The sideways movement	The contact interface	Friction coefficient
Case 1	$9.81 \cdot 10^3$ mN/kg	1 mm	sliding with gaps	0.2

CASE 1

The first characteristic that needs to be noted is the fact that the convergence of this simulation does not go very smooth. In the first few steps of the solution, the body 'twitches' from side to side, as shown in the snapshots in Figure 4.10. When looking closely it can be seen that the sphere has moved to the right in the second snapshot, and has moved back in the fourth. In the final snapshot (at $t = 0.01686$), the sphere is in the correct position and the convergence continues smoothly.

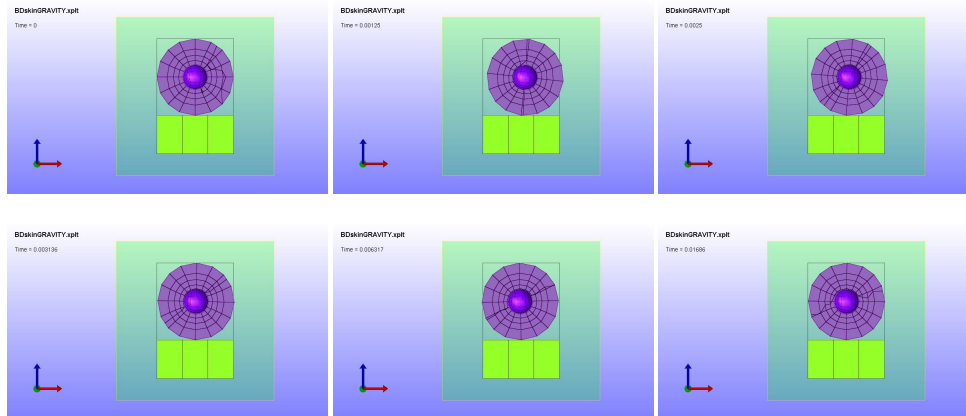
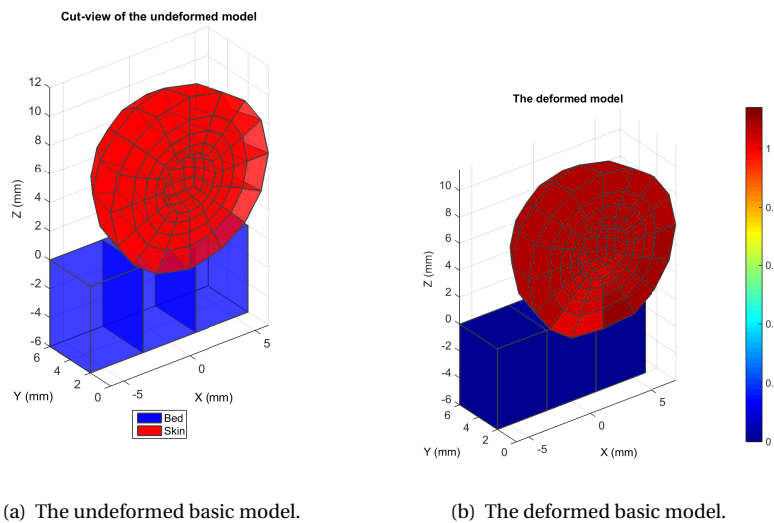


Figure 4.10: Twitches in the first few steps of the solution

In the first case the sliding with gaps interface is used with a friction coefficient of 0.2. The deformation results of this case when using the body load are given in Figure 4.11.



(a) The undeformed basic model.

(b) The deformed basic model.

Figure 4.11: Deformation results of the small basic model with a body load.

It can be seen that the body hardly deforms. To see the movement in more detail, FEBio's post processor PostView is used. Figure 4.12 shows the displacement of the body in the z-direction at $t = 1$ when the downward movement is complete. It can be seen that the maximum downward displacement is around 0.4 mm, which is very small. It does however seem close to reality as the model only consists of a hollow sphere with a 6mm radius. Comparing this to a human body is similar to considering a fingertip. As the weight of such a fingertip is very small, it will hardly deform.

Looking at the maximum shear stress values (Figure 4.13), it can be seen that they are always less than 0.5kPa, which, when considering it's the size of a fingertip might even be a lot.

Figure 4.14 shows the maximum values of the maximum shear stress (denoted by the red line) and the shear strength of the skin (denoted by the blue line), and as expected, the skin will not break.

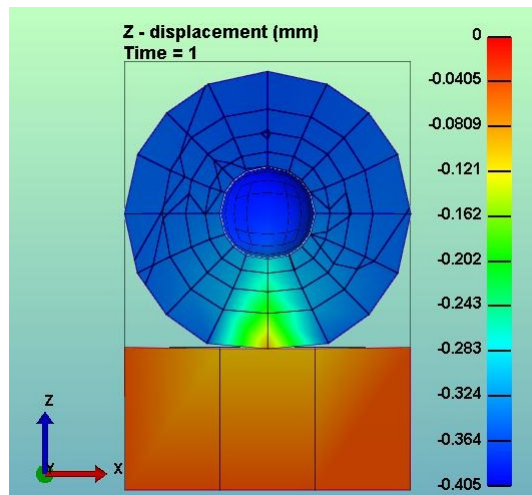


Figure 4.12: Downward displacement due to gravity for the small basic model.

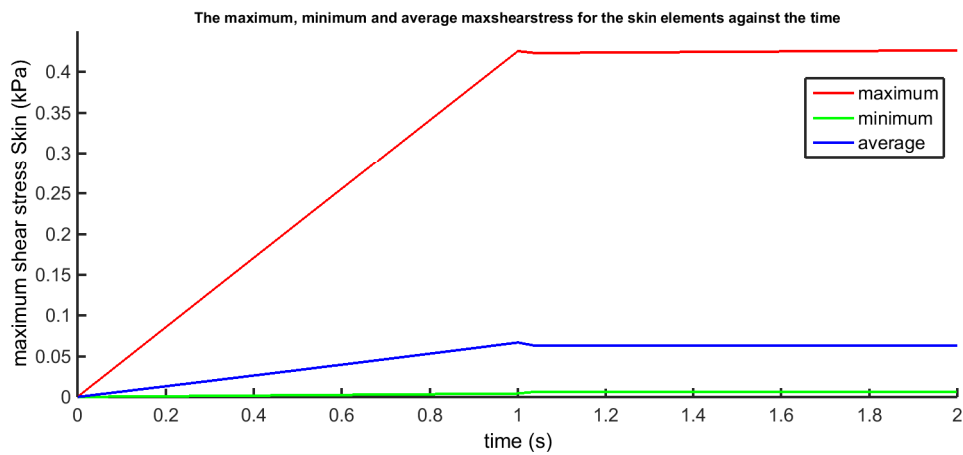


Figure 4.13: The maximum shear stress of the skin elements in the small basic model with a body load.

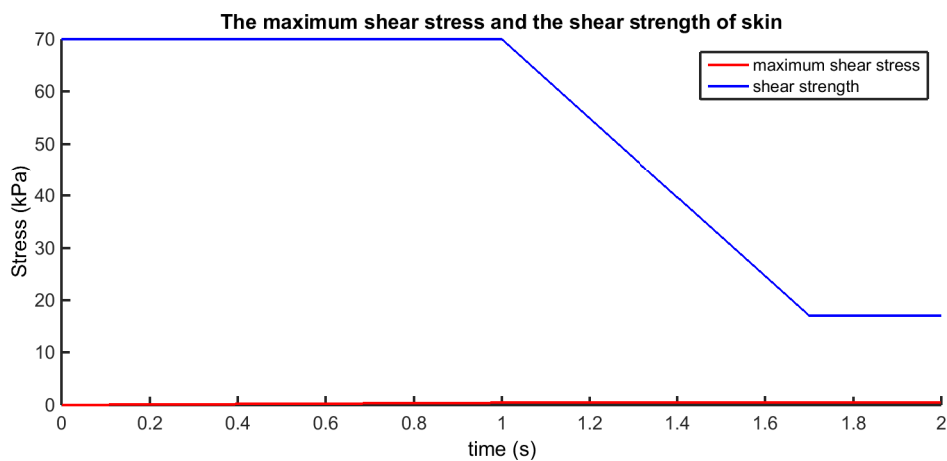


Figure 4.14: The maximum shear stress of the skin compared with the shear strength for the small basic model with a body load.

Another interesting result from this simulation is the location of the shear stress. Right from the beginning of the contact the shear stress goes all the way to the center of the sphere. Figure 4.15 shows the maximum shear stress indicated by color for two different time steps. Note that the stress in the center of the sphere could result in deep tissue injury.

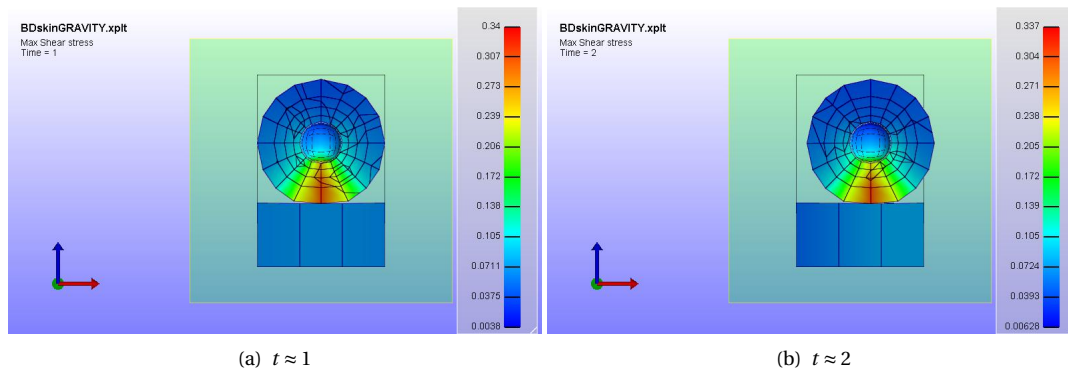


Figure 4.15: The maximum shear stress in the small basic body.

4.2.3. THE BIG MODEL (MODEL B) WITH PRESCRIBED BOUNDARY CONDITIONS

The results of the big model will be discussed using only one case. This is done as the convergence of the big model is rather bad. This case will use the facet-to-facet contact interface. The case is summarized in Table 4.3.

Table 4.3: A single case for the big basic model with prescribed boundary conditions.

	The downward movement	The sideways movement	The contact interface	Friction coefficient
Case 1	5 mm	5 mm	facet-to-facet	no friction

CASE 1

This case considers the facet-to-facet contact interface, which does not include friction. The deformations of the model are shown in Figure 4.16. It can be seen that the deformations are very small. Looking at the

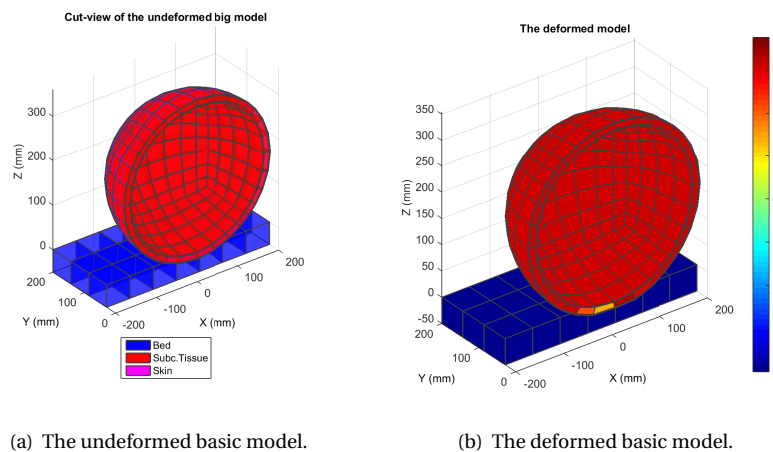


Figure 4.16: Deformation results of the big basic model with prescribed boundary conditions.

maximum shear stress in Figure 4.17, one immediately notices the sudden change around $t = 1$. At this time the body is ordered to move sideways, which in this model is very difficult for the body. For this reason the body moves upwards just a little, which causes the stress to decrease. The body then moves sideways, which causes the stress levels to slightly increase again. Figure 4.18 shows the plot with both the maximum values of the maximum shear stress and the shear strength of the skin. It can be seen that the lines do not intersect, hence there will be no skin failure.

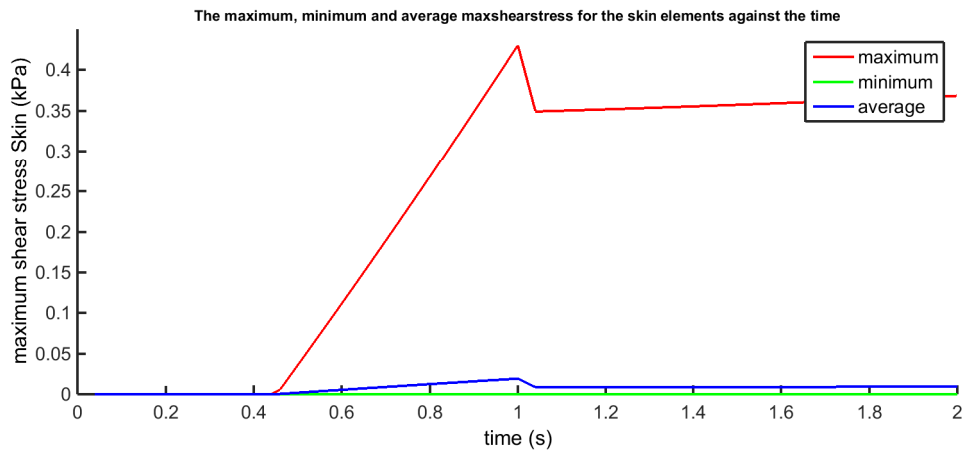


Figure 4.17: The maximum shear stress of the skin elements in the big basic model with prescribed boundary conditions.

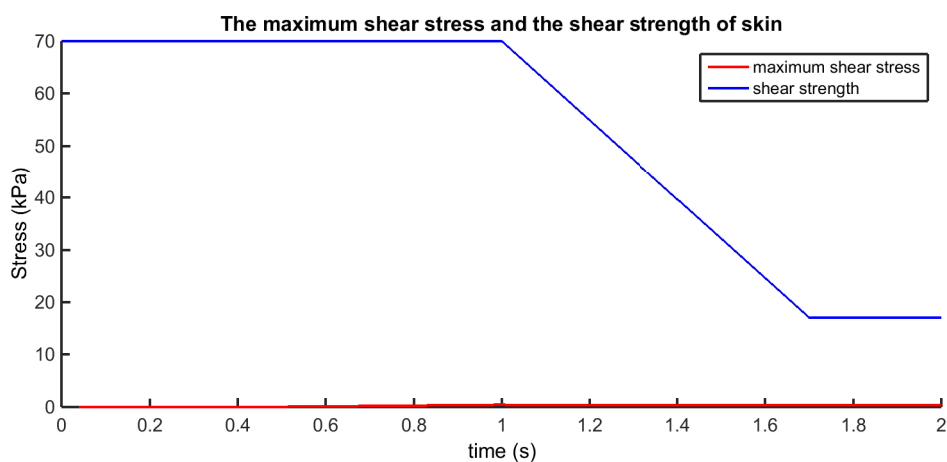


Figure 4.18: The maximum shear stress of the skin compared with the shear strength for the big basic model with prescribed boundary conditions.

4.2.4. RESULTS OF THE BASIC MODEL

Considering all the results obtained using the basic model, several things can be noted.

1. The maximum value of the maximum shear stress does not come close to the value of the shear strength of the skin, which means that when working with this model there will be no skin failure. This is most likely due to the absence of weight in the model. As the model exists of a hollow sphere, it does not really represent the human body in a realistic way.
2. Using the facet-to-facet contact interface results in lower stresses than those obtained with the sliding with gaps interface. This makes sense, as the friction makes the contact and especially the movement across the bed more difficult.
3. Increasing the Young's modulus will lead to an increase in the maximum shear stress values. Again this is to be expected since a higher Young's modulus corresponds to a stiffer skin, which will deform less easily.

4.3. RESULTS OF THE MODEL INCLUDING MICROCLIMATE FACTORS

In this section the results obtained with the model including microclimate factors will be given. The following three steps are taken:

1. In the first step the body undergoes a downward motion caused by either a body force or prescribed boundary condition of which the last is either applied on the inner sphere or the outer sphere.
2. The body does not move. In this step the coefficient of friction changes according to

$$\mu = 0.5 \frac{\Delta V(t)}{V} + 0.4. \quad (4.2)$$

For the skin temperature given as $T_s = 30^\circ\text{C}$ the coefficient of friction is shown in Figure 4.19.

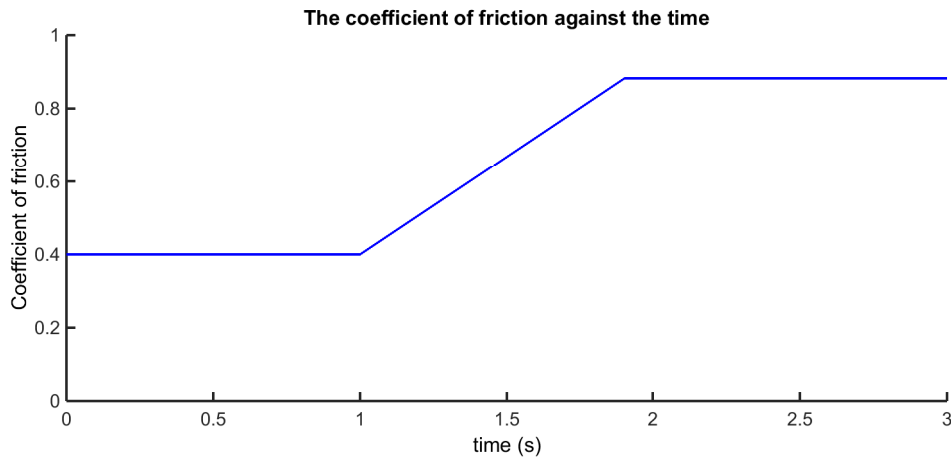


Figure 4.19: The coefficient of friction for a skin temperature of $T_s = 30^\circ\text{C}$.

3. In the third step the body moves across the bed, modeled using a prescribed boundary condition. The condition is applied to the same surface as the prescribed boundary condition in step 1.

Similar to the basic model, different cases will be discussed. For this model it should be noted though that the facet-to-facet contact interface will not be used, as this interface does not include friction. Since this model is specifically created to change the coefficient of friction in time, friction needs to be a part of the solving method.

From this section on, we will only consider the small model with the body load. This because using gravity gives more realistic results, and the small problem converges a lot better than the big model.

4.3.1. THE SMALL MODEL WITH MICROCLIMATE FACTORS

When using the body load to simulate gravity a coarser mesh is used as before, and also the body will be made up of skin. Only one case will be considered:

Table 4.4: A single case for the small model including microclimate factors with a body load.

	The applied acceleration	The sideways movement	The contact interface	Friction coefficient
Case 1	$9.81 \cdot 10^3 \text{ mN/kg}$	1 mm	sliding with gaps	$\mu = 0.5 \frac{\Delta V(t)}{V} + 0.4$.

CASE 1

Similar to the basic model, using a body load for the downward motion makes the problem harder to solve. In the first few steps of the solution, the body 'twitches' again from side to side, but after 0.01 time step the problem converges normally. The deformation due to the gravity is shown in Figure 4.20.

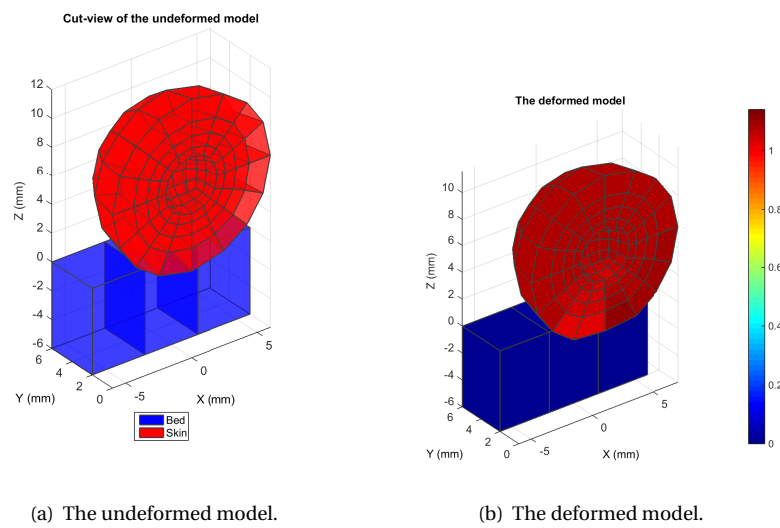


Figure 4.20: Deformation results of the small model including microclimate factors with a body load.

Looking at the maximum shear stress values (Figure 4.21), it can be noted that also in the case of gravity, the shear stress does not increase when the coefficient of friction changes. This is in contradiction with the idea presented in the article on microclimate factors written by Amit Gefen [1].

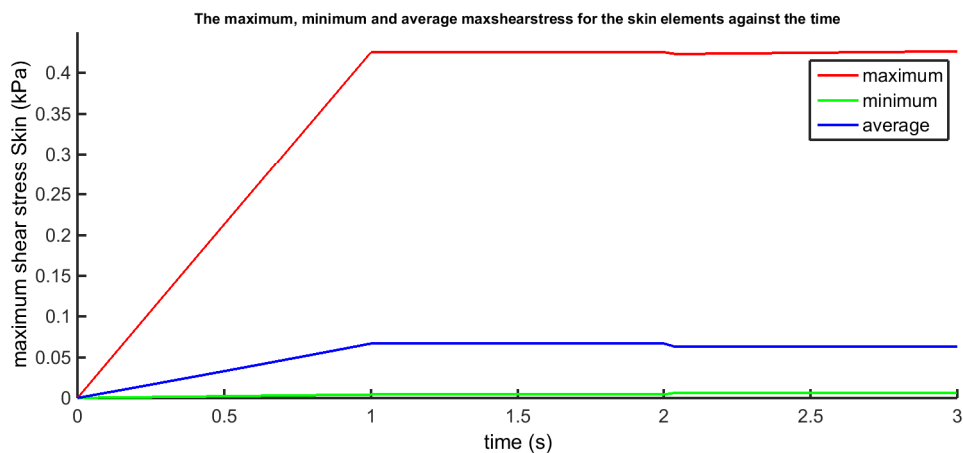


Figure 4.21: The maximum shear stress of the skin elements in the small model including microclimate factors with a body load.

Figure 4.22 shows the maximum values of the maximum shear stress (denoted by the red line) and the shear strength of the skin (denoted by the blue line). Note that the changing coefficient of friction hardly affects the shear stress values, and hence the skin will still not break.

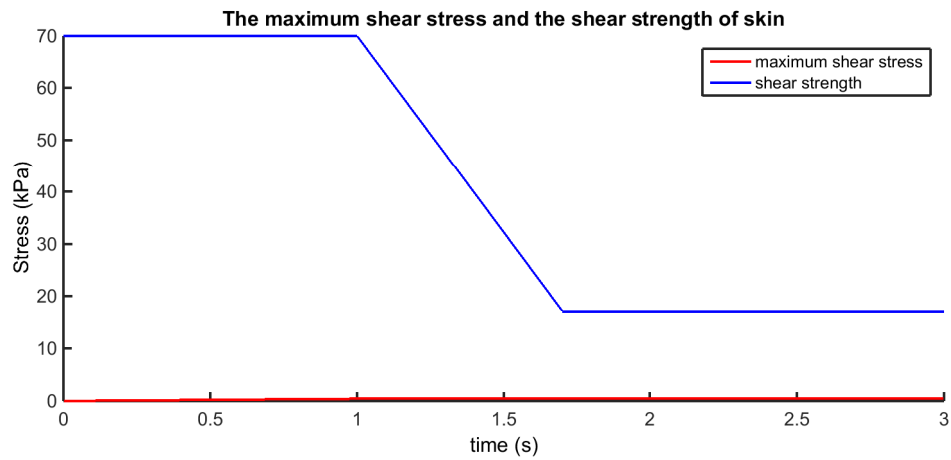


Figure 4.22: The maximum shear stress of the skin compared with the shear strength for the small model including microclimate factors with a body load.

4.4. RESULTS OF FINAL MODEL

In chapter 2.4.3, three different improvements have been discussed. In this chapter, these improvements are added to the model one by one, starting with the changing Young's modulus. Once this improvement is included, additional weight will be added to the model. Finally, the results of the model with a different temperature will be shown. The results of each improvement is shown using the small model with a body load.

4.4.1. CHANGING THE YOUNG'S MODULUS

The first change in the model is making the Young's modulus dependent of the time. This was done using the loadcurve [0 15.2; 1 15.2; 1.5 50; 2 100; 3 100]. The sideways movement is taken to be 1mm. The deformations of the small model in which the Young's modulus is changed in time are shown in Figure 4.23. It can be seen that the downward deformation at the final time step is close to zero. The

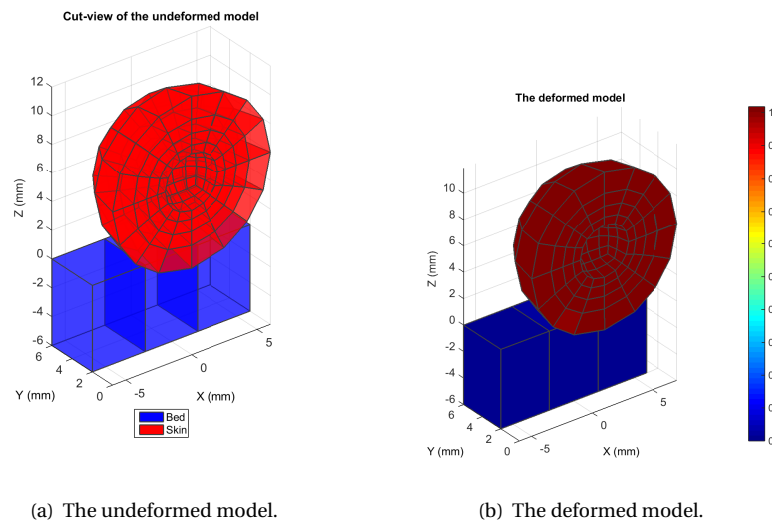


Figure 4.23: Deformation results of the small model with a changing Young's modulus with a body load.

downward displacement of the model is shown in more detail in Figure 4.24.

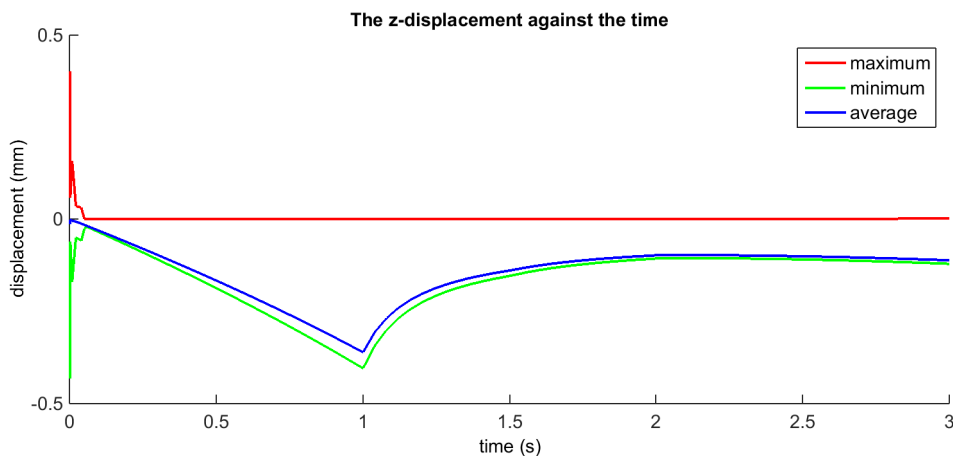


Figure 4.24: The downward of the small model with a changing Young's modulus.

It can be seen that during the first time step the body moves downwards, but during the second step this movement is reversed. This reversed movement is due to the changing stiffness of the skin. As the skin gets stiffer, it cannot handle the deformation, and hence will move upwards to try to return to its original geometry.

Looking at the maximum shear stress of the skin it can be seen that the stress now slightly changes during the second time step. This is probably due to the movement caused by the changing Young's modulus.

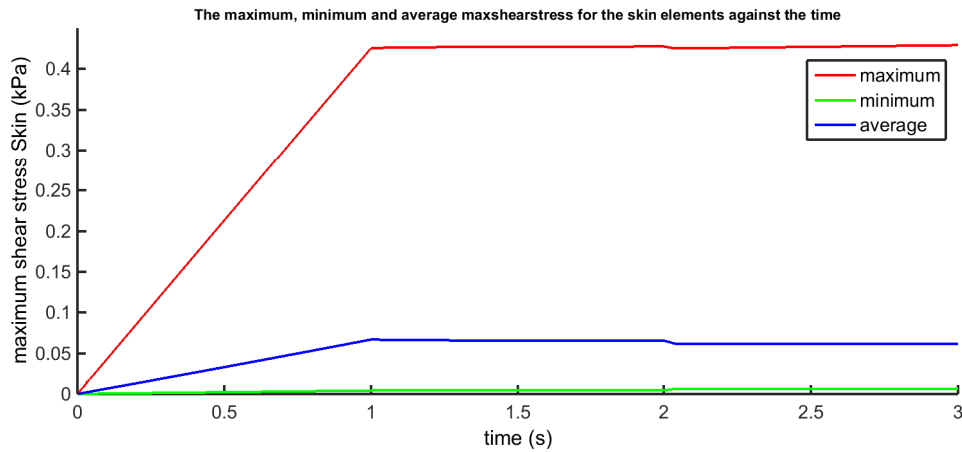


Figure 4.25: The maximum shear stress of the skin elements in the small model with a changing Young's modulus with a body load.

Comparing the maximum shear stress of the skin with the shear strength of the skin, Figure 4.26 is obtained. Still the lines do not intersect, and hence there is no skin-failure.

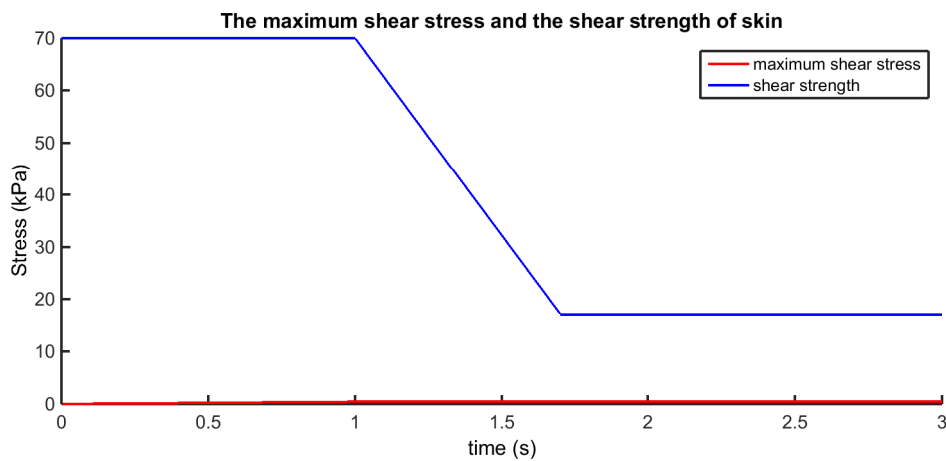


Figure 4.26: The maximum shear stress of the skin compared with the shear strength for the small model with a changing Young's modulus with a body load.

4.4.2. ADDING WEIGHT

The second change in the model is adding more weight to the model. This is done by decreasing the size of the hollow sphere in the center. Instead of a radius of 2mm the inner sphere now has a radius of 0.5 mm. The results of this change are shown below. First of all we will look at the deformation of this heavier model (Figure 4.27). Looking at the downward displacement against the time (Figure 4.28) it can be seen

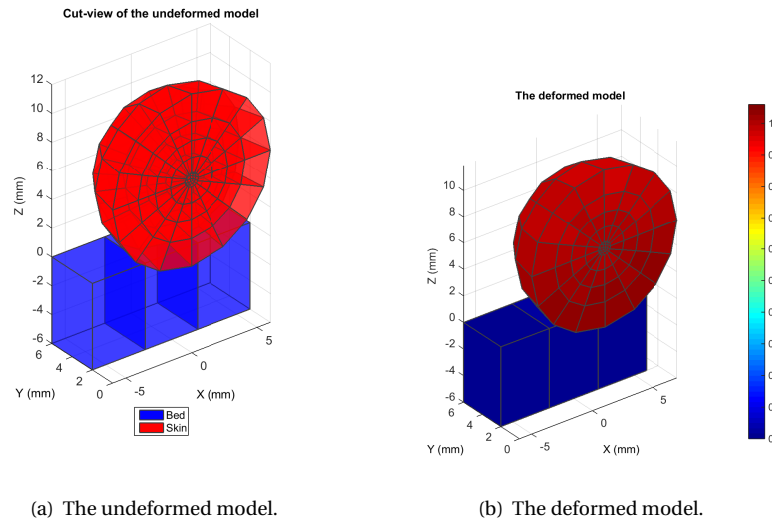


Figure 4.27: Deformation results of the small model with additional weight modeled with a body load.

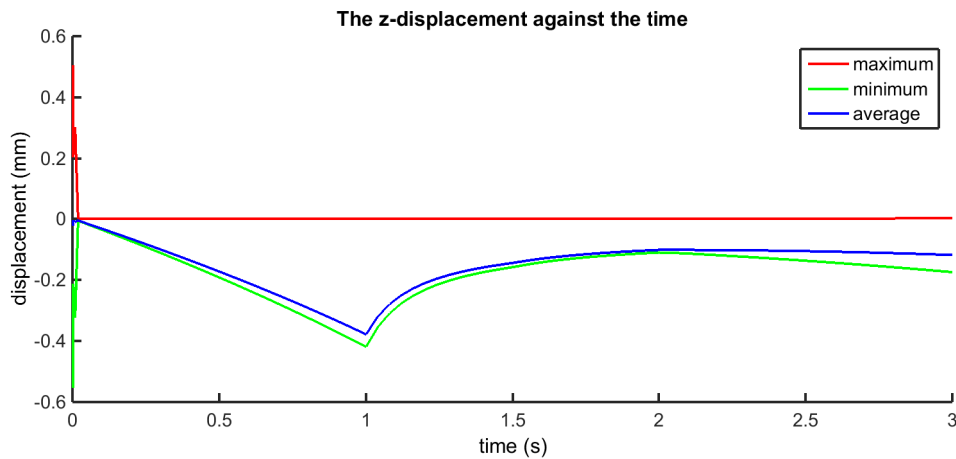


Figure 4.28: The downward of the small model with additional weight.

that, compared to the model without additional weight, the downward displacement of both models is quite similar. Again it can be seen that the body moves upwards while the Young's modulus changes. Looking at the maximum shear stresses it can be seen that the additional weight results in slightly higher values. However, as Figure 4.30 shows, the lines do not yet intersect, and hence there will be no skin failure.

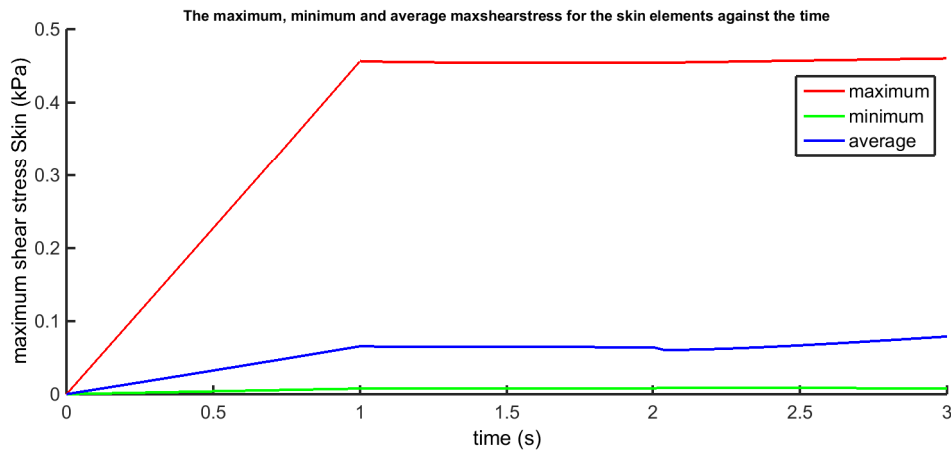


Figure 4.29: The maximum shear stress of the skin elements in the small model with additional weight modeled with a body load.

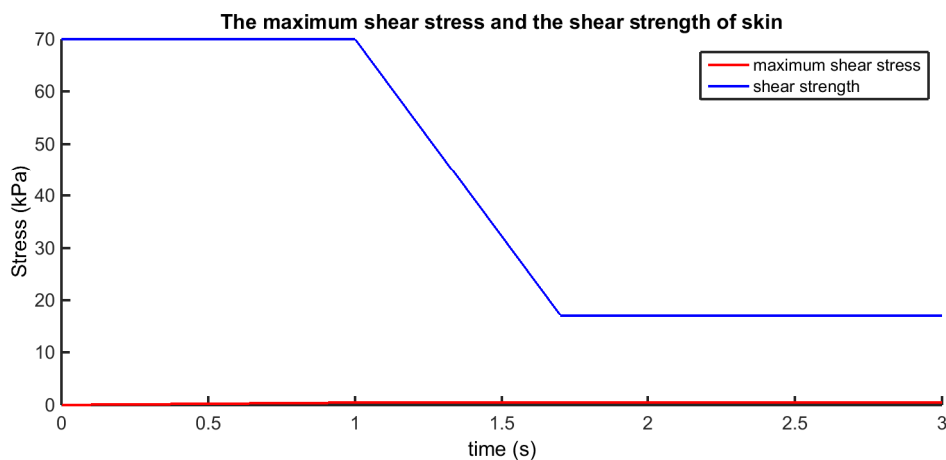


Figure 4.30: The maximum shear stress of the skin compared with the shear strength for the small model with additional weight modeled with a body load.

4.4.3. CHANGING THE TEMPERATURE

When changing the temperature of the skin from 30°C to 35°C one must note that all parts of the microclimate factors will change. Figures 4.31, 4.32 and 4.33 show respectively the change in the accumulation of perspiration, the coefficient of friction and the shear strength of the skin caused by the change in temperature.

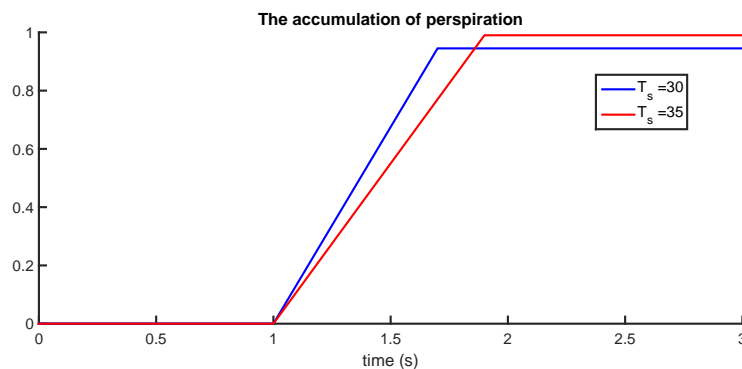


Figure 4.31: The accumulation of perspiration for different skin temperatures.

To see the effects of the changing temperature the small model is solved for a skin temperature of 35°C.

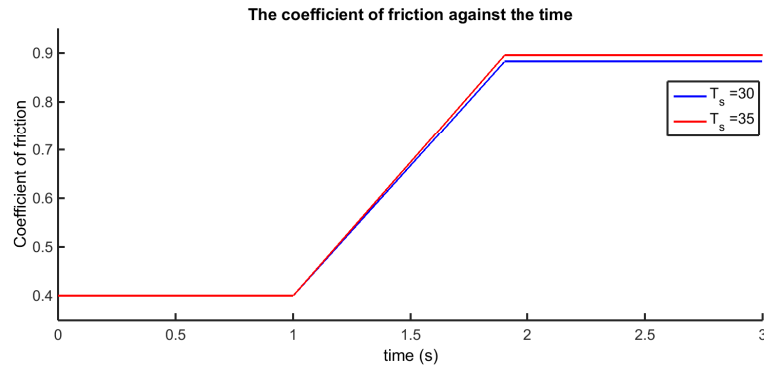


Figure 4.32: The coefficient of friction for different skin temperatures.

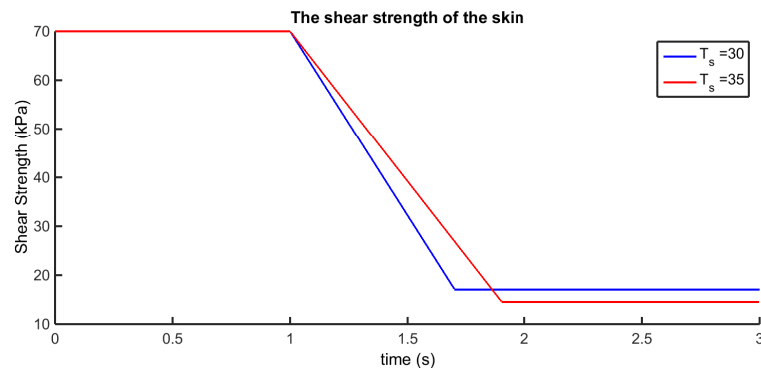


Figure 4.33: The shear strength of the skin for different skin temperatures.

The model that is used is the model with changing Young's modulus and additional weight (inner radius is 1mm instead of 2mm).

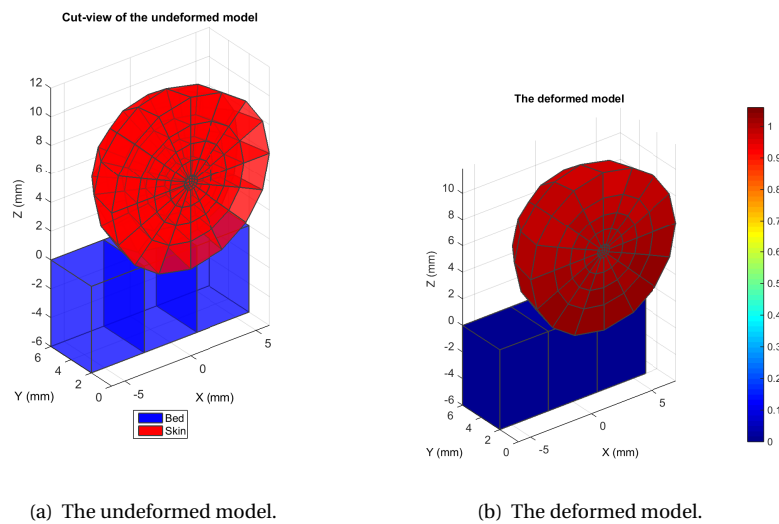


Figure 4.34: Deformation results of the small model with $T_s = 35^\circ\text{C}$ modeled with a body load.

Looking at the results shown in figures 4.35 and 4.36 it can be seen that the maximum shear stress does not become higher than the shear strength.

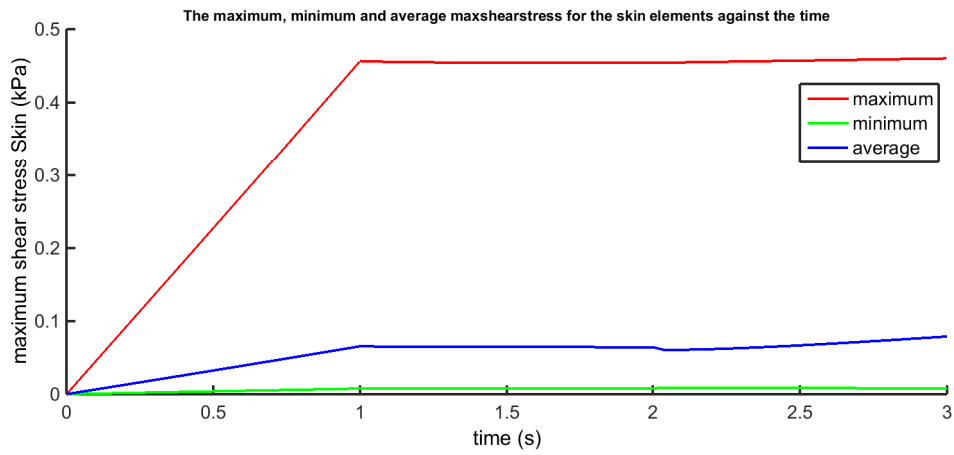


Figure 4.35: The maximum shear stress of the skin elements in the small model with $T_s = 35^\circ\text{C}$ modeled with a body load.

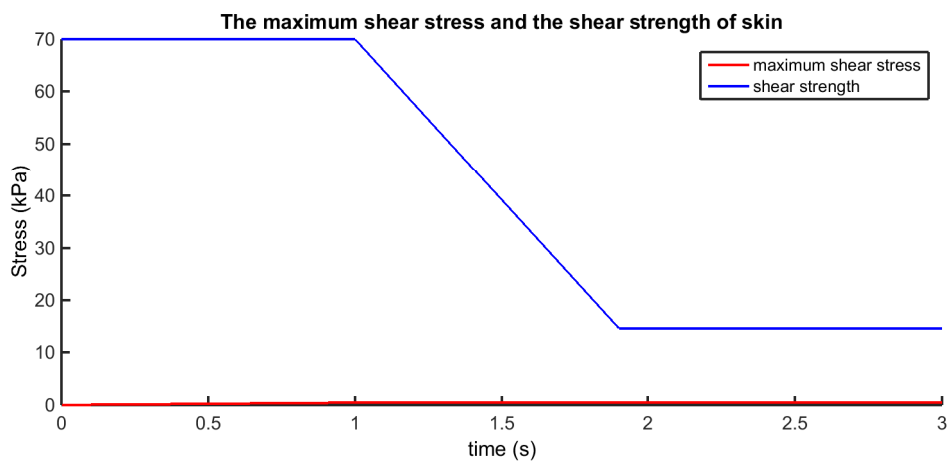


Figure 4.36: The maximum shear stress of the skin compared with the shear strength for the small model with $T_s = 35^\circ\text{C}$ modeled with a body load.

4.5. OVERALL RESULTS

For all models the first time step is the step in which the shear stress increases the most. In the second step the shear stress only changes when the Young's modulus is changed.

Having looked at all the models the results of the different simulations can be compared. To get a clear idea of the differences in the maximum shear stress values, all the models have been solved for the same displacements using the body load. For the small models all cases were solved for a sideways displacement of 1 mm. The resulting maximum shear stresses is shown in Figure 4.37.

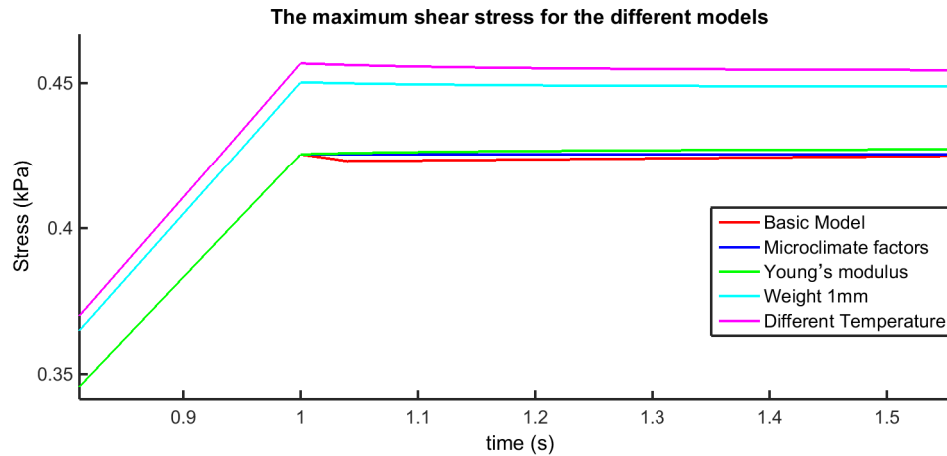


Figure 4.37: The maximum shear stress of the skin for all different models.

It can be seen that every element that was added to the model results in an increase of the values of the maximum shear stress. Especially adding additional weight and increasing the skin temperature show higher values. Though the value increases, the values always remain far below the value of the shear strength of the skin.

We have also seen that when using the body load the shear stress is also present inside the model, not only on the skin.

5

DISCUSSIONS AND CONCLUSIONS

5.1. CONCLUSIONS

The main goal of this thesis was to combine the two models described in the articles written by Amit Gefen ([1] and [2]), which means that the effect of microclimate factors should be included in the contact model between a human body and a hospital bed. The main conclusion is that this goal was accomplished, and a model now exists in which the contact between the human body and a hospital bed changes due to the accumulation of sweat. In the model the body experiences gravity which creates a downwards motion towards the bed, after which the body is moved across the bed as part of the repositioning.

Starting with a small basic model of a body on a bed and enhancing this model with different steps, several conclusions can be drawn.

First of all the Young's modulus has a substantial influence on the stress levels measured in the body. Stiffer skins, that is, higher values of the modulus, result in higher stress levels while experiencing the same movements. This is to be expected, as the body will have more trouble deforming. This result is similar to the results given in [2], in which it is stated that older people (with stiffer skins) have a higher chance of developing pressure ulcers.

When adding the microclimate factors as described in [1] only the coefficient of friction is changed. This is done while the body is at rest on the bed. In the article written by Gefen it is assumed that the shear stress is dependent on the friction coefficient, and hence the stress will increase when the coefficient increases. However, this is not seen in our results. While the coefficient of friction changes, the maximum shear stress of the skin remains constant, which makes sense as the body is at rest.

Though not specifically mentioned in the article on microclimate factors, we assumed that the stiffness of the skin changes when exposed to fluids as sweat. This was modeled by changing the Young's modulus simultaneously with the coefficient of friction. What was not expected beforehand is that increasing the Young's modulus would result in an upwards motion of the body. It does however make sense that this happens, as the body cannot handle the deformation that is created in the first step.

A significant influence on the maximum shear stress levels is given by the weight of the model. Though the model shown here is still very small (a sphere of 12mm diameter corresponds maybe to a single finger) it can be seen that a small increase of weight leads to an increase of the stress levels.

The final addition to the model was using a different temperature of the skin. It is seen that when a higher temperature is used, higher stress levels occur and also the strength of the skin decreases slower but more profoundly. From this it can be noted that patients with a fever will have a higher chance of developing a pressure ulcer.

Regarding the solution method it can be concluded that, though FEBio gives the user many options, the convergence of the solution remains a problem. Solving the small model using a body load takes about a minute, but it does not always converge. The problem has to run several times before it converges. The bigger, more realistic problem has even more problems converging, which is why it is not included in this thesis.

While the small model works the same as the bigger model, the stress levels will be higher for the bigger model. Using only the small model we have not experienced an intersection between the strength of the skin

and the stress levels of the skin, which is why we cannot give any conclusions regarding the time it takes to develop a pressure ulcer.

5.2. DISCUSSION

Though a model was created in which the microclimate factors are included in the contact between a body and a bed, several improvements can still be made. Some of these improvements and remarks will be discussed in this chapter.

The first big remark that can be made is the model that is most discussed in this thesis is the small model with a diameter of 12mm. When looking at the human body this might represent a toe. Drawing results from this model regarding the actual development of pressure ulcers is not very realistic. Though the mechanics of this model and a bigger model will be the same, the stress levels will differ, which will lead to actual usable results.

Secondly, the reason why the small model is used is the issue of convergence. The fact that contact problems are hard to solve directly shows in the convergence of the model. Though the small model is solved, it took multiple runs for each problem to find a solution. For the big model a solution was not always found. Specifically when also using a body load to act as gravity, the convergence gets very slow.

Another remark concerns the material used in the model. The small model that is used most often in this thesis only exists of skin, while of course a human body contains a lot more. Also the human body is now modeled as a sphere, which for now is a proper geometry, but when this research is continued the body should eventually be modeled more realistic.

It should be noted that in the solved models not all steps described in the article on microclimate factors ([1]) have been included. First of all the sideways motion is not as big as the movement described in the article, and secondly, the additional downward movement caused by the weight of the caretaker is not included. This was omitted because of the additional difficulty it would bring along in the model, but in the future should be taken into account.

It is currently assumed in the model that the temperatures of the skin and the room are constant. In reality this is not the case though.

5.3. RECOMMENDATIONS FOR FUTURE WORK

From the remarks given above some recommendations can be formulated for future work.

- The model should be increased in order to obtain more realistic and useful results. The most important part in this is finding a mesh and proper values for the solving variables. Different element types could be used, and with this some research could be done concerning the convergence. Different solving methods could be used to find an optimal solving method.
- The geometry of human body should be improved, as well as the materials used in the body. One could for example model a human body as an ellipsoid, with at the center a rigid cylinder to model the bone, around that some muscle tissue, followed by subcutaneous tissue and skin. Even more advanced would be to use an actual model of the human skin including all its organs, as is already being used in the research done in certain hospitals. As those models are not available to the public I have not managed to obtain one.
- It should be noted that the different body parts of the patient are connected. This means that considering only a foot is not realistic, as the effects of the attached leg are omitted. A possible solution for this could be to include additional loading to the sphere.
- As mentioned above, the temperatures are assumed to be constant during this case. In real life however the temperature of the room can change as well as the temperature of the skin. It would be interesting to change the temperature of the skin during the simulation to see for example the effects of a patient developing a fever.
- As FEBio has the option of solving heat equations the temperature of the skin could be calculated during the simulation, which could lead to better results. Combined with the previous idea this would allow the user to model more realistic circumstances regarding the temperature.
- In the current model three steps have been used to model all actions. It could however be interesting to see what would happen if the patient were to remain at rest for a longer period of time. This could be modeled by simply adding a few steps between the lying down and the repositioning.
- In changing the Young's modulus it was now assumed that the skin 'ages' when exposed to fluids. The values used here were not based on any literature, only on the values used by Gefen ([2]). It would be interesting to find information on the actual changing of the skin in the literature. Even better would be to make the Young's modulus dependent on the stress values and accumulated perspiration. This could for instance be done by using the shear modulus (see Appendix A) which can be expressed in terms of the stress.
- As a final recommendation the current model can be used to investigate specific cases of the development of pressure ulcers. An interesting case for example is the situation in which a tube (or something similar) is stuck between a baby or other patient who is not able to move himself and the bed. This additional deformation could be modeled by simply adding a small geometry between the body and the bed and would probably lead to higher stress values around the tube.



ELASTICITY, STRESS AND STRAIN

In contact between solids the concepts of elasticity, stress and strain are very important. In the subject of pressure ulcers, especially stress and strain are of importance. This section will therefore provide some additional information regarding these topics. The knowledge used in this section and its subsections is acquired a.o. from the books Theory of Elasticity, by S. Timoshenko and J.N. Goodier [16], and Introduction to Finite Element Analysis Using MATLAB ® and Abaqus by Amar Khennane, chapter 5 [18].

A.1. ELASTICITY

The property of elasticity is something that all structural materials possess to a certain extent. It means that when external forces cause an object to deform up to a certain limit, the deformation will disappear when the external forces are removed. An object is said to be *perfectly elastic* when it resumes its initial form completely after the removal of all external forces.

Often when modeling elastic bodies it will be assumed that the matter of the body is *homogeneous*. This means that when taking a very small element of the body the same specific physical properties as for the entire body will apply. Another assumption that is often made is that the body is *isotropic*. This means that the elastic properties are the same in all directions.

Even though many structural materials do not satisfy these assumptions, experience has shown that the solutions of the theory of elasticity using these assumptions give very good results for these materials. When the elastic properties however are not the same in all directions, and also cannot be assumed to be the same, the condition of *anisotropy* must be considered.

A.2. STRESS AND STRAIN

Stress and strain are the words most commonly used when talking about applying pressure on an object or when objects are deformed due to external forces. The topic of stress is discussed in detail in Section 2.1.3. In this Appendix we will therefore focus on strain.

STRAIN

When one applies pressure or other external forces on the outside of an object while this object is being restrained against rigid body movement, one not only induces internal forces, but may also cause material points inside the body to be displaced. When this displacement causes the distance between two points in the body to change one speaks of straining.

Similar to stress the strain in a certain point exists of different components. These components are again denoted using the subscripts x , y and z . Same as stress the strain is also divided into two parts; the unit elongations and the shearing strains. These are respectively denoted as ϵ_i and γ_{ij} or as ϵ_{ii} and ϵ_{ij} , where $\gamma_{ij} = \epsilon_{ij} + \epsilon_{ji}$. Here the unit elongation means that the distance between two points in the body only changes in one direction. In the shearing stresses the distance between the points will change in two different coordinates.

The displacements in the Euclidean space are denoted using the letters u , v and w for respectively displace-

ments in the x -plane, y -plane and z -plane. The strain components are then given by

$$\begin{aligned} \epsilon_x &= \frac{\partial u}{\partial x} & \epsilon_y &= \frac{\partial v}{\partial y} & \epsilon_z &= \frac{\partial w}{\partial z} \\ \epsilon_{xy} &= \frac{1}{2} \left(\frac{\partial u}{\partial y} + \frac{\partial v}{\partial x} \right) & \epsilon_{xz} &= \frac{1}{2} \left(\frac{\partial u}{\partial z} + \frac{\partial w}{\partial x} \right) & \epsilon_{yz} &= \frac{1}{2} \left(\frac{\partial v}{\partial z} + \frac{\partial w}{\partial y} \right) \\ \gamma_{xy} &= \frac{\partial u}{\partial y} + \frac{\partial v}{\partial x} & \gamma_{xz} &= \frac{\partial u}{\partial z} + \frac{\partial w}{\partial x} & \gamma_{yz} &= \frac{\partial v}{\partial z} + \frac{\partial w}{\partial y} \end{aligned} \quad (\text{A.1})$$

It can be easily seen that

$$\begin{aligned} \gamma_{xy} &= \gamma_{yx} & \gamma_{xz} &= \gamma_{zx} & \gamma_{yz} &= \gamma_{zy} \\ \epsilon_{xy} &= \epsilon_{yx} & \epsilon_{xz} &= \epsilon_{zx} & \epsilon_{yz} &= \epsilon_{zy} \end{aligned} \quad (\text{A.2})$$

Also the strain can be given in matrix form. One obtains the following matrix

$$\boldsymbol{\epsilon} = \begin{bmatrix} \epsilon_x & \gamma_{xy} & \gamma_{xz} \\ \gamma_{yx} & \epsilon_y & \gamma_{yz} \\ \gamma_{zx} & \gamma_{zy} & \epsilon_z \end{bmatrix}.$$

Using equations (A.2) it can be seen that $\boldsymbol{\epsilon}$ is symmetric. Since the strain matrix consists of only six independent components, some engineers prefer to use a vector notation to represent the strain components. The following vector notations are commonly used in the literature:

$$\vec{\epsilon} = \begin{Bmatrix} \epsilon_x \\ \epsilon_y \\ \epsilon_z \\ \gamma_{xy} \\ \gamma_{yz} \\ \gamma_{xz} \end{Bmatrix} = \begin{Bmatrix} \epsilon_{xx} \\ \epsilon_{yy} \\ \epsilon_{zz} \\ \gamma_{xy} \\ \gamma_{yz} \\ \gamma_{xz} \end{Bmatrix} = \begin{Bmatrix} \epsilon_{xx} \\ \epsilon_{yy} \\ \epsilon_{zz} \\ \epsilon_{xy} + \epsilon_{yx} \\ \epsilon_{yz} + \epsilon_{zy} \\ \epsilon_{xz} + \epsilon_{zx} \end{Bmatrix} = \begin{Bmatrix} \epsilon_{xx} \\ \epsilon_{yy} \\ \epsilon_{zz} \\ 2\epsilon_{xy} \\ 2\epsilon_{yz} \\ 2\epsilon_{xz} \end{Bmatrix},$$

or

$$\vec{\epsilon} = \begin{Bmatrix} \epsilon_{xx} \\ \epsilon_{yy} \\ \epsilon_{zz} \\ \epsilon_{xy} \\ \epsilon_{yz} \\ \epsilon_{xz} \end{Bmatrix} = \begin{Bmatrix} \epsilon_{11} \\ \epsilon_{22} \\ \epsilon_{33} \\ \epsilon_{12} \\ \epsilon_{23} \\ \epsilon_{13} \end{Bmatrix} = \begin{Bmatrix} \epsilon_1 \\ \epsilon_2 \\ \epsilon_3 \\ \epsilon_4 \\ \epsilon_5 \\ \epsilon_6 \end{Bmatrix}.$$

A.3. HOOKE'S LAW

In the previous section the different components for stress and strain are given. The relation between these components are given in Hooke's law. This law says the following.

$$\vec{\sigma} = \mathbf{D}\vec{\epsilon} \quad (\text{A.3})$$

Here the matrix \mathbf{D} is called the stiffness tensor.

Using the vectors $\vec{\sigma}$ and $\vec{\epsilon}$, which both contain only six elements due to symmetry, one can see that the matrix \mathbf{D} has size 6 by 6. These elements contain information regarding the materials of the solids. This information is given using the coefficients of Elasticity. In total there are five different coefficients which are all related to one another. The coefficients are called the Lamé's constants (Lamé's first constant and the shear modulus), Young's modulus, the Poisson's ratio and the Bulk modulus.

Of these parameters, three are moduli of elasticity. These are the shear modulus, Young's modulus and the Bulk modulus. All three describe the ratio of the stress to the strain, hence they are equal to the slope of a stress-strain curve. The elasticity modulus is the mathematical description of an objects tendency to deform elastically when forces are applied to it.

LAMÉ CONSTANTS

The Lamé constants are two constants described by the French mathematician Gabriel Lamé; Lamé's first parameter λ and the shear modulus denoted by μ or G .

The first parameter, λ , is an elastic modulus, but is often said to have no physical interpretation.

The second parameter, denoted as μ or G , is mostly referred to as the shear modulus. Other names for this elastic modulus are rigidity or the modulus of rigidity. This parameter is defined to be the ratio of the shear

stress to the shear strain. The modulus measures the stiffness of the material. It can be considered as measuring the response of a material to shear stress, for example when cutting it with dull scissors. The SI unit of the shear modulus is Pascal ($\text{Pa} = \text{N}/\text{m}^2$).

Where the shear modulus always has to be positive, the first Lamé constant can be negative. For most materials however, the constant will be positive.

YOUNG'S MODULUS

Young's modulus is the most common elastic modulus, named after the British scientist Thomas Young. The modulus is also known as the modulus of elasticity, the elastic modulus or the Tensile modulus. This parameter measures the stiffness of an elastic isotropic material, and is therefore specific for the material. The modulus is defined as the ratio between the stress and the strain along a specific axis. It can be considered as the material's response to linear stress. Examples of such stress are pulling the ends of a wire and putting a weight on top of a column.

Since the elastic modulus is defined as the ratio between stress and strain, its SI unit is the same as the SI unit of the stress, Pascal (Pa).

In anisotropic materials the Young's modulus can have different values for the different directions of the applied force with respect to the material's structure. The value of the Young's modulus can be seen as a measure for the rigidity of the material. When the material has a high modulus, it is very rigid.

POISSON'S RATIO

One of the other elastic parameters is called the Poisson's ratio and is denoted using the Greek letter nu (ν). This parameter is defined as the ratio of the transverse strain to the longitudinal strain. Since strain has no dimension, the Poisson's ratio is also dimensionless. The ratio describes the material's response to when the object is squeezed (i.e. how much the material expands outwards) and the response to when the object is stretched (i.e. how much the material contracts).

The value of the ratio hence depends on the material of the object. When the material is incompressible, the ratio will have a value of approximately 0.5. A value equal to 0 means that the material does not expand radially when it is compressed. When the value of the ratio is negative it means that the material has an opposite response to compression, i.e. the material gets thinner when compressed. These materials are called *auxetic*.

BULK MODULUS

The third elasticity modulus is called the Bulk modulus and is denoted by K or B . It measures the material's response to uniform pressure. An example of such uniform pressure is the pressure at the bottom of the ocean or a deep swimming pool. It can be defined as the ratio of the volume stress to the volume strain. In other words it can be described as "the ratio of the infinitesimal pressure increase to the resulting relative decrease of the volume". The modulus is measured in Pascal (Pa).

In working with elasticity usually two of the above mentioned coefficients are used. In this thesis Young's modulus and the Poisson's ratio (E, ν) are used. In Table A.1 the relations between the different coefficients are given.

Table A.1: Relationships between the Coefficients of Elasticity
From [18]

(λ, μ)		(E, ν)	(E, G)
λ	λ	$\frac{E\nu}{(1+\nu)(1-2\nu)}$	$\frac{G(E-2G)}{3G-E}$
μ	μ	$\frac{E}{2(1+\nu)}$	G
E	$\frac{\mu(3\lambda+2\mu)}{\lambda+\mu}$	E	E
ν	$\frac{\lambda}{2(\lambda+\mu)}$	ν	$\frac{E-2G}{2G}$
K	$\lambda + \frac{2}{3}\mu$	$\frac{E}{3(1-2\nu)}$	$\frac{GE}{3(3G-E)}$

Equation (A.3) gives Hooke's law as $\vec{\sigma} = \mathbf{D}\vec{\epsilon}$. For several situations the matrix \mathbf{D} is actually known. (Note that the elements of this matrix will consist of factors of E and ν .) Writing Hooke's Law in index notation, one obtains

$$\sigma_{ij} = D_{ijkl}\epsilon_{kl}. \quad (\text{A.4})$$

Here D_{ijkl} is called the stiffness tensor, which is a fourth order tensor with a total of 81 components. Equation (A.4) can also be written as a system of nine equations.

$$\left\{ \begin{array}{l} \sigma_{11} = D_{1111}\epsilon_{11} + D_{1112}\epsilon_{12} + D_{1113}\epsilon_{13} + D_{1121}\epsilon_{21} + D_{1122}\epsilon_{22} + D_{1123}\epsilon_{23} \\ \quad + D_{1131}\epsilon_{13} + D_{1132}\epsilon_{32} + D_{1133}\epsilon_{33} \\ \sigma_{12} = D_{1211}\epsilon_{11} + D_{1212}\epsilon_{12} + D_{1213}\epsilon_{13} + D_{1221}\epsilon_{21} + D_{1222}\epsilon_{22} + D_{1223}\epsilon_{23} \\ \quad + D_{1231}\epsilon_{13} + D_{1232}\epsilon_{32} + D_{1233}\epsilon_{33} \\ \sigma_{13} = D_{1311}\epsilon_{11} + D_{1312}\epsilon_{12} + D_{1313}\epsilon_{13} + D_{1321}\epsilon_{21} + D_{1322}\epsilon_{22} + D_{1323}\epsilon_{23} \\ \quad + D_{1331}\epsilon_{13} + D_{1332}\epsilon_{32} + D_{1333}\epsilon_{33} \\ \sigma_{21} = D_{2111}\epsilon_{11} + D_{2112}\epsilon_{12} + D_{2113}\epsilon_{13} + D_{2121}\epsilon_{21} + D_{2122}\epsilon_{22} + D_{2123}\epsilon_{23} \\ \quad + D_{2131}\epsilon_{13} + D_{2132}\epsilon_{32} + D_{2133}\epsilon_{33} \\ \sigma_{22} = D_{2211}\epsilon_{11} + D_{2212}\epsilon_{12} + D_{2213}\epsilon_{13} + D_{2221}\epsilon_{21} + D_{2222}\epsilon_{22} + D_{2223}\epsilon_{23} \\ \quad + D_{2231}\epsilon_{13} + D_{2232}\epsilon_{32} + D_{2233}\epsilon_{33} \\ \sigma_{23} = D_{2311}\epsilon_{11} + D_{2312}\epsilon_{12} + D_{2313}\epsilon_{13} + D_{2321}\epsilon_{21} + D_{2322}\epsilon_{22} + D_{2323}\epsilon_{23} \\ \quad + D_{2331}\epsilon_{13} + D_{2332}\epsilon_{32} + D_{2333}\epsilon_{33} \\ \sigma_{31} = D_{3111}\epsilon_{11} + D_{3112}\epsilon_{12} + D_{3113}\epsilon_{13} + D_{3121}\epsilon_{21} + D_{3122}\epsilon_{22} + D_{3123}\epsilon_{23} \\ \quad + D_{3131}\epsilon_{13} + D_{3132}\epsilon_{32} + D_{3133}\epsilon_{33} \\ \sigma_{32} = D_{3211}\epsilon_{11} + D_{3212}\epsilon_{12} + D_{3213}\epsilon_{13} + D_{3221}\epsilon_{21} + D_{3222}\epsilon_{22} + D_{3223}\epsilon_{23} \\ \quad + D_{3231}\epsilon_{13} + D_{3232}\epsilon_{32} + D_{3233}\epsilon_{33} \\ \sigma_{33} = D_{3311}\epsilon_{11} + D_{3312}\epsilon_{12} + D_{3313}\epsilon_{13} + D_{3321}\epsilon_{21} + D_{3322}\epsilon_{22} + D_{3323}\epsilon_{23} \\ \quad + D_{3331}\epsilon_{13} + D_{3332}\epsilon_{32} + D_{3333}\epsilon_{33} \end{array} \right. \quad (\text{A.5})$$

Using the symmetry of σ and ϵ it follows that the above equations can be simplified as the stiffness tensor is also symmetric, i.e.

$$D_{ijkl} = D_{ijlk} = D_{jikl} = D_{jilk}.$$

This means that instead of 81 different elements, the stiffness tensor only has 36 independent elastic coefficients. Using more simplifications the number of coefficients can even be reduced to 21.

A.3.1. ISOTROPIC MATERIALS

In this thesis the skin and subcutaneous will be modeled as *isotropic* materials. Here isotropy means uniformity in all orientations, or in other words, the elastic properties of the material are the same in any direction and therefore do not depend on the choice of the coordinates system ([18]). Since none of the properties of the material depend on the orientation, the material is perfectly rotational and symmetric with respect to three orthogonal planes. Using this assumption the matrix \mathbf{D} can be simplified to exist of only two independent coefficients, E and ν , obtaining the following stress-strain relationship for the elastic matrix

$$\begin{pmatrix} \sigma_{xx} \\ \sigma_{yy} \\ \sigma_{zz} \\ \sigma_{xy} \\ \sigma_{yz} \\ \sigma_{xz} \end{pmatrix} = \frac{E}{(1+\nu)(1-2\nu)} \begin{bmatrix} 1-\nu & \nu & \nu & 0 & 0 & 0 \\ \nu & 1-\nu & \nu & 0 & 0 & 0 \\ \nu & \nu & 1-\nu & 0 & 0 & 0 \\ 0 & 0 & 0 & \frac{1-2\nu}{2} & 0 & 0 \\ 0 & 0 & 0 & 0 & \frac{1-2\nu}{2} & 0 \\ 0 & 0 & 0 & 0 & 0 & \frac{1-2\nu}{2} \end{bmatrix} \begin{pmatrix} \epsilon_x \\ \epsilon_y \\ \epsilon_z \\ \gamma_{xy} \\ \gamma_{yz} \\ \gamma_{xz} \end{pmatrix}. \quad (\text{A.6})$$

In equation (A.6) the relation between stress and strain is given for an isotropic material, with the stress as a function of the strain. Here the stiffness tensor is called the elasticity matrix \mathbf{D} .

It is also possible to write Hooke's Law differently, i.e. with the strain as a function of the stress. The equation will then become $\vec{\epsilon} = \mathcal{C}\vec{\sigma}$. In this case instead of the elastic matrix one speaks of the compliance matrix, denoted by \mathcal{C} . Equation (A.7) shows the relation between stress and strain using this compliance matrix.

$$\begin{pmatrix} \epsilon_x \\ \epsilon_y \\ \epsilon_z \\ \gamma_{xy} \\ \gamma_{yz} \\ \gamma_{xz} \end{pmatrix} = \frac{1}{E} \begin{bmatrix} 1 & -\nu & -\nu & 0 & 0 & 0 \\ -\nu & 1 & -\nu & 0 & 0 & 0 \\ -\nu & -\nu & 1 & 0 & 0 & 0 \\ 0 & 0 & 0 & 2(1+\nu) & 0 & 0 \\ 0 & 0 & 0 & 0 & 2(1+\nu) & 0 \\ 0 & 0 & 0 & 0 & 0 & 2(1+\nu) \end{bmatrix} \begin{pmatrix} \sigma_{xx} \\ \sigma_{yy} \\ \sigma_{zz} \\ \sigma_{xy} \\ \sigma_{yz} \\ \sigma_{xz} \end{pmatrix} \quad (\text{A.7})$$

A.4. PLANE STRESS AND PLANE STRAIN

Working with solids, hence in three dimensions, the vectors describing the stress and strain both contain six elements, and the stiffness tensor is six by six. This causes most problems to be quite large. Fortunately it is often possible to make some assumptions that lead to simplifications.

PLANE STRESS

An example of a situation in which simplifying assumptions can be made is when working with a solid with one dimension relatively small compared to the two others and loaded in its plane. In such a situation the problem can be analyzed using the plane stress approach. This approach means that the stress on the small dimension is assumed to be zero throughout the entire solid. The only forces applied to the object will be parallel to the plate of this dimension. In other words, the stress vector is zero across a particular surface. This approach is usually taken when working with thin plates and beams. Look for example at Figure A.1.

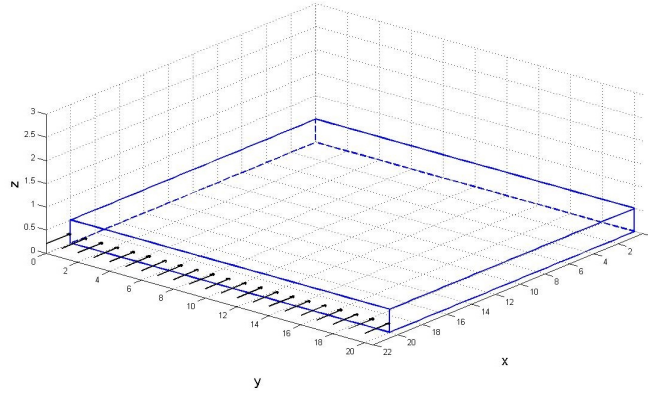


Figure A.1: In plane stress one of the dimensions is very small compared to the others. In this thin body, the z-component is small.

In this figure one can see that the thickness of the beam (z-component) is small compared to the other two dimensions. It is also clear that the surfaces of the beam are free of forces. This leads to the stress components σ_{xz} , σ_{yz} and σ_{zz} being equal to zero. If the beam is thin, as it is shown in the figure, it can be assumed that these stress components are equal to zero throughout the entire thickness of the beam. Furthermore, it is reasonable to assume that the other stress components, σ_{xx} , σ_{yy} and σ_{xy} remain constant. We find that in the case of plane stress the stress vector will only exist of three non-zero components, and using this the stress-strain relation using the elastic matrix shown in equation (A.6) will simplify to

$$\begin{pmatrix} \sigma_{xx} \\ \sigma_{yy} \\ \sigma_{xy} \end{pmatrix} = \frac{E}{1-\nu^2} \begin{bmatrix} 1 & \nu & 0 \\ \nu & 1 & 0 \\ 0 & 0 & \frac{1-\nu}{2} \end{bmatrix} \begin{pmatrix} \epsilon_{xx} \\ \epsilon_{yy} \\ \gamma_{xy} \end{pmatrix}. \quad (\text{A.8})$$

Note that instead of a three dimensional problem, a two dimensional problem will now be solved. Furthermore, since σ_{zz} is equal to zero, and using that

$$\sigma_{zz} = \frac{E}{(1+\nu)(1-2\nu)} (\nu\epsilon_{xx} + \nu\epsilon_{yy} + (1-\nu)\epsilon_{zz}) \quad (\text{A.9})$$

(from equation (A.6)), ϵ_{zz} can be determined. To do this, take

$$A = \frac{E}{(1+\nu)(1-2\nu)}.$$

Substituting $\sigma_{zz} = 0$ into (A.9) one obtains a result for ϵ_{zz} .

$$\begin{aligned} 0 &= Av(\epsilon_{xx} + \epsilon_{yy}) + A(1 - \nu)\epsilon_{zz} \\ A(1 - \nu)\epsilon_{zz} &= -Av(\epsilon_{xx} + \epsilon_{yy}) \\ \epsilon_{zz} &= \frac{-\nu}{1 - \nu}(\epsilon_{xx} + \epsilon_{yy}) \end{aligned} \quad (\text{A.10})$$

This expression can be rewritten further using equation (A.8). From Hooke's Law for plane stress it follows that

$$\begin{aligned} \sigma_{xx} &= \frac{E}{1 - \nu^2}(\epsilon_{xx} + \nu\epsilon_{yy}), \\ \sigma_{yy} &= \frac{E}{1 - \nu^2}(\nu\epsilon_{xx} + \epsilon_{yy}), \\ \sigma_{xx} + \sigma_{yy} &= \frac{E}{1 - \nu^2}(1 + \nu)(\epsilon_{xx} + \epsilon_{yy}), \\ \sigma_{xx} + \sigma_{yy} &= \frac{E}{1 - \nu}(\epsilon_{xx} + \epsilon_{yy}). \end{aligned} \quad (\text{A.11})$$

Multiplying equation (A.11) by $\frac{-\nu}{E}$ and comparing this with equation (A.10), equation (A.12) can be derived as

$$\epsilon_{zz} = \frac{-\nu}{E}(\sigma_{xx} + \sigma_{yy}). \quad (\text{A.12})$$

As before, Hooke's Law can also be given using the compliance matrix. This relation is given by

$$\begin{pmatrix} \epsilon_{xx} \\ \epsilon_{yy} \\ \gamma_{xy} \end{pmatrix} = \frac{1}{E} \begin{bmatrix} 1 & -\nu & 0 \\ -\nu & 1 & 0 \\ 0 & 0 & 2(1 + \nu) \end{bmatrix} \begin{pmatrix} \sigma_{xx} \\ \sigma_{yy} \\ \sigma_{xy} \end{pmatrix}. \quad (\text{A.13})$$

PLANE STRAIN

Another example in which certain assumptions can simplify the problem is called plane strain. In this case one of the dimensions of an object will be very large compared to the other two dimensions. In this case the loads are uniformly distributed with respect to the large dimension and act perpendicular to it. An example of this situation is shown in Figure A.2.

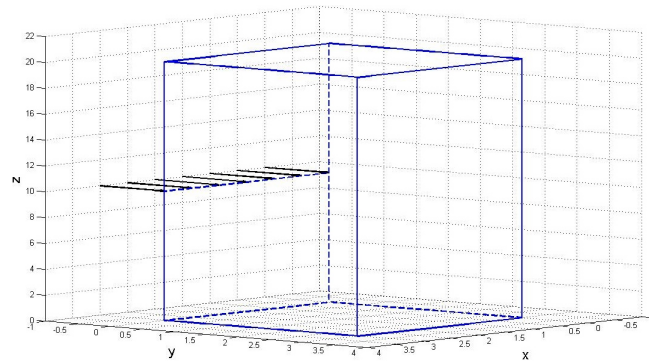


Figure A.2: In plane strain one of the dimensions is very large compared to the others. In this thick body, the z -component is large.

Instead of the z -component being very small compared to the other two dimension as in plane stress, here the z -component is very large compared to the other two. In this case the strain components γ_{xz} , γ_{yz} and ϵ_{zz} are equal to zero. This holds throughout the beam because the displacements of all faces in the z -direction

are kept equal to zero.

The strain components that are nonzero are ϵ_{xx} , ϵ_{yy} and γ_{xy} .

As in the case of plane stress we find that Hooke's law will be smaller, since the strain vector exists of only three nonzero components. The stress-strain relation using the elastic matrix shown in equation (A.6) becomes

$$\begin{pmatrix} \sigma_{xx} \\ \sigma_{yy} \\ \sigma_{xy} \end{pmatrix} = \frac{E}{(1+\nu)(1-2\nu)} \begin{bmatrix} 1-\nu & \nu & 0 \\ \nu & 1-\nu & 0 \\ 0 & 0 & \frac{1-2\nu}{2} \end{bmatrix} \begin{pmatrix} \epsilon_{xx} \\ \epsilon_{yy} \\ \gamma_{xy} \end{pmatrix}. \quad (\text{A.14})$$

Hooke's Law can also be given the other way around, using the compliance matrix. This relation is given by equation (A.15):

$$\begin{pmatrix} \epsilon_{xx} \\ \epsilon_{yy} \\ \gamma_{xy} \end{pmatrix} = \frac{1+\nu}{E} \begin{bmatrix} 1-\nu & -\nu & 0 \\ -\nu & 1-\nu & 0 \\ 0 & 0 & 2 \end{bmatrix} \begin{pmatrix} \sigma_{xx} \\ \sigma_{yy} \\ \sigma_{xy} \end{pmatrix}. \quad (\text{A.15})$$

Furthermore, ϵ_{zz} is equal to zero, but σ_{zz} is not. Looking at Hooke's Law in equation (A.6) and writing zero for γ_{xz} , γ_{yz} and ϵ_{zz} the following equation is obtained.

$$\begin{pmatrix} \sigma_{xx} \\ \sigma_{yy} \\ \sigma_{zz} \\ \sigma_{xy} \\ \sigma_{yz} \\ \sigma_{xz} \end{pmatrix} = \frac{E}{(1+\nu)(1-2\nu)} \begin{bmatrix} 1-\nu & \nu & \nu & 0 & 0 & 0 \\ \nu & 1-\nu & \nu & 0 & 0 & 0 \\ \nu & \nu & 1-\nu & 0 & 0 & 0 \\ 0 & 0 & 0 & \frac{1-2\nu}{2} & 0 & 0 \\ 0 & 0 & 0 & 0 & \frac{1-2\nu}{2} & 0 \\ 0 & 0 & 0 & 0 & 0 & \frac{1-2\nu}{2} \end{bmatrix} \begin{pmatrix} \epsilon_{xx} \\ \epsilon_{yy} \\ 0 \\ \gamma_{xy} \\ 0 \\ 0 \end{pmatrix} \quad (\text{A.16})$$

Equation (A.17) follows directly from this relation:

$$\sigma_{zz} = \nu(\epsilon_{xx} + \epsilon_{yy}). \quad (\text{A.17})$$

REVIEW PLANE STRESS AND PLANE STRAIN

In Figure A.3 the two states plane stress and plane strain are quickly compared.

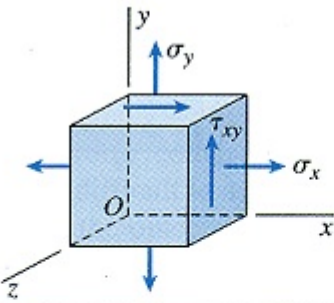
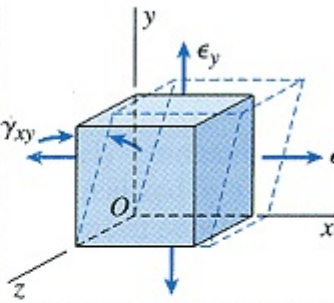
	Plane stress	Plane strain
		
Stresses	$\sigma_z = 0$ $\tau_{xz} = 0$ $\tau_{yz} = 0$ σ_x , σ_y , and τ_{xy} may have nonzero values	$\tau_{xz} = 0$ $\tau_{yz} = 0$ σ_x , σ_y , σ_z , and τ_{xy} may have nonzero values
Strains	$\gamma_{xz} = 0$ $\gamma_{yz} = 0$ ϵ_x , ϵ_y , ϵ_z , and γ_{xy} may have nonzero values	$\epsilon_z = 0$ $\gamma_{xz} = 0$ $\gamma_{yz} = 0$ ϵ_x , ϵ_y , and γ_{xy} may have nonzero values

Figure A.3: Comparison between plane stress and plane strain.

Source: http://classes.mst.edu/civeng110/concepts/13/strain/plane_stress_vs_strain.gif

B

CONTACT MECHANICS

Contact mechanics is the area that involves situations in which multiple solids are in contact with one another. This area is very big, since there are many different options when looking at contacting solids. The solids themselves for example can be rigid or elastic, they can deform or stay the same as an effect of the contact, and the contact between the solids can be conforming or non-conforming. These latter options mean that without applying pressure the bodies either touch at multiple points (i.e. they "fit together") or they only touch at one point or one line (i.e. the shapes do not "fit together"). In the case of non-conforming contact, the contact area is very small compared to the sizes of the bodies, which causes the stresses to be high in this area. In this case the contact will also be called concentrated. In the case of a larger contact area the stresses will be more spread out and the contact will be called diversified.

In the general contact problem there are three components that can be of importance.

1. Due to the load that presses the bodies together, deformation of the separate bodies will occur. The deformation depends on the material and structure of the body.
2. Secondly the bodies have an overall motion relative to each other. Possibilities are the bodies being at rest, approaching each other (after which impact follows), sliding and rolling over each other.
3. Thirdly there are the processes at the contact area: compression and adhesion in the direction perpendicular to the area, and friction and micro-slip in the tangential directions.

This last component can be described using conditions called the contact conditions.

- First of all the gap between the two bodies should always be greater than or equal to zero: $e_n \geq 0$, where equality holds in case of contact and inequality when the bodies are separated.
- Secondly, the normal stress acting on each body should also be greater than or equal to zero: $p_n \geq 0$, where equality means the bodies are separated and inequality holds when the bodies are in contact. In this latter case the normal stress is compressive.

Note that:

- The functions e_n and p_n depend on the location of the body surfaces.
- The product of e_n with p_n will always be equal to zero: $e_n p_n = 0$.

The first important component of contact problems is, as given above, the deformation of the solids in contact. Researchers have been investigating this deformation for a long time. In 1882, Hertz published an article called "On the contact of elastic solids". This article was one of the first steps in the research of contact mechanics. After this, many more models were created, such as the JKR model (Johnson, Kendall and Roberts), and the Bradley model.

There are many different models regarding contact between two solids. Some of these models are useable for contact problems of solids that are only pressed together (normal contact problems), while other models

can be used when either one or both solids are being moved with respect to the other (tangential contact problems). Four common models regarding normal contact problems are described in Section B.1. The contact problems with tangential movement are described in Section B.2.

B.1. NORMAL CONTACT MECHANICS

The information described in this subsection is mostly obtained from the books Contact Mechanics by Johnson [27] and Contact Mechanics and Friction by Popov [4] and the website Wikipedia [28].

The following models will be described in this section. A more elaborate description of these models is given in respectively Section B.1.1 and B.1.2.

Hertz fully elastic model.

JKR fully elastic model considering adhesion in the contact zone.

Bradley purely van der Waals model with rigid spheres.

DMT fully elastic, adhesive and van der Waals model.

B.1.1. THE HERTZIAN THEORY OF ELASTIC DEFORMATIONS

The Hertzian Theory of Elastic Deformations is one of the first models regarding the geometrical effects on local elastic deformation properties. It was created around 1882 when Hertz solved the problem of contact between two elastic bodies with curved surfaces. The result described in the model forms a basis for contact mechanics today. The most common problem is called the *normal contact problem*. This problem revolves around two bodies which are brought into contact with another by forces perpendicular to their surfaces [4], or in other words, are being pressed together. The Hertzian Theory of Elastic Deformations considers such a normal contact problem between a rigid sphere and an elastic half-space. In the theory all adhesive forces are neglected. The information in this section closely follows the information from the book Contact Mechanics and Friction by V.L. Popov [4].

Figures B.1 and B.2 shows the contact between the elastic half-space and the rigid sphere schematically.

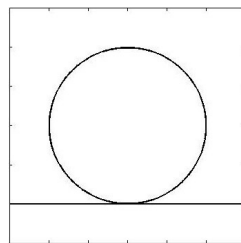


Figure B.1: Contact with no force acting upon the contact.

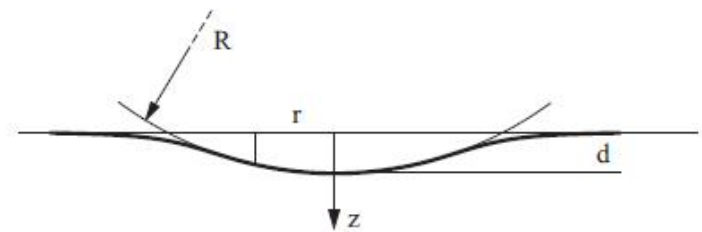


Figure B.2: Contact with a normal force acting upon the contact. Source: [4]

The original theory of Heinrich Hertz has three results:

- the contact radius was determined,
- the maximum pressure was determined and
- the normal force of the contact was determined.

To obtain these results Hertz used the displacement of the points on the surface in the contact area between an originally even surface and a rigid sphere of radius R . This displacement is equal to¹

$$u_z = d - \frac{r^2}{2R}, \quad (\text{B.1})$$

¹Only the z -component of the displacement is of interest within the framework of the half-space approximation in contact problems without friction [4].

where u_z denotes the surface displacement, d the indentation depth, $r = \sqrt{x^2 + y^2}$ and R the radius of the sphere. The relation between the before mentioned parameters is shown in Figure B.2.

In solving the contact problem to obtain the three results a pressure distribution has to be assumed. The pressure distribution that is assumed in the theory of Hertz is $p = p_0(1 - r^2/a^2)^n$, with $n = 1/2$. In this pressure distribution p_0 is the maximum pressure. This *Hertzian Pressure Distribution*

$$p = p_0 \left(1 - \frac{r^2}{a^2}\right)^{\frac{1}{2}}, \quad r^2 = x^2 + y^2, \quad (\text{B.2})$$

leads to a vertical displacement equal to

$$u_z = \frac{\pi p_0}{4E^* a} (2a^2 - r^2), \quad r \leq a. \quad (\text{B.3})$$

Equation (B.3) can be obtained as follows.² When working with a continuous distribution of the normal pressure $p(x, y)$, the displacement of the surface is calculated as

$$u_z = \frac{1}{\pi E^*} \iint p(x', y') \frac{dx' dy'}{r} \quad \text{with } r = \sqrt{(x - x')^2 + (y - y')^2} \quad \text{and } E^* = \frac{E}{1 - \nu^2}. \quad (\text{B.4})$$

Using a change of coordinates, taking $\alpha = a^2 - r^2$, $\beta = r \cos(\phi)$ and substituting equation (B.2), equation (B.4) becomes

$$u_z = \frac{1}{\pi E^*} \frac{p_0}{a} \int_0^{2\pi} \left(\underbrace{\int_0^{s_1} (\alpha^2 - 2\beta - s^2)^{\frac{1}{2}} ds}_{*} \right) d\phi. \quad (\text{B.5})$$

The expression (*) can be calculated as

$$\begin{aligned} (*) &= \int_0^{s_1} (\alpha^2 - 2\beta - s^2)^{\frac{1}{2}} ds \\ &= \frac{1}{2} \alpha \beta + \frac{1}{2} (\alpha^2 + \beta^2) \cdot \left(\frac{\pi}{2} - \arctan(\beta/\alpha) \right). \end{aligned}$$

Integrating the above over ϕ from 0 to 2π , the terms $\alpha\beta$ and $\arctan(\beta/\alpha)$ vanish since $\beta = r \cos(\phi)$. This leads to the following result:

$$\begin{aligned} u_z &= \frac{1}{\pi E^*} \frac{p_0}{a} \int_0^{2\pi} \left(\int_0^{s_1} (\alpha^2 - 2\beta - s^2)^{\frac{1}{2}} ds \right) d\phi \\ &= \frac{1}{\pi E^*} \frac{p_0}{a} \int_0^{2\pi} \frac{\pi}{4} (\alpha^2 + \beta^2) d\phi \\ &= \frac{1}{4E^*} \frac{p_0}{a} \int_0^{2\pi} (a^2 - r^2 + r^2 \cos(\phi)) d\phi \\ &= \frac{\pi p_0}{4E^* a} (2a^2 - r^2), \end{aligned}$$

which gives equation (B.3).

The total force of the contact is

$$F = \int_0^a p(r) 2\pi r dr = \frac{2}{3} p_0 \pi a^2. \quad (\text{B.6})$$

To solve the contact problem, one can now use the fact that both equation (B.1) and equation (B.3) describe the same vertical displacement and hence should be equal:

$$\frac{\pi p_0}{4E^* a} (2a^2 - r^2) = d - \frac{r^2}{2R}.$$

²This derivation is explained in Appendix A of [4].

From this equality the variables a and d can be derived. One obtains

$$a = \frac{\pi p_0 R}{2E^*} \quad \text{and} \quad d = \frac{\pi a p_0}{2E^*}. \quad (\text{B.7})$$

Equation (B.7) leads to the first result of Hertz theory, the contact radius between the rigid sphere and the elastic half-space:

$$1. \quad a^2 = Rd. \quad (\text{B.8})$$

Using equations (B.7) and (B.8) the second result can also be obtained, which is the maximum pressure:

$$2. \quad p_0 = \frac{2E^*}{\pi} \left(\frac{d}{R} \right)^{\frac{1}{2}}. \quad (\text{B.9})$$

Substituting both equations (B.8) and (B.9) into the equation of total force (B.6), the third result is obtained; the normal force

$$3. \quad F = \frac{4}{3} E^* \left(\frac{d^3}{R} \right)^{\frac{1}{2}}. \quad (\text{B.10})$$

From this last result, the potential energy of the elastic deformation U can be determined using $-F = \partial U / \partial d$:

$$U = \frac{8}{15} E^* (Rd^5)^{\frac{1}{2}}.$$

The above results are explicitly for the contact between a rigid sphere and an elastic half space. The results can be used to obtain results for other scenarios, such as the contact between two elastic bodies, the contact between two spheres, the contact between two elastic cylinders, and more.

If the contact is for instance between two elastic bodies, the only difference with the previous result is that the expression of E^* must be changed into

$$\frac{1}{E^*} = \frac{1 - \nu_1^2}{E_1} + \frac{1 - \nu_2^2}{E_2}, \quad (\text{B.11})$$

where E_1 and E_2 are the moduli of elasticity of the two bodies, and ν_1 and ν_2 the respective Poisson's ratios.

B.1.2. BRADLEY'S VAN DER WAALS MODEL, THE JKR-THEORY AND THE DMT-THEORY

Fifty years after Hertz solved the normal contact problem without adhesion between elastic bodies in 1882, Bradley presented the solution for the normal contact problem with adhesion between a rigid sphere and a rigid plane.

In 1971 an article was written by K.L. Johnson, K. Kendall and A.D. Roberts. In this article a new contact mechanics model called the JKR-theory is described in which the contact adhesive interactions are taken into account. The JKR-theory is often referred of as the classical theory of adhesive contact. The JKR-theory is based on the Hertzian theory. However, as has been noted before, Hertz did not include any adhesive forces in his model. It was found by Roberts and Kendall [29] that these contact forces are of little significance when two spheres are pressed together by a high load, but become more important when this load reduces. This means that for low loads the model of Hertz will be less accurate.

The DMT-theory is yet another theory that includes adhesive forces. This theory is created as a combination of the Hertzian theory and Bradleys model. When the two bodies are separated and significantly apart, the DMT-theory will simplify to *Bradleys's Van der Waals model*.

All three models describe the adhesive normal contact problem, only between different types of bodies.

Bradley solved the adhesive normal contact problem between a rigid sphere and a rigid plane. The resulting adhesive force was found to be $F_A = 4\pi\gamma R$, with γ the surface energy and R the radius of the sphere.

JKR solved the adhesive contact problem between elastic bodies. They found the adhesive force to be equal to $F_A = 3\pi\gamma R$.

DMT described a different adhesive theory while they considered the case of deformable bodies by adding the adhesive force of Bradleys model to the theory of Hertz.

In 1976 Tabor realized that the above mentioned models were all valid for different scenarios. The DMT-Theory and JKR-Theory are both special cases of the general problem. He stated that the theories had only very small differences, but that ([4])

Bradleys model is correct for absolutely rigid bodies,

The JKR-Theory is valid for large, flexible spheres, and

The DMT-Theory is valid for small, rigid spheres.

B.2. TANGENTIAL CONTACT PROBLEMS

In the previous models, the two solids were only pressed together and both had absolutely smooth and frictionless surfaces. In these cases the shear forces in the contact area are equal to zero.

In this section contacts are examined in which the point of contact is also loaded in the tangential direction. Now static and kinetic frictional forces will become interesting, and the shear forces will thus be nonzero. These Tangential Contact Problems belong to the field of Frictional contact mechanics, which is the study of the deformation of bodies in the presence of frictional effects.

In case of tangential contact problems there are additional contact conditions, coming from the fact that the shear stress should always be smaller than or equal to the so-called traction bound which depends on the position. This is called the local friction law. The friction law that is most commonly used is called Coulomb's law (see Section B.2.4), which states that $F_x \leq \mu F_N$. Here F_x is the tangential force, F_N is the normal force and μ is the coefficient of friction.

In this law equality holds in case of sliding and inequality holds in case of sticking.

Generally the contact area and the sticking and sliding parts are unknown in advance. If these were known, then the elastic fields in the two bodies could be solved independently from each other and the problem would not be a contact problem anymore.

B.2.1. CATTANEO PROBLEM

A commonly known tangential contact problem is called the Cattaneo problem. This contact problem is between an elastic sphere with radius R and an elastic plane (half space). The sphere is pressed onto the plane and then shifted over the plane's surface by a tangential force F_x .

When starting with only the normal force F_N the sphere will be pressed onto the plane. The contact point will turn into a contact area as both bodies deform and the center of the sphere moves down by a distance of δ_n called the approach (see Figure B.3). The contact area will be circular and a Hertzian normal pressure distribution arises.

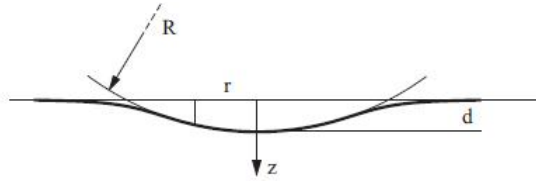


Figure B.3: The center of the sphere moves down by a distance of $d = \delta_n$. Source: [4]

When both the sphere and the plane are from the same material (same elastic properties), the Hertzian solution reads

$$p_n(x, y) = p_0 \sqrt{1 - r^2/a^2} \quad r = \sqrt{x^2 + y^2} \leq a \quad a = \sqrt{R\delta_n},$$

$$p_0 = \frac{2}{\pi i} E^* (\delta_n/R)^{1/2} \quad F_N = \frac{4}{3} E^* R^{1/2} \delta_n^{3/2} \quad E^* = \frac{E}{2(1-\nu^2)},$$

where E and ν are respectively the Young's modulus and the Poisson's ratio. This is the same as was shown earlier in Section B.1.1.

When the sphere and the plane are made of different materials, the same solution holds, only now using

$$\frac{1}{E^*} = \frac{1-\nu_1^2}{E_1} + \frac{1-\nu_2^2}{E_2}. \quad (\text{B.12})$$

Assumed before is that after the normal pressure is applied, a tangential force F_x will be applied that 'pushes' against the sphere.

When this force is lower than the Coulomb friction bound ($F_x < \mu F_N$) the center of the sphere will move sideways for a small distance δ_x , which is called the shift. An equilibrium will be obtained in which the bodies are deformed and frictional shear stresses occur. When the tangential force is removed the sphere will (mostly) shift back.

This problem was solved analytically by Cattaneo. In his solution he combined two Hertzian distributions which showed that partial sliding occurs during the tangential loading (see Section B.2.3). Before this combination of distributions is shown, some information regarding working with half-spaces, the deformations that will occur in these and the stress distributions causing these deformations are given.

B.2.2. HALF-SPACE APPROACHES

It is often useful to work with half-spaces instead of fixed and bounded planes. We will therefore look into the deformations that will occur when a tangential stress distribution acts upon an elastic half-space.

As is done in the book of Valentin L. Popov [4] the problems will be considered using a half-space approximation. This means that "the gradient of the surface of the contacting bodies should be small in the vicinity relevant to the contact problem" ([4]).

A point is taken on the surface of this elastic half-space which is chosen to be the origin. A concentrated force acts on this origin, which for simplicity only has a component in the x -direction. When considering the surface $z = 0$ the following equations describe the displacements ([30]³)

$$\begin{aligned} u_x &= F_x \frac{1}{4\pi G} \left\{ 2(1-\nu) + \frac{2\nu x^2}{r^2} \right\} \frac{1}{r}, \\ u_y &= F_x \frac{1}{4\pi G} \cdot \frac{2\nu}{r^3} xy, \\ u_z &= F_x \frac{1}{4\pi G} \cdot \frac{(1-2\nu)}{r^2} x. \end{aligned} \quad (\text{B.13})$$

In these equations G is the shear modulus also denoted by μ , described further in Section A.3 and Table A.1.

To make the problem more realistic one can look at a tangential force distribution acting upon the displacement of the surface. Assuming this force acts in the x -direction it can be denoted by

$$\sigma_{zx}(x, y) = \tau(x, y).$$

Using this distribution, the displacement in the x -direction can be calculated using the integral

$$u_x = \frac{1}{4\pi G} \cdot 2 \iint_A \left\{ \frac{1-\nu}{s} + \nu \frac{(x-x')^2}{s^3} \right\} \tau(x', y') dx' dy', \quad (\text{B.14})$$

where

$$s^2 = (x-x')^2 + (y-y')^2.$$

It is obvious that a different force distribution will lead to a different displacement in the x -direction. The following possibilities are given in Chapter 8 of Contact Mechanics and Friction, by V.L. Popov [4].

- For example, a constant value of the displacement will be found if the following force distribution is taken

$$\tau(x, y) = \tau_0 (1 - r^2/a^2)^{-1/2} \quad \text{with} \quad r^2 = x^2 + y^2 \leq a^2.$$

Substituting this into equation (B.14) and integrating, the displacement inside the loaded area ($r \leq a$) is found to be

$$u_x = \frac{\pi(2-\nu)}{4G} \tau_0 a = \text{constant}. \quad (\text{B.15})$$

Due to symmetry, in this case $u_y = 0$. The z -component of the displacement however is not equal to zero and can be calculated using equation (B.13). The total force F_x that acts on the contact area can be calculated as

$$F_x = \int_0^a \tau(r) 2\pi r dr = 2\pi \tau_0 a^2. \quad (\text{B.16})$$

³referred to by [4]

- Another possible force distribution is the distribution

$$\tau(x, y) = \tau_0 (1 - r^2/a^2)^{1/2}. \quad (\text{B.17})$$

Substituting this into equation (B.14) the x -displacement of the surface points in the loaded area ($r \leq a$) is obtained as

$$u_x = \frac{\tau_0 \pi}{32Ga} [4(2 - \nu)a^2 - (4 - 3\nu)x^2 - (4 - \nu)y^2], \quad (\text{B.18})$$

with the total force equal to

$$F_x = \frac{2}{3} \pi \tau_0 a^2. \quad (\text{B.19})$$

- A third possibility would be that the force distribution acting in the x - direction upon an elastic body within a strip of width $2a$ is given by

$$\tau(x, y) = \tau_0 (1 - x^2/a^2)^{1/2}. \quad (\text{B.20})$$

In this the displacement of the surface points is given by [4]

$$u_x = \text{constant} - \tau_0 \frac{x^2}{aE^*}. \quad (\text{B.21})$$

- The last case that is given in [4] is a special case. Now the tangential loading is presented as *torsion*. This phenomena occurs when working in a round contact area (radius a) and the tangential forces are directed perpendicular to the respective polar radius r . The stresses in this situation are give by

$$\sigma_{zx} = \tau(r) \sin(\phi) \quad \text{and} \quad \sigma_{zy} = \tau(r) \cos(\phi). \quad (\text{B.22})$$

Here the force distribution τ is given as

$$\tau(r) = \tau_0 \frac{r}{a} \left(1 - \left(\frac{r}{a} \right)^2 \right)^{-1/2}. \quad (\text{B.23})$$

According to Johnson in his book Contact Mechanics ([27]), the displacement of the surface is given by (in polar components)

$$\begin{aligned} u_\phi &= \frac{\pi \tau_0 r}{4G}, \\ u_r &= 0, \\ u_z &= 0. \end{aligned} \quad (\text{B.24})$$

Looking at these displacement components it is clear that the surface area turns, which happens if the chosen torsion is in fact the torsion of the rigid cylindrical indenter sticking to the surface. In this case the torsional moment is equal to [4]

$$M_z = \frac{4}{3} \pi a^3 \tau_0. \quad (\text{B.25})$$

Now that some information is available regarding the deformations that occur due to different force distributions, the cases of sticking and sliding will be examined.

COMPLETE STICKING - A CONTACT PROBLEM WITHOUT SLIP

In the case of complete sticking, no sliding exists in the contact. These type of problems are also called *tangential contact problems without slip*. Here the coefficient of friction (COF) between the two bodies is very high (tends to infinity), or the bodies are "glued together".

In most cases, however, the no-slip condition will not hold near the boundary, which means that relative sliding will occur. The fact that the no-slip condition often does not hold is due to the fact that in these cases the shear stress approaches infinity in these areas, while the normal stress tends to zero [4].

A CONTACT PROBLEM ACCOUNTING FOR SLIP

An example of a contact problem accounting for slip is the Cattaneo problem described earlier. Many other examples can be considered as well. As said above, in most cases there will be slip in the boundary of the contact area. When sliding occurs in (part of) the contact area, the contact problem accounts for slip. In these problems one could deal with both sliding and sticking, or only sliding.

To get an idea of a contact problem accounting for slip, consider two bodies in contact where normal and tangential forces act simultaneously. As an example [4] two spheres are being pressed together with a normal force F_N while also being pulled in the tangential direction with force F_x . The friction between the two bodies is assumed to be according to Coulomb's law of friction; the maximum static friction stress τ_{\max} is equal to the kinetic friction stress τ_k . Both are equal to the normal stress p multiplied with a constant coefficient of friction (COF) μ :

$$\tau_{\max} = \mu p \quad \text{and} \quad \tau_k = \mu p. \quad (\text{B.26})$$

Now in the area where sticking occurs, the stress τ will have to be smaller than or equal to the normal stress multiplied with this coefficient of friction, i.e.

$$\tau \leq \mu p. \quad (\text{B.27})$$

When one assumes the bodies completely adhere in the contact area, the following equations for the distributions of the normal and tangential stresses are obtained according to Valentin L. Popov [4]:

$$\text{Normal stress} \quad p = p_0 (1 - (r/a)^2)^{\frac{1}{2}}, \quad F_N = \frac{2}{3} p_0 \pi a^2, \quad (\text{B.28})$$

$$\text{Tangential stress} \quad \tau = \tau_0 (1 - (r/a)^2)^{-\frac{1}{2}}, \quad F_x = 2\pi \tau_0 a^2. \quad (\text{B.29})$$

Looking at these distributions it is clear that at the boundary of the area the normal stress p approaches zero, while the tangential stress τ tends to infinity. This means that here the sticking condition (B.27) will always be invalid and hence there will always be slip near the boundary of the contact area. Sticking will occur however inside of the area, when the tangential forces are sufficiently small (see Figure B.4). The sticking and sliding domains are separated by the boundary circle on which holds that $\tau = \mu p$.

It can be shown that the shear stress distribution given in equation (B.29) is only valid for contact without sliding. However, using this distribution one can prove that there will always be sliding at the boundary, which is a contradiction to the assumption.

A new distribution needs to be constructed, which is correct for a situation with both sliding and sticking. Such a distribution can be constructed as a combination of the known distributions. This need for a new and better stress distribution is the same as the need in the Cattaneo problem.

B.2.3. FORMING A NEW STRESS DISTRIBUTION

In Contact mechanics and Friction [4] it is described that in the case of sliding and sticking (such as in the Cattaneo problem) a distribution can be formed using two "Hertzian" stress distributions, obtaining

$$\begin{aligned} \tau &= \tau^{(1)} + \tau^{(2)} \\ &= \tau_1 (1 - r^2/a^2)^{1/2} - \tau_2 (1 - r^2/c^2)^{1/2}, \end{aligned} \quad (\text{B.30})$$

where a is the contact radius and c is the radius of the sticking domain as is shown in Figure B.4.

Since this stress distribution is of the form given in equation (B.17) the displacement will be similar to the one shown in equation (B.18). The following displacement can be obtained.

$$\begin{aligned} u_x &= \frac{\tau_0 \pi}{32Ga} [4(2 - \nu)a^2 - (4 - 3\nu)x^2 - (4 - \nu)y^2] \\ &\quad - \frac{\tau_0 \pi}{32Gc} [4(2 - \nu)c^2 - (4 - 3\nu)x^2 - (4 - \nu)y^2] \end{aligned} \quad (\text{B.31})$$

Now combining this displacement with the fact that sticking occurs within the circle with radius c it is clear that the displacement in this area should be constant:

$$u_x(r) = \text{constant} \quad \text{if } r < c.$$

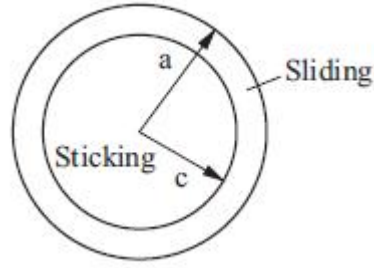


Figure B.4: Sticking and sliding domains in a round tangential contact. Source: [4, Ch. 8].

The fact that sliding occurs in the rest of the domain means that in that area Coulomb's law of friction is met:

$$\tau(r) = \mu p(r), \quad \text{if } c < r < a.$$

Using these conditions, the following stress distribution can be found:

$$\tau(r) = \mu p_0(1 - r^2/a^2)^{1/2} - \mu p_0 \frac{c}{a}(1 - r^2/c^2)^{1/2} \quad \text{if } 0 \leq r \leq c, \quad (\text{B.32})$$

$$\tau(r) = \mu p(r) \quad \text{if } c \leq r \leq a. \quad (\text{B.33})$$

The displacement for the points in the sticking area and the sliding area can be determined. From these displacements, the tangential force can be given in terms of the normal force, using that $F_N = \frac{2}{3} p_0 \pi a^2$. One obtains

$$F_x = \mu F_N \left(1 - \left(\frac{c}{a}\right)^3\right). \quad (\text{B.34})$$

Rewriting this equation, a radius for the static area is found as

$$\frac{c}{a} = \left(1 - \frac{F_x}{\mu F_N}\right)^{1/3}. \quad (\text{B.35})$$

From this relationship it can be seen that complete sliding occurs when

$$F_x = \mu F_N,$$

where μ is the coefficient of friction from Coulomb's Law of Friction.

B.2.4. COULOMB'S LAW OF FRICTION

Coulomb's Law of Friction is a very simple model to describe the extremely complicated phenomenon of friction in case of dry friction (or Coulomb friction). Despite the simplicity of the law it is shown to be very widely applicable [4].

The law is given by the following inequality

$$F_f \leq \mu F_N, \quad (\text{B.36})$$

where F_f is the frictional force, F_N the normal force and μ the coefficient of friction.

The coefficient of friction is a constant which can depend on a.o.

- the contact time,
- the normal force,
- the sliding speed,
- the surface roughness and
- the temperature.

In the article of Gefen on microclimate factors [1], the effect of the temperature of the room, the temperature of the patient and the production of sweat on the risk for pressure ulcers is being examined. It could therefore be important to include these factors in the contact model. A change in the temperature could for instance change the elastic properties of the materials (i.e. the skin, subcutaneous tissue and the mattress) and when sweat is produced it might be necessary to include the presence of fluid in the model.

B.2.5. THE CONTACT MECHANICS MODEL FOR CONTACT BETWEEN HUMAN AND BED

In the previous sections, several contact mechanics models have been described. In this section they will briefly be compared to see which contact model is most applicable for the problem in this thesis.

In this thesis the contact is between a human body, which is elastic, and a hospital mattress which also is elastic. The human body is pressed against the mattress, but is simultaneously moved along the mattress. The body is not glued to the mattress, and the coefficient of friction between the patient and the bed does not tend to infinity, which means that sliding will occur during the movement.

These factors lead to the conclusion that the problem is in fact a tangential contact problem accounting for slip. For this reason, the contact models describing the normal contact problem (see Section B.1) can be discarded. The information given in Section B.2, such as the solving process of the Cataneo problem, can be used to solve the problem described in this thesis. However, since other factors are of interest too the model needs to be expended. For instance, this thesis will also include the effect of moisture on the risk of pressure ulcers. This means that the presence of fluids might have to be included in the contact model. Also, the effect of the temperature on the risk of pressure ulcers is being examined. Therefore it might be important to include the temperature changes in the contact model.

Very important is that the contact is between a human body and a hospital mattress. This means that the exact contact area is not known as opposed to all examples shown above. This in turn means that the integrals used in the models above, in which is integrated over the contact area, can not be calculated as simple as shown. This is similar to the **Signorini problem** which is explained in Section B.3. We will have to determine the contact area using a sort of trial and error system in which the contact area is estimated and improved until it is obtained right.

B.3. THE SIGNORINI PROBLEM

The Signorini problem is a problem posed in 1959 regarding the equilibrium configuration of an elastic body resting on a rigid surface. In this contact only the mass forces on the body were taken into account.

The problem is to find the elastic equilibrium configuration of this elastic body subject to only its mass forces. In other words, the problem is to find the deformation of the body, only subject to its body forces. The difficulty in the problem is that the contact area between the elastic body and the sphere is not known prior to solving the problem. Due to this the problem originally was named the problem with ambiguous boundary conditions. These ambiguous boundary conditions consist of both equalities and inequalities and represent the difference between contact and separation. Every point in the body has to satisfy one of the two sets of boundary conditions, i.e. it will either be in the contact area or in the separation.

Antonio Signorini posed the problem asking his students whether the problem is well-posed or not in a physical sense, i.e. if its solution exists and is unique or not. This eventually was solved by one of his students, Gaetano Fichera, who named the problem after his teacher.

Fichera, as opposed to Signorini, did not consider only incompressible bodies and a plane rest surface, which made the problem more general.

The goal of the problem is to [31] "find the displacement vector from the natural configuration $\mathbf{u}(\mathbf{x}) = (u_1(\mathbf{x}), u_2(\mathbf{x}), u_3(\mathbf{x}))$ of an anisotropic non-homogeneous elastic body that lies in a subset A of the three dimensional euclidean space, whose boundary δA and whose interior normal is the vector \mathbf{n} , resting on a rigid frictionless surface whose contact surface (or contact set) is Σ and subject only to its body forces $\mathbf{f}(\mathbf{x}) = (f_1(\mathbf{x}), f_2(\mathbf{x}), f_3(\mathbf{x}))$, and surface forces $\mathbf{g}(\mathbf{x}) = (g_1(\mathbf{x}), g_2(\mathbf{x}), g_3(\mathbf{x}))$ applied on the free surface $\delta A \setminus \Sigma$: the set A and the contact surface Σ characterize the natural configuration of the body and are known a priori. Therefore the body has to satisfy the general equilibrium equations:

$$\frac{\delta \sigma_{ik}}{\delta x_k} - f_i = 0 \quad \text{for } i = 1, 2, 3, \quad (\text{B.37})$$

the ordinary boundary conditions on $\delta A \setminus \Sigma$

$$\sigma_{ik}n_k - g_i = 0 \quad \text{for } i = 1, 2, 3, \quad (\text{B.38})$$

and the following two sets of boundary conditions on Σ , where $\vec{\sigma} = \vec{\sigma}(\vec{\mathbf{u}})$ is the Cauchy stress tensor."

As said before, each point has to satisfy one of two sets of ambiguous boundary conditions. These sets are the following:

$$\left\{ \begin{array}{l} u_i n_i = 0 \\ \sigma_{ik} n_i n_k \geq 0 \\ \sigma_{ik} n_i \tau_k = 0 \end{array} \right. \quad \text{or} \quad \left\{ \begin{array}{l} u_i n_i > 0 \\ \sigma_{ik} n_i n_k = 0 \\ \sigma_{ik} n_i \tau_k = 0 \end{array} \right. , \quad (\text{B.39})$$

where $\boldsymbol{\tau} = (\tau_1, \tau_2, \tau_3)$ is a tangent vector to the contact set Σ .

Looking at these sets of boundary conditions it can be seen ([31]) that points which satisfy the first set of conditions are the points which do not leave the contact set Σ in the equilibrium configuration. This area is called the area of support. The points which satisfy the second set of conditions are those which do leave this contact set, and are referred to as the area of separation.

C

MATLAB CODES

C.1. EFFECT OF MICROCLIMATE FACTORS ON THE PATIENTS RISK OF PRESSURE ULCERS - MATLAB CODE

```
% This Matlab code repeats the calculation which are done in the article by
% Gefen.
3 clear all;

taus = 70;
P = 7;
alpha = 2;
8 beta = 1;
gamma = 0.1;
RH = 0.5;
Ts = 30:0.5:33;

13 % Start with the subplot(2,2,1), which plots different values of the
% ambient temperature Ta
x = zeros(1,6);
matrix = zeros(6,7);
for Ta = 35:40;
18     counter = taus-0.4*P;
        nD1 = (0.5*P+0.8*taus);
        nD2 = alpha * ((Ta-30)/10);
        nD3 = beta * ((Ta-Ts)/10)*(1-RH);
        nD4 = gamma;
23     tX = counter ./ (nD1.*(nD2- nD3 - nD4));
        matrix(Ta-34,:) = tX;
        x(Ta-34) = tX(1);
    end;
matrix = matrix./max(x);
28 subplot(2,2,1);
    plot(Ts,matrix);
    axis([30,33,0.4,1]);
    xlabel('T_s [°C]');
    ylabel('Dimensionless time for skin breakdown');
33 hold on;

% Continue with the second subplot, which takes Ta=35 and plots for
% different values of RH.
x = zeros(1,5);
38 matrix = zeros(5,7);
    Ta = 35;
    clear RH;
    for RH = 0:0.25:1;
        counter = taus-0.4*P;
43     nD1 = (0.5*P+0.8*taus);
        nD2 = alpha * ((Ta-30)/10);
        nD3 = beta * ((Ta-Ts)/10)*(1-RH);
        nD4 = gamma;
```

```

        tX = counter ./ (nD1.*(nD2- nD3 - nD4));
48     matrix(RH*4+1,:) = tX;
        x(RH*4+1) = tX(1);
    end;
    matrix = matrix./max(x);
    subplot(2,2,2);
53     plot(Ts,matrix);
        axis([30,33,0.4,1]);
        xlabel('T_s [°C]');
        ylabel('Dimensionless time for skin breakdown');
    hold on;
58     % In the third subplot, RH is taken to be 0.5, and different values of P
        % are plotted.
        x = zeros(1,8);
        matrix = zeros(8,7);
63     RH =0.5;
    clear P;
    for P = 3:10;
        counter = taus-0.4.*P;
        nD1 = (0.5.*P+0.8*taus);
68         nD2 = alpha * ((Ta-30)/10);
            nD3 = beta * ((Ta-Ts)/10)*(1-RH);
            nD4 = gamma;
            tX = counter ./ (nD1.*(nD2- nD3 - nD4));
            matrix(P-2,:) = tX;
73         x(P-2) = tX(1);
    end;
    matrix = matrix./max(x);
    subplot(2,2,3);
    plot(Ts,matrix);
78     axis([30,33,0.7,1]);
        xlabel('T_s [°C]');
        ylabel('Dimensionless time for skin breakdown');
    hold on;

83     % In the final subbplot P=7 and gamma is being changed.
        x = zeros(1,5);
        matrix = zeros(5,7);
        P=7;
    clear gamma;
88     for gamma = 0:0.05:0.2;
        counter = taus-0.4.*P;
        nD1 = (0.5.*P+0.8*taus);
        nD2 = alpha * ((Ta-30)/10);
        nD3 = beta * ((Ta-Ts)/10)*(1-RH);
93         nD4 = gamma;
            tX = counter ./ (nD1.*(nD2- nD3 - nD4));
            matrix(gamma*20+1,:) = tX;
            x(gamma*20+1) = tX(1);
    end;
98     matrix = matrix./max(x);
    subplot(2,2,4);
    plot(Ts,matrix);
        axis([30,33,0.6,1]);
        xlabel('T_s [°C]');
103    ylabel('Dimensionless time for skin breakdown');
    hold on;

```

C.2. MATLAB CODE OF THE FINAL MODEL

```

1 %% Small Final model with Gravity
  % We consider a body and a bed that will be in contact. In the first time
  % step the gravity is applied, which will cause the body to move down
  % towards the bed. In the second step (gravity is still applied), the body
  % is at rest and the effects of the microclimate factors are applied
6  % (changing COF and changing Youngs Modulus). In the third step the body
  % is repositioned by moving it across the bed.

  % In this final model the coefficient of friction and the Young's modulus
  % change in time. Also the model has extra weight and the temperature is
11 % set to 35 degrees.
  %%
  clear; close all; clc;
  %Since the convergence of the problems with gravity is not very good,
  %the problem will run until solved. Usually takes about 5 minutes.
16 x=0;
  clearvars -except x; clc;
  while x==0
  close all; clc;
  Ts = 35;%Skin temperature
21 Ta = 35; %Ambient temperature
  %Calculate the perspiration as given in the article on microclimate factors by Amit
  Gefen.
  %This function calculates for three time steps, in which the first time
  %step is constant, as well as the third time step.
  [time,deltaV] = perspiration(Ta,Ts);
26
  %% Plot settings
  figColor='w'; figColorDef='white';
  fontSize=15;
  faceAlpha1=0.5;
31 faceAlpha2=1;
  edgeColor=0.25*ones(1,3);
  edgeWidth=1.5;
  markerSize=25;
  lineWidth=3;
36
  %% Control parameters: Some basic information is saved here
  % path names
  filePath=mfilename('fullpath');
  savePath=fullfile(fileparts(filePath),'data','temp');
41 modelName=fullfile(savePath,'CBGravitySmallFullTemp');

  %Specifying dimensions and number of elements
  sampleWidth=12;
  sampleThickness=12;
46 sampleHeight=6;
  pointSpacing=4.3;
  initialArea=sampleWidth*sampleThickness;

  numElementsWidth=round(sampleWidth/pointSpacing);
51 numElementsThickness=round(sampleThickness/pointSpacing);
  numElementsHeight=round(sampleHeight/pointSpacing);

  contactInitialOffset=0;%0.2
  sphereRadius=6;
56 sphereRadiusInner=0.5;

  %% CREATING MESHED BOX
  %Create box 1 using Gibbon Toolbox
  boxDim=[sampleWidth sampleThickness sampleHeight]; %Dimensions
61 boxE1=[numElementsWidth numElementsThickness numElementsHeight]; %Number of elements
  [box1]=hexMeshBox(boxDim,boxE1);
  E1=box1.E;
  V1=box1.V;
  F1=box1.F;
66 Fb1=box1.Fb;
  faceBoundaryMarker=box1.faceBoundaryMarker;
  V1(:,3)=V1(:,3)-(sampleHeight/2); %The top of the bed is now at z=0

```

```

%% CREATING MESHED SPHERE
71 %Control settings
    cPar.sphereRadius=sphereRadius;
    cPar.coreRadius=sphereRadiusInner;
    cPar.numElementsMantel=4;
    cPar.numElementsCore=4;
76 cPar.makeHollow=1; %1 means the sphere is hollow
    %Creating sphere using Gibbon Toolbox
    [meshStruct]=hexMeshSphere(cPar);

    %Access ouput
81 E2=meshStruct.E; %The elements
    V2=meshStruct.V; %The vertices
    Fb2=meshStruct.Fb; %The boundary faces
    faceBoundaryMarker2=meshStruct.faceBoundaryMarker;

86 %Offset sphere
    V2(:,3)=V2(:,3)+sphereRadius+contactInitialOffset; %The bottom of the body is now at z
        =0.

    %% Plotting surface models
    hf=figuremax(figColor,figColorDef);
91 title('Model surfaces','FontSize',fontSize);
    xlabel('X','FontSize',fontSize); ylabel('Y','FontSize',fontSize); zlabel('Z','FontSize',
        ,fontSize);
    hold on;
    patch('Faces',Fb1,'Vertices',V1,'FaceColor','flat','CData',faceBoundaryMarker,'
        FaceAlpha',faceAlpha1,'lineWidth',edgeWidth,'edgeColor',edgeColor);
    patch('Faces',Fb2,'Vertices',V2,'FaceColor','r','FaceAlpha',faceAlpha1,'lineWidth',
        edgeWidth,'edgeColor',edgeColor);
96 colormap(jet(6)); colorbar;
    set(gca,'FontSize',fontSize);
    view(3); axis tight; axis equal; grid on;
    drawnow;

101 %% MERGING NODE SETS
    %For simplicity we need all the nodes to be in one set.
    V=[V1;V2;]; %Nodes
    E2=E2+size(V1,1);
    Fb2=Fb2+size(V1,1);
106

    %% Plotting surface models using the merged sets
    hf=figuremax(figColor,figColorDef);
    title('Merged node sets','FontSize',fontSize);
    xlabel('X','FontSize',fontSize); ylabel('Y','FontSize',fontSize); zlabel('Z','FontSize',
        ,fontSize);
111 hold on;
    patch('Faces',Fb1,'Vertices',V,'FaceColor','b','FaceAlpha',faceAlpha1,'lineWidth',
        edgeWidth,'edgeColor',edgeColor);
    patch('Faces',Fb2,'Vertices',V,'FaceColor','r','FaceAlpha',faceAlpha1,'lineWidth',
        edgeWidth,'edgeColor',edgeColor);
    set(gca,'FontSize',fontSize);
    view(3); axis tight; axis equal; grid on;
116 drawnow;

    %% Define contact surfaces
    %Here the surfaces need to be defined which will be in contact
    Fc1=Fb2(faceBoundaryMarker2==1,:); %The outer surface of the sphere
121

    logicContactSurf1=faceBoundaryMarker==6;
    Fc2=Fb1(logicContactSurf1,:);%The top surface of the bed

    % Plotting surface models of the contact surfaces
126 hf=figuremax(figColor,figColorDef);
    title('Contact sets','FontSize',fontSize);
    xlabel('X','FontSize',fontSize); ylabel('Y','FontSize',fontSize); zlabel('Z','FontSize',
        ,fontSize);
    hold on;
    patch('Faces',Fb1,'Vertices',V,'FaceColor','b','FaceAlpha',0.2,'edgeColor','none');
131 patch('Faces',Fc1,'Vertices',V,'FaceColor','g','FaceAlpha',1,'lineWidth',edgeWidth,'

```

```

    edgeColor',edgeColor);
[hp]=patchNormPlot(Fc1,V,1);
patch('Faces',Fc2,'Vertices',V,'FaceColor','g','FaceAlpha',1,'lineWidth',edgeWidth,'
    edgeColor',edgeColor);
[hp]=patchNormPlot(Fc2,V,1);
set(gca,'FontSize',fontSize);
136 view(3); axis tight; axis equal; grid on;
drawnow;

%% DEFINE BC's
%Here the surface for the boundary conditions are defined
141 %The bottom of the bed is the first surface, as this will be constricted
%later on.
logicRigid=faceBoundaryMarker==5;
Fr=Fr1(logicRigid,:);
bcRigidList=unique(Fr(:));
146
%The Inner surface of the sphere is used to apply the prescribed boundary
%conditions
Fr=Fr2(faceBoundaryMarker2==2,:); %Inner sphere
bcPrescribeList=unique(Fr(:));
151
%The magnitude of the prescribed boundary condition is defined to be 1mm in the x
direction.
displacementMagnitude2=[1 0 0];
bcPrescribeMagnitudes2=displacementMagnitude2(ones(1,numel(bcPrescribeList)),:);

156 %% Visualize BC's
hf=figuremax(figColor,figColorDef);
title('Complete model','FontSize',fontSize);
xlabel('X','FontSize',fontSize); ylabel('Y','FontSize',fontSize); zlabel('Z','FontSize',
    ,fontSize);
hold on;
161 patch('Faces',Fb1,'Vertices',V,'FaceColor','b','FaceAlpha',faceAlpha1,'lineWidth',
    edgeWidth,'edgeColor',edgeColor);
patch('Faces',Fb2,'Vertices',V,'FaceColor','r','FaceAlpha',faceAlpha1,'lineWidth',
    edgeWidth,'edgeColor',edgeColor);
plotV(V(bcRigidList,:),'k.','MarkerSize',markerSize);
plotV(V(bcPrescribeList,:),'k.','MarkerSize',markerSize);
set(gca,'FontSize',fontSize);
166 view(3); axis tight; axis equal; grid on;
drawnow;

%% Visualize the Inside of the model
hf1=figuremax(figColor,figColorDef);
171 title('Cut-view of the undeformed model','FontSize',fontSize);
xlabel('X (mm)','FontSize',fontSize); ylabel('Y (mm)','FontSize',fontSize); zlabel('Z (
    mm)','FontSize',fontSize); hold on;
%Create cut view
Y=V(:,2); YE=mean(Y(E1),2);
L=YE>mean(Y);
176 [Fs,~]=element2patch(E1(L,:),[],'hex8');
patch('Faces',Fs,'Vertices',V,'FaceColor','b','FaceAlpha',faceAlpha1,'lineWidth',
    edgeWidth,'edgeColor',edgeColor);
%Create cut view
Y=V(:,2); YE=mean(Y(E2),2);
L=YE>mean(Y);
181 [Fs,~]=element2patch(E2(L,:),[],'hex8');
patch('Faces',Fs,'Vertices',V,'FaceColor','r','FaceAlpha',faceAlpha1,'lineWidth',
    edgeWidth,'edgeColor',edgeColor);
view(3); axis tight; axis equal; grid on;
colormap jet; colorbar;
% camlight headlight;
186 set(gca,'FontSize',fontSize);
legend('Bed','Skin','Location','southoutside');
drawnow;

%% CONSTRUCTING FEB MODEL
191 %Setting some basic information
FEB_struct.febio_spec.version='2.0';
FEB_struct.Module.Type='solid';

```

```

% Defining file names
196 FEB_struct.run_filename=[modelName,'.feb']; %FEB file name
    FEB_struct.run_logname=[modelName,'.txt']; %FEBio log file name

%Creating FEB_struct
    FEB_struct.Geometry.Nodes=V; %The node set
201 FEB_struct.Geometry.Elements={E1 E2}; %The element sets
    FEB_struct.Geometry.ElementType={'hex8','hex8'}; %The element types
    %The materials are assigned as follows: All elements in E1 are material 1,
    %all elements in E2 are material 2FEB_struct.Geometry.ElementMat={[1*ones(1,size(E1,1))
        ]; [2*ones(1,size(E2,1))]; };
    FEB_struct.Geometry.ElementsPartName={'Bed','Body'};
206
% DEFINING MATERIALS
%Material 1: Mattress
density=30e-9;
E=10;
211 v=0.3;
    FEB_struct.Materials{1}.Type='isotropic elastic';
    FEB_struct.Materials{1}.Properties={'density','E','v'};
    FEB_struct.Materials{1}.Values={density,E,v};

216 %Material 2: Skin
density=1100e-9;
E=1;
v=0.49;
    FEB_struct.Materials{2}.Type='isotropic elastic';
221 FEB_struct.Materials{2}.Properties={'density','E','v'};
    FEB_struct.Materials{2}.Values={density,E,v};
    FEB_struct.Materials{2}.lc={0,5,0}; %A load curve is connected to the Youngs modulus

%Control sections
226 %here the information regarding the solution method are defined.
    FEB_struct.Control.AnalysisType='static';
    FEB_struct.Control.Properties={'time_steps','step_size',...
        'max_refs','max_ups',...
        'dtol','etol','rtol','lstol'};
231 FEB_struct.Control.Values={25,0.04,...
        25,10,...
        0.001,0.01,0,0.9};
    FEB_struct.Control.TimeStepperProperties={'dtmin','dtmax','max_retries','opt_iter','
        aggressiveness'};
    FEB_struct.Control.TimeStepperValues={1e-4,0.04,5,5,1};
236
    FEB_struct.Step{2}.Control = FEB_struct.Control;%The second step is defined the same as
        the first step

    FEB_struct.Step{3}.Control = FEB_struct.Control;%The third step is defined the same as
        the first step

241 %Defining surfaces
    %The earlier defined contact surfaces are now called the master and slave
    %surfaces.
    FEB_struct.Geometry.Surface{1}.Set=Fc1;
    FEB_struct.Geometry.Surface{1}.Type='quad4';
246 FEB_struct.Geometry.Surface{1}.Name='Contact_master';

    FEB_struct.Geometry.Surface{2}.Set=Fc2;
    FEB_struct.Geometry.Surface{2}.Type='quad4';
    FEB_struct.Geometry.Surface{2}.Name='Contact_slave';
251
%Defining node sets
    FEB_struct.Geometry.NodeSet{1}.Set=bcRigidList;
    FEB_struct.Geometry.NodeSet{1}.Name='bcRigidList';
    FEB_struct.Geometry.NodeSet{2}.Set=bcPrescribeList;
256 FEB_struct.Geometry.NodeSet{2}.Name='bcPrescribeList';

%Adding fixed BC's
%The bottom of the bed is restricyed from all movements (in x,y and z directions)
    FEB_struct.Boundary.Fix{1}.bc='x';

```

```

261 FEB_struct.Boundary.Fix{1}.SetName=FEB_struct.Geometry.NodeSet{1}.Name;
FEB_struct.Boundary.Fix{2}.bc='y';
FEB_struct.Boundary.Fix{2}.SetName=FEB_struct.Geometry.NodeSet{1}.Name;
FEB_struct.Boundary.Fix{3}.bc='z';
FEB_struct.Boundary.Fix{3}.SetName=FEB_struct.Geometry.NodeSet{1}.Name;
266 %The inner sphere is only restricted in the y-direction
FEB_struct.Boundary.Fix{4}.bc='y';
FEB_struct.Boundary.Fix{4}.SetName=FEB_struct.Geometry.NodeSet{2}.Name;

%In the third step a prescribed boundary condition is used to move the
271 %inner sphere 1 mm in the x-direction.
FEB_struct.Step{3}.Boundary.Prescribe{1}.Set=bcPrescribeList;
FEB_struct.Step{3}.Boundary.Prescribe{1}.bc='x';
FEB_struct.Step{3}.Boundary.Prescribe{1}.lc=2;
FEB_struct.Step{3}.Boundary.Prescribe{1}.nodeScale=bcPrescribeMagnitudes2(:,1);
276
%Adding Loads
%Here the body load is defined.
FEB_struct.Loads.Body_force{1}.Directions={'z'};
FEB_struct.Loads.Body_force{1}.Values={1};%Value 1 will be multiplied by the values in
the loadcurve.
281 FEB_struct.Loads.Body_force{1}.lc={3};%the loadcurve wil have a final value of 9810 mN/
kg = 9.81N/kg =gravity acceleration
FEB_struct.Loads.Body_force{1}.Type='const';

%Adding contact information
%The contact method is defined. First the master and slave are defined,
286 %then the contact interface with the details.
FEB_struct.Contact{1}.Surface{1}.SetName=FEB_struct.Geometry.Surface{1}.Name;
FEB_struct.Contact{1}.Surface{1}.Type='master';

FEB_struct.Contact{1}.Surface{2}.SetName=FEB_struct.Geometry.Surface{2}.Name;
291 FEB_struct.Contact{1}.Surface{2}.Type='slave';

FEB_struct.Contact{1}.Type='sliding_with_gaps';
FEB_struct.Contact{1}.Properties={'penalty','auto_penalty','two_pass',...
'laugon','tolerance',...
296 'gaptol','minaug','maxaug',...
'fric_coeff','fric_penalty',...
'seg_up',...
'search_tol'};

FEB_struct.Contact{1}.Values={100,1,1,...
301 0,0.1,...
0,0,10,...
0.2,1,...
0,...
0.01};
306 FEB_struct.Contact{1}.lc={0,0,0,...
0,0,...
0,0,0,...
7,0,... %A loadcurve is applied to the COF
0,...
311 0};

%Adding output requests
FEB_struct.Output.VarTypes={'displacement','stress','relative volume','shell thickness'
};

316 %Specify log file output
%The outputs that are saved in logfiles are specified here. The current
%outputs are the displacements, the forces, the Cauchy stresses and the
%eigenvalues.
run_disp_output_name=[FEB_struct.run_filename(1:end-4),'_node_out.txt'];
321 run_force_output_name=[FEB_struct.run_filename(1:end-4),'_force_out.txt'];
run_stress_output_name=[FEB_struct.run_filename(1:end-4),'_stress.txt'];
run_eigenvalues_output_name=[FEB_struct.run_filename(1:end-4),'_eigenval.txt'];
FEB_struct.run_output_names={run_disp_output_name,run_force_output_name,
run_stress_output_name,run_eigenvalues_output_name};
FEB_struct.output_types={'node_data','node_data','element_data','element_data'};
326 FEB_struct.data_types={'ux;uy;uz','Rx;Ry;Rz','sx;sy;sz;sxy;syz;sxz','s1;s2;s3'};

```

```

%Load curves
taus = 70; %strength of dry skin is 70kPa
COF = 0.5*deltaV +0.4;%The COF is calculated using the perspiration
331 FEB_struct.LoadData.LoadCurves.id=[1 2 3 4 5 6 7];
FEB_struct.LoadData.LoadCurves.type={'linear','linear','linear','linear','linear','
linear','smooth'};
FEB_struct.LoadData.LoadCurves.loadPoints={[0 0;1 1];[0 0;1 0;2 0;3 1];[0 0; 1 9810; 2
9810; 3 9810];[0 1; 1 1];[0 15.2; 1 15.2;1.5 50; 2 100];[0 0.2; 1 0.2; 2 0.8];[time
' COF']];

336 %% SAVING .FEB FILE
FEB_struct.disp_opt=0; %Display waitbars option
febStruct2febFile(FEB_struct); %This function uses the abpue informaton to create a .
feb file (from Gibbon Toolbox)

%% RUNNING FEBIO JOB
341 FEBioRunStruct.FEBioPath='C:\Users\Thyrza\FEBio2p0\bin\Febio2x64.exe';
FEBioRunStruct.run_filename=FEB_struct.run_filename;
FEBioRunStruct.run_logname=FEB_struct.run_logname;
FEBioRunStruct.disp_on=1;
FEBioRunStruct.disp_log_on=1;
346 FEBioRunStruct.runMode='external';%'internal'; %External uses the febio interface,
internal shows all calculations in matlab.
FEBioRunStruct.t_check=0.25; %Time for checking log file (dont set too small)
FEBioRunStruct.maxtpi=1e99; %Max analysis time
FEBioRunStruct.maxLogCheckTime=3; %Max log file checking time

351 [runFlag]=runMonitorFEBio(FEBioRunStruct);%START FEBio NOW!

%%
if runFlag==1 %i.e. a succesful run the following results will be shown
x=1;
356 %% The NODAL DISPLACEMENT RESULTS
% Importing nodal displacements from a log file
[~, N_disp_mat,~]=importFEBio_logfile(FEB_struct.run_output_names{1}); %Nodal
displacements

DN=N_disp_mat(:,2:end,end); %Final nodal displacements
361

% CREATING NODE SET IN DEFORMED STATE
V_def=V+DN;
DN_magnitude=sqrt(sum(DN.^2,2));

366 %Plotting the displacements
hf1=figuremax(figColor,figColorDef);
title(['The deformed model'],'FontSize',fontSize);
xlabel('X (mm)','FontSize',fontSize); ylabel('Y (mm)','FontSize',fontSize); zlabel(
'Z (mm)','FontSize',fontSize); hold on;
%Create cut view
371 Y=V(:,2); YE=mean(Y(E1),2);
L=YE>mean(Y);
[Fs,~]=element2patch(E1(L,:),[],'hex8');
%[Fs,~]=element2patch(E1(:,2),[],'hex8');
patch('Faces',Fs,'Vertices',V_def,'FaceColor','flat','CData',DN_magnitude,'
FaceAlpha',1,'lineWidth',edgeWidth,'edgeColor',edgeColor);
376 %Create cut view
Y=V(:,2); YE=mean(Y(E2),2);
L=YE>mean(Y);
[Fs,~]=element2patch(E2(L,:),[],'hex8');
patch('Faces',Fs,'Vertices',V_def,'FaceColor','flat','CData',DN_magnitude,'
FaceAlpha',1,'lineWidth',edgeWidth,'edgeColor',edgeColor);
381 view(3); axis tight; axis equal; grid on;
colormap jet; colorbar;
% camlight headlight;
set(gca,'FontSize',fontSize);
drawnow;
386 hold on;

%% The Elemental STRESS RESULTS
% Importing elemental STRESS from a log file

```

```

[time_mat, N_stress_mat, ~]=importFEBio_logfile(FEB_struct.run_output_names{3}); %
    elemental stresses
391
%% Calculating the maximum shear stress
Sntime=squeeze(N_stress_mat(1,end,:));
[~, N_eigenvalues_mat, ~]=importFEBio_logfile(FEB_struct.run_output_names{4}); %
    Elemental eigenvalues
principalstress = principalStress(N_stress_mat, N_eigenvalues_mat);
396 [maxshearstress, maxmaxshearstress, minmaxshearstress, avgmaxshearstress]=
    maxShearStress(principalstress); % matrix: nr elements x nr timesteps.
maxmaxshearstressSkin = max(maxshearstress(end-size(E2,1)+1:end,:));
minmaxshearstressSkin = min(maxshearstress(end-size(E2,1)+1:end,:));
avgmaxshearstressSkin = mean(maxshearstress(end-size(E2,1)+1:end,:));
shearStrength = (1-0.8*deltaV)*taus;
401
%Plotting the maximum shear stress
hf2=figuremax(figColor, figColorDef);
title('The maximum, minimum and average maxshearstress for the skin elements
    against the time', 'FontSize', 11);
xlabel('time (s)'); ylabel('maximum shear stress Skin (kPa)'); hold on;
406 plot(time_mat, maxmaxshearstressSkin, 'r', 'LineWidth', 2);
    hold on;
    plot(time_mat, minmaxshearstressSkin, 'g', 'LineWidth', 2);
    hold on;
    plot(time_mat, avgmaxshearstressSkin, 'b', 'LineWidth', 2);
411 h_legend = legend('maximum', 'minimum', 'average');
    set(gca, 'fontsize', 14)
    set(h_legend, 'FontSize', 14);

%Plotting the shear strength and the maximum shear stress
416 hf3=figuremax(figColor, figColorDef);
title('The maximum shear stress and the shear strength of skin');
xlabel('time (s)'); ylabel('Stress (kPa)'); hold on;
plot(time_mat, maxmaxshearstressSkin, 'r', 'LineWidth', 2);
    hold on;
421 plot(time, shearStrength, 'b', 'LineWidth', 2);
    legend('maximum shear stress', 'shear strength');
    set(gca, 'fontsize', 14)
    set(h_legend, 'FontSize', 14);
end
426 end

```


D

FEBIO FILES

D.1. FEBIO FILE OF THE FINAL MODEL

```
<?xml version="1.0" encoding="utf-8"?>
<!-- Created using GIBBON, 12-Mar-2015 21:14:35-->
<febio_spec version="2.0">
4   <Module type="solid"/>
    <Control>
        <time_steps>25.000000</time_steps>
        <step_size>0.040000</step_size>
        <max_refs>25.000000</max_refs>
9       <max_ups>10.000000</max_ups>
        <dtol>0.001000</dtol>
        <etol>0.010000</etol>
        <rtol>0.000000</rtol>
        <lstol>0.900000</lstol>
14      <analysis type="static"/>
        <time_stepper>
            <dtmin>0.000100</dtmin>
            <dtmax>0.040000</dtmax>
            <max_retries>5.000000</max_retries>
19          <opt_iter>5.000000</opt_iter>
            <aggressiveness>1.000000</aggressiveness>
        </time_stepper>
    </Control>
    <Material>
24      <material id="1" name="mat_1" type="isotropic elastic">
        <density>3.000000e-08</density>
        <E>1.000000e+01</E>
        <v>3.000000e-01</v>
    </material>
29      <material id="2" name="mat_2" type="isotropic elastic">
        <density>1.100000e-06</density>
        <E lc="5">1.000000e+00</E>
        <v>4.900000e-01</v>
    </material>
34 </Material>
    <Geometry>
        <Nodes>
            <node id="1">-6.000000e+00, -6.000000e+00, -6.000000e+00</node>
            .....
39          <node id="522">3.4641016e+00, 3.4641016e+00, 9.4641016e+00</node>
        </Nodes>
        <Elements mat="1" name="Bed" type="hex8">
            <elem id="1"> 1, 5, 6, 2, 17, 21, 22, 18</elem>
            .....
44          <elem id="9"> 11, 15, 16, 12, 27, 31, 32, 28</elem>
        </Elements>
        <Elements mat="2" name="Body" type="hex8">
            <elem id="10"> 34, 39, 38, 33, 132, 137, 136, 131</elem>
            .....
```

```

49     <elem id="393"> 418, 423, 424, 419, 516, 521, 522, 517</elem>
      </Elements>
      <Surface name="Contact_master">
        <quad4 id="1"> 426, 431, 430, 425</quad4>
          .....
54     <quad4 id="96"> 516, 521, 522, 517</quad4>
      </Surface>
      <Surface name="Contact_slave">
        <quad4 id="1"> 17, 21, 22, 18</quad4>
          .....
59     <quad4 id="9"> 27, 31, 32, 28</quad4>
      </Surface>
      <NodeSet name="bcRigidList"> 1, 2, 3, 4, .., 13, 14, 15, 16</NodeSet>
      <NodeSet name="bcPrescribeList"> 33, 34, 35, 36, 37, 38, 39, 40, 41,
        .....
64     117, 118, 119, 120, 121, 122, 123, 124, 125, 126, 127, 128, 129, 130</NodeSet>
      </Geometry>
      <Boundary>
        <fix bc="x" set="bcRigidList"/>
        <fix bc="y" set="bcRigidList"/>
69     <fix bc="z" set="bcRigidList"/>
        <fix bc="y" set="bcPrescribeList"/>
      </Boundary>
      <Loads>
        <body_load type="const">
74     <z lc="3">1.000000e+00</z>
        </body_load>
      </Loads>
      <Contact>
        <contact type="sliding_with_gaps">
79     <penalty>1.000000e+02</penalty>
        <auto_penalty>1.000000e+00</auto_penalty>
        <two_pass>1.000000e+00</two_pass>
        <laugon>0.000000e+00</laugon>
        <tolerance>1.000000e-01</tolerance>
84     <gaptol>0.000000e+00</gaptol>
        <minaug>0.000000e+00</minaug>
        <maxaug>1.000000e+01</maxaug>
        <fric_coeff lc="7">2.000000e-01</fric_coeff>
        <fric_penalty>1.000000e+00</fric_penalty>
89     <seg_up>0.000000e+00</seg_up>
        <search_tol>1.000000e-02</search_tol>
        <surface set="Contact_master" type="master"/>
        <surface set="Contact_slave" type="slave"/>
        </contact>
94     </Contact>
      <LoadData>
        <loadcurve id="1" type="linear">
          <loadpoint>0.000000, 0.000000</loadpoint>
          <loadpoint>1.000000, 1.000000</loadpoint>
99     </loadcurve>
        <loadcurve id="2" type="linear">
          <loadpoint>0.000000, 0.000000</loadpoint>
          <loadpoint>1.000000, 0.000000</loadpoint>
          <loadpoint>2.000000, 0.000000</loadpoint>
104    <loadpoint>3.000000, 1.000000</loadpoint>
        </loadcurve>
        <loadcurve id="3" type="linear">
          <loadpoint>0.000000, 0.000000</loadpoint>
          <loadpoint>1.000000, 9810.000000</loadpoint>
109    <loadpoint>2.000000, 9810.000000</loadpoint>
          <loadpoint>3.000000, 9810.000000</loadpoint>
        </loadcurve>
        <loadcurve id="4" type="linear">
          <loadpoint>0.000000, 1.000000</loadpoint>
114    <loadpoint>1.000000, 1.000000</loadpoint>
        </loadcurve>
        <loadcurve id="5" type="linear">
          <loadpoint>0.000000, 15.200000</loadpoint>
          <loadpoint>1.000000, 15.200000</loadpoint>
119    <loadpoint>1.500000, 50.000000</loadpoint>

```

```

    <loadpoint>2.000000, 100.000000</loadpoint>
  </loadcurve>
  <loadcurve id="6" type="linear">
    <loadpoint>0.000000, 0.200000</loadpoint>
124    <loadpoint>1.000000, 0.200000</loadpoint>
    <loadpoint>2.000000, 0.800000</loadpoint>
  </loadcurve>
  <loadcurve id="7" type="smooth">
129    <loadpoint>0.000000, 0.400000</loadpoint>
    <loadpoint>1.000000, 0.400000</loadpoint>
    <loadpoint>1.100000, 0.455000</loadpoint>
    <loadpoint>1.200000, 0.510000</loadpoint>
    <loadpoint>1.300000, 0.565000</loadpoint>
134    <loadpoint>1.400000, 0.620000</loadpoint>
    <loadpoint>1.500000, 0.675000</loadpoint>
    <loadpoint>1.600000, 0.730000</loadpoint>
    <loadpoint>1.700000, 0.785000</loadpoint>
    <loadpoint>1.800000, 0.840000</loadpoint>
139    <loadpoint>1.900000, 0.895000</loadpoint>
    <loadpoint>2.000000, 0.895000</loadpoint>
    <loadpoint>3.000000, 0.895000</loadpoint>
  </loadcurve>
</LoadData>
<Step name="Step_1">
144   <Module type="solid"/>
</Step>
<Step name="Step_2">
   <Module type="solid"/>
   <Control>
149     <time_steps>25.000000</time_steps>
     <step_size>0.040000</step_size>
     <max_refs>25.000000</max_refs>
     <max_ups>10.000000</max_ups>
154     <dtol>0.001000</dtol>
     <etol>0.010000</etol>
     <rtol>0.000000</rtol>
     <lstol>0.900000</lstol>
     <analysis type="static"/>
     <time_stepper>
159       <dtmin>0.000100</dtmin>
       <dtmax>0.040000</dtmax>
       <max_retries>5.000000</max_retries>
       <opt_iter>5.000000</opt_iter>
       <aggressiveness>1.000000</aggressiveness>
164     </time_stepper>
   </Control>
</Step>
<Step name="Step_3">
   <Module type="solid"/>
169   <Boundary>
     <prescribe bc="x" lc="2">
       <node id="33">1.000000e+00</node>
       .....
       <node id="130">1.000000e+00</node>
174     </prescribe>
   </Boundary>
   <Control>
179     <time_steps>25.000000</time_steps>
     <step_size>0.040000</step_size>
     <max_refs>25.000000</max_refs>
     <max_ups>10.000000</max_ups>
     <dtol>0.001000</dtol>
     <etol>0.010000</etol>
     <rtol>0.000000</rtol>
184     <lstol>0.900000</lstol>
     <analysis type="static"/>
     <time_stepper>
189       <dtmin>0.000100</dtmin>
       <dtmax>0.040000</dtmax>
       <max_retries>5.000000</max_retries>
       <opt_iter>5.000000</opt_iter>

```

```
        <aggressiveness>1.000000</aggressiveness>
      </time_stepper>
    </Control>
194 </Step>
    <Output>
      <plotfile type="febio">
        <var type="displacement"/>
        <var type="stress"/>
199 </plotfile>
      <logfile>
        <node_data data="ux;uy;uz" delim=", " file="C:\..\CBGrFullT_node_out.txt"/>
        <node_data data="Rx;Ry;Rz" delim=", " file="C:\..\CBGrFullT_force_out.txt"/>
        <element_data data="sx;sy;sz;sxy;syz;sxz" delim=", " file="C:\..\
          CBGrFullT_stress.txt"/>
204 <element_data data="s1;s2;s3" delim=", " file="C:\..\CBGrFullT_eigval.txt"/>
      </logfile>
    </Output>
  </febio_spec>
```

BIBLIOGRAPHY

- [1] A. Gefen, *How do microclimate factors affect the risk for superficial pressure ulcers: A mathematical modeling study*, Journal of tissue viability **20**, 81 (2011).
- [2] E. Shaked and A. Gefen, *Modeling the effects of moisture-related skin-support friction on the risk for superficial pressure ulcers during patient repositioning in bed*, frontiers in bioengineering and biotechnology **1** (2013).
- [20] T. A. Laursen, *Computational Contact and Impact Mechanics* (Springer, Durham, USA, 2002).
- [4] V. L. Popov, *Contact Mechanics and Friction. Physical Principles and Applications* (Springer, Heidelberg, Germany, 2010).
- [3] EPUAP, *European pressure ulcer advisory panel*, .
- [5] R. M. Christensen, *Failure theory for materials science and engineering*, .
- [6] eFunda Inc., *Engineering fundamentals*, .
- [7] M. C. M. R. S. R. V. R. J. Black and C. Dealey, *Microclimate in context. international guidelines. pressure ulcer prevention: pressure shear, friction and microclimate in context*, London: Wounds International , 19 (2010).
- [8] A. Gefen, *Pressure-sensing devices for assessment of soft tissue loading under bony prominences: technological concepts and clinical utilization*. Wounds **19**, 350 (2007).
- [9] J. B. R. Wildnauer and A. Douglass, *Stratum corneum biomechanical properties. i. influence of relative humidity on normal and extracted human stratum corneum*. J Invest Dermatol **56**, 72 (1971).
- [10] D. K. Bathe and associates, *Adina - finite element analysis software*, .
- [11] U. of Utah's Musculoskeletal Research Laboratories and C. M. B. Laboratory, *Febio - finite elements for biomechanics*, ().
- [12] U. of Utah's Musculoskeletal Research Laboratories and C. M. B. Laboratory, *Preview - finite element pre processing*, ().
- [13] U. of Utah's Musculoskeletal Research Laboratories and C. M. B. Laboratory, *Postview - finite element post processing*, ().
- [14] K. M. Moerman, *Gibbon (hylobates agilis)*, (2014).
- [15] D. Systemes, *Abaqus fea*, .
- [16] S. Timoshenko and J. Goodier, *Theory of Elasticity* (McGraw-Hill Book Company, Inc., 1951).
- [17] J. Bonet and R. D. Wood, *Nonlinear Continuum Mechanics for Finite Element Analysis* (Cambridge University Press, Cambridge, United Kingdom, 1997).
- [18] A. Khennane, *Introduction to Finite Element Analysis Using MATLAB® and Abaqus* (CRC Press, 2013).
- [19] P. Kelly, *Solid mechanics part iii: Foundations of continuum solid mechanics*, .
- [21] R. Haberman, *Applied Partial Differential Equations with Fourier Series and Boundary Value Problems* (Pearson Prentice Hall, Upper Sadle River, New Jersey 07458, 2004).
- [22] S. M. D. R. D. J. Weiss and D. G. Ateshian, *FEBio - Finite Elements for Biomechanics - User Manual* (2014).

- [23] U. of Utah's Musculoskeletal Research Laboratories and C. M. B. Laboratory, [Postview - finite element post processing](#), ().
- [24] P. N. Kuster, [It's for health](#), .
- [25] R. J. de Dear, Edward A Arens, Hui Zhang and M. Oguro", *Convective and radiative heat transfer coefficients for individual human body segments*, Int J Biometeorol **40**, 141 (1997).
- [26] S. M. D. R. D. J. Weiss and D. G. Ateshian, *FEBio - Finite Elements for Biomechanics - Theory Manual* (2014).
- [27] K. Johnson, *Contact mechanics* (Cambridge University Press, 1985).
- [28] Wikipedia, [Frictional contact mechanics](#), (2014).
- [29] K. J. K. Kendall and A. Roberts, *Surface energy and the contact of elastic solids*, Proceedings of the Royal Society of London. Series A, Mathematical and Physical Sciences **324**, 301 (1971).
- [30] L. Landau and E. Lifschitz, *Theory of elasticity* (Pergamon Press, Butterworth-Heinemann, Oxford, 1999).
- [31] Wikipedia, [Signorini problem](#), (2014).